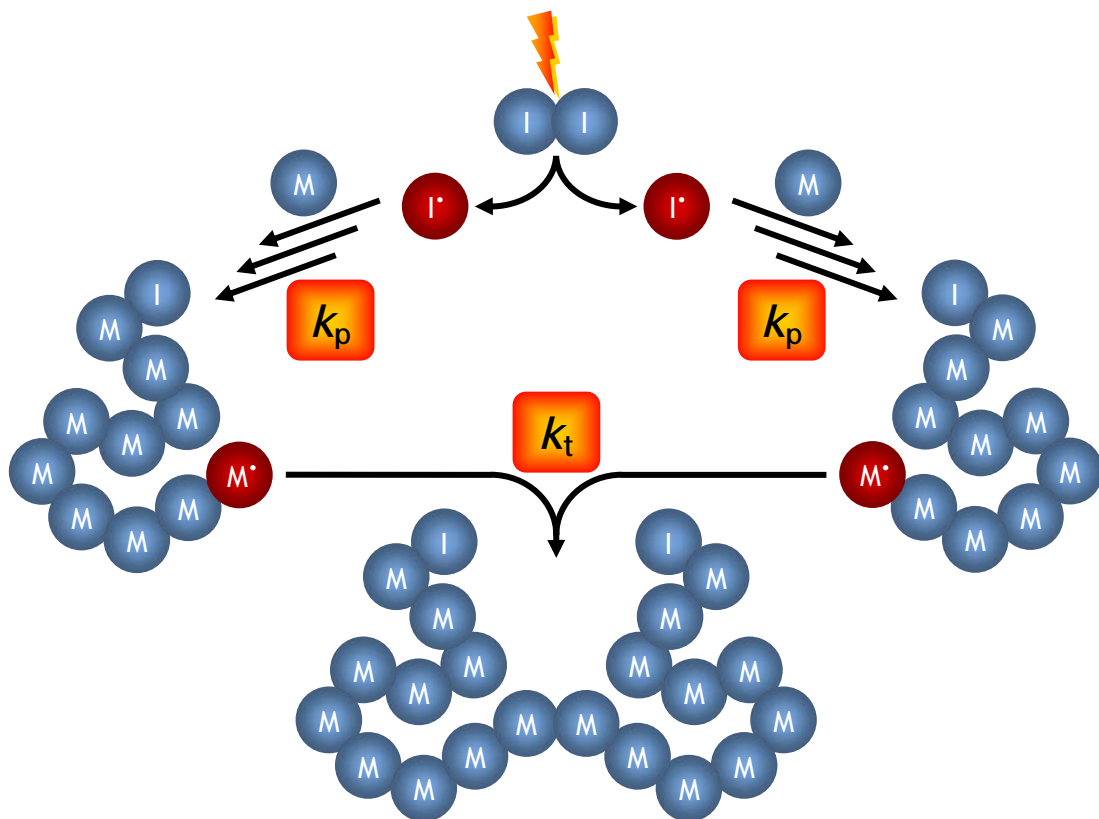


Investigations into the Propagation and Termination Kinetics of the Radical Polymerization of Polar Monomers in Aqueous Solution



Investigations into the Propagation and Termination Kinetics of the Radical Polymerization of Polar Monomers in Aqueous Solution

Dissertation

zur Erlangung des mathematisch-naturwissenschaftlichen Doktorgrades
„Doctor rerum naturalium“
der Georg-August-Universität Göttingen

im Promotionsprogramm Chemie
der Georg-August University School of Science (GAUSS)

vorgelegt von
Jens Schrooten
aus Göttingen

Göttingen, 2012

Betreuungsausschuss

Prof. Dr. M. Buback, Technische und Makromolekulare Chemie, Institut für Physikalische Chemie, Georg-August-Universität Göttingen

Prof. Dr. P. Vana, Makromolekulare Chemie, Institut für Physikalische Chemie, Georg-August-Universität Göttingen

Mitglieder der Prüfungskommission

Referent: Prof. Dr. M. Buback, Technische und Makromolekulare Chemie, Institut für Physikalische Chemie, Georg-August-Universität Göttingen

Korreferent: Prof. Dr. P. Vana, Makromolekulare Chemie, Institut für Physikalische Chemie, Georg-August-Universität Göttingen

Weitere Mitglieder der Prüfungskommission:

Prof. Dr. P. Botschwina, Theoretische Chemie, Institut für Physikalische Chemie, Georg-August-Universität Göttingen

Jun.-Prof. Dr. R. Mata, Computerchemie und Biochemie, Institut für Physikalische Chemie, Georg-August-Universität Göttingen

Prof. Dr. J. Schroeder, Physikalische Chemie I, Institut für Physikalische Chemie, Georg-August-Universität Göttingen

Prof. Dr. M. Suhm, Physikalische Chemie II, Institut für Physikalische Chemie, Georg-August-Universität Göttingen

Tag der mündlichen Prüfung: 24. Oktober 2012

Contents

1	Abstract	1
2	Introduction	3
3	Theoretical Background	7
3.1	Radical Homopolymerization	7
3.1.1	Formation of Primary Radicals and Initiation.....	7
3.1.2	Propagation	10
3.1.3	Termination	15
3.1.4	Steady-State Kinetics.....	23
3.1.5	Chain Transfer	24
3.1.6	Chain Scission.....	26
3.1.7	Inhibition and Retardation.....	26
3.2	Propagation in Binary Copolymerizations	27
3.3	Pressure and Temperature Effects on Rate Coefficients	31
3.4	Size-Exclusion Chromatography.....	34
3.5	PLP–SEC Technique	36
3.6	Fourier-Transform Near-Infrared Spectroscopy	37
3.7	SP–PLP–NIR Technique	38
3.8	Viscometry	39
3.9	Oscillating U-Tube	40
3.10	Nuclear Magnetic Resonance Spectroscopy	40
4	Materials and Equipment	43
4.1	Chemical Substances	43

4.1.1	Monomers.....	43
4.1.2	Solvents.....	45
4.1.3	Initiators.....	45
4.1.4	Further Chemical Substances	46
4.2	Purificants.....	47
4.3	Cuvettes	48
4.4	Optical High-Pressure Cell	48
4.5	Pressure Generation and Measurement.....	51
4.6	Temperature Control	52
4.7	Laser Energy Meter.....	53
4.8	PLP–SEC Technique	54
4.8.1	PLP Setup.....	54
4.8.2	Size-Exclusion Chromatographs.....	55
4.9	FTIR Spectrometer	57
4.10	SP–PLP–NIR Setup.....	58
4.11	NMR Spectrometer	65
4.12	Density Meter	65
4.13	Viscometer	65
4.14	Electrical Conductivity/pH Meter	65
5	Experimental Procedures and Data Evaluation	67
5.1	Determination of Density	67
5.2	Viscometry	67
5.3	PLP–SEC Experiments.....	67
5.3.1	Experimental Procedure	67
5.3.2	Data Evaluation.....	68

5.4	FT–NIR Spectroscopy	71
5.5	Chemically Initiated Polymerizations	71
5.5.1	Experimental Procedure	71
5.5.2	Data Evaluation.....	72
5.6	SP–PLP–NIR Experiments	75
5.6.1	Experimental Procedure	75
5.6.2	Data Evaluation.....	77
5.7	Curve Fitting	85
5.8	Determination of Joint Confidence Regions	85
5.9	Experimental Conditions	86
5.9.1	Photoinitiator	86
5.9.2	Tube Material of the Internal Cell.....	89
5.9.3	Reaction Conditions	89
5.10	^1H NMR Spectroscopy	91
5.11	Error Estimates	93
6	Termination Kinetics of 1-Vinylpyrrolidin-2-one Polymerization	97
6.1	Multidimensional Dependence of the Propagation Rate Coefficient on Reaction Conditions.....	98
6.2	Dynamic Viscosity of Monomer–Water Mixtures.....	99
6.3	Dependence on Initial Monomer Mass Fraction and Degree of Monomer Conversion.....	100
6.4	Pressure Dependence	116
7	Propagation Kinetics of the Polymerization of Prop-2-enamides	117
7.1	Dependence on Laser-Pulse Repetition Rate	123
7.2	Temperature Dependence	125

7.3	Concentration Dependence.....	136
7.4	Pressure Dependence	145
7.5	Multidimensional Dependence on Reaction Conditions	149
8	Termination Kinetics of the Polymerization of Prop-2-enamides	153
8.1	Dynamic Viscosity of Monomer–Water Mixtures.....	154
8.2	SP–PLP–NIR Investigations into the Dependence of the Termination Rate Coefficient on Initial Monomer Mass Fraction and Degree of Monomer Conversion.....	155
8.3	Pressure Dependence	170
8.4	Chemically Initiated Polymerizations	175
9	Propagation Kinetics of Sodium Acrylate–1-Vinylpyrrolidin-2-one Copolymerization	187
10	Closing Remarks and Outlook	197
10.1	Experimental Techniques	197
10.2	Kinetic Parameters.....	201
10.3	Monomers.....	202
	Acknowledgements	205
	Appendix A: Experimental Data	209
A.1	Propagation Rate Coefficients	209
A.2	Termination Rate Coefficients	220
A.3	Densities and Viscosities	233
A.4	Analysis of ^1H NMR Spectra	234
A.5	Copolymer Composition	235

Appendix B: C++ Source Codes	237
B.1 Script for the Calibration of the Laser and the UV Diode.....	237
B.2 Script for the Electronic Control of the SP–PLP–NIR Setup	242
Appendix C: Flowcharts	259
C.1 Flowchart of the Main Steps of Laser Calibration.....	259
C.2 Flowchart of the Main Steps of SP–PLP–NIR Experiments	260
Appendix D: MATLAB® Functions	263
D.1 Function for the Adjustment of <i>I002</i> Values	263
D.2 Function for the Calculation of the Relative Monomer Concentration Versus Time Profile and for the Curve Fitting to Experimental Data	271
Abbreviations and Symbols	291
References	309

1 Abstract

Propagation and termination rate coefficients of radical polymerizations in aqueous solution were determined from pulsed-laser induced polymerizations and chemically initiated polymerizations. Pulsed-laser induced polymerizations of *N*,2-dimethylprop-2-enamide, *N,N*-dimethylprop-2-enamide, 2-methylprop-2-enamide, and prop-2-enamide were performed. Subsequent analysis of the products by size-exclusion chromatography provided access to propagation rate coefficients. The obtained variation of the propagation rate coefficients with monomer concentration may be explained by the degree to which internal rotations and vibrations in the transition state of the propagation step are hindered. The dependence of the degree of hindrance on monomer concentration may be ascribed to an increase of intermolecular interactions of the transition-state structure with solvating molecules towards higher monomer content. Pressure and temperature were varied from ambient pressure to 2000 bar and from 10 °C to 80 °C, respectively, to allow for determination of volumes of activation and Arrhenius activation energies for propagation. The activation energy and the absolute value of the volume of activation in case of 2-methylprop-2-enamide are larger compared to *N,N*-dimethylprop-2-enamide. This finding may be ascribed to the circumstance that *N,N*-dimethylprop-2-enamide lacks an α -methyl group. Both activation parameters in case of *N*,2-dimethylprop-2-enamide are close to the ones of *N,N*-dimethylprop-2-enamide. This is unexpected because *N*,2-dimethylprop-2-enamide exhibits an α -methyl group. Differences between both monomers regarding the conformation of the carbon–carbon double bond relative to the carbon–oxygen double bond may explain this observation. Initiation of a polymerization by a single laser pulse and subsequent detection of monomer-to-polymer conversion by time-resolved near-infrared spectroscopy was used to measure termination rate coefficients. The time resolution has been improved to 0.33 μ s. Repetitive application of laser pulses in conjunction with near-infrared spectroscopic analysis yields termination rate coefficients as a function of the degree of monomer conversion. Investigations into the termination kinetics of prop-2-enamide,

2-methylprop-2-enamide, *N*,2-dimethylprop-2-enamide, *N,N*-dimethylprop-2-enamide, and 1-vinylpyrrolidin-2-one were performed at 2000 bar because of the better signal-to-noise ratio at high pressure. Additional measurements were conducted at pressures of 500 bar, 1000 bar, and 1500 bar in case of most prop-2-enamides. The so-obtained volumes of activation may be used to estimate termination rate coefficients at ambient pressure. The volumes of activation amount to $12.4 \text{ cm}^3 \cdot \text{mol}^{-1}$ and $14.3 \text{ cm}^3 \cdot \text{mol}^{-1}$ for the termination rate coefficients of *N*,2-dimethylprop-2-enamide and prop-2-enamide, respectively. The volume of activation in case of *N,N*-dimethylprop-2-enamide ($4.9 \text{ cm}^3 \cdot \text{mol}^{-1}$) is lower than expected. Termination rate coefficients of 1-vinylpyrrolidin-2-one could be obtained for a large range of initial monomer concentrations and degrees of monomer conversion. This information allows for a detailed analysis of the parameters used to describe the monomer-conversion dependence of the termination rate coefficient. Within the monomer-conversion ranges under investigation the termination rate coefficient is assumed to be controlled by segmental, translational, and reaction diffusion.

In case of *N,N*-dimethylprop-2-enamide and 1-vinylpyrrolidin-2-one, dynamic viscosities of monomer–water mixtures were determined at ambient pressure to assist the understanding of termination kinetics. A large set of termination rate coefficients in dependence on initial monomer concentration was obtained for these two monomers by pulsed-laser induced polymerization.

Chemically initiated polymerizations of prop-2-enamide were conducted to determine termination rate coefficients at ambient pressure as a function of the degree of monomer conversion. The obtained data are in good agreement with data determined by pulsed-laser induced polymerizations.

Investigations into the binary copolymerization of 1-vinylpyrrolidin-2-one and sodium acrylate revealed a strong incorporation of sodium acrylate into the copolymer, as was measured by nuclear magnetic resonance spectroscopy. Monomer reactivity ratios were determined by means of the Mayo–Lewis equation.

2 Introduction

Synthetic polymers have developed to versatile and common materials within the last decades. This gain in importance was initiated by the invention of the first synthetic, mass-produced polymer Bakelite, which was announced by Baekeland^[1] in 1907, and Staudinger's^[2] fundamental studies into polymerization. Nowadays, polymeric materials can be found in many areas of everyday life. Because of their tunable physical properties, applications range from automotive parts over packaging materials, textiles, and construction materials to components of varnish, adhesives, and cosmetics. The benefit of polymeric materials is reflected in world polymer production, which increased from 1.7 Mt in 1950 to 280 Mt in 2011.^[3] The main products concerning market share are polyethene (29 %), polypropene (19 %), poly(vinyl chloride) (11 %), polystyrene (7.5 %), polyurethane (7 %), and poly(ethylene terephthalate) (6.5 %).^[3] Moreover, polymerization of prop-2-enamide and its substituted derivatives, of acrylic acid as well as of 1-vinylpyrrolidin-2-one, which were studied within this thesis, lead to products for special applications like adhesives, film-forming agents, setting lotions, coatings, emulsifiers, gels for chemical analysis, soft tissue fillers, foam in the automotive and aerospace industry, superabsorbents, stabilizers of beverages or even in cosmetics.^[4–9] Industrial polymers are mainly synthesized via conventional radical polymerization, also by polyaddition, polycondensation, ionic polymerization, and to a minor degree via reversible-deactivation polymerization.

The physical properties of polymeric materials are to a great extent governed by the composition and the microstructure of its macromolecules. Both properties strongly depend on the kinetics of the different reactions occurring during polymerization. Knowledge of the reactions contributing to polymerization and of the associated rate coefficients is essential for modeling and optimizing polymerization processes. They are thus of fundamental academic as well as of industrial interest. Alternatively, polymerization processes may also be optimized by conducting experiments in pilot plants. However, this procedure requires a large number of experiments to vary process variables such as temperature, monomer concentration, initiator concentration, reactor

dimensioning and type, method of the polymerization process (primarily bulk polymerization, emulsion polymerization, precipitation polymerization, solution polymerization, and suspension polymerization), and dimensioning of the cooling system in an adequate range. Since such an approach demands a high amount of material and manpower, the determination of relevant rate coefficients and further universally valid quantities of importance, like viscosities and heat-transfer coefficients, and subsequent modeling is much more cost-effective.

Pulsed-laser polymerization (PLP) techniques have turned out to be a powerful tool to determine the rate coefficients of propagation, k_p , and termination, k_t , as well as to investigate chain-transfer reactions and the corresponding rate coefficients. For the latter purpose, the polymerization is initiated by a single laser pulse (SP) while the radical concentration is monitored by time-resolved electron paramagnetic resonance (EPR) spectroscopy.^[10] This rather novel technique, referred to as SP–PLP–EPR, yields chain-length dependent k_t values and provides insight into chain-transfer reactions. However, studies of highly viscous systems being present, for example, at high polymer content may be expensive due to difficulties in cleaning the EPR tubes. Moreover, precise determination of radical concentrations is hardly feasible because the spectrometer has to be calibrated with a solution that is as similar as possible to the reaction solution. For this purpose, the highly viscous reaction solution, containing stable radicals instead of initiator, has to be filled into the EPR tubes. Because of the absence of initiator, it is not possible to produce the polymer directly inside the tube. Furthermore, investigations into polar systems result in a low signal-to-noise ratio and access to kinetic data of monomers which bear a nitrogen atom connected to the carbon–carbon double bond has turned out to be rather difficult due to band assignment problems.^[11] Volumes of activation, which may provide further insight into the termination mechanism, are so far inaccessible as well since SP–PLP–EPR experiments may only be conducted at ambient pressure. These drawbacks can be overcome by time-resolved near-infrared (NIR) spectroscopy, monitoring the monomer concentration, in combination with initiation by a single laser pulse (SP–PLP–NIR).^[12] Even though this technique does not allow for studies into the kinetics of chain transfer, it is the method of choice to determine k_t as a function of the

degree of monomer-to-polymer conversion. The SP–PLP–NIR technique is recommended by the IUPAC Subcommittee on “Modeling of Polymerization Kinetics and Processes” for deducing k_t .^[13] The primary result is, however, not the pure rate coefficient but the ratio of k_p to k_t , so that k_p values are required. These are accessible via PLP and subsequent analysis of the produced polymer by size-exclusion chromatography (SEC). The PLP–SEC technique has been introduced by Olaj et al. a quarter of a century ago^[14] and has been applied to various monomers in organic solution and in bulk^[15–32]. The implementation of aqueous solution SEC about ten years ago^[33] has offered the possibility to investigate polymerizations in aqueous solution as well^[33–47]. Polymerizations in water being a so-called green solvent are of particular ecologic interest. The results of studies into polymerization kinetics in aqueous solution revealed significant differences compared to the kinetics in organic solution, especially concerning the dependence of k_p on monomer concentration. Thus, investigations of homo- and copolymerizations of a wide range of monomers seem to be worthwhile. Up to date, detailed studies of copolymerization kinetics in aqueous solution are scarce. Available data include monomer reactivity ratios of binary copolymerizations of acrylic acid with 1-vinylpyrrolidin-2-one,^[48] *N*-vinylformamide with 1-vinylpyrrolidin-2-one,^[49] prop-2-enamide with *N*-vinylformamide,^[50] and acrylic acid with prop-2-enamide^[51].

While the above-mentioned methods are based on instationary radical concentrations, rate coefficients may also be determined by stationary methods. Chemically initiated polymerizations, for example, result in the ratio of k_p over the square root of k_t . The experimental data need to be combined with data determined by PLP–SEC or SP–PLP–NIR to deduce absolute rate coefficients. Combining data of chemically initiated polymerizations and SP–PLP–NIR poses problems when the radical chain-length distributions of both experiments differ significantly^[52] or side reactions such as transfer to polymer^[53] occur. Combination of the results of chemically initiated polymerizations and PLP–SEC is therefore more useful.

This work deals with propagation and termination rate coefficients of radical homopolymerizations in aqueous solution. The monomers under investigation are prop-2-enamide, 2-methylprop-2-enamide, *N*,2-dimethylprop-2-enamide, and

N,N-dimethylprop-2-enamide. Furthermore, termination rate coefficients of 1-vinylpyrrolidin-2-one as well as monomer reactivity ratios of the binary copolymerization of 1-vinylpyrrolidin-2-one and sodium acrylate are presented. Activation energies and volumes of activation have been determined to allow for predictions of rate coefficients at various pressures and temperatures.

3 Theoretical Background

3.1 Radical Homopolymerization

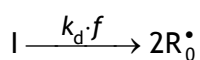
Radical polymerization consists of initiation, propagation, and termination as well as in some cases of chain transfer, chain scission or chain deactivation.^[54] The first three reactions are considered in the so-called “ideal polymerization kinetics” which is based on the following assumptions:^[55]

- All reactions are irreversible.
- All reaction rates are independent of the molar mass of the growing macroradicals.
- Monomer is solely consumed by propagation.
- Termination occurs only by mutual deactivation of two radicals.
- All primary radicals are generated by initiator decomposition and consumed by initiation.

The individual reactions are described below. Chain deactivation is not covered because it is of no significance to this work.

3.1.1 Formation of Primary Radicals and Initiation

Radical polymerization starts with the formation of primary radicals, R_0^\bullet , followed by the addition of these radicals to monomer molecules to initiate chain growth. Primary radicals can be formed chemically (for example by redox initiation), electrochemically (electrochemical initiation), by decomposition of an initiator, I , or in special cases thermally by monomer self-initiation (thermal initiation), like in case of styrene. More specifically, the initiator decomposition can be induced thermally (chemical initiation), or photochemically (photochemical initiation) and can most often be described by the following reaction scheme.^[56]



k_d represents the rate coefficient of the reaction and f the initiator efficiency, which describes the ratio of the number of initiated growing chains to the number of produced primary radicals.^[54] In “ideal polymerization kinetics” the initiator efficiency is assumed to be unity. However, f is usually lower than unity because of the recombination of primary radicals, as in the case of the cage effect, and because of the side-reactions of primary radicals with other species.^[56] At high degrees of monomer-to-polymer conversion and thus low monomer concentration, the viscosity is significantly increased as compared to the one of the initial solution. All chemical reactions with molecularity other than unity are preceded by mutual approach of the reactants by diffusion. Diffusion rate is strongly decreased towards higher viscosity. Thus, chain initiation may become diffusion-controlled, also known as encounter-controlled, at high degrees of monomer-to-polymer conversion. The concomitant increase of the time interval between initiator decomposition and chain initiation favors the probability of the primary radicals undergoing a reaction other than chain initiation.^[57] Experimental evidence for such decrease in initiator efficiency at high degrees of monomer conversion has been obtained from comparison of bulk and emulsion polymerizations of methyl methacrylate (MMA)^[58] as well as by EPR spectroscopy studies into the polymerizations of MMA^[59] and styrene^[60,61].

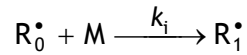
Finally, the rate of formation of primary radicals, which describes the change of the radical concentration, c_R , with time, t , can be expressed by equation 3.1 using the initiator concentration, c_I .

$$\frac{dc_R}{dt} = 2 \cdot k_d \cdot f \cdot c_I \quad (\text{eq. 3.1})$$

Neglecting recombination of primary radicals, the concentration of a thermally decomposing initiator may be described by the following integrated first-order rate law taking the initial initiator concentration, c_i^0 , into account:

$$c_i = c_i^0 \cdot \exp(-k_d \cdot t) \quad (\text{eq. 3.2})$$

The produced primary radicals can react with a monomer molecule, M, to initiate chain growth with the rate coefficient k_i resulting in radicals R_1^\bullet .



In case of a laser-induced photochemical initiation with a laser pulse width of a few nanoseconds or less, the formation of radicals can be regarded as instantaneous in comparison to all other reactions occurring in radical polymerization. The radical concentration when applying the laser pulse at time zero, $c_R(t=0)$, may be determined by means of the quantum yield, Φ , the initiator efficiency, the amount of absorbed photons, n_{abs} , and the irradiated sample volume, V . The quantum yield represents the fraction of photons that leads to initiator decomposition.

$$c_R(t=0) = 2 \cdot \Phi \cdot f \cdot \frac{n_{\text{abs}}}{V} \quad (\text{eq. 3.3})$$

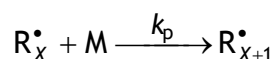
According to the Beer–Lambert–Bouguer law^[62–64], the amount of absorbed photons can be expressed via equation 3.4.

$$n_{\text{abs}} = n_{\text{tot}} \cdot \left(1 - \frac{I(\tilde{\nu})}{I_0(\tilde{\nu})} \right) = \frac{E_p}{E_\lambda \cdot N_A} \cdot (1 - 10^{-\varepsilon(\tilde{\nu}) \cdot c_i \cdot l_{\text{rc}}}) \quad (\text{eq. 3.4})$$

n_{tot} corresponds to the amount of photons entering the sample cell, $I(\tilde{\nu})$ to the light intensity of a certain wavenumber behind the sample cell, $I_0(\tilde{\nu})$ to the light intensity in front of the sample cell, E_p to the energy of a laser pulse, E_λ to the energy of a photon of the laser wavelength λ , N_A to the Avogadro constant, $\varepsilon(\tilde{\nu})$ to the molar decadic absorption coefficient, and l_{tc} to the path length of the sample cell.

3.1.2 Propagation

The term chain propagation describes the reaction of monomer molecules with a radical R_X^\bullet with a degree of polymerization of X resulting in a new radical, R_{X+1}^\bullet , with a degree of polymerization of $X + 1$.



The rate of consumption of monomer is described by:

$$-\frac{dc_M}{dt} = k_p \cdot c_M \cdot c_R \quad (\text{eq. 3.5})$$

with c_M being the monomer concentration.

Dependence of the Propagation Rate Coefficient on Monomer Conversion

As propagation is a bimolecular reaction, it may be subdivided into two consecutive steps. These are a diffusive approach of the reactants followed by the chemical reaction. In case of the diffusive step, the corresponding rate coefficient, k_D , may be described by the Smoluchowski equation:^[65]

$$k_D = 4 \cdot \pi \cdot N_A \cdot (D_S^A + D_S^B) \cdot r_c \quad (\text{eq. 3.6})$$

in which D_S^A and D_S^B are the diffusion coefficients of species A and B, respectively, and r_c is the capture radius. Therefore, the corresponding rate coefficient of the diffusive step of propagation, $k_{p,D}$, is proportional to the sum of the diffusion coefficients of monomer and macroradical.

Assuming negligible ionic interactions, the individual diffusion coefficients, D_S , may be approximated by the Stokes–Einstein relationship:^[66]

$$D_S = \frac{k_B \cdot T}{6 \cdot \pi \cdot r_{h,X} \cdot \eta} \quad (\text{eq. 3.7})$$

with k_B representing the Boltzmann constant, T the thermodynamic temperature, $r_{h,X}$ the hydrodynamic radius of the monomer or the macroradical with a degree of polymerization X , and η the dynamic solution viscosity. Due to the small hydrodynamic radius of the monomer, $k_{p,D}$ is mainly governed by the diffusion coefficient of the monomer. Based on $k_{p,D}$ being diffusion-controlled, the rate coefficient may be expressed by:^[67]

$$k_{p,D} = \frac{k_{p,D}^0}{\eta_r(\alpha)} \quad (\text{eq. 3.8})$$

with $k_{p,D}^0$ representing $k_{p,D}$ at a degree of monomer-to-polymer conversion, α , being equal to zero and $\eta_r(\alpha)$ representing the relative dynamic viscosity of the reaction solution at degree of monomer-to-polymer conversion α (equation 3.10). The degree of monomer-to-polymer conversion is defined by equation 3.9.

$$\alpha = \frac{n_M^0 - n_M}{n_M^0} \quad (\text{eq. 3.9})$$

n_M^0 and n_M represent the amount of monomer at degrees of monomer conversion of zero and of α , respectively. The relative dynamic viscosity may be expressed as:

$$\eta_r(\alpha) = \frac{\eta(\alpha)}{\eta^0} \quad (\text{eq. 3.10})$$

with $\eta(\alpha)$ and η^0 referring to absolute dynamic viscosities.

Because chain propagation is a consecutive reaction, its rate coefficient can be expressed by the following sum:

$$\frac{1}{k_p} = \frac{1}{k_{p,D}} + \frac{1}{k_{p,C}} \quad (\text{eq. 3.11})$$

$k_{p,C}$ is the rate coefficient of the chemical reaction of the propagation.

A significant decrease of k_p due to diffusion control, that is the contribution of $k_{p,D}$ in equation 3.11, is only expected at very high viscosity where the chemical reaction may be faster than the diffusive approach. In bulk polymerization, k_p may thus be assumed to be constant up to degrees of monomer conversion of about 0.8, from where on a pronounced drop of the propagation rate coefficient may set in.^[57] In the last-mentioned case, the mobility of the monomer molecules is reduced, which is known as glass effect. Via EPR spectroscopy, the decrease in k_p has been shown experimentally for styrene and MMA polymerization in non-polar solvents.^[59,68–70] In solution polymerization, not only viscosity of the reaction solution changes but also solvent composition. This is because monomer, which actually is a co-solvent, is continuously converted into polymer. Hence, in systems with pronounced solvent effects, k_p may even change during polymerization at low degrees of monomer conversion. Further details are given in the following paragraph.

Dependence of the Propagation Rate Coefficient on Monomer Concentration

As stated above, propagation may be assumed to be chemically controlled up to high degrees of monomer conversion. Thus, the absolute value of k_p is determined by the partition functions and the Gibbs energies of the reactants and of the activated complex. About a decade ago, the first detailed investigations into the propagation kinetics of polar monomers in polar solvents, especially water, have been conducted. These investigations and further studies carried out within the last years reveal a dependence of k_p on the initial monomer concentration.^[33–38,40–42,45–47,71] The propagation rate coefficients were determined by PLP–SEC. The primary result is the product of monomer concentration and k_p . Generally, it is assumed that overall monomer concentration is identical to the “local” monomer concentration. If overall and “local” monomer concentrations are different, both monomer concentrations will not necessarily be proportional to each other. Therefore, deviations of the change in the product of monomer concentration and k_p from the change in initial monomer content may also be attributed to a difference in overall and “local” monomer concentrations. However, in case of polymerizations in aqueous solution, this assumption requires an enormously large difference. At low monomer concentrations almost all monomer molecules would have to be located in the direct vicinity of macroradicals. As a consequence, the reaction solution consists of a few radicals with associated monomer molecules dissolved in almost pure water.^[41] This is unlikely in case of the investigated systems.

A variation of the activation energy with monomer concentration was also taken into account. In case of a smaller activation energy at low monomer concentration, k_p would decrease towards higher monomer content. Nevertheless, detailed investigations into the propagation kinetics of methacrylic acid (MAA) have shown that the activation energy is more or less insensitive to a variation of the monomer content within a large concentration range.^[41] Calculations of Thickett and Gilbert^[72] demonstrate that the introduction of a water solvent field lowers the activation energy for addition of acrylic acid (AA) to the corresponding monomeric radical by about $10 \text{ kJ}\cdot\text{mol}^{-1}$ relative to the associated gas-phase value. In contrast, the activation energy in a toluene solvent field is not significantly different from the gas-phase value. Since no calculations have been

conducted for the reaction in a monomer solvent field, the work of Thickett and Gilbert does not allow for a statement whether the activation energy changes with monomer concentration.

The variation of k_p may be assigned to a change in the pre-exponential factor,^[42,72] which is composed of the partition functions per volume for the reactants, \tilde{q}_M and \tilde{q}_R , and for the activated complex, \tilde{q}^\ddagger , as reflected in equation 3.12.^[73–75]

$$k_p = \kappa \cdot \frac{k_B \cdot T}{h_p} \cdot \frac{\tilde{q}^\ddagger}{\tilde{q}_M \cdot \tilde{q}_R} \cdot \exp\left(-\frac{E_0}{k_B \cdot T}\right) \quad (\text{eq. 3.12})$$

κ represents the transmission coefficient, h_p the Planck constant, and E_0 the difference of zero-point energies of the reactants and of the transition state.

The pre-exponential factor is essentially determined by the geometry of the rotating groups in the reactants and in the activated complex and by the rotational potentials of the relevant internal motions in the activated complex.^[76] The solvent molecules in the direct vicinity of the activated complex may impose a hindrance to the internal rotational and vibrational motions of the activated complex via intermolecular interactions. The stronger intermolecular interactions of the activated complex with an environment that essentially consists of monomer molecules result in a lower rotational and vibrational mobility and thus lead to a reduced pre-exponential factor towards higher monomer content.^[41,42,72]

In addition to the dependence of the pre-exponential factor on monomer concentration, it cannot be ruled out that the activation energy slightly changes with monomer content.^[45,46]

Chain-Length Dependence of the Propagation Rate Coefficient

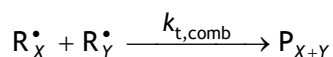
Macroradicals of various chain lengths occur during polymerization because of chain propagation. In literature,^[77–79] experimental evidence for a dependence of k_p on chain length can be found. It is also supported by theoretical approaches which apply the transition state theory on propagation kinetics in conjunction with, for example, *ab initio*

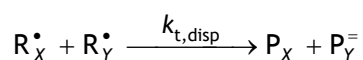
quantum-chemical calculations.^[76] The propagation rate coefficient described so far, consequently is a chain-length-averaged value, correctly denoted by $\langle k_p \rangle$.

Predictions and experiments indicate significantly higher k_p values for small radicals compared to long-chain ones.^[76,77,80–85] Yet, it remains unclear to which extent k_p varies with chain length and up to which degree of polymerization the variation is significant. Recent simulations, however, indicate that even in the case that the chain-length dependence of k_p does not exceed $X \approx 10$, strong macroscopic kinetic effects may be seen for systems with degrees of polymerization of up to at least 100.^[80,81,86–88] This can be understood given that the average k_p is the arithmetic mean of all individual propagation rate coefficients of the degrees of polymerization less or equal to the one of the produced polymer. Moreover, the rate of the first propagation step of a radical exceeds the long-chain limit by about one order of magnitude.^[77,80,81] Despite the chain-length dependence, the propagation rate coefficient will be denoted by k_p in the following because of the high chain length of the polymers produced to determine the rate coefficients presented in this thesis.

3.1.3 Termination

Chain termination is characterized by the reaction of two radicals by which both radical functions are lost. This reaction can occur via combination, which is a formation of a covalent bond between the active centers of propagating radicals, or via disproportionation, which is associated with the transfer of a β -hydrogen atom from one radical to the other resulting in a macromolecule carrying a saturated chain end, P_X , and another one carrying an unsaturated chain end, P_Y^- . In case of combination, the degree of polymerization, $X + Y$, of the resulting macromolecule, P_{X+Y} , is the sum of the degrees of polymerization of the two terminating radicals, whereas disproportionation does not change the degrees of polymerization of the reactants.





The termination rate coefficient is the sum of the rate coefficient of combination, $k_{t,\text{comb}}$, and the rate coefficient of disproportionation, $k_{t,\text{disp}}$. The ratio of combination to disproportionation primarily depends on the structure of the monomer molecule. Combination dominates in case of less sterically demanding monomer molecules, mostly monosubstituted ethene derivatives like styrene.^[89] Termination by disproportionation is preferably found with higher substituted ethene derivatives like MMA.^[89] The individual rate coefficients of the two modes of termination may be determined by analysis of the produced polymer. However, since termination is diffusion-controlled, the contributions of combination and disproportionation to termination are not of concern regarding termination kinetics and are thus not of interest for this work. Only the overall k_t will be discussed in what follows.

The rate of consumption of radicals is described by a second-order rate equation. Although being under discussion to the present,^[90] the equation including a factor of 2, as recommended by the IUPAC,^[52] is used throughout this work.

$$-\frac{dc_R}{dt} = 2 \cdot k_t \cdot c_R^2 \quad (\text{eq. 3.13})$$

Dependence of the Termination Rate Coefficient on Monomer Conversion

As with propagation, bimolecular termination consists of a diffusive approach of the reactants followed by the chemical reaction. Since the chemical reaction of two radicals is fast, termination is considered to be diffusion controlled.^[57,91] The diffusive mobility of the macroradicals may, in addition to pressure and temperature, strongly depend on factors like solvent viscosity, monomer conversion, chain flexibility, dynamics of entanglements, chain length of the terminating macroradicals, and molar mass distribution of the

surrounding polymer matrix. For the sake of comparability, it is therefore necessary to report precisely all reaction conditions chosen for determining k_t data.^[13,52,91,92]

The diffusional step may be described by two parallel mechanisms. On the one hand, the diffusive approaching can occur by two consecutive reactions.^[93,94] In the first step, the macroradicals come into contact by centre-of-mass diffusion, which is also called translational diffusion (TD). Subsequently, the active sites have to come into close proximity by reorientation of the chain segments. This process is called segmental diffusion (SD) and is mainly determined by the dynamics of entanglement and disentanglement of the polymer coils and by the freedom of movement of the growing chain end. On the other hand, the macroradicals can also approach one another by propagation.^[67,95,96] This contribution to k_t is denoted by reaction diffusion (RD) and may become dominant in highly viscous media, where most coils are trapped in a polymer environment.^[67,96,97]

The termination rate coefficient, $k_{t,DM}$, of the primarily described mechanism which is based on diffusion occurring by motion of the macroradical or segments of it, in other words by SD and TD, may be expressed by:

$$\frac{1}{k_{t,DM}} = \frac{1}{k_{t,SD}} + \frac{1}{k_{t,TD}} + \frac{1}{k_{t,C}} \quad (\text{eq. 3.14})$$

with $k_{t,SD}$ denoting the termination rate coefficient based on segmental diffusion, $k_{t,TD}$ denoting the termination rate coefficient based on translational diffusion, and $k_{t,C}$ denoting the rate coefficient of the chemical reaction of termination. $k_{t,TD}$ describes the centre-of-mass diffusion and similar to equation 3.8 it may be written as:

$$k_{t,TD} = \frac{k_{t,TD}^0}{\eta_r(\alpha)} \quad (\text{eq. 3.15})$$

with $k_{t,TD}^0$ representing $k_{t,TD}$ at α being equal to zero. Equation 3.6 may be used for $k_{t,TD}$ as well. However, assuming that only radical pairs with singlet spin multiplicity can terminate, the right-hand side of equation 3.6 may be multiplied with a spin-statistical factor of 0.25.^[98–102] This value is based on the fact that by reaction of two radicals three product triplet states but only one product singlet state are possible. In solution, the radicals may be trapped in a solvent cage before reaction. Therefore, the spin-statistical factor may amount to values up to unity in case the residence time within the solvent cage is sufficient for spin flips to occur.^[102]

The overall termination rate coefficient may be written as:

$$k_t = k_{t,DM} + k_{t,RD} \quad (\text{eq. 3.16})$$

where $k_{t,RD}$ represents the rate coefficient based on reaction diffusion. Since reaction diffusion is based on propagation, $k_{t,RD}$ is proportional to k_p and the actual monomer concentration.^[97]

$$k_{t,RD} = C_{RD} \cdot \frac{C_M}{C_M^0} \cdot k_p = C_{RD} \cdot (1 - \alpha) \cdot k_p \quad (\text{eq. 3.17})$$

Studies into the termination kinetics of ethylene^[103,104] revealed that the reaction-diffusion constant, C_{RD} , might be estimated with the help of the volume-swept-out model which considers the diameter, d , of the macroradical and the jump distance, s .^[95,105]

$$C_{RD} = \pi \cdot d^2 \cdot s \cdot N_A \cdot C_M^0 \quad (\text{eq. 3.18})$$

The jump distance, which describes the displacement of the active site, may be taken from the size of a monomer molecule. The diameter of the macroradical should be looked upon as an effective diameter due to the flexibility of the coil and to the fact that the shape of

the coil usually differs from a perfect sphere.^[67,106] Typically, C_{RD} is independent of temperature but it decreases towards higher pressure.^[97,107]

Under the assumption that $k_{t,C}$ is much higher than $k_{t,SD}$ and $k_{t,TD}$, the combination of equations 3.14, 3.15, 3.16, and 3.17 leads to:

$$k_t = \left(k_{t,SD}^{-1} + \frac{\eta_r(\alpha)}{k_{t,TD}^0} \right)^{-1} + C_{RD} \cdot (1 - \alpha) \cdot k_p \quad (\text{eq. 3.19})$$

In most cases no information about reduced viscosity is available. Nevertheless, as it increases towards higher monomer conversion, it might be expressed by equation 3.20 to a first approximation.^[67]

$$\ln(\eta_r(\alpha)) = C_\eta \cdot \alpha \quad (\text{eq. 3.20})$$

C_η denotes a proportionality factor. Implementation of equations 3.8, 3.11, and 3.20 in equation 3.19 yields:

$$k_t = \left(k_{t,SD}^{-1} + \frac{\exp(C_\eta \cdot \alpha)}{k_{t,TD}^0} \right)^{-1} + \frac{C_{RD} \cdot (1 - \alpha)}{\frac{\exp(C_\eta \cdot \alpha)}{k_{p,D}^0} + \frac{1}{k_{p,C}}} \quad (\text{eq. 3.21})$$

The three modes of diffusion, that is SD, TD, and RD, do not influence the overall k_t to the same extent over the entire range of monomer conversion. Thus, the variation of k_t with monomer conversion may be subdivided into different conversion regimes as indicated in figure 3.1, which shows the variation of k_t with the degree of monomer-to-polymer conversion for MMA bulk polymerization. At low degrees of monomer conversion, k_t remains almost constant indicating that SD is the rate-controlling step and that $k_{t,SD}$ is much lower than $k_{t,TD}$ but significantly larger than $k_{t,RD}$. The increase in

polymer content and the concomitant increase in bulk viscosity do not affect the mobility of the growing chain end at low degree of conversion. However, a further increase in conversion reduces the translational mobility of the macroradical accompanied by a distinct decrease in $k_{t,TD}$. This decrease may lead to TD becoming rate-determining which manifests itself in a pronounced decrease in k_t . The strong decrease of the termination rate in this regime, which results in a steep increase in polymerization rate, is often referred to as gel effect or Trommsdorff–Norrish–Smith effect.^[108,109] At even higher monomer conversion, a second regime of almost constant k_t is obtained because of control by reaction diffusion. The translational diffusion of macroradicals, in contrast to the one of monomer molecules, almost ceases and $k_{t,RD}$ exceeds $k_{t,DM}$. The slight decrease in this regime can be traced back to the reduction in monomer concentration and thus in $k_{t,RD}$.

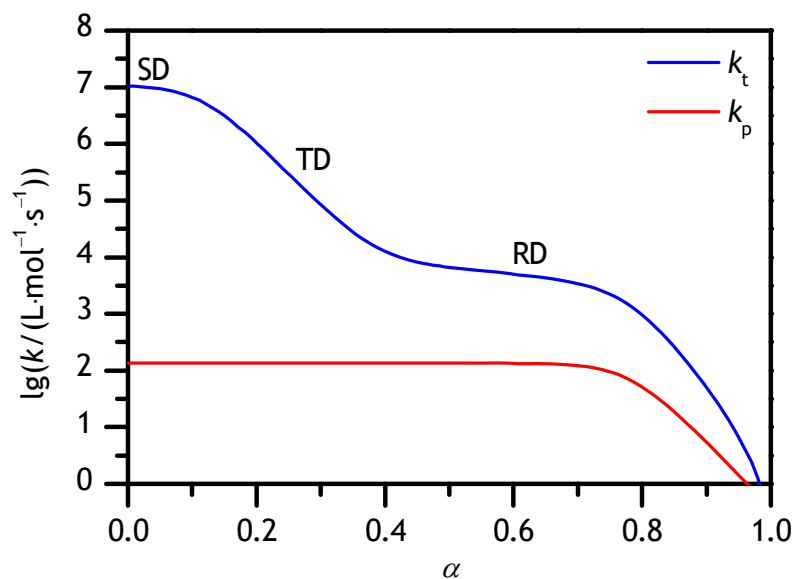


Figure 3.1: Dependence of propagation and termination rate coefficients of MMA at 0 °C and ambient pressure on the degree of monomer-to-polymer conversion according to equations 3.8, 3.11, 3.20, and 3.21 with the parameters taken from the literature.^[67,97]

The much stronger decrease of k_t at very high degrees of monomer conversion is due to k_p becoming diffusion controlled, as can be seen in figure 3.1, as well as to the monomer concentration approaching zero. It should be noted that the onset of the gel and the glass effects as well as the magnitude of the decrease in k_t strongly depend on solute concentration^[110–113] and molar-mass distribution (MMD) of the polymer matrix.

Chain-Length Dependence of the Termination Rate Coefficient

The diffusion-controlled nature of the termination rate coefficient engenders a chain-length dependence of k_t because the chain length has an impact on the mobility of the growing chain end and of the macroradical. In fact, an individual rate coefficient, $k_t(u, v)$, should be assigned to each termination between two radicals of chain length u and v , respectively. The values of u and v are considered to exceed the corresponding degrees of polymerization by one unit since the degree of polymerization disregards the fragment of the initiating species. The difference of one unit assumes that the fragment of the initiating species is identical to a monomer molecule. However, by virtue of the structural and electronic mismatch of this fragment and a monomeric unit, a difference by one can only be regarded as an approximation. The overall termination rate coefficient corresponds to the average over the individual rate coefficients governed by the distribution of radical chain length in the time span under investigation and will be denoted by $\langle k_t \rangle$ in the following.

To describe $k_t(u, v)$ in its dependence on u and v , three simple models are commonly used. The difference between these models, which are the diffusion mean (equation 3.22), the geometric mean (equation 3.23), and the harmonic mean (equation 3.24) model, is the weighting of the impact of the larger and the smaller radical on the rate coefficient.^[57,114–116]

$$k_t(u, v) = \frac{1}{2} \cdot k_t(1, 1) \cdot (u^{-\beta} + v^{-\beta}) \quad (\text{eq. 3.22})$$

$$k_t(u, v) = k_t(1, 1) \cdot (\sqrt{u \cdot v})^{-\beta} \quad (\text{eq. 3.23})$$

$$k_t(u, v) = k_t(1, 1) \cdot \left(\frac{2 \cdot u \cdot v}{u + v} \right)^{-\beta} \quad (\text{eq. 3.24})$$

$k_t(1, 1)$ represents the rate coefficient of termination of two radicals of chain length unity and the power-law exponent β quantifies the extent of the chain-length dependence of k_t . The diffusion mean model, known as Smoluchowski mean model, provides a reasonable description of termination of small radicals and is expected to be suitable if translational diffusion is rate-determining.^[57,116] The geometric mean model has been suggested to describe best termination under segmental diffusion control, whereas the harmonic mean may be used in cases where chain-end encounter upon coil overlap is the rate-determining step.^[57,116] In case of the termination between radicals of identical chain length, equations 3.22, 3.23, and 3.24 reduce to equation 3.25, which can be applied to flash-initiated polymerizations, for example polymerizations initiated by a single laser pulse. As long as chain transfer is negligible, termination in flash-initiated polymerizations occurs between radicals of more or less identical degree of polymerization because the growth of individual radicals in the time after initiation is close to uniform.

$$k_t(u, u) = k_t(1, 1) \cdot u^{-\beta} \quad (\text{eq. 3.25})$$

The drawback of this simple power-law model is that it does not account for changes in the termination mode during propagation. Hence, an increase in chain length may induce a variation in the exponent β . An approach to overcome this problem is the so-called composite model introduced by Smith et al.^[117] This model suggests a rather strong decrease of k_t at small chain lengths and a less pronounced decrease at higher chain lengths. Thus, k_t may be described by two different exponents β_s and β_l for the small-chain-length and the high-chain-length regime, respectively. The transition between both

regimes occurs at the so-called crossover chain length, u_c . In the regime of short chains, equation 3.25 is used with the modification that β is replaced by β_s . The long-chain-length regime is represented by:

$$k_t(u, u) = k_t(1, 1) \cdot u^{-\beta_l} \cdot u_c^{-\beta_s + \beta_l} = k_t^0 \cdot u^{-\beta_l} \quad (\text{eq. 3.26})$$

k_t^0 is the rate coefficient of termination of two hypothetically coiled radicals of chain length unity, whereas $k_t(1, 1)$ represents the actual termination rate coefficient of two non-coiled monomeric radicals as stated above.

3.1.4 Steady-State Kinetics

Under steady-state conditions with respect to the radical concentration, the rates of consumption and of formation of radicals are identical. Equations 3.1 and 3.13 may then be combined to:

$$k_d \cdot f \cdot c_I = \langle k_t \rangle \cdot c_R^2 \quad (\text{eq. 3.27})$$

Solving for c_R and plugging into equation 3.5, the rate of polymerization reads:

$$-\frac{dc_M}{dt} = c_M \cdot \frac{k_p}{\sqrt{\langle k_t \rangle}} \cdot \sqrt{k_d \cdot f \cdot c_I} \quad (\text{eq. 3.28})$$

which is equivalent to:

$$-\frac{d(\ln c_M)}{dt} = \frac{k_p}{\sqrt{\langle k_t \rangle}} \cdot \sqrt{k_d \cdot f \cdot c_I} \quad (\text{eq. 3.29})$$

This equation neglects chain initiation as it proceeds much faster than initiator decomposition, which is thus the rate-determining step. In case of bulk polymerization or solution polymerization in a non-polar solvent, usually all quantities on the right-hand side of equation 3.29 are more or less constant at low degrees of monomer conversion. This results in a linear decrease of the logarithmic monomer concentration with polymerization time.

In case of a conversion-independent sample volume, equation 3.9 may be written as:

$$\alpha = \frac{c_M^0 - c_M}{c_M^0} \quad (\text{eq. 3.30})$$

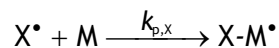
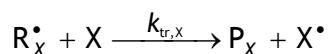
with c_M^0 denoting the initial monomer concentration.

By means of equations 3.28 and 3.30 the increase of the degree of monomer conversion with time may be expressed by:

$$\frac{d\alpha}{dt} = \frac{c_M}{c_M^0} \cdot \frac{k_p}{\sqrt{\langle k_t \rangle}} \cdot \sqrt{k_d \cdot f \cdot c_i} \quad (\text{eq. 3.31})$$

3.1.5 Chain Transfer

In extension of ideal polymerization kinetics, in some cases chain transfer reactions have to be taken into account, in which the radical function of a macroradical is transferred to another molecule, which can be a deliberately added chain-transfer agent, an initiator molecule, a macromolecule, a monomer molecule, a solvent molecule or just another site of the macroradical itself. A transfer, for example, of a hydrogen or a halogen atom occurs simultaneously. The newly formed radical, X^\bullet , can undergo further propagation resulting in the molecule $X-M^\bullet$.



The corresponding rate coefficients of chain transfer to the molecule, X, to which the radical function has been transferred and of the first propagation step of the radical X^\bullet are designated as $k_{tr,X}$ and $k_{p,X}$, respectively. The decrease of the concentration of X, c_X , is described by:

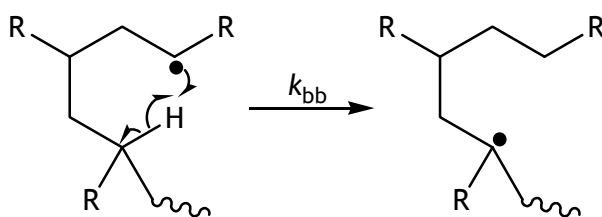
$$-\frac{dc_X}{dt} = k_{tr,X} \cdot c_R \cdot c_X \quad (\text{eq. 3.32})$$

The chain-transfer constant, $C_{tr,X}$, is defined as:

$$C_{tr,X} = \frac{k_{tr,X}}{k_p} \quad (\text{eq. 3.33})$$

Provided that X is a small molecule, chain transfer reduces the average degree of polymerization by introducing additional termination and initiation events.

Chain transfer to polymer may be subdivided into inter- and intramolecular chain transfer, the latter being known as backbiting.^[118] Whereas intermolecular chain transfer usually leads to long-chain branching, the intramolecular reaction normally results in short-chain branches. The latter effect is caused by a transition state incorporating a six-membered ring structure as shown below. The rate coefficient of backbiting is denoted by k_{bb} . Chain transfer to polymer occurs at significant rate only when the propagating radical, with its radical function located at the chain end, is less stable than the newly formed radical. Therefore, chain transfer may influence the constitution of the macromolecules, the degree of polymerization as well as the polymerization rate.



R represents an organic substituent group.

3.1.6 Chain Scission

The degree of polymerization is in some cases reduced by breaking of backbone bonds, which process is named chain scission. Apart from deliberately caused chain scissions, β -scission may occur in all radical polymerizations. It refers to a breaking of a carbon–carbon bond in beta position to the carbon atom bearing the radical function.^[119] If the original radical function is not located at the chain end, the products will be a macroradical with the radical function being located at the chain end and a macromolecule with an unsaturated chain end. If the original radical function is located at the chain end, the products will be a macroradical with the radical function again being located at the chain end and a monomer molecule. This process is called chain depropagation^[54] and is in equilibrium with propagation.

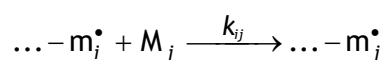
3.1.7 Inhibition and Retardation

Retarders are chemical substances that decrease the rate of polymerization,^[120] whereas inhibitors suppress polymerization.^[54] Inhibitors are usually used to prevent monomers from polymerization during their synthesis and storage. Oxygen is known to retard polymerization.^[121–125] Via the fast combination^[121,122,126] of an oxygen molecule and a macroradical a resonance-stabilized peroxy radical is generated. This radical may add further monomer and oxygen, thus resulting in a binary copolymerization.^[121–124] In case of acrylic acid, for example, the copolymerization proceeds faster than polymerization of the

monomer.^[123] Oxygen is, however, hardly capable of inhibiting polymerization.^[122] Therefore, stabilizers are usually added to monomers. Benzene-1,4-diol is often used as stabilizer although it is neither an inhibitor nor a retarder. However, in the presence of oxygen it is oxidized to cyclohexa-2,5-diene-1,4-dione. The oxygen-centered radicals, formed by reaction of cyclohexa-2,5-diene-1,4-dione and a propagating radical, are much less prone to initiation due to their resonance stabilization. Another common stabilizer is 4-methoxyphenol.^[121–124] After formation of peroxy radicals by reaction of a radical with oxygen, these radicals abstract the hydrogen atom from the hydroxy function of 4-methoxyphenol.^[121–123] The generated radical may undergo addition of another peroxy radical. Thus, one 4-methoxyphenol molecule can trap two oxygen molecules. Direct abstraction of a hydrogen atom from 4-methoxyphenol by a carbon-centered radical occurs only at low rate.^[122]

3.2 Propagation in Binary Copolymerizations

The simplest model describing propagation in binary copolymerizations is the so-called terminal model which considers the influence of the last (terminal) monomeric unit in a macroradical on the propagation rate coefficient and on copolymer composition.^[127,128] The basic kinetic scheme reads:



with i and j being 1 or 2. \mathbf{M}_j denotes the monomer j and k_{ij} the corresponding propagation rate coefficient. $\dots - \dot{\mathbf{m}}_i$ and $\dots - \dot{\mathbf{m}}_j$ represent macroradicals with a terminal monomer unit of type \mathbf{M}_i and \mathbf{M}_j , respectively.

Monomer reactivity ratios, r_{ij} , are defined as the ratio of the rate coefficient of homopropagation, k_{ii} , to the rate coefficient of cross-propagation, k_{ij} . The following equation is valid for i being unequal to j .

$$r_{ij} = \frac{k_{ji}}{k_{ij}} \quad (\text{eq. 3.34})$$

The instantaneous composition of the binary copolymer can be determined by means of the monomer reactivity ratios, r_{12} and r_{21} , and the instantaneous monomer concentrations, c_{M1} and c_{M2} , of the comonomers M_1 and M_2 .

$$\frac{dc_{M1}}{dc_{M2}} = \frac{c_{M1} \cdot (r_{12} \cdot c_{M1} + c_{M2})}{c_{M2} \cdot (c_{M1} + r_{21} \cdot c_{M2})} \quad (\text{eq. 3.35})$$

This equation,^[127–130] known as copolymerization composition equation or Mayo–Lewis equation, is equivalent to:

$$F_1 = \frac{r_{12} \cdot f_1^2 + f_1 \cdot f_2}{r_{12} \cdot f_1^2 + 2f_1 \cdot f_2 + r_{21} \cdot f_2^2} \quad (\text{eq. 3.36})$$

with F_1 being the mole fraction of component 1 in the copolymer, f_1 the mole fraction of component 1 in the monomer mixture, and f_2 the mole fraction of component 2 in the monomer mixture.

The rate of consumption of monomer can be deduced from the overall propagation rate coefficient, $k_{p,copo}$, the overall monomer concentration, c_M , and the radical concentration.

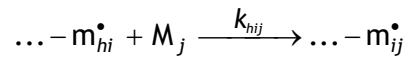
$$-\frac{dc_M}{dt} = k_{p,copo} \cdot c_M \cdot c_R \quad (\text{eq. 3.37})$$

For a binary copolymerization the overall copolymer propagation rate coefficient can be expressed by:^[131]

$$k_{p, \text{copo}} = \frac{r_{12} \cdot f_1^2 + r_{21} \cdot f_2^2 + 2 \cdot f_1 \cdot f_2}{(r_{12} \cdot f_1 / k_{11}) + (r_{21} \cdot f_2 / k_{22})} \quad (\text{eq. 3.38})$$

with k_{11} and k_{22} being the rate coefficients of homopropagation of the monomers M_1 and M_2 , respectively.

However, the overall copolymer propagation rate coefficient cannot be described by the terminal model in most systems.^[132] A few systems have even been found, where copolymer composition cannot be adequately described by the terminal model.^[132–134] In these systems, at least the penultimate monomeric unit of a macroradical has an influence on the propagation kinetics. Therefore, a penultimate-unit effect (PUE) model^[131,135] has been developed, which accounts for the terminal and its preceding monomeric unit. The eight occurring reactions can be summarized to:



with h , i , and j adopting the values 1 or 2. $\dots - \mathbf{m}_{hi}^\bullet$ represents a macroradical with a terminal monomer unit of type M_i and an adjacent, penultimate monomer unit M_h . $\dots - \mathbf{m}_{ij}^\bullet$ represents a macroradical having a terminal monomer unit of type M_j and an adjacent, penultimate monomer unit M_i . k_{hij} is the corresponding propagation rate coefficient.

For i being unequal to j the monomer reactivity ratios, r_{ij} and r_{ji} , in accordance with the PUE model and the chain-end reactivity ratios, s_i , are defined by the following equations.

$$r_{ij} = \frac{k_{iii}}{k_{ijj}} \quad (\text{eq. 3.39})$$

$$r_{ji} = \frac{k_{jii}}{k_{jij}} \quad (\text{eq. 3.40})$$

$$s_i = \frac{k_{jii}}{k_{iii}} \quad (\text{eq. 3.41})$$

k_{iii} , k_{ijj} , k_{jii} , and k_{jjj} represent the propagation rate coefficients corresponding to a propagation step with the types of the penultimate monomer unit, the terminal monomer unit, and the monomer molecule indicated by the first, the second, and the last index, respectively.

Monomer reactivity ratios describe the addition of different monomer molecules to the same radical whereas chain-end reactivity ratios describe the addition of the same monomer molecule to different terminal diads.

In the terminal model the monomer reactivity ratios r_{ij} and r_{ji} reduce to r_{12} for i being 1 and j being 2 and to r_{21} for i being 2 and j being 1, respectively. The chain-end reactivity ratios become unity. The relations between the monomer reactivity ratios and homopropagation rate coefficients, respectively, in accordance with the terminal and the PUE model are given by equations 3.42 and 3.43.^[136,137]

$$r_{ij} = r_{jj} \cdot \frac{r_{ijj} \cdot f_i + f_j}{r_{jjj} \cdot f_i + f_j} \quad (\text{eq. 3.42})$$

$$k_{ii} = k_{iii} \cdot \frac{r_{ijj} \cdot f_i + f_j}{r_{ijj} \cdot f_i + f_j / s_i} \quad (\text{eq. 3.43})$$

f_i and f_j represent the mole fractions of component i and j in the monomer mixture, respectively.

The overall copolymerization propagation rate coefficient and copolymer composition according to the PUE model can be calculated by inserting equations 3.42 and 3.43 in equations 3.36 and 3.38.

Contrary to this so-called explicit PUE model, an implicit PUE model was suggested to describe systems, where copolymer composition, unlike the overall copolymerization

propagation rate coefficient, can be described by the terminal model.^[131,132,138] The implicit PUE model, which adequately describes the kinetics in most binary copolymerizations, correlates with the explicit PUE model under the following restrictions (with i being unequal to j):^[138]

$$r_{ijj} = r_{jij} = r_{ij} \quad (\text{eq. 3.44})$$

Thus, the monomer reactivity ratios of the implicit PUE model are equal to the ones of the terminal model, whereas the chain-end reactivity ratios are not equal to unity. As a result, effects of the penultimate unit on the selectivity of the macroradical are neglected in contrast to effects on reactivity.

3.3 Pressure and Temperature Effects on Rate Coefficients

Pressure Dependence

Rate coefficients may be expressed according to the transition-state theory^[120,139] via:

$$k_x = \kappa \cdot \frac{k_B \cdot T}{h_p} \cdot \exp\left(-\frac{\Delta^\ddagger G^\circ}{R \cdot T}\right) \quad (\text{eq. 3.45})$$

with $\Delta^\ddagger G^\circ$ representing the standard Gibbs energy of activation.

k_x in equation 3.45 is a first-order rate coefficient. Rate coefficients for reactions of order e can be derived by multiplication with the standard concentration to the power of $(e - 1)$.^[140]

Based on the fundamental equation for the Gibbs energy,^[141] the following equation of state may be derived:

$$\left(\frac{\partial \Delta^\ddagger G^\circ}{\partial p} \right)_T = \Delta^\ddagger V^\circ \quad (\text{eq. 3.46})$$

with $\Delta^\ddagger V^\circ$ denoting the volume of activation which may be regarded as the difference of partial molar volumes of the transition state and of the reactants. p is the pressure.

Under the assumption of the transmission coefficient κ being pressure-independent, the volume of activation may be determined by combining equations 3.45 and 3.46.

$$\Delta^\ddagger V^\circ = -R \cdot T \cdot \left(\frac{\partial \ln k_x}{\partial p} \right)_T - R \cdot T \cdot (e - 1) \cdot \kappa_T \quad (\text{eq. 3.47})$$

κ_T denotes the isothermal compressibility.

The assumption made is justifiable since even the error caused by assuming the coefficient κ to be unity is negligible for many reactions.^[139] Depending on the system under investigation, the second term on the right-hand side of equation 3.47 may vary between 1 and 5 cm³·mol⁻¹ for second-order reactions at 25 °C (1.1 cm³·mol⁻¹ for water).^[142–145] This term is assigned to the loss of translational degrees of freedom.^[146] At low isothermal compressibility or in case of first-order reactions equation 3.47 may be converted to equation 3.48.

$$\Delta^\ddagger V^\circ = -R \cdot T \cdot \left(\frac{\partial \ln k_x}{\partial p} \right)_T \quad (\text{eq. 3.48})$$

The volume of activation may be considered to be a sum of an intrinsic and a solvation part. The intrinsic part represents changes in bond length as well as in bond angles. It should be negative for bond-forming reactions and positive in case of bond cleavage. The solvation part of the volume of activation represents effects due to changes in the intermolecular interactions of the surrounding solvent molecules. The intrinsic

contribution, which characterizes the reaction mechanism, may be smaller than the solvation part in case of reactions with large polarity changes.^[144]

In reactions where diffusion contributes to the rate coefficient, a third term has to be considered which takes diffusional aspects into account. This contribution to the volume of activation is always positive^[147] and is considered to be closely related to the molar volume of the solvent^[143].

Temperature Dependence

Several equations have been developed to describe the temperature dependence of rate coefficients. Reviews of such equations can be found in the literature.^[148,149] The temperature dependence of rate coefficients, k_x , may in most cases be described by the Arrhenius equation which was derived by van't Hoff^[150] and Arrhenius^[151] based on thermodynamic theory:

$$k_x = A \cdot \exp\left(-\frac{E_A}{R \cdot T}\right) \quad (\text{eq. 3.49})$$

A represents the Arrhenius pre-exponential factor, E_A the Arrhenius activation energy and R the gas constant. A and E_A are often treated as temperature-independent quantities.

Assuming that the rate coefficient of a diffusion-controlled reaction is inversely proportional to solution viscosity, as implied by combining equations 3.6 and 3.7, the activation energy of the rate coefficient may conform to the activation energy of the viscosity. The latter may be closely related to the internal energy of vaporization of the solvent (approximately one fourth to one third of the internal energy of vaporization).^[152–155] In solutions where hydrogen bonds are present the activation energy decreases towards higher temperature due to the reduced strength of the hydrogen bonds.^[156]

An equation taking the dependence of k_x on both variables, pressure and temperature, into account may be derived by combining equations 3.48 and 3.49. For reasons of consistency, another pre-exponential factor, A' , is used.

$$k_x = A' \cdot \exp\left(-\frac{E_A + \Delta^\ddagger V^\circ \cdot p}{R \cdot T}\right) \quad (\text{eq. 3.50})$$

The numerator in equation 3.50 has already been described by Glasstone et al.^[157] and interpreted as pressure dependence of the activation energy. For most reactions at ambient pressure, the product of volume of activation and pressure is much lower than the activation energy and may thus be neglected which converts equation 3.50 into the Arrhenius equation.

3.4 Size-Exclusion Chromatography

Size-exclusion chromatography (SEC) is a technique to separate molecules mainly according to their hydrodynamic volumes.^[158] In case of the stationary phase being a swollen gel, the term gel-permeation chromatography may be used.^[158] This situation applies to the SEC setups used within the present work. The term size-exclusion chromatography will be used in the following. In SEC a dilute polymer solution is passed through a column that contains a porous material. Most often this material is based on crosslinked polystyrene or crosslinked polyacrylamides for organic or aqueous eluents, respectively.^[159] Separation is based on the diffusion of polymer coils into the pores of the stationary phase. Low-molar-mass material, forming coils of small hydrodynamic volume, will spend more time in the column than macromolecules of higher molar mass as more pores are accessible.^[159] Low-molar-mass material passes thus more slowly through the column. After separation, the relative concentration of the eluted chains can be detected by measuring changes in, for example, absorption of UV light or refractive index (RI). Retention times strongly depend on experimental conditions (polymer type, column

packing, eluent). For concentration-sensitive detectors a calibration curve is required which correlates elution volume with molar mass. The calibration curve may be constructed using polymeric standard samples of known narrow molar-mass distribution. Since SEC separates by size and not by molar mass, the calibration is referred to as “relative”. Calibration standards are only available for a limited number of polymers. Without such standards, molar-mass distributions may be estimated via the principle of universal calibration^[160] as the retention volume only depends on a size parameter of the molecules. Usually the product of intrinsic viscosity, $[\eta]$, and molar mass, M , is used as size parameter. The hydrodynamic volume, V_h , of a macromolecule in solution may be described by:^[161]

$$V_h = \frac{[\eta] \cdot M}{2.5 \cdot N_A} \quad (\text{eq. 3.51})$$

with N_A representing the Avogadro constant.

After calibrating the SEC setup with a standard, the MMD of the polymer sample is calculated using the Kuhn–Mark–Houwink–Sakurada equation (equation 3.52) which describes the correlation of intrinsic viscosity and relative molecular mass, M_r .^[162–166]

$$[\eta] = K \cdot M_r^a \quad (\text{eq. 3.52})$$

Two sets of Kuhn–Mark–Houwink–Sakurada parameters, K and a , are required for this transformation, one for the polymer used for calibration and one for the polymer under investigation. The combination of equations 3.51 and 3.52 leads to the desired relation:

$$\lg M_{r,p} = \frac{1}{1+a_p} \cdot \lg \frac{K_{st}}{K_p} + \frac{1+a_{st}}{1+a_p} \cdot \lg M_{r,st} \quad (\text{eq. 3.53})$$

with subscript P denoting the polymer under investigation and St the polymer used as calibration standard.

If Kuhn–Mark–Houwink–Sakurada parameters are not available, direct MMD determination can be performed by using an SEC system with multiple detectors, most commonly refractive index measurements in combination with on-line viscometry^[167] or on-line light scattering^[168]. Such a setup yields absolute polymer molar masses.

3.5 PLP–SEC Technique

PLP–SEC is a powerful technique for determination of propagation rate coefficients. A solution containing monomer, photoinitiator, and, optionally, solvent is irradiated by a sequence of short laser pulses, which are applied at a constant laser-pulse repetition rate (LPRR), ν_{LPRR} , and thus at a constant time interval, t_0 . Each laser pulse generates almost instantaneously primary radicals which initiate chain growth. Due to the high radical concentration being produced by each pulse, significant termination of growing radicals with primary radicals occurs right after their formation by one of the subsequent laser pulses.^[14,169,170] Preferential termination after integer multiples of t_0 results in maxima of a multimodal molar-mass distribution. Concerning ideal polymerization kinetics, variations in chain length of produced macromolecules may originate from propagation being a statistical process^[14,52,171–173] and from bimolecular termination of two grown radicals. Additionally, SEC, which is used for polymer analysis, is subject to axial dispersion.^[170,172,173] These features usually lead to asymmetrical broadening of the MMD. Thereby, the maxima of the obtained MMD are shifted in molar mass compared to the positions expected from theory. The degree of polymerization, X_b , of macroradicals, which are terminated by a primary radical right after application of a laser pulse, is usually best identified with the point of inflection (POI) featuring a maximum in the first derivative of the logarithmic MMD.^[14,52,172,174] X_b can be expressed by equation 3.54.

$$X_b = b \cdot k_p \cdot c_M \cdot t_0 = b \cdot k_p \cdot c_M \cdot \frac{1}{\nu_{\text{LPRR}}} \quad (\text{eq. 3.54})$$

b represents the number of the corresponding maximum in the first derivative of the MMD in case the first of these maxima on the low-molar-mass side of the MMD is denoted by unity. The reliability of the determined rate coefficients can be verified by consistency criteria.^[174,175] These require the existence of at least two POIs conforming to X_1 and X_2 as well as the independence of k_p on initiator concentration, LPRR, and laser pulse energy. Chain transfer and side reactions may result in a violation of the consistency criteria or even in a loss of a simple multimodality of the first derivative of the MMD due to increased broadening. Polymer production in PLP–SEC experiments requires an almost constant monomer concentration and therefore a low degree of monomer conversion. A change in monomer concentration and hence in chain length would result in a loss of a simple multimodality of the first derivative of the MMD because of the superposition of several MMDs each corresponding to a single monomer concentration.

3.6 Fourier-Transform Near-Infrared Spectroscopy

The Fourier-transform near-infrared (FT–NIR) spectroscopy is a powerful technique to determine a near-infrared spectrum of a chemical substance. First, a scanning interferometer splits a beam of light into at least two components and then recombines these with a variable phase difference.^[176] The most common interferometer is a continuous-wave Michelson interferometer.^[177] After determination of the temporal coherence of the resulting beam, the raw data in the time domain are converted into frequency-domain data by Fourier-transformation (FT). The time-domain signal is called interferogram.

For experimental reasons the phase difference is finite. Therefore, the interferogram comes to an abrupt ending. To reduce resulting sidelobes of the original spectral line, the interferogram is multiplied by a window function before carrying out the FT. This process is called apodization.^[177,178]

By zero filling, the interferogram is extended with zeros. Due to the artificial increase in data points, the number of points of the spectrum is increased by the same factor yielding a higher digital resolution.

Because of experimental errors, the interferogram is usually not mirror-symmetrical about the point where the phase difference equals zero. As a result, FT generates a complex spectrum and a phase correction is required. Using the Mertz method, the complex spectrum in its exponential notation is multiplied by the inverse of the phase exponential and taking the real part.^[177,179]

The final absorption spectrum is obtained by division of the sample spectrum by a background spectrum.

3.7 SP–PLP–NIR Technique

In SP–PLP–NIR experiments, polymerization is initiated by a single laser pulse. The induced decrease of monomer concentration is monitored via on-line NIR spectroscopy with a time resolution less than a microsecond. The radical concentration, $c_R(t)$, at time t after applying the laser pulse, can be derived by integration of equation 3.13 and reads:

$$c_R(t) = \left(2 \cdot \langle k_t \rangle \cdot t + \frac{1}{c_R(t=0)} \right)^{-1} \quad (\text{eq. 3.55})$$

$c_R(t=0)$ denotes the radical concentration when applying the laser pulse.

As the macroradical chain length varies with time after application of the laser pulse, the resulting rate coefficient should be referred to as $\langle k_t \rangle$. Plugging of equation 3.55 in equation 3.5 and subsequent integration results in equation 3.56 which describes the ratio of the monomer concentration, $c_M(t)$, at time t after application of the laser pulse to the monomer concentration, $c_M(t=0)$, when applying the laser pulse.

$$\frac{c_M(t)}{c_M(t=0)} = (2 \cdot \langle k_t \rangle \cdot c_R(t=0) \cdot t + 1)^{-k_p / 2 \cdot \langle k_t \rangle} \quad (\text{eq. 3.56})$$

Fitting of equation 3.56 to the data provides access to the product of $\langle k_t \rangle$ and initial radical concentration as well as to the ratio of k_p to $\langle k_t \rangle$. The radical concentration is not accessible by SP–PLP–NIR experiments. Therefore, k_p needs to be known for determination of the termination rate coefficient. Conducting several successive SP–PLP–NIR experiments may yield the dependence of $\langle k_t \rangle$ on degree of monomer conversion.

3.8 Viscometry

Viscosities of liquids are most often measured with capillary viscometers of the Ostwald, Cannon–Fenske, or Ubbelohde type.^[180] These instruments exhibit a capillary of inside radius r_{cap} and length l_{cap} . The time needed for a solution of volume V_{sol} and density ρ_{sol} to pass between two marks in the viscometer under hydrostatic pressure is determined to calculate the dynamic viscosity by means of the Hagen–Poiseuille law^[181–185] given in equation 3.57. This law assumes a laminar viscous flow.

$$\eta = \frac{\pi \cdot r_{\text{cap}}^4 \cdot \rho_{\text{sol}} \cdot g \cdot h_{\text{cap}} \cdot t}{8 \cdot l_{\text{cap}} \cdot V_{\text{sol}}} \quad (\text{eq. 3.57})$$

g denotes the acceleration of free fall. h_{cap} represents the distance of the two marks of the viscometer.

To correct for the formation of eddies and the loss of part of the potential energy by friction, the right-hand side of equation 3.57 is lowered by the Hagenbach–Couette correction term, resulting in equation 3.58.^[180]

$$\eta = \frac{\pi \cdot r_{\text{cap}}^4 \cdot \rho_{\text{sol}} \cdot g \cdot h_{\text{cap}} \cdot t}{8 \cdot l_{\text{cap}} \cdot V_{\text{sol}}} - \frac{k_{\text{HC}} \cdot V_{\text{sol}}}{8 \cdot \pi \cdot l_{\text{cap}} \cdot t} \quad (\text{eq. 3.58})$$

k_{HC} is an empirical constant.

3.9 Oscillating U-Tube

The oscillating U-tube^[186] is a common technique used to determine the density of solutions. The liquid is filled into a U-shaped glass tube, which is electronically excited into undamped oscillation. The natural frequency, f_n , which is determined electromagnetically, depends on the mass and thus on the density, ρ_{Osc} , of the oscillator. The densities of two substances 1 and 2 are related via equation 3.59.

$$\rho_{\text{Osc},1} - \rho_{\text{Osc},2} = k_{\text{Osc}} \cdot (f_{n,1}^{-2} - f_{n,2}^{-2}) \quad (\text{eq. 3.59})$$

The instrument constant, k_{Osc} , can be determined by means of two substances of known density.

3.10 Nuclear Magnetic Resonance Spectroscopy

A common method to identify chemical substances in inorganic and especially in organic chemistry is the nuclear magnetic resonance (NMR) spectroscopy. In the presence of a magnetic field, atomic nuclei with nuclear spin may absorb electromagnetic radiation due to a splitting of their spin energy levels. The resonance frequency is different for each isotope but depends on the magnetic and thus the chemical environment as well. Nowadays the magnetic field strength is kept constant while a short radio-wave pulse is applied to the sample. This external magnetic field causes a precession of the spins around an axis parallel to the external magnetic field, which is hereafter referred to as main axis. The frequency of this precession is the resonance frequency. In combination with the splitting of the spin energy levels, a net macroscopic magnetization is generated. The radio-wave pulse, which is applied at right angles to the external magnetic field, causes the

spins to precess around the magnetic field vector of the radio-wave pulse as well. Therefore, the orientation of the net macroscopic magnetization is changed. After application of the pulse, this orientation should return exponentially with time to the original one being parallel to the main axis. In view of the fact that the spins still precess around this axis, the vector of the net macroscopic magnetization spirals back around it. An induction coil, being installed at right angles to the main axis, determines the net macroscopic magnetization. The detected signal resembles a superposition of exponentially decaying sine waves of the individual nuclei. This signal is called free induction decay (FID). As well as in case of FT-NIR spectroscopy, the FID, representing data in the time domain, is converted into frequency-domain data by FT. Similar to the data processing described in chapter 3.6, apodization, zero filling, and phase correction are applied to the data in NMR spectroscopy. Generally the abscissa in an NMR spectrum shows the chemical shift, δ . Therefore, the frequency-domain spectrum has to be converted via:^[187]

$$\delta = \frac{\nu_n - \nu_{\text{ref}}}{\nu_{\text{ref}}} \quad (\text{eq. 3.60})$$

with ν_n being the resonance frequency of the nucleus under investigation and ν_{ref} being the resonance frequency of a standard. For ^1H NMR in trichloro(^2H)methane the reference signal is usually that of tetramethylsilane.^[187]

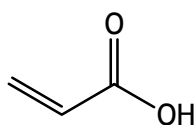
4 Materials and Equipment

4.1 Chemical Substances

4.1.1 Monomers

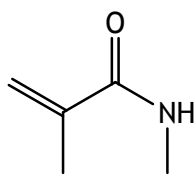
Monomers may come into contact with ground glass joints during purification and storage. To reduce impurities, PTFE rings (Dr. Dietmar Glindemann, GLINDEMANN® PTFE sealing rings for ground taper (conical) joints) instead of grease were used to seal ground glass joints and PTFE stopcocks were used for column chromatography. The chemical substances were stored at ambient temperature where not otherwise indicated.

Acrylic Acid



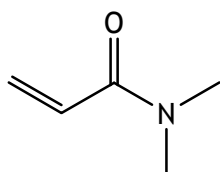
Acrylic acid (AA, Fluka, purum, $\geq 99\%$, anhydrous, stabilized with 0.02 % 4-methoxyphenol, CASRN: 79-10-7, $M = 72.06 \text{ g}\cdot\text{mol}^{-1}$) was used as received.

N,2-Dimethylprop-2-enamide



N,2-Dimethylprop-2-enamide (M-MPAm, *N*-methylmethacrylamide, ABCR, 95 %, stabilized with 100 ppm 4-methoxyphenol, CASRN: 3887-02-3, $M = 99.13 \text{ g}\cdot\text{mol}^{-1}$) was used without further purification and stored at 4 °C.

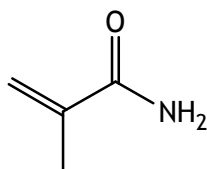
N,N-Dimethylprop-2-enamide



N,N-Dimethylprop-2-enamide (DM-PAm, *N,N*-dimethylacrylamide, Aldrich, 99 %, stabilized with 500 ppm 4-methoxyphenol, CASRN: 2680-03-7, $M = 99.13 \text{ g}\cdot\text{mol}^{-1}$) was used as received or passed through a column containing inhibitor remover

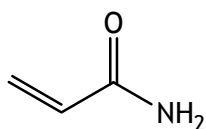
(chapter 4.2) where remarked. Purified monomer was stored at $-21\text{ }^{\circ}\text{C}$.

2-Methylprop-2-enamide



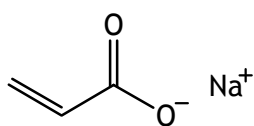
2-Methylprop-2-enamide (MPAm, methacrylamide, Fluka, purum, $\geq 98\%$, stabilized, CASRN: 79-39-0, $M = 85.11\text{ g}\cdot\text{mol}^{-1}$) was used as received or recrystallized from methanol where remarked. Purified monomer was stored at $-21\text{ }^{\circ}\text{C}$.

Prop-2-enamide



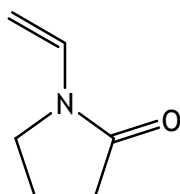
Prop-2-enamide (PAm, acrylamide, Fluka, purum, $\geq 98.0\%$, stabilized with Cu^{2+} ,^[188] CASRN: 79-06-1, $M = 71.08\text{ g}\cdot\text{mol}^{-1}$) was used without further purification or recrystallized from acetone where remarked. Purified monomer was stored at $-21\text{ }^{\circ}\text{C}$.

Sodium Acrylate



Sodium acrylate (NaA, Aldrich, purum, 97% , stabilized with 140 ppm 4-methoxyphenol,^[188] CASRN: 7446-81-3, $M = 94.04\text{ g}\cdot\text{mol}^{-1}$) was used as received.

1-Vinylpyrrolidin-2-one



1-Vinylpyrrolidin-2-one (VP, Fluka, purum, $\geq 97.0\%$, stabilized with 0.001% N,N' -di(butan-2-yl)-benzene-1,4-diamine, CASRN: 88-12-0, $M = 111.14\text{ g}\cdot\text{mol}^{-1}$) was purified by distillation under reduced pressure. Purified monomer was stored at $-21\text{ }^{\circ}\text{C}$.

4.1.2 Solvents

Demineralized Water

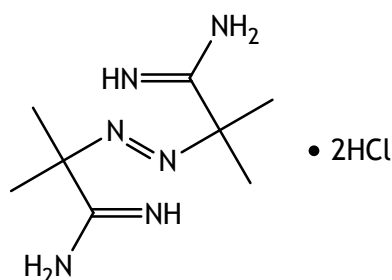
Demineralized water (CASRN: 7732-18-5, $M = 18.02 \text{ g}\cdot\text{mol}^{-1}$) was taken from an internal cycle.

Dideuterium Oxide

Dideuterium oxide (Aldrich or Deutero, 99.9 %, CASRN: 7789-20-0, $M = 20.03 \text{ g}\cdot\text{mol}^{-1}$) was used without further purification.

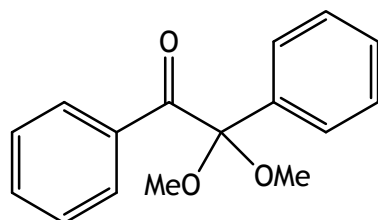
4.1.3 Initiators

2-[(*E*)-2-(1-carbamimidoyl-1-methylethyl)diazen-1-yl]-2-methylpropanimidamide dihydrochloride

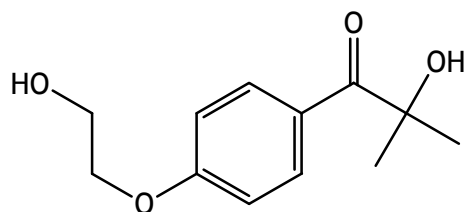


2-[(*E*)-2-(1-carbamimidoyl-1-methylethyl)diazen-1-yl]-2-methylpropanimidamide dihydrochloride (V-50, Aldrich, 97 %, CASRN: 2997-92-4, $M = 271.20 \text{ g}\cdot\text{mol}^{-1}$) was used as received.

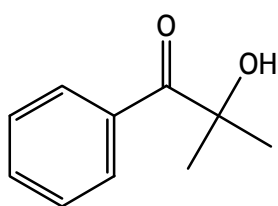
2,2-Dimethoxy-1,2-diphenylethan-1-one



2,2-Dimethoxy-1,2-diphenylethan-1-one (DMPA, 2,2-dimethoxy-2-phenylacetophenone, Aldrich, 99 %, CASRN: 24650-42-8, $M = 256.30 \text{ g}\cdot\text{mol}^{-1}$) was used without further purification.

2-Hydroxy-1-[4-(2-hydroxyethoxy)phenyl]-2-methylpropan-1-one

2-Hydroxy-1-[4-(2-hydroxyethoxy)phenyl]-2-methylpropan-1-one (HHMP, Aldrich, 98 %, CASRN: 106797-53-9, $M = 224.25 \text{ g}\cdot\text{mol}^{-1}$) was used as received and stored at 4 °C.

2-Hydroxy-2-methyl-1-phenylpropan-1-one

2-Hydroxy-2-methyl-1-phenylpropan-1-one (Darcucur 1173, Aldrich, 97 %, CASRN: 7473-98-5, $M = 164.20 \text{ g}\cdot\text{mol}^{-1}$) was used without further purification.

4.1.4 Further Chemical Substances**Acetone**

Acetone (Carl Roth, ROTIPURAN®, p.a., $\geq 99.8 \%$, CASRN: 67-64-1) was used without further purification.

Argon

Argon ($\geq 99.999 \%$, CASRN: 7440-37-1) was used as received.

Benzene-1,4-diol

Benzene-1,4-diol (Fluka, puriss., p.a., $\geq 99 \%$, CASRN: 123-31-9) was used without further purification.

Heptane

Heptane (Carl Roth, for synthesis, $\geq 99\%$, CASRN: 142-82-5) was used as received.

Methanol

Methanol (Sigma-Aldrich, puriss., p.a., $\geq 99.8\%$, CASRN: 67-56-1) was used without further purification.

Nitrogen

Nitrogen ($\geq 99.999\%$, CASRN: 7727-37-9) was used as received.

4.2 Purificants

Dialysis Tubing

The prewetted dialysis tubing Spectra/Por[®] 6 (Spectrum Laboratories, Inc., standard grade, regenerated cellulose, flat width of 18 mm, 11.5 mm in diameter) with an *MWCO* of 2 kDa was used for removing small molecules and ions from polymer solutions. The membrane was stored at 4 °C in an aqueous solution of 0.1 % sodium azide. Spectra/Por[®] closures (Spectrum Laboratories, Inc., polypropylene, sealing width of 12 or 23 mm) were used to seal the tubing.

Inhibitor Remover

Inhibitor remover (Aldrich, “replacement packing for removing hydroquinone and monomethyl ether hydroquinone”) was used to free monomer from 4-methoxyphenol.

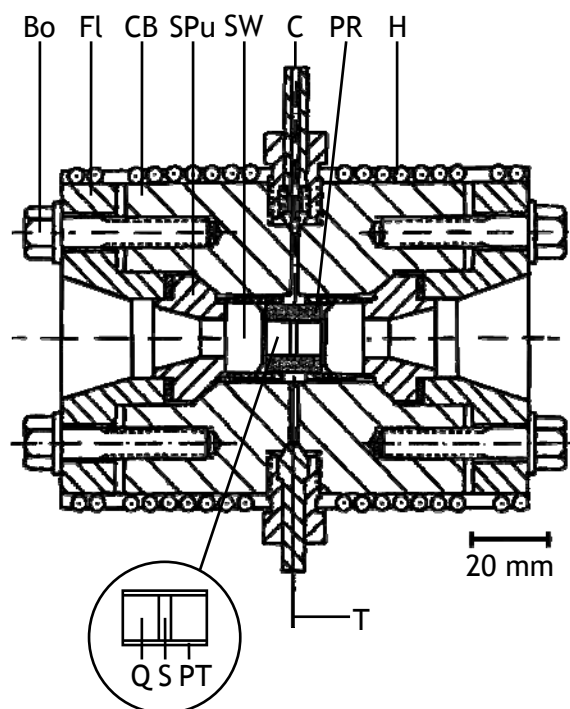
4.3 Cuvettes

Cuvettes were used for measurements at ambient pressure. PLP–SEC experiments were conducted with cylindrical cuvettes (Starna, 65.14/Q/10, Spectrosil® fused quartz, transmission of at least 0.8 for 190–2700 nm, path length of 10 mm). These cells exhibit a separate chamber surrounding the sample compartment through which a heat-transfer fluid can be circulated. For chemically initiated polymerizations either these cylindrical cuvettes or cuboidal cuvettes (Starna, 21/MS/Q/10, Spectrosil® fused quartz, transmission of at least 0.8 for 190–2700 nm, path length of 10 mm) were used. The sample contained in the latter cuvettes was stirred by means of a magnetic stir bar (6 mm long, 3 mm in diameter, PTFE coated) and a magnetic stirrer (Thermo Scientific, Variomag™ Magnetic Stirrer MINI 07 with control unit TELEMODUL, 130–1000 rpm). Both cuvette types were closed with PTFE stoppers.

4.4 Optical High-Pressure Cell

The optical high-pressure cell^[189] used for pulsed-laser induced polymerizations under high pressure is illustrated in scheme 4.1. The cell is designed for pressures up to 3000 bar and temperatures up to 300 °C. The cylindrical cell body (CB) is made of a nickel-base alloy (Arbed Saerstahl, material no. 2.4668, RGT 601). The length of the cell body is 100 mm and the outer and inner diameters are 80 and 22 mm, respectively. The material exhibits a high ultimate tensile strength of $> 1 \text{ kN}\cdot\text{mm}^{-2}$ up to 500 °C, which ensures stability at the above-defined reaction conditions including a safety factor of 2.5. The cell is sealed at each end by a conical sealing punch (SPu) (Arbed Saerstahl, material no. 2.4969, RGT 12). Because of RGT 12 being softer than RGT 601, attrition is limited to the sealing punches. Each punch is pressed into the cell cone by a flange (Fl) (Arbed Saerstahl, material no. 2.4668, RGT 601) which is fixed by six high-pressure bolts (Bo) (material no. 2.4969, RGT 12). These bolts have to be evenly tightened to 30 N·m. The punches exhibit an opening angle of 75° which is lower than the one of the cell cone with 78°. The cell is sealed due to the compression of the surface of the punches and the inner edge of the cell

body. The optical path length may be varied from 0.1 mm up to 20 mm by using punches of different length. The central drilled hole of the punches offers 10 mm in diameter for light to pass the sample chamber.



Scheme 4.1: Full section view of the optical high-pressure cell consisting of bolts (Bo), flanges (Fl), a cell body (CB), sealing punches (SPu), sapphire windows (SW), a high-pressure capillary (C), a positioning ring (PR), a heating jacket (H), and a sheathed thermocouple (T). The enlargement depicts the full section view of the optical internal cell composed of quartz windows (Q), the sample (S), and a PTFE tube (PT).

The high-pressure optical windows (SW) used in this work were made from synthetic sapphire single crystals (Roditi/Union Carbide, 18 mm in diameter, 10 mm in height, UV-grade, polished surfaces normal to the optical axis) produced by the Czochralski process. This material offers high transparency in the wavenumber range from 2000 to 50000 cm^{-1} (200 to 5000 nm). Each high-pressure window is fitted against the polished (micron diamond, grit size of 4 to 8 μm) surface of a punch and held in place by a stainless steel

screwcap. To compensate for surface area irregularities, an about 12 μm thick PTFE film (Huth Industry) is placed between the polished surfaces of the window and the punch. This setup is self-sealing under pressure according to the principle described by Poulter.^[190] Four internal screw threads perpendicular to the cylindrical axis allow for connecting high-pressure capillaries (C) (Autoclave Engineers, inside diameter of 1/16 in, outside diameter of 1/4 in) and a sheathed thermocouple (T) (CGE Alsthom, chromel–alumel, CIA S250). Unused screw threads are closed by a filler plug. The cell is heated by an insulated electric resistance heater (Les Cables de Lyon, Pyrolon-M16, $16\ \Omega\cdot\text{m}^{-1}$) which is imbedded into a two-part brazen heating jacket (H). The heating jacket is pulled over the cell.

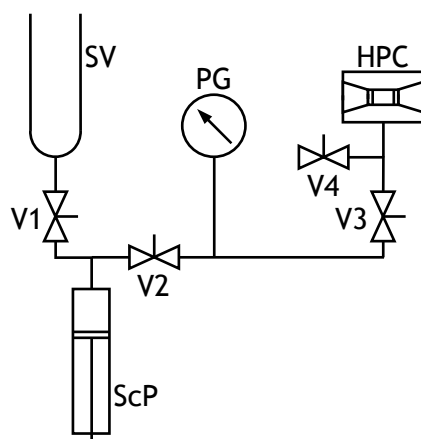
To avoid conceivable catalytic effects of the inside cell wall on the reactions, an internal cell (see below) containing the actual sample was placed inside the high-pressure cell. The internal cell was fixed in place by a PTFE positioning ring (PR). The usage of an internal cell also renders the cleaning of the high-pressure cell unnecessary and simplifies purging the sample with inert gas.

Optical Internal Cell

The internal cell depicted as enlargement in scheme 4.1 consists of a PTFE tube (PT) (inside diameter of 9.00 mm, outside diameter of 10.00 mm) into which an optical quartz window (Q) (Heraeus Quarzglas, INFRASIL® 301, 10.0 mm in diameter, thickness of 5.0 mm, polished surfaces normal to the optical axis) is inserted from each side. The lateral surfaces of the windows were polished with a diamond compound (Joke Technology, Hyprez® S, grit size of 6 μm) to improve the sealing. The sample (S) is contained between the two windows. The optical windows exhibit high transmittance between 270 and 2500 nm.

4.5 Pressure Generation and Measurement

Heptane was used as pressurizing medium and to provide efficient heat transfer from the high-pressure cell to the internal cell. The setup for pressurization is given in scheme 4.2.



Scheme 4.2: Setup for high-pressure generation consisting of a storage vessel (SV), a pressure gauge (PG), the high-pressure cell (HPC), a screw press (ScP), and stop valves (V).

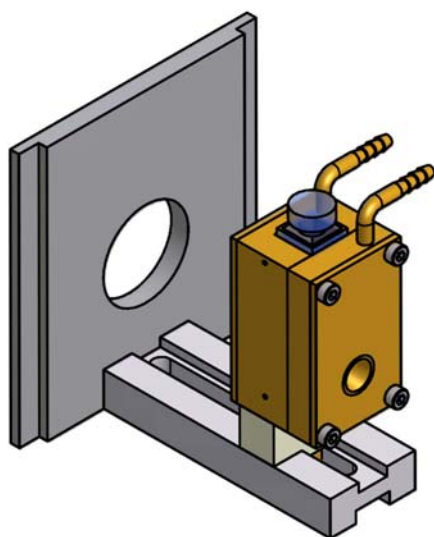
The manually operated syringe-type screw press (ScP) (maximum volume of 12 cm³), used for pressurizing the high-pressure cell (HPC), was filled up with heptane provided in a storage vessel (SV). Pressure was monitored either by a Bourdon tube pressure gauge (PG) (WIKA Alexander Wiegand, precision test gauge, 0–2.5 kbar, accuracy class 0.1, nominal size of 250 mm, scale interval of 5 bar), another Bourdon tube pressure gauge (WIKA Alexander Wiegand, precision test gauge, 0–4 kbar, accuracy class 0.1, nominal size of 250 mm, scale interval of 10 bar) or with the help of an absolute pressure transducer (Hottinger Baldwin Messtechnik, P3MB, 0–3 kbar, accuracy class 0.2) which is connected to a measuring amplifier (Hottinger Baldwin Messtechnik, MVD 2510, accuracy class 0.1). The Bourdon tube pressure gauges were used for investigations into the polymerization kinetics of *N,N*-dimethylprop-2-enamide, 2-methylprop-2-enamide, and 1-vinylpyrrolidin-2-one, the absolute pressure transducer for the latest measurements with prop-2-enamide being the monomer. The first-mentioned Bourdon tube pressure gauge

was used for PLP–SEC studies, whereas the last-mentioned Bourdon tube pressure gauge was applied to SP–PLP–NIR experiments.

4.6 Temperature Control

High-pressure experiments were conducted using a PID controller (Eurotherm, 815) for SP–PLP–NIR and another PID controller (Eurotherm, 820) for PLP–SEC experiments. These controllers were connected to the thermocouple and the electric resistance heater to determine temperature and to provide the electric current for heating purposes.

Experiments at ambient pressure were performed in cylindrical or cuboidal cuvettes. The cuboidal cuvettes used for FT–NIR spectroscopy were placed in a brazen cuvette holder (see scheme 4.3) that exhibits a separate chamber surrounding the cuvette compartment (depth and width of 13 mm, height of 50 mm) through which a heat-transfer fluid can be circulated.



Scheme 4.3: View drawing of the cuvette holder with an inserted cuvette.

The cuvette holder is designed such that the magnetic stirrer can be set into the cuvette compartment. The diameter (inside diameter of 5.0 mm) as well as the angle (opening

angle of 17°) of the holder's aperture are constructed as small as possible for a best possible temperature control, but as large as is necessary for a maximum throughput of light. In other words, the cuvette holder is adapted to the spectrometer. To control temperature, the hose barbs of the cylindrical cuvettes or the brazen sample holder were connected with a heated/refrigerated circulating bath (Haake, F3-K) operated with an aqueous ethane-1,2-diol solution used as heat transfer fluid. Temperature inside cuvettes was monitored in case of a few chemically initiated polymerizations by a thermocouple (chapter 4.4) which was connected to a PID controller (Eurotherm, 91e). The thermocouple was inserted through a hole drilled in the PTFE stopper of the cuvette.

A clear-view thermostat (Lauda Dr. R. Wobser, D40) was used for viscosity measurements. The temperature inside is determined with a Pt100 connected to a PID controller (Eurotherm, 2460). The PID controller regulates a universal relay box (Lauda Dr. R. Wobser, R3) which controls the power supply of an immersion heater. The bath was filled with demineralized water.

Density measurements were performed by means of a heating water bath circulator (Haake, D2-L). To reduce overheating, the water bath circulator is connected with a water circulation cooler (Lauda Dr. R. Wobser, WK 500). Temperature monitoring was carried out by means of a digital thermometer (Votcraft 302 K/J Thermometer).

4.7 Laser Energy Meter

Determination of the laser pulse energy was carried out with a laser energy meter (Coherent, LabMaxTM-TOP) and an appropriate sensor (Coherent, EnergyMaxTM J-50MT-10KHZ, 0.3–2.1 μm , 500 μJ –1 J, repetition rate ≤ 10 kHz, pulse width ≤ 1.7 μs). The sensor was connected to a heat sink (Coherent, large heat sink) to increase the maximum average power, which may be applied nondestructively to the sensor.

4.8 PLP–SEC Technique

4.8.1 PLP Setup

PLP–SEC experiments were performed using an exciplex laser with a pulse width of 20 ns operated on the XeF-line at 351 nm. The internal laser energy meters were calibrated via an external energy meter (chapter 4.7). Within the present work, the setup has been changed. Two different setups are described in chronological order.

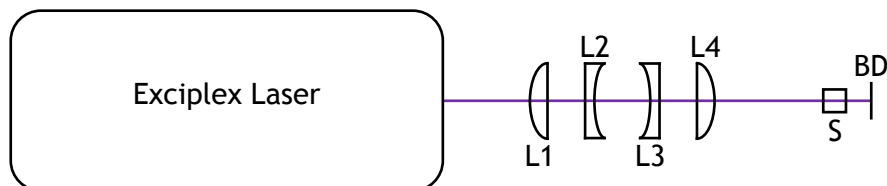
Setup A

The width of the laser (Lambda Physik, LPX 210i, maximum pulse energy of 320 mJ, maximum repetition rate of 100 Hz) beam is reduced via two cylindrical plano-convex lenses resulting in chosen pulse energies at the sample cell between 10 and 55 mJ·cm⁻². The energies are much lower than the specified ones because of the use of helium instead of neon as buffer gas. This setup was used for all homopolymerizations except for PAm homopolymerization.

Setup B

The laser (Coherent, LPXpro 240, maximum pulse energy of 120 mJ, maximum repetition rate of 400 Hz) beam is reduced in width to 16 mm, by means of a plano-convex (L1) and a plano-concave (L2) lens, and expanded to a height of 20 mm, by the use of a plano-concave (L3) and a plano-convex (L4) lens, resulting in chosen pulse energies at the sample cell between 10 and 40 mJ·cm⁻² (all lenses: CVI Melles Griot, cylindrical, UV-grade fused silica, V-type antireflective coating wavelength of 351 nm, reflectance < 0.25 % per surface; L1: SCX-50.8-127.1-UV-351, $f_L = 250.0$ mm; L2: RCC-40.0-30.0-101.7-UV-351, $f_L = -200.0$ mm; L3: RCC-40.0-25.4-25.4-UV-351, $f_L = -50.0$ mm; L4: SCX-30.0-50.9-UV-351, $f_L = 100.0$ mm). To reduce spherical aberration, Galilean-type lens configurations have been chosen for this setup (scheme 4.4) with the curved surfaces of the lenses facing the parallel beam. For safety reasons a beam dump (BD) (CVI Melles

Griot, 48-10M) is used to absorb light passing through the sample (S) cell. Additionally, all components except for the laser are set up in a wooden, internally black anodized box. Moreover, such a shielding reduces ambient UV light impinging on the sample. This setup was used for all binary copolymerizations as well as PAm homopolymerization.



Scheme 4.4: Setup B for PLP experiments consisting of an exciplex laser, lenses (L), a sample (S), and a beam dump (BD).

4.8.2 Size-Exclusion Chromatographs

Depending on the polymer under investigation, different setups were used to determine molar-mass distributions. The MMDs were kindly determined by I. Lacík, DSc, and M. Stach, PhD, and coworkers at the Polymer Institute of the Slovak Academy of Sciences in Bratislava, Slovakia.

Setup A

The aqueous-solution SEC setup consists of an in-line degasser (Waters), a pump (Waters, 515 HPLC pump) equipped with a plunger washing kit, an injector (Rheodyne, 7725i), a guard and three main columns (both types: PSS Polymer Standards Service, PSS SUPREMA, guard column length of 50 mm, main column length of 300 mm, inner diameter of 8 mm, particle size of 10 μm , main column pore sizes of 100, 1000 and 3000 Å) positioned in a column heater module (Waters) set to 60 °C as well as a differential refractive index detector (Waters, Waters® 2410). The measurements were performed using demineralized water as eluent which contained 0.1 mol·L⁻¹ sodium

nitrate. The eluent was permanently stirred to avoid concentration changes as a consequence of salt sedimentation. Ethane-1,2-diol was used as flow rate marker to adjust eluent flow to a rate of $1 \text{ mL} \cdot \text{min}^{-1}$. Calibration of the SEC setup was performed with poly(prop-2-enamide) (poly(PAm)) standards (American Polymer Standards Corporation, dispersities between 1.2 and 2.0) for peak molar masses between 2950 and $950\,000 \text{ g} \cdot \text{mol}^{-1}$. Data acquisition and analysis were performed via the WinGPC software (PSS Polymer Standards Service, version 6 or 7.2). This setup was used for poly(MPAm) and poly(PAm).

Setup B

SEC analysis for weakly polar polymers was performed with *N,N*-dimethylacetamide (DMAc) as the eluent containing $0.001 \text{ g} \cdot \text{g}^{-1}$ lithium bromide pumped through a guard column and three main columns (both types: PSS Polymer Standards Service, PSS GRAM, guard column length of 50 mm, main column length of 300 mm, inner diameter of 8 mm, particle size of $10 \mu\text{m}$, main column pore sizes of 100, 1000 and 3000 \AA) placed in a column heater set to $45 \text{ }^{\circ}\text{C}$. The instrumentation is otherwise identical to setup A. The flow rate of $0.8 \text{ mL} \cdot \text{min}^{-1}$ was controlled by toluene as the flow rate marker. Calibration of the SEC setup was performed with polystyrene standards (PSS Polymer Standards Service, dispersities between 1.03 and 1.11) exhibiting a narrow molar-mass distribution for peak molar masses between 376 and $2\,300\,000 \text{ g} \cdot \text{mol}^{-1}$. This SEC setup was used for analysis of poly(M-MPAm) and poly(DM-PAm).

Narrow poly(MPAm), poly(M-MPAm), and poly(DM-PAm) calibration standards are not available. Therefore, as already described for *N*-vinylformamide (NVF)^[46] and VP^[45], direct molar-mass determination is required. An on-line multi-angle laser light scattering (MALLS) detector (PSS Polymer Standards Service, SLD7000, working at 633 nm) in combination with the differential refractive index detector provided absolute molar masses (MALLS–RI detection). Narrow pullulan (Polymer Laboratories) and polystyrene (PSS Polymer Standards Service) calibration standard samples exhibiting mass-average molar masses of $113\,000 \text{ g} \cdot \text{mol}^{-1}$ and $65\,000 \text{ g} \cdot \text{mol}^{-1}$, respectively, were used as isotropic

scatterers. The refractive index increments, $\partial n / \partial c$, were determined on a differential refractometer (Phoenix Precision Instrument Company, Brice-Phoenix, BP-2000-V) in the eluent which was used for SEC analysis of the respective polymer to be $0.161 \text{ mL} \cdot \text{g}^{-1}$ for poly(MPA_m), $0.0730 \text{ mL} \cdot \text{g}^{-1}$ for poly(M-MPA_m), $0.0723 \text{ mL} \cdot \text{g}^{-1}$ for poly(DM-PA_m), $0.165 \text{ mL} \cdot \text{g}^{-1}$ for polystyrene, and $0.135 \text{ mL} \cdot \text{g}^{-1}$ for pullulan, respectively. These numbers were estimated^[191] from the values measured at 436 and 546 nm for the wavelength of 633 nm at which the MALLS detector operates. The factor which correlates the positions of the primary points of inflection obtained by direct (MALLS–RI detection) MMD determination and by calibrant-relative (RI detection) calibration was found to be: $M_{\text{POI}}(\text{MALLS–RI}) / M_{\text{POI}}(\text{RI}) = 3.58 \pm 0.31$ for poly(MPA_m), 2.80 ± 0.05 for poly(M-MPA_m), and 1.13 ± 0.03 for poly(DM-PA_m), respectively. These correction factors were used for obtaining POI positions and thus k_p values.

4.9 FTIR Spectrometer

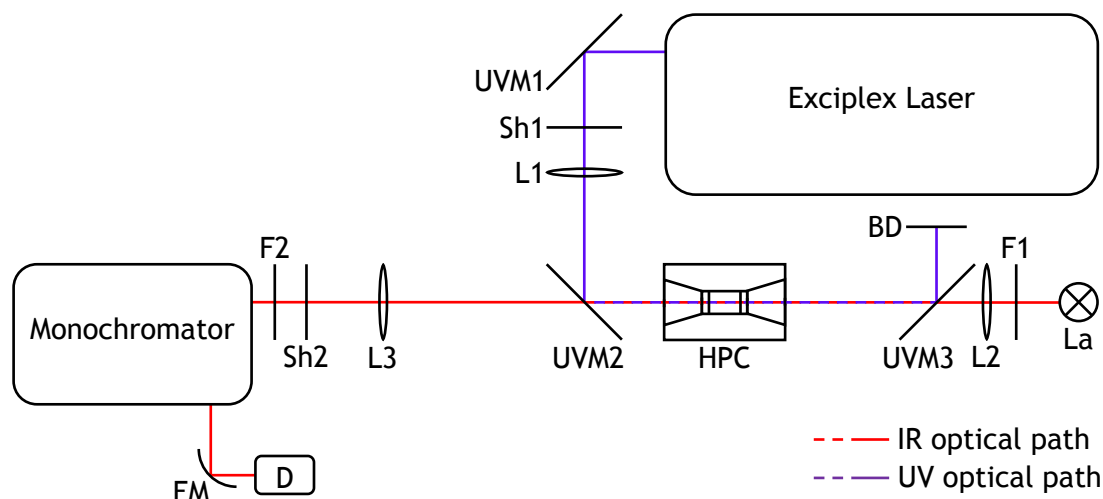
NIR spectra were recorded with an FTIR spectrometer (Bruker Optik, IFS 88). To accommodate the optical high-pressure cell, the default sample compartment of the spectrometer has been enlarged in height. A water-cooled cell holder is used to reduce heat transfer from the cell to spectrometer components. The compartment as well as the optical system are permanently purged with compressed dry (ZANDER Aufbereitungstechnik, adsorption dryer) air. For the present work, the optical configuration consisted of a tungsten halogen lamp (Gilway Technical Lamp, L7417A, 12 V, 50 W), a silicon-coated calcium difluoride beam splitter (model T8401), and a liquid-nitrogen-cooled InSb detector (InfraRed Associates, model D413, 1 mm in diameter, peak detectivity of $1.75 \cdot 10^{11} \text{ cm} \cdot \text{Hz}^{0.5} \cdot \text{W}^{-1}$). The sample compartment is separated from the optical system by calcium difluoride windows. This configuration allows for optimal recording in the spectral range of 2500 to 11000 cm^{-1} . Data acquisition and data analysis were performed using the software OPUS (Bruker Optik, version 4.2 or 6.0).

4.10 SP–PLP–NIR Setup

The setup has been modified within the present work. The two setups used in this work are described in chronological order.

Setup A

The optical setup for the SP–PLP–NIR experiments of this work is illustrated in scheme 4.5. The setup may be divided into two units, the optical path of the UV irradiation light and the path of the IR probing light.



Scheme 4.5: Optical setup for SP–PLP–NIR experiments consisting of an exciplex laser, UV mirrors (UVM), shutters (Sh), lenses (L), the high-pressure cell (HPC), a beam dump (BD), filters (F), a lamp (La), a monochromator, an ellipsoidal mirror (EM), and a detector (D).

The UV light, which is generated by a pulsed XeF exciplex laser (Lambda Physik, LEXtra 50, pulse width of 20 ns, maximum pulse energy of 100 mJ, maximum repetition rate of 30 Hz), is reflected by a UV mirror (UVM1) and passes through an electromagnetic shutter (Sh1) (PRONTOR, PRONTOR magnetic E/40, PTFE-coated blades, blade material grade C100S, material no. 1.1274) as well as a plano-concave lens (L1)

($f_L = 16$ cm). The lens concentrates the light before it is reflected at a second UV mirror (UVM2) to impinge on the high-pressure cell (HPC). A third UV mirror (UVM3) redirects the laser light to a beam dump (BD). The UV mirrors are transparent in the infrared region (INFRASIL®, ZnSe-coated, 45° angle of incidence, 90° beam deflection). Depending on the selected operating high voltage of the laser, the pulse energies at the exit of the high-pressure cell were chosen to be between 3.5 and 5.5 mJ·cm⁻². The maximum laser pulse energy of approximately 12.5 mJ·cm⁻² is relatively low because of using helium instead of neon as buffer gas.

A tungsten-halogen lamp (La) (65 W, filament size of 3 × 5 mm²), which is mounted with vertical positioning of the filament (lamp in horizontal orientation) inside a water-cooled metal holder, serves as a source of infrared radiation. Water cooling is necessary to prevent the lamp from burning out and to ensure a constant temperature of the filament. The lamp is, to a large extent, surrounded by an aluminum sheet to reduce the amount of stray light that may reach the detector. The lamp is powered by a lead accumulator (Varta, M 13 t, 968 001 000 3100, “Antrieb und Beleuchtung”, semi-traction, 12 V, 180 A·h (5 h), 230 A·h (20 h)) instead of a common direct-current power supply to provide a stable light intensity. Initiation processes caused by UV light from the tungsten-halogen lamp are suppressed by introducing a colored glass filter (F1) (long-wave pass type, glass type RG-695). The analysis light is focused by a lens (L2) (CaF₂, $f_L = 100$ mm, $d = 50$ mm) onto the sample contained in the optical high-pressure cell. A second lens (L3) (CaF₂, $f_L = 100$ mm, $d = 50$ mm) focuses the analysis light onto the slit of a Czerny–Turner monochromator (B & M Spektronik, BM 50, collimator focal length f_L of 0.5 m, f-number of $f_L/6.9$). The entrance and exit slits (B & M Spektronik, SP 0.0003) can be varied up to a height of 20 mm and a width of 5 mm. The width can be adjusted with a precision of 0.01 mm. An electromagnetic shutter (Sh2) (PRONTOR, PRONTOR magnetic E/40, PTFE-coated blades, blade material grade C100S, material no. 1.1274), in front of the monochromator, is used to block the analysis light which allows for determination of the background detector signal without infrared radiation. The light is diffracted by a diffraction grating (Bausch & Lomb, 3599, substrate dimensions of 76 × 76 mm², thickness of 16 mm, planar, groove density of 600 mm⁻¹, blaze wavelength of 1.6 μm,

blaze angle of $28^{\circ}41'$, efficiencies of 78 % at $1.7\text{ }\mu\text{m}$, 82 % at $1.8\text{ }\mu\text{m}$, 74 % at $2.0\text{ }\mu\text{m}$) and redirected to a fast InAs-detector (D) (EG&G Judson, J12D-M204-R02M-60, 2.0 mm in diameter, peak detectivity of $1.50\cdot 10^{11}\text{ cm}\cdot\text{Hz}^{0.5}\cdot\text{W}^{-1}$, peak responsivity of $1.3\text{ A}\cdot\text{W}^{-1}$, cooled by liquid nitrogen) by an ellipsoidal mirror (EM) (Bruker Analytische Meßtechnik, f-number of $f_l/6$, $f_{l1} = 200\text{ mm}$, $f_{l2} = 40\text{ mm}$, 90° beam deflection) which is metalized with aluminum. The detector is powered by two battery packs (NiMH, $15 \times 1.2\text{ V}$ per pack, typically $800\text{ mA}\cdot\text{h}$ per cell) to avoid adverse impact due to ripple of a direct-current power supply. Voltage regulators (STMicroelectronics, L79L12 and L7812) reduce the output voltage to $+12\text{ V}$ and -12 V , respectively. The combination of the diffraction grating and the focusing mirror of the monochromator results in a reciprocal linear dispersion of approximately $4.1\text{ nm}\cdot\text{mm}^{-1}$. The diffraction grating can be turned by means of a stepper motor which is controlled via an Atari computer. A monochromator order sorting filter (F2) (Oriel, 1 mm silicon, long-wave pass, 50 % cut-off wavelength of $1.05\text{ }\mu\text{m}$, transmission in the $2500\text{ to }8000\text{ cm}^{-1}$ range), directly in front of the monochromator, ensures that only one order of diffraction hits the detector. All optical components are set up in a darkened room to reduce ambient UV light impinging on the sample.

After appropriate amplification, the detector signal is recorded by a transient recorder (Spectrum Systementwicklung Microelectronic, PAD 164 2 MHz, voltage resolution of 16 bit, $2\text{ kHz} \leq \text{sample rate} \leq 2\text{ MHz}$, 4 MSamples on-board memory) and transferred via an ISA bus to a personal computer (operating system Windows® 98) for further evaluation. The software SBench 4.55 (Spectrum Systementwicklung Microelectronic) was used for signal processing. For mechanical decoupling from background laboratory vibrations, for example of the building services, all components in the IR optical path are placed on a solid granite slab supported by rubber inner tubes. A scheme of the electronic SP–PLP–NIR setup is given elsewhere.^[192] Of major importance for signal processing is the amplifier and compensator unit. For shielding against electromagnetic interference, the amplifier and compensator unit is placed in a grounded steel housing and metal film resistors have been used solely. Single-ended signaling is used to transmit the electrical signals. The circuit diagram is given in the PhD thesis of Degener,^[193] whereas an

additional output channel, which provides the Atari computer with a signal, is connected to the output line of the second operational amplifier (OPA) inside the preamplifier. Furthermore, all operational amplifiers OP27 and OP37 have been replaced by ultra-low noise precision operational amplifiers OPA27 (Burr-Brown®, $4.5 \text{ nV} \cdot \text{Hz}^{-0.5}$ at 1 kHz, typical GBP of 8 MHz) and OPA37 (Burr-Brown®, $4.5 \text{ nV} \cdot \text{Hz}^{-0.5}$ at 1 kHz, typical GBP of 63 MHz), respectively, except for the OP37 inside the preamplifier, which has been replaced by an OPA27. The output channel labeled $\times 50$ Atari is not used any more. Within the amplifier and compensator unit, which is directly attached to the infrared detector, the voltage signal is amplified and transferred to the transient recorder. After each single laser pulse, the compensator electronics reset the voltage at the transient recorder (determined via the so-called channel 10) to the prepulse voltage level to ensure that the input range of the transient recorder is not exceeded. Otherwise it would be necessary to reduce the amplification factor significantly, resulting in a worse voltage resolution. As source of the compensating voltage a multifunction data-acquisition board (Computer Boards, CIO-DAS1602/16, 16 bit resolution of analog input, 12 bit resolution of analog output), which is controlled by C++ programs compiled with Microsoft® Visual C++ 6.0 (Microsoft), is used. Applying another compensating voltage of up to 12 V (adjustable by means of a potentiometer) to the input line of the second OPA inside the preamplifier allows for determination of small changes in the signal relative to a high underlying voltage. This reduces the compensating voltage applied via channel 10 that is limited to the maximum output voltage of the multifunction data-acquisition board. The electronics of the amplifier and compensator unit are also used to determine the initial light intensity prior to any polymerization activity as well as before and after each individual pulse sequence (via the so-called channel 8). Without applying a compensating voltage, the signal at the transient recorder is a hundred times higher than the one at channel 8. The measured signals are transferred to the personal computer via the multifunction data-acquisition board. The light intensities are used by a program which converts the voltage versus time signals to monomer concentration versus time signals to calculate the degree of overall monomer conversion. The cable which links the amplifier and compensator unit with the so-called connection board I has a double-layer shield

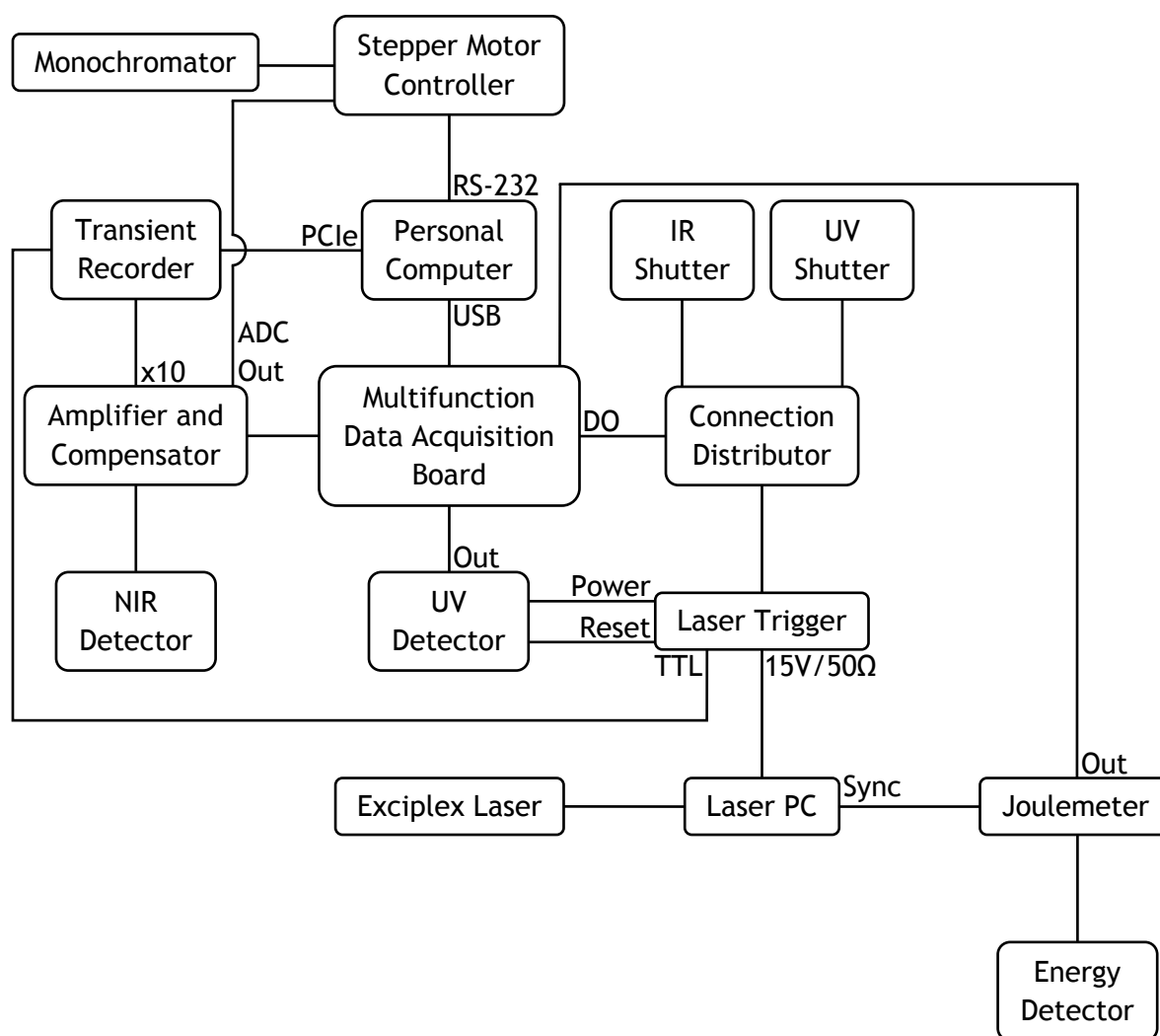
consisting of a foil and a braid to reduce electromagnetic interference. The multifunction data-acquisition board exhibits an 8 bit input/output port capable of providing TTL signals. The analog-to-digital converting function of the board is used (via the connection board I) to collect voltage signals during SP–PLP experiments from a joulemeter, a UV detector as well as the amplifier and compensator unit. The joulemeter, in turn, determines the voltage at the pyroelectric energy detector (Gentec Electro-Optics, ED-200, 0.19–40 μm , typical rise time of 1 ms, accuracy of $\pm 5\%$, sensitivity of $9.32 \text{ V}\cdot\text{J}^{-1}$), which is incorporated in a sample-and-hold circuit which holds the analog input voltage for approximately 17 ms. The UV detector can be placed between lens L1 and mirror UVM2 and thus be used to determine the energy of each laser pulse. The energy detector is used for calibration. Due to its opacity, it cannot be employed to SP–PLP experiments. The UV detector is a peak energy detector consisting of a beam splitter (Heraeus Quarzglas, Suprasil®, thickness of 1 mm, angle of incidence of 45°) which reflects a small amount of the UV light, after passing through a diffusion plate (roughened fused silica), onto a silicon photodiode (EG&G Judson, FND-100Q, 200–1150 nm, rise time less than 1 ns). The photodiode, operated in reverse direction, is incorporated in a sample-and-hold circuit which holds the analog input voltage until the occurrence of a reset signal. Nevertheless, the UV detector has not been installed within the present work but is mentioned for the sake of completeness. The two photo shutters and a laser trigger unit are controlled via connection board II, which handles data transfer from the 8 bit input/output port. The laser trigger unit serves multiple purposes. It provides power for the UV detector, arms, and resets it once it has been charged by a laser pulse. Moreover, it converts the TTL signal from the 8 bit input/output port, which triggers the laser, to a 15 V signal that in turn is transferred to the laser control computer. The laser trigger unit is also responsible for synchronizing the beginning of the recording of the transient recorder with the firing of the laser pulse. All power supplies of the electronic components are connected to an alternating-current line filter (Corcom, 10VK3) to reduce electromagnetic interference. All grounding cables of the electronic components are plugged in a central grounding point to avoid ground loops.

Setup B

The optical setup is identical to setup A with the modification that the lamp has been replaced by a new tungsten-halogen lamp (L) (OSRAM, XENOPHOT[®], HLX 64623, NAED 54251, ANSI code EVA, LIF code M/28, 100 W, 12 V, 2800 lm, filament size of $2.7 \times 4.7 \text{ mm}^2$, burning position s 90 horizontal to vertical, base down) which is powered by a switching-mode power supply (Manson, reichelt elektronik, output of 0–10 A and 1–36 V). Switching-mode power supplies deliver a constant voltage whereas voltage slightly decreases with operating time in case of lead accumulators due to an increasing internal resistance. Moreover, unlike switching-mode power supplies, lead accumulators are explosive due to gassing and they require maintenance. With the frequency of the ripple of switching-mode power supplies being in the kHz range, it is unlikely that the filament of the lamp oscillates with such a high frequency. Such an oscillation would affect the stability of the detector output. The stepper motor of the monochromator is controlled by means of the main personal computer, which controls all other components of the setup except for the laser, via an RS-232 port (DE-9 plug). For this purpose, a VEE program compiled with Agilent VEE Pro (Agilent Technologies, version 9.2) has been written by Dr. H.-P. Vögele. Because of malfunctions, the main personal computer and the transient recorder had to be replaced. The new transient recorder (Spectrum Systementwicklung Microelectronic, M2i.4650-exp, voltage resolution of 16 bit, $1 \text{ kHz} \leq \text{sample rate} \leq 3 \text{ MHz}$, 128 MSamples on-board memory) is plugged in a PCIe $\times 1$ slot of the personal computer (operating system Windows[®] 7 Professional). The software SBench 5.3 (Spectrum Systementwicklung Microelectronic) was used for signal processing. Because of the personal computer lacking an ISA slot, a USB multifunction data-acquisition board (Measurement Computing, minilab 1008, 12 bit resolution of analog input, 10 bit resolution of analog output) has been installed. The labeling of channels 8 and 10 in setup A has been changed to channels 2 and 3, respectively. Contrary to the transient recorder, the inputs of the multifunction data-acquisition board are used in differential mode. The electronic setup is depicted in scheme 4.6.

Replacement of the operational system of the personal computer required a new C++ compiler (Microsoft, Microsoft[®] Visual C++[®] 2010 Express, version 10.0). Since the

previously used C++ source codes did not contain C++ code alone but a mixture of C and C++ codes, a feature that is not supported any longer by the latest compilers, the source codes have been rewritten. Besides, the program sequence has been changed. The C++ source codes and the corresponding flowcharts are given in appendices B.1, B.2, C.1, and C.2. To avoid damage of the electronic equipment or incorrectly measured values due to electrostatic discharge, the operator has to be connected continuously to ground via an antistatic wrist strap (1 M Ω). The whole setup is placed in an air-conditioned lab to reduce deformations of optical components and concomitant changes in the light intensity as a result of shifts of the room temperature during measurement.



Scheme 4.6: Electronic setup (setup B) for SP-PLP-NIR experiments.

4.11 NMR Spectrometer

^1H NMR spectra were recorded via a Varian spectrometer (Varian, *MERCURY VxWorks-Powered* NMR Spectrometer System, 300 MHz) combined with a Varian processing software (Varian, VNMR 6.1C) or via another Varian spectrometer (Varian, VNMRs, 300 MHz) combined with another Varian processing software (Varian, VnmrJ 2.2C). Data analysis was performed using the software MestReNova (MESTRELAB RESEARCH, version 7).

4.12 Density Meter

A density meter based on the oscillating U-tube principle and consisting of a data acquisition unit (Anton Paar, DMA 60), a measuring unit (Anton Paar, DMA 602TP), and a high-temperature cell (Anton Paar, DMA 602 H, DURAN® 50, $-10 \leq \theta \leq 150$ °C) was used within the present work. The temperature inside the U-tube was monitored via a digital thermometer (chapter 4.6).

4.13 Viscometer

The kinematic viscosity, ν , was measured with an Ubbelohde viscometer (SCHOTT, 0a, inside diameter of 0.53 mm). The viscometer was mounted inside a clear-view thermostat (chapter 4.6).

4.14 Electrical Conductivity/pH Meter

A combined measuring instrument (Mettler-Toledo, S47 SevenMulti™ dual meter pH / conductivity, $-2.000 \leq \text{pH} \leq 20.000$, $0.001 \mu\text{S}\cdot\text{cm}^{-1} \leq \kappa \leq 1\,000 \text{ mS}\cdot\text{cm}^{-1}$) was used to determine electrical conductivity as well as pH values. For pH measurements a glass-body electrode (Mettler-Toledo, InLab® Routine Pro, $0 \leq \text{pH} \leq 14$, $0 \leq \theta \leq 100$ °C)

with integrated temperature sensor (NTC thermistor, 30 k Ω) was used. The electrical conductivity was determined by means of a conductivity probe (Mettler-Toledo, InLab[®]730, $K_{\text{cell}} = 0.56 \text{ cm}^{-1}$, $0.01 \text{ mS} \cdot \text{cm}^{-1} \leq \kappa_c \leq 1000 \text{ mS} \cdot \text{cm}^{-1}$, $-5 \leq \theta \leq 100 \text{ }^{\circ}\text{C}$) with integrated temperature sensor (NTC thermistor, 30 k Ω).

5 Experimental Procedures and Data Evaluation

5.1 Determination of Density

Unpurified monomer and demineralized water were mixed and filled into the U-tube which was subsequently brought to the desired temperature. The number of oscillations used to determine the natural frequency was chosen to be 10000. The instrument constant was determined by means of demineralized water and air^[194,195] allowing for calculation of the density via equation 3.59.

5.2 Viscometry

Unpurified monomer and demineralized water were mixed and filled into the viscometer. The viscometer was calibrated with demineralized water at 20 °C^[194,196] under the assumption that the Hagenbach–Couette correction given by the manufacturer is independent of manufacturing accuracy. The capillary was thermostated for about 15 min prior to measurement. Dynamic viscosities were determined via combination of the measured kinematic viscosity and density, ρ , by:

$$\eta = \nu \cdot \rho \quad (\text{eq. 5.1})$$

5.3 PLP–SEC Experiments

5.3.1 Experimental Procedure

For PLP–SEC experiments, unpurified monomer and, optionally, solvent were mixed and poured at ambient temperature into a volumetric flask containing the initiator. In case of ambient-pressure experiments, the reaction solution was transferred into a cuvette

(chapter 4.3) and purged with nitrogen for 5 min to remove oxygen. The cuvette was closed with a PTFE stopper and thermostated for about 15 min prior to laser pulsing.

For high-pressure experiments, the reaction solution was purged with argon or nitrogen for 5 min and filled into an internal cell (chapter 4.4), which was fitted into the high-pressure cell. The length of the sealing punches was chosen such that the path length of the high-pressure cell amounted to approximately 17.0 mm allowing for a path length of the internal cell of about 7 mm, which ensures sufficient amount of produced polymer for analysis. The high-pressure cell was pressurized and brought to the desired temperature. Temperature constancy was checked on-line.

All flasks and cuvettes were wrapped in aluminum foil until start of laser irradiation to reduce ambient-light induced initiator decomposition. Post-PLP polymerization was suppressed by transferring the reaction solution into a sample vial containing benzene-1,4-diol. In case of NaA and VP copolymerization as well as PAm and MPAm homopolymerizations residual monomer was removed by dialysis against demineralized water since NaA, PAm, and MPAm are solid at ambient pressure and temperature. Dialysis was carried out for up to two weeks until constant conductivity was attained. Solvent and volatile monomer were removed under reduced pressure at ambient temperature.

5.3.2 Data Evaluation

The degree of monomer conversion was determined by gravimetric analysis for all monomer systems. Molar monomer concentrations at zero monomer conversion may be described by equation 5.2 and were calculated using ambient pressure densities of DM-PAm,^[197] M-MPAm,^[198] PAm, VP, as well as Vienna Standard Mean Ocean Water (VSMOW) given by equations 5.3 to 5.9 under the assumption of ideal mixing.

$$c_M^0 = \frac{m_M/M_M}{m_M/\rho_M + m_{Sol}/\rho_{Sol}} \quad (\text{eq. 5.2})$$

m_M denotes monomer mass, M_M monomer molar mass, ρ_M monomer density, m_{Sol} solvent mass, and ρ_{Sol} solvent density.

$$\rho_{DM-PAm} = 0.962 \text{ g} \cdot \text{cm}^{-3} \quad (\text{eq. 5.3})$$

$$\rho_{M-MPAm} = 0.97 \text{ g} \cdot \text{cm}^{-3} \quad (\text{eq. 5.4})$$

$$0.10 \text{ g} \cdot \text{g}^{-1}: \rho_{aqPAm} / (\text{g} \cdot \text{cm}^{-3}) = 1.012 - 3.52 \cdot 10^{-4} \cdot \theta / ^\circ\text{C} - 3.19 \cdot 10^{-6} \cdot \theta^2 / ^\circ\text{C}^2 \quad (\text{eq. 5.5})$$

$$0.20 \text{ g} \cdot \text{g}^{-1}: \rho_{aqPAm} / (\text{g} \cdot \text{cm}^{-3}) = 1.020 - 1.71 \cdot 10^{-4} \cdot \theta / ^\circ\text{C} - 4.39 \cdot 10^{-6} \cdot \theta^2 / ^\circ\text{C}^2 \quad (\text{eq. 5.6})$$

$$0.30 \text{ g} \cdot \text{g}^{-1}: \rho_{aqPAm} / (\text{g} \cdot \text{cm}^{-3}) = 1.020 - 4.96 \cdot 10^{-5} \cdot \theta / ^\circ\text{C} - 6.91 \cdot 10^{-6} \cdot \theta^2 / ^\circ\text{C}^2 \quad (\text{eq. 5.7})$$

$$\rho_{VP} / (\text{g} \cdot \text{cm}^{-3}) = 1.0592 - 7.7772 \cdot 10^{-4} \cdot \theta / ^\circ\text{C} - 4.6649 \cdot 10^{-7} \cdot \theta^2 / ^\circ\text{C}^2 \quad (\text{eq. 5.8})$$

$$\rho_{VSMOW} / (\text{g} \cdot \text{cm}^{-3}) = 0.9999 + 2.3109 \cdot 10^{-5} \cdot \theta / ^\circ\text{C} - 5.44807 \cdot 10^{-6} \cdot \theta^2 / ^\circ\text{C}^2 \quad (\text{eq. 5.9})$$

The density of D₂O was estimated assuming that the ratio of the density of D₂O to the density of H₂O is identical to the ratio of the molar mass of D₂O, M_{D_2O} , to the molar mass of H₂O, M_{H_2O} . This is associated with the assumption that the average required space of a molecule is independent of isotope. The contribution of the monomer to the sample volume is negligible in case of MPAm at monomer mass fractions up to 0.20 g·g⁻¹. For PAm, temperature-dependent densities for various monomer mass fractions, w_M , in water were provided by the Lacík group.^[199] Densities of aqueous solutions of PAm containing more than 0.30 g·g⁻¹ PAm were assumed to be identical to the density of

0.30 g·g⁻¹ PAm in water. It was assumed that water used by the Lacík group as well as water used within the present work conform with VSMOW. In case of solutions of PAm in D₂O, ideal mixing of PAm with D₂O and H₂O, respectively, was assumed so that equations 5.5, 5.6, and 5.7 may be converted into densities of PAm in D₂O, $\rho_{\text{PAmD}_2\text{O}}$, via equation 5.10. The resulting densities were applied to ρ_M as well as ρ_{sol} .

$$\rho_{\text{PAmD}_2\text{O}} = \rho_{\text{aqPAm}} \cdot \left(\frac{M_{\text{D}_2\text{O}}}{M_{\text{H}_2\text{O}}} \cdot (1 - w_M) + w_M \right) \quad (\text{eq. 5.10})$$

The dependences of the density of bulk VP^[45] and VSMOW^[33] on temperature were taken from the literature, whereas the densities of DM-PAm and M-MPAm are valid for 25 °C. Temperature effects were neglected where unknown. Due to the lack of information on pressure effects, densities at high pressure were determined such that the relative change in density going from ambient pressure to high pressure is identical to the change in case of VSMOW. Densities of VSMOW given in table 5.1 for 40 °C and various pressures were estimated by linear interpolation of literature values^[200] given for 310 and 315 K. The value at 1 500 bar was determined by linear interpolation of the values at 1 000 and 2 000 bar.

Table 5.1: Density of VSMOW at 40 °C estimated by linear interpolation of literature values^[200] given for 310 and 315 K.

p/bar	$\rho_{\text{VSMOW}}/(\text{g}\cdot\text{cm}^{-3})$
1.01325	0.9922
500	1.0130
1000	1.0319
1500	1.0485
2000	1.0652

The degrees of polymerization at the inflection points of the MMD are calculated by dividing the corresponding molar mass by the molar mass of the monomer. k_p is

determined from the first POI via equation 3.54 with ϵ_M being the arithmetic mean of the monomer concentration before and after PLP.

5.4 FT–NIR Spectroscopy

FT–NIR spectra were recorded at an interferometer mirror speed of 80 kHz using the single-sided fast-return mode. 32 interferograms were co-added to improve the signal-to-noise ratio and the three-term Blackman–Harris window was applied for apodization. Combination of a zero-filling factor of two and a spectral resolution of 2 cm^{-1} resulted in a data-point distance of 1 cm^{-1} . The Mertz method was used for phase correction. To allow for quantitative analysis of the spectra, the optical path length was chosen such that the absorbance did not exceed 2 in the wavenumber range of interest, thus ensuring the validity of the Beer–Lambert–Bouguer law (detector linearity). Spectra analysis is described in chapters 5.5.2 and 5.6.2.

5.5 Chemically Initiated Polymerizations

5.5.1 Experimental Procedure

Chemically initiated polymerizations were conducted in cylindrical or cuboidal cuvettes where denoted. Sample preparation was as described for the ambient-pressure experiments in chapter 5.3.1 with the modification that argon instead of nitrogen was used to purge the samples. The cuvettes were allowed to thermostat for about 3 min before starting the experiment. Spectra were taken every 10 to 16 s until full monomer conversion.

5.5.2 Data Evaluation

The decrease in monomer concentration during polymerization was monitored via NIR spectroscopy. For this purpose, the vibrational band at about 6100–6250 cm⁻¹, which is assigned to the first overtone of the antisymmetric carbon–hydrogen stretching vibration of the methyldene group,^[201–204] was used. Usually, this band is not overlapped by other bands of similar or lower half-width. Influences due to overlap with much broader bands may be reduced via baseline correction. Monomer conversion was determined applying the Beer–Lambert–Bouguer law^[62–64] (equation 5.11) which relates the decadic absorbance, A_{10} , at wavenumber $\tilde{\nu}$ to monomer concentration.

$$A_{10}(\tilde{\nu}) = \lg \left(\frac{I_0(\tilde{\nu})}{I(\tilde{\nu})} \right) = \varepsilon(\tilde{\nu}) \cdot c_M \cdot l_{rc} \quad (\text{eq. 5.11})$$

The degree of monomer conversion at time t may be determined via equation 5.13 which is derived from equation 3.30 by using the integrated decadic absorbance, A_{int} , described by equation 5.12 with ε_{int} being the integrated molar decadic absorption coefficient.

$$A_{\text{int}} = \int A_{10}(\tilde{\nu}) d\tilde{\nu} = \varepsilon_{\text{int}} \cdot c_M \cdot l_{rc} \quad (\text{eq. 5.12})$$

$$\alpha(t) = 1 - \frac{c_M}{c_M^0} = 1 - \frac{A_{\text{int}}(t)}{A_{\text{int}}(t=0)} \quad (\text{eq. 5.13})$$

A typical representation of FT–NIR spectra recorded during the chemically initiated polymerization of PAm in D₂O is given in figure 5.1. The arrows indicate the course of absorbance during the reaction. The bands between 5900 and 6250 cm⁻¹, which decrease during polymerization, correlate with the overtone of carbon–hydrogen vibrations of the monomer. In contrast, the bands at lower wavenumber, which increase towards higher degree of conversion, correlate with the overtone of carbon–hydrogen vibrations of the

produced polymer. H₂O absorption bands of the first overtones of the stretching vibrations^[205] would overlap with the monomer absorption bands and thus reduce the signal-to-noise ratio. Therefore, D₂O was used because its absorption band appears at lower wavenumber compared to H₂O. Monomer absorption bands are, however, overlapped by at least one broad band, as indicated by the brown spectrum in figure 5.1 at nearly full conversion, showing its maximum at about 6000 cm⁻¹. It might be due to nitrogen–hydrogen or oxygen–hydrogen vibrations. Taking the approximate linearity of the absorbance curve between the monomer absorption band at about 6100–6250 cm⁻¹ and the bands at wavenumbers below 6050 cm⁻¹ into account, one may conclude that the monomer absorption bands of these two wavenumber ranges do not overlap. The change in absorbance between 6050 and 6100 cm⁻¹ with monomer conversion might be explained by a change in the shape of underlying absorption bands.

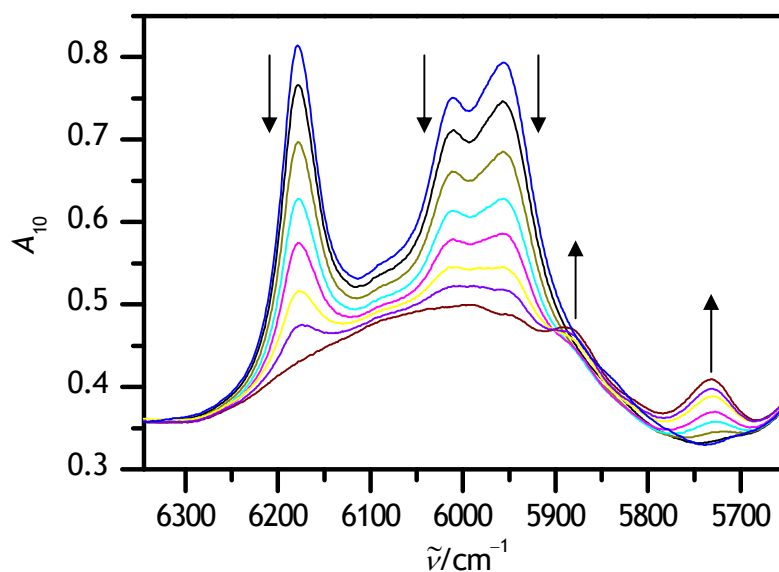


Figure 5.1: FT–NIR absorption spectra recorded during a chemically initiated polymerization of 0.10 g·g⁻¹ PAm in D₂O at 50 °C, ambient pressure, and an initiator concentration of $c_{V-50} = 0.050 \text{ mol}\cdot\text{L}^{-1}$. The arrows indicate the course of absorbance during polymerization.

The spectral series of chemically initiated polymerizations was evaluated by integration of the band between 6180 and 6260 cm^{-1} via OPUS method F. For this purpose, an individual baseline was generated for each spectrum by least-squares fitting of a parabola to the data points between 6070 and 6100 cm^{-1} as well as between 6269 and 6300 cm^{-1} . Data in the initial polymerization period, in which the reaction is usually subject to inhibition, are not considered. The rate of polymerization was determined from the first derivative of the monomer concentration versus time profile, which was calculated via equation 5.13. The Savitzky–Golay smoothing filter was chosen to perform a second-order regression on 5 to 60 data points, depending on the scatter of the data. The ratio of k_p to the square root of $\langle k_t \rangle$ was determined by means of equation 3.28 assuming an ideal initiator efficiency of unity. Initiator concentration was calculated via equation 3.2 and the rate coefficient of initiator decomposition was estimated via equation 5.14 which was fitted to data provided by the manufacturer^[206] for solutions in water. The experimental data and the fitted function are depicted in figure 5.2.

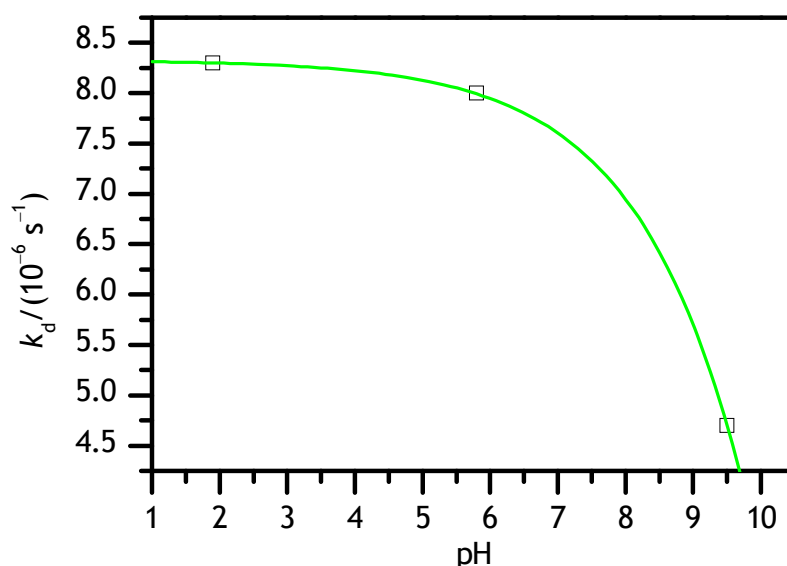


Figure 5.2: Rate coefficients of initiator decomposition of V-50 in water at 50 °C provided by the manufacturer.^[206] The line represents equation 5.14.

$$k_d/s^{-1} = 8.33 \cdot 10^{-6} - 2.70 \cdot 10^{-8} \cdot \exp\left(\frac{pH-1.90}{1.55}\right) \quad (\text{eq. 5.14})$$

pa_{D^+} values for solutions of PAm in D₂O were determined by adding 0.40 to the values measured with a conventional pH meter (chapter 4.14) as recommended in the literature.^[207] This goes along with the assumption that the summand of 0.40 is valid at 50 °C and that the influence of protons originating from PAm on the results is negligible. The pa_{D^+} values and rate coefficients of initiator decomposition determined by equation 5.14 at 50 °C are given in table 5.2. It was assumed that equation 5.14 is valid for solutions in D₂O as well so that pa_{D^+} values can be used as pH values.

Table 5.2: pa_{D^+} values and rate coefficients of initiator decomposition of V-50 determined by equation 5.14 at 50 °C and various PAm mass fractions, w_{PAm} , in D₂O.

$w_{PAm}/(g \cdot g^{-1})$	pa_{D^+}	$k_d/(10^{-6} s^{-1})$
0.10	7.98	6.97
0.20	7.72	7.18
0.30	7.41	7.39

5.6 SP–PLP–NIR Experiments

5.6.1 Experimental Procedure

The length of the sealing punches of the optical high-pressure cell was chosen such that the path length of the internal cell amounted to approximately 1.6 mm. This small path length was chosen to ensure detector linearity for various monomer concentrations. The optical high-pressure cell was equipped with an empty internal cell, pressurized to 50 bar and brought to the desired temperature. Temperature constancy was checked on-line. The cell was positioned into the optical path of the SP–PLP–NIR setup and the solid granite slab was brought to a horizontal position. The operating high voltage of the exciplex laser

was calibrated against the energy detector being placed between high-pressure cell and UV mirror UVM3 by means of the C++ program “Calibration.cpp” (appendices B.1 and C.1). Subsequently, the high-pressure cell was inserted into the sample compartment of the FT–NIR spectrometer to record the background signal. InSb-detectors usually show a less pronounced dependence of detectivity on wavelength than InAs-detectors. Therefore, an InSb-detector was used to determine FT–NIR spectra of the entire absorption band. However, the detectivity of InSb-detectors at the absorption maximum of the band of interest is lower compared to InAs-detectors. Thus, for SP–PLP–NIR experiments, in which light of a small wavelength range impinges on the detector, an InAs-detector was used.

The samples for SP–PLP–NIR experiments were prepared as described in chapter 5.3.1 for PLP–SEC high-pressure experiments, however, purified monomers were used instead. Initial photoinitiator concentrations between 1 and 5 mmol·L⁻¹ were used. The internal cell was inserted into the high-pressure cell. After pressurization, an initial FT–NIR spectrum was recorded and the cell was inserted into the SP–PLP–NIR setup. The monochromator diffraction grating was oriented such that the wavenumber of light which predominantly passes the monochromator corresponds to the absorption maximum of the first overtone of the antisymmetric carbon–hydrogen stretching vibration of the methyldene group at about 6100–6250 cm⁻¹. In SP–PLP–NIR experiments all light intensities are determined as voltages. The light intensity at channel 2 (denoted as channel 8 in setup A) prior to polymerization, *I*₀₀₂, was recorded by means of the USB multifunction data-acquisition board. This value was adjusted to approximately 0.3 V via the width of the monochromator slits. Significantly lower values result in a small signal-to-noise ratio whereas too high values would hamper the application of a compensating voltage because it could exceed the maximum output voltage of the multifunction data-acquisition board. The operating high voltage of the exciplex laser was chosen to yield adequate pulse energies. In SBench the number of data points collected during measurement was set to be 2¹⁴ in the time interval prior to the trigger event and 3·2¹⁴ in the post-trigger region. For setup A, an input range of ±1 V was used whereas ±500 mV were used for setup B. Neither the SBench signal scaling function nor a software-

selectable input offset was applied. The sampling rate can be varied from 1 kHz to 3 MHz in setup B with the phase-locked loop using an internal 10 MHz reference. Therefore, time resolutions of 1 ms to 333 ns are available. In setup A the maximum sampling rate was limited to 2 MHz yielding a time resolution of down to 500 ns. The sampling time is defined by the sampling rate and the number of collected data points. In SP–PLP–NIR experiments the light intensity after application of a single laser pulse is monitored in dependence on time. To increase the signal-to-noise ratio, several consecutive intensity versus time profiles were averaged while keeping the total range of the degree of monomer conversion below approximately 0.05. The number of pulses of such a sequence was set in SBench as well as in the C++ program “Measurement.cpp” which is responsible for controlling the electronic devices of the setup and for determination of signals other than time-resolved ones. Prior to each laser pulse the signal at channel 3 (denoted as channel 10 in setup A) with electromagnetic shutter Sh2 being open was determined and applied as compensating voltage to the amplifier and compensator unit. Before and after each pulse sequence the signal at channel 2 was measured and saved as *I02* and *I2*, respectively. FT–NIR spectra were recorded at an interval of the degree of monomer conversion of about 0.05. The correct positioning of the high-pressure cell in the SP–PLP–NIR setup was verified checking for a proper signal at channel 2. Pulse sequences were applied until the sample became inhomogeneous. The C++ source codes and the corresponding flowcharts of setup B given in appendices B.1, B.2, C.1, and C.2 provide detailed insight into the course of the experiment. The source codes of setup A were written by Feldermann.^[208]

5.6.2 Data Evaluation

The overall degree of monomer conversion may, in principal, be determined via the data measured at channel 2. However, the IR light is refracted and scattered by the sample to different extents during the course of polymerization resulting in large uncertainties in monomer conversion. In case of FT–NIR spectra, focusing or dispersing the light would result in a shift of the baseline which is overcome by integration of the absorption band over a large wavenumber range using a baseline fitted to the boundary points of the band.

To a small extent, these integrals are, nevertheless, affected by refraction and scattering of the light as well because of the frequency dependence of refraction and scattering. Background absorption additionally hampers the determination of monomer conversion via the data measured at channel 2. Reliable integration of the absorption band may be obtained by proper baseline fitting to reduce interference caused by band overlap. Degrees of monomer conversion determined by means of FT–NIR spectra were used to calculate virtual *I002* values for each pulse sequence to conform with absolute degrees of monomer-to-polymer conversion whereas time-resolved data remain unchanged.

FT–NIR spectra were evaluated similar to the procedure given in chapter 5.5.2 to determine degrees of monomer conversion. The absorption band of PAm was integrated between 6105 and 6270 cm^{-1} via OPUS method F. An individual baseline was generated for each spectrum by least-squares fitting of a parabola to the data points between 6075 and 6100 cm^{-1} as well as between 6275 and 6300 cm^{-1} . In case of VP, OPUS method F was used to integrate the absorption band between 6110 and 6280 cm^{-1} . The baseline was generated using the data points between 6105 and 6110 cm^{-1} as well as between 6300 and 6400 cm^{-1} . DM-PAm spectra, however, were analyzed using OPUS method G, which looks for the highest peak between two boundary values and for the minima on the two sides of the peak. The boundary values were chosen to be 6090 and 6280 cm^{-1} . The baseline linearly connects the two minima, which define the integration range in addition.

The determination of virtual *I002* values, which is described in the following, was mainly carried out by using the software MATLAB® (MathWorks, release R2011a, version 7.12) with the functions given in appendix D.1 for setup B. The computation in case of setup A was performed with MATLAB® functions (MathWorks, release R12.1, version 6.1) described by Junkers.^[209] Several quantities are needed to determine virtual *I002* values for a pulse sequence. It is assumed that each laser pulse applied between recording two consecutive FT–NIR spectra results in the same consumption of monomer. Such average degree of conversion, $\bar{\alpha}$, may be expressed by:

$$\bar{\alpha} = \frac{\alpha_{ak} - \alpha_{bj}}{\sum_{i=j}^k n_i} \quad (\text{eq. 5.15})$$

with α_{ak} being the degree of monomer conversion after applying pulse sequence k , which is the last of a set of pulse sequences applied between the recordings of the two FT–NIR spectra, and α_{bj} being the degree of monomer conversion prior to pulse sequence j , which is the first of the set of pulse sequences. n_i denotes the number of pulses of pulse sequence i .

The degree of monomer conversion before pulse sequence i , α_{bi} , may be calculated by means of the sum of the number of laser pulses of sequences l , n_l .

$$\alpha_{bi} = \alpha_{bj} + \bar{\alpha} \cdot \left(\sum_{l=j}^i n_l - n_i \right) \quad (\text{eq. 5.16})$$

The degree of monomer conversion after pulse sequence i , α_{ai} , is given by:

$$\alpha_{ai} = \alpha_{bj} + \bar{\alpha} \cdot \sum_{l=j}^i n_l \quad (\text{eq. 5.17})$$

The solution density at reaction conditions and zero monomer conversion, ρ^0 , was estimated via:

$$\rho^0 = \frac{m_M + m_{\text{Sol}}}{m_M/\rho_M + m_{\text{Sol}}/\rho_{\text{Sol}}} \quad (\text{eq. 5.18})$$

Combining ρ^0 with the degrees of monomer conversion given in equations 5.16 and 5.17, artificial density losses before and after pulse sequence i , $\Delta\rho_{\text{art},bi}$ and $\Delta\rho_{\text{art},ai}$, respectively,

can be described by equations 5.19 and 5.20. These density losses have no exact physical meaning but may be expressed in units of a density.

$$\Delta\rho_{\text{art},bi} = \alpha_{bi} \cdot \rho^0 \quad (\text{eq. 5.19})$$

$$\Delta\rho_{\text{art},ai} = \alpha_{ai} \cdot \rho^0 \quad (\text{eq. 5.20})$$

Monomer concentration at zero monomer conversion and reaction pressure was determined via:

$$c_{M,p}^0 = c_{M,p^\circ}^0 \cdot \frac{\rho^0}{\rho_{p^\circ}^0} \quad (\text{eq. 5.21})$$

with the subscript p° denoting ambient pressure.

A virtual molar mass, M_{virt} , taking the presence of monomer and solvent into account may be described by:

$$M_{\text{virt}} = \frac{\rho^0}{c_{M,p}^0} \quad (\text{eq. 5.22})$$

By means of equations 3.30, 5.19, and 5.22, $\Delta\rho_{\text{art},bi}$ may also be described by:

$$\Delta\rho_{\text{art},bi} = M_{\text{virt}} \cdot \alpha_{bi} \cdot c_{M,p}^0 = M_{\text{virt}} \cdot (c_{M,p}^0 - c_{M,p,bi}) \quad (\text{eq. 5.23})$$

with $c_{M,p,bi}$ denoting the monomer concentration before applying pulse sequence i . The same holds for $\Delta\rho_{\text{art},ai}$.

The path length of the internal cell at reaction conditions may be estimated via the path length determined at ambient pressure and temperature, $l_{p^0,rt}$, the solution density at ambient pressure, ambient temperature, and zero monomer conversion, $\rho_{p^0,rt}^0$, and the solution density at reaction conditions and zero monomer conversion. This estimate is associated with the assumption that pressurization influences the path length, as a result of a displacement of the optical windows of the internal cell, but not the diameter of the internal cell.

$$l_{rc} = l_{p^0,rt} \cdot \frac{\rho_{p^0,rt}^0}{\rho^0} \quad (\text{eq. 5.24})$$

$\rho_{p^0,rt}^0$ may be determined via equation 5.18 using the densities given in equations 5.3 to 5.9.

In case of identical monochromator entrance and exit slit widths, B , the spectral range exiting the monochromator, $\Delta \tilde{\nu}$, may be estimated by:

$$\Delta \tilde{\nu} = \left(\frac{1}{\tilde{\nu}_{\text{peak}}} - \frac{B}{2} \cdot \left(\frac{d\lambda}{dx} \right) \right)^{-1} - \left(\frac{1}{\tilde{\nu}_{\text{peak}}} + \frac{B}{2} \cdot \left(\frac{d\lambda}{dx} \right) \right)^{-1} \quad (\text{eq. 5.25})$$

$\tilde{\nu}_{\text{peak}}$ represents the wavenumber at the maximum of the absorption band and $d\lambda/dx$ the reciprocal linear dispersion.

The effective decadic absorbance, $A_{10,\text{eff}}$, may be determined by integration of the absorption band in the range which is defined by the two bracketed terms of equation 5.25 combined with:

$$A_{10,\text{eff}} = \frac{\int A_{10}(\tilde{\nu}) d\tilde{\nu}}{\Delta \tilde{\nu}} \quad (\text{eq. 5.26})$$

Integration was conducted by using the methods given above. DM-PAm spectra, however, were analyzed using OPUS method C, which uses a straight line connecting two predefined points as baseline. The baseline points were chosen to be 6090 and 6280 cm^{-1} . The effective decadic molar absorption coefficient corresponding to $A_{10,\text{eff}}$, ε_{eff} , reads:

$$\varepsilon_{\text{eff}} = \frac{A_{10,\text{eff}}}{c_{\text{M},p}^0 \cdot l_{\text{rc}}} \quad (\text{eq. 5.27})$$

Plugging the results of equations 5.19, 5.22, 5.24, and 5.27 into equation 5.28 allows for determination of the $I002$ value before pulse sequence i , $I002_{bi}$, according to the Beer–Lambert–Bouguer law and equation 5.23.

$$I002_{bi} = I02_i \cdot 10^{-\varepsilon_{\text{eff}} \cdot \frac{\Delta\rho_{\text{art},bi}}{M_{\text{virt}}} \cdot l_{\text{rc}}} \quad (\text{eq. 5.28})$$

The $I002$ value after pulse sequence i , $I002_{ai}$, may be expressed analogously:

$$I002_{ai} = I2_i \cdot 10^{-\varepsilon_{\text{eff}} \cdot \frac{\Delta\rho_{\text{art},ai}}{M_{\text{virt}}} \cdot l_{\text{rc}}} \quad (\text{eq. 5.29})$$

The $I002$ value for pulse sequence i , $I002_i$, may be described as the arithmetic mean of $I002_{bi}$ and $I002_{ai}$:

$$I002_i = \frac{I002_{bi} + I002_{ai}}{2} \quad (\text{eq. 5.30})$$

A second MATLAB[®] function with its subfunctions (appendix D.2) was used to determine termination rate coefficients. The artificial densities $\rho_{\text{art},bi}$ and $\rho_{\text{art},ai}$ are reevaluated using virtual $I002$ values.

$$\Delta\rho_{\text{art},bi} = -M_{\text{virt}} \cdot \frac{\lg\left(\frac{1002_i}{102_i}\right)}{l_{\text{rc}} \cdot \varepsilon_{\text{eff}}} \quad (\text{eq. 5.31})$$

$$\Delta\rho_{\text{art},ai} = -M_{\text{virt}} \cdot \frac{\lg\left(\frac{1002_i}{12_i}\right)}{l_{\text{rc}} \cdot \varepsilon_{\text{eff}}} \quad (\text{eq. 5.32})$$

Compared with equation 5.23, the absolute value of the arithmetic mean of the artificial densities may be described by:

$$\overline{\Delta\rho_{\text{art},i}} = \left| \frac{\Delta\rho_{\text{art},bi} + \Delta\rho_{\text{art},ai}}{2} \right| = M_{\text{virt}} \cdot \alpha_i \cdot c_{\text{M},p}^0 \quad (\text{eq. 5.33})$$

α_i represents the arithmetic mean of the degrees of monomer conversion before and after pulse sequence i and may be described by:

$$\alpha_i = 1 - \frac{c_{\text{M},p,i} \cdot M_{\text{virt}}}{\rho^0} \quad (\text{eq. 5.34})$$

with $c_{\text{M},p,i}$ being the average monomer concentration occurring during pulse sequence i .

The artificial density occurring during pulse sequence i , $\rho_{\text{art},i}$, may be expressed by:

$$\rho_{\text{art},i} = \rho^0 - \overline{\Delta\rho_{\text{art},i}} \quad (\text{eq. 5.35})$$

Plugging in equations 5.22 and 5.33 yields:

$$\rho_{\text{art},i} = M_{\text{virt}} \cdot (c_{\text{M},p}^0 - \alpha_i \cdot c_{\text{M},p}^0) \quad (\text{eq. 5.36})$$

which is equivalent to:

$$c_{\text{M},p,i} = \frac{\rho_{\text{art},i}}{M_{\text{virt}}} \quad (\text{eq. 5.37})$$

The decadic absorbance before pulse sequence i , $A_{10,bi}$, may be calculated via:

$$A_{10,bi} = \varepsilon_{\text{eff}} \cdot l_{\text{rc}} \cdot \left(\frac{\rho^0}{M_{\text{virt}}} - \frac{\Delta \rho_{\text{art},bi}}{M_{\text{virt}}} \right) \quad (\text{eq. 5.38})$$

Time-resolved data, determined by the transient recorder, do not allow for determination of monomer concentrations due to the application of a compensating voltage which hampers detection of absolute voltages. Monomer concentration versus time profiles have therefore to be derived by combination of the time-resolved data with data determined by the above-mentioned procedure which may be done via equation 5.39 for single pulses. Before, 16 consecutively measured time-resolved voltage values were averaged to improve the signal-to-noise ratio. The corresponding time value was set to be the mean value of the first and the last time values.

$$\frac{c_{\text{M},p,i}(t)}{c_{\text{M},p,bi}} = 1 - \frac{1}{A_{10,bi}} \cdot \lg \left(\frac{102_i + (U_{\text{post}}(t) - \overline{U_{\text{pre}}}) / \text{amp}}{102_i} \right) \quad (\text{eq. 5.39})$$

$U_{\text{post}}(t)$ denotes the voltage value determined by the transient recorder after applying a laser pulse, $\overline{U_{\text{pre}}}$ denotes the average value of a chosen number of voltage values determined before applying the laser pulse, and amp is the amplification factor mentioned in chapter 4.10 to be one hundred. The logarithmic term in equation 5.39 is proportional

to the difference in absorbances when applying the laser pulse and at time t . However, equation 5.39 cannot be used for a sequence of pulses by using voltages determined by the transient recorder which were averaged for several pulses. Instead, the total difference in absorbances has to be determined for the pulse sequence and averaged afterwards because of the virtual change in initial light intensity. This may be carried out via:

$$\frac{c_{M,p,i}(t)}{c_{M,p,bi}} = 1 - \frac{1}{A_{10,bi} \cdot n_i} \cdot \lg \left(\frac{102_i + n_i \cdot (U_{\text{post}}(t) - \overline{U_{\text{pre}}}) / \text{amp}}{102_i} \right) \quad (\text{eq. 5.40})$$

Equation 3.56 was fitted to the resulting monomer concentration versus time profiles using the Levenberg–Marquardt algorithm. The MATLAB® function used for this purpose allows for fitting to a set data range starting at $t = 0$. Termination rate coefficients may thereby be fitted up to a predefined degree of polymerization of the growing radicals.

5.7 Curve Fitting

Fitting of mathematical functions to experimental data was conducted by means of the software ORIGIN® (OriginLab®, version 6.1 or version Pro 8.0951) except for curve fitting described in chapter 5.6.2. Linear fitting with ORIGIN® is carried out applying the method of least squares. For non-linear curve fitting the Levenberg–Marquardt algorithm is used to iteratively adjust the parameters. The tolerance required for the fitting algorithm was set to $1 \cdot 10^{-9}$.

5.8 Determination of Joint Confidence Regions

The program Contour (A. M. van Herk, version 1.8) was used to generate ellipses corresponding to 95 % joint confidence regions for the Arrhenius activation energy and

the Arrhenius pre-exponential factor of k_p . The principles of the program are outlined in the literature.^[210,211]

5.9 Experimental Conditions

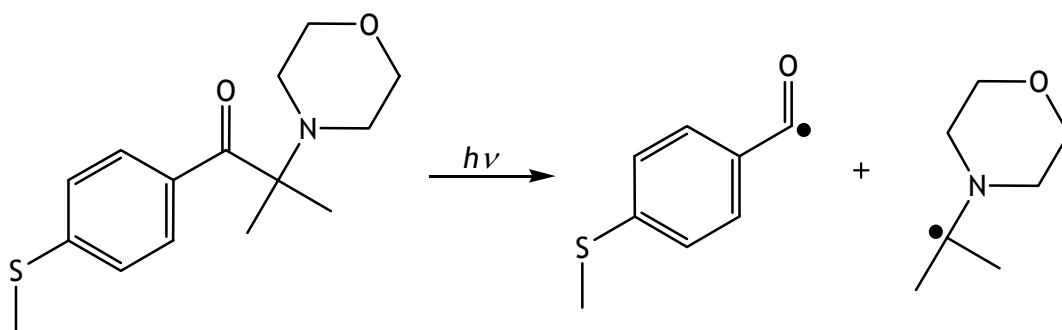
5.9.1 Photoinitiator

Photoinitiators used for PLP experiments are subject to several requirements. They have to decompose at the wavelength of the laser which has been chosen to be 351 nm. This wavelength is convenient because most monomers do not absorb at this wavelength. Applying lower energy radiation may be inefficient for initiator decomposition whereas at lower wavelength the monomer may absorb part of the light. Photoinitiator decomposition has to be fast compared to chain initiation in order to ensure a narrow molar-mass distribution of the produced polymer which requires identical fast reactivity of both primary radicals concerning chain initiation and chain termination as well. Furthermore, the photoinitiator should neither undergo side reactions nor decompose thermally at the chosen reaction conditions. Using photoinitiators fulfilling all of these requirements, so-called ideal initiators, results in the narrowest possible molar-mass distribution of the produced polymer. Thereby, the chain-length dependence of the termination rate coefficient may be evaluated by fitting time-resolved data on monomer consumption. Moreover, the accuracy of PLP–SEC experiments is increased.

Azo compounds may decompose thermally or photochemically. Only azo compounds exhibiting a low rate coefficient of initiator decomposition can be taken into account for PLP studies. However, nitrogen production may hamper spectroscopic analysis in SP–PLP–NIR experiments. In addition, quantum yields of such initiators are usually rather low. Aliphatic acyclic azo compounds usually exist as *trans* isomer and are, by UV irradiation, excited to a state which decays, to similar extents, to *cis* and *trans* ground states. If the *cis* isomer is thermally instable, it may decompose as distinguished from the *trans* isomer. Therefore, the quantum yield of initiator decomposition is usually below 0.5.^[212]

Peroxides may be used as thermally or photochemically decomposing initiator as well. This requires taking the rate coefficient of initiator decomposition into account. Furthermore, the primary radicals generated from peroxides may undergo side reactions.^[213–215]

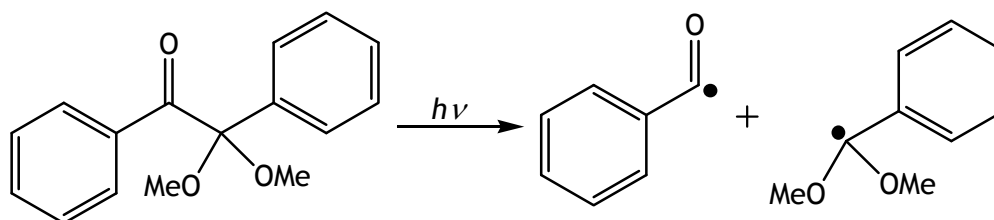
Commonly used photoinitiators for PLP experiments are carbonyl compounds which may undergo a Norrish type I^[216] photoreaction. Investigations into polymerizations of methyl acrylate^[217,218] and dicyclohexyl 2-methylidenebutanedioate^[218] initiated by 2-methyl-1-[4-(methylsulfanyl)phenyl]-2-(morpholin-4-yl)propan-1-one (MMMP) revealed that MMMP is a close-to-ideal photoinitiator, at least for these two monomers. The decomposition of the initiator generates two radicals, one of which may be stabilized by the electron-donating capability of the adjacent nitrogen atom.



A general statement concerning the ideality of MMMP cannot be made because detailed investigations were conducted for only two monomers. As one of the two primary radicals is electron-rich and the carbon–carbon double bonds of methyl acrylate and dicyclohexyl 2-methylidenebutanedioate are electron-deficient, it is unlikely that MMMP is appropriate for polymerizations of monomers bearing electron-rich double bonds. Only initiators generating two identical primary radicals may overcome this problem.

Due to the poor solubility in aqueous solution, MMMP was not used within the present work. Darocur 1173, DMPA, and HHMP were used instead. Darocur 1173 and HHMP may be electronically similar to MMMP and thus be close-to-ideal for monomers resembling methyl acrylate and dicyclohexyl 2-methylidenebutanedioate. DMPA is known to be a non-ideal initiator. It decomposes into a benzoyl radical and an

α,α -dimethoxybenzyl radical which is stabilized via the phenyl ring as well as via the electron-donating capability of two adjacent oxygen atoms.^[219]



The α,α -dimethoxybenzyl radical contributes to chain termination whereas its reactivity relating to initiation is low.^[219–222] Due to this predominantly inhibiting nature of one primary radical, the monomer concentration versus time traces determined by SP–PLP–NIR experiments at different initial DMPA contents, but otherwise identical reaction conditions, may intersect each other.^[223] At low radical concentrations, the impact of the poorly initiating primary radical is, however, negligible and the resulting $\langle k_t \rangle$ values are close to true average termination rate coefficients, although non-ideal behavior of the initiator is not contained in the kinetic scheme used for data analysis.^[224] Low radical concentrations can be obtained by suitable selection of initiator concentration and laser pulse energy. In PLP–SEC experiments, the non-ideality of DMPA does not influence the results as the inhibiting fragment may only increase the amount of background polymer which does not show a PLP structure. In the worst case, the PLP structure may be lost thus allowing for no k_p determination.

DMPA was mostly used because the weighing out of predefined small amounts of substances is easier in case of solids. Darocur 1173, which is liquid at ambient pressure and temperature, was used for low monomer contents where DMPA is poorly soluble. HHMP was chosen for the binary copolymerizations.

5.9.2 Tube Material of the Internal Cell

The tube material of the optical internal cell for high-pressure experiments has been chosen to be PTFE due to its chemical resistance^[225] and its low permeability towards gases. With respect to gas permeability, the focus is on oxygen because of its influence on the kinetics. A comparison with other materials such as PFA is, however, hardly feasible.^[226] The permeability depends on various factors, such as the material's microstructure^[227] and thus the manufacturing process as well as temperature^[228]. Furthermore, the gas tightness of the contact area of PTFE tube und optical window has to be taken into account. This tightness strongly depends on the dimensions of both tube and window, on the individual surface finish of tube and window as well as on the abrasion resistance of the tube material.

5.9.3 Reaction Conditions

PLP–SEC Experiments

Arrhenius activation energies for ambient pressure PLP–SEC experiments were determined in a wide range of temperature from 10 to 80 °C. The upper limit results from the recommended temperature range for the aqueous ethane-1,2-diol solution, which was used as heat transfer fluid, and for the quick disconnect couplings, which were used to connect cuvettes and heated/refrigerated circulating bath. At temperatures below 10 °C freezing of aqueous monomer solutions and condensation of water on the cuvettes' surfaces may be expected.

Further experiments were conducted at 40 °C and pressures up to 2000 bar to determine the volume of activation of k_p . Monomer concentrations were chosen such as to cover a wide concentration range. Whereas DM-PAm is soluble in water at ambient pressure and temperature in the full concentration range, M-MPAm is soluble from 0.60 g·g⁻¹ on, MPAm is soluble up to 0.20 g·g⁻¹, and PAm up to at least 0.50 g·g⁻¹. Initiator concentrations of 1 to 3 mmol·L⁻¹ and laser pulse energies of 10 to 55 mJ·cm⁻² were mostly used to obtain well-pronounced PLP structures. The number of pulses was

selected to be between 5 and 1000, such as to reach a degree of monomer conversion of approximately 0.05 to produce a sufficient amount of polymer for SEC analysis. The LPRR was mostly chosen to be 20 Hz in case of MPAm and M-MPAm, whereas 100 Hz was used for DM-PAm, 150 Hz for PAm, and 40 to 400 Hz for the binary copolymerization of NaA and VP. Copolymerizations were conducted at a total monomer mole fraction of $0.05 \text{ mol} \cdot \text{mol}^{-1}$. This rather small amount of monomer allows for a variation of the composition of the reaction solution from pure aqueous NaA to pure aqueous VP solution. Contrary to VP, which is soluble in water at ambient pressure and temperature in the full concentration range, sodium acrylate is solid and thus limits the maximum monomer content.

SP–PLP–NIR Experiments

The signal-to-noise ratio in SP–PLP–NIR experiments scales with monomer conversion per pulse. This ratio is favored by high propagation and low termination rate coefficients. As k_p increases towards higher pressure whereas k_t decreases, experiments at high pressure are beneficial for the signal-to-noise ratio. Increasing temperature may also improve the signal-to-noise ratio due to the Arrhenius activation energy of k_t usually being lower than the one of k_p . However, the small difference in activation energies makes pressure variations much more effective than changes in temperature. Therefore, the experiments have mostly been performed at 40 °C and 2000 bar. The volume of activation of k_t was determined by reducing the pressure down to 500 bar. SP–PLP–NIR experiments were usually carried out up to the monomer conversion where the reaction mixture turned inhomogeneous. Initial monomer concentrations were chosen such as to cover a large concentration range. To obtain a sufficient signal-to-noise ratio, monomer mass fractions of at least $0.20 \text{ g} \cdot \text{g}^{-1}$ were used.

Chemically Initiated Polymerizations

In case of chemically initiated polymerizations, the reaction was induced by thermal decomposition of V-50. Experiments were conducted at 50 °C and ambient pressure. Initiator concentrations of 0.05 to 0.005 mol·L⁻¹ were used. Monomer concentrations of 0.10, 0.20, and 0.30 g·g⁻¹ were chosen. Lower monomer concentrations result in poor signal-to-noise ratios. At higher monomer contents the reaction solution gets highly viscous which renders sample removal from the cuvette almost impossible.

More details on the selection of experimental conditions are given in the experimental results section in chapters 6 to 9.

5.10 ¹H NMR Spectroscopy

¹H NMR spectra were recorded in thin-walled tubes (VWR, 4.95 mm outside diameter, wall thickness of 0.43 mm, length of 178 mm, camber of 2.5 μm, concentricity of 3.8 μm, suitable for 700 MHz) at solute mass concentrations of typically 5 to 30 g·L⁻¹. Spectra were determined at 35 °C in dideuterium oxide using an acquisition time of 3.128 s and an FID resolution of 0.160 Hz. To improve the signal-to-noise ratio, 16 or 32 FIDs were co-added. The number of data points within the measuring range was 31 968 in case of the *MERCURY* spectrometer and 30 264 for the *VNMRS* spectrometer. Because of differing relaxation times of the individual spins, either the time difference between two consecutive radio-wave pulses or the pulse angle has to be adapted to the sample under investigation. Owing to a limited memory capacity, an increase in acquisition time was not possible. Therefore, an additional time delay without data acquisition was introduced. In case of polymer samples, a time delay of 5 s and a pulse angle of 84° were used. These parameters were verified to be suitable by checking for consistency of signal intensities of poly[(acrylic acid)-*co*-(1-vinylpyrrolidin-2-one)] (poly(AA-*co*-VP)) using delay times of 5, 30, 60, and 90 s. In case of monomer solutions, a time delay of 3 s and a significantly reduced pulse angle of 10° were chosen. These parameters were determined to be adequate by studying ¹H NMR spectra of acrylic acid in dideuterium oxide. The signals corresponding

to the three hydrogen atoms connected to the carbon–carbon double bond were investigated under variation of the pulse angle at a constant time delay of 3 s as well as under variation of the time delay at a constant pulse angle of 90° . The integrals are given in tables 5.3 and 5.4. Small deviations from the ideal ratio of 1:1:1 may be ascribed to errors in data analysis. The hydrogen atoms are denoted as α , *cis*, and *trans* referring to the hydrogen atoms joined to the α -carbon and in *cis* and *trans* position to the alpha hydrogen atom, respectively.

Table 5.3: Relative ^1H NMR signal intensities of the hydrogen atoms connected to the carbon–carbon double bond of acrylic acid at a pulse angle of 90° ; α , *cis*, and *trans* denote the hydrogen atoms joined to the α -carbon and in *cis* and *trans* position to the alpha hydrogen atom, respectively.

<i>delay/s</i>	α	<i>cis</i>	<i>trans</i>
60	1.000	0.992	1.000
50	1.000	1.046	1.026
40	1.000	1.049	1.038
30	1.000	1.098	1.090
20	1.000	1.196	1.188
3	1.000	1.604	1.511

Comparison of the set of spectra at constant pulse angle tells that the change in intensity of the signal corresponding to the hydrogen atom denoted by α is most pronounced. This indicates that the relaxation time of this hydrogen atom is much larger compared to the other two which is in agreement with the finding that the intensity of the signal corresponding to the hydrogen atom denoted by α is lowest.

Table 5.4: Relative ^1H NMR signal intensities of the hydrogen atoms connected to the carbon–carbon double bond of acrylic acid at a delay time of 3 s; α , *cis*, and *trans* denote the hydrogen atoms joined to the α -carbon and in *cis* and *trans* position to the alpha hydrogen atom, respectively.

<i>pulse angle</i>	α	<i>cis</i>	<i>trans</i>
10°	1.000	0.993	0.994
20°	1.000	1.033	1.028
30°	1.000	1.106	1.091
40°	1.000	1.189	1.147
50°	1.000	1.297	1.260
60°	1.000	1.377	1.315
70°	1.000	1.467	1.394
80°	1.000	1.540	1.450
90°	1.000	1.604	1.511

A zero-filling factor of two was applied to the FID. The built-in MestReNova window functions “Exponential” and “Sync” (2.000) were used for apodization. Baseline correction was conducted using the Bernstein Polynomial Fit algorithm which uses a polynomial for interpolation. The residual proton signal of the deuterated solvent served as internal standard for the ^1H NMR spectra using chemical shifts known from the literature.^[229]

5.11 Error Estimates

Pressure

The Bourdon tube pressure gauges described in chapter 4.5 feature an accuracy class of 0.1 which describes the inaccuracy at the maximum rated pressure expressed as percentage. Absolute errors of the Bourdon tube pressure gauges may be assumed to be less than ± 2.5 bar in case of PLP–SEC studies and less than ± 4 bar concerning SP–PLP–

NIR experiments. At 2000 bar, an error of ± 6 bar may be assumed for the absolute pressure transducer in combination with the measuring amplifier. The inaccuracies should be smaller at lower pressure because the pressure gauges and the transducer were adjusted at ambient pressure prior to each experiment.

Temperature

The thermocouple used in high-pressure experiments is specified to be accurate to ± 0.25 °C. The PID controllers are accurate to ± 0.2 °C. They regulate the temperature within ± 0.2 °C, which results in an overall accuracy of ± 0.65 °C.

In case of ambient pressure experiments in cuvettes as well as in case of viscosity determination, an error of ± 1 °C is estimated on the basis of manufacturer's information.

The temperature in the pH measurements is precise to ± 0.1 °C. The temperature accuracy in density measurements is expected to be ± 0.2 °C.

pH

The inaccuracy of the pH values is given by the manufacturer to be ± 0.002 . However, an accuracy of ± 0.01 may be assumed because of fluctuations.

Density

The density meter is specified to be accurate to $\pm 1.5 \cdot 10^{-6}$ g·cm⁻³. Because of fluctuations and small changes in temperature, the measurement inaccuracy is assumed to be $\pm 5 \cdot 10^{-4}$ g·cm⁻³.

Viscosity

The accuracy of viscosity measurement is expected to be better than ± 0.01 mPa·s.

¹H NMR Integral

Integrals of signals corresponding to hydrogen atoms within monomer molecules are estimated to be precise to ± 1 %. Spectral analysis of polymer samples is much more challenging, especially because of baseline correction which may result in an overall inaccuracy of ± 5 %.

Initial Concentration

For preparing the reaction solutions, an analytical balance with an accuracy of ± 0.1 mg and volumetric flasks with an uncertainty in volume of ± 0.5 % were used. Concentrations were extrapolated to reaction conditions using reported density data. The overall error is estimated to be less than ± 3 %.

Monomer Concentration from FT–NIR

Repeated recording of spectra of the same sample shows slightly different results. Further errors are introduced by the window function used for apodization and the mode of phase correction. In conjunction with uncertainties of the baseline, the error of the integrated absorbance is estimated to be less than ± 3 % at monomer concentrations above $0.10 \text{ g}\cdot\text{g}^{-1}$ but may increase up to ± 50 % at monomer concentrations below $0.01 \text{ g}\cdot\text{g}^{-1}$.

Propagation Rate Coefficient from PLP–SEC

The error of k_p determination by PLP–SEC originates from inaccuracies in monomer concentration and in degree of polymerization. The latter error may be ascribed to broadening of the MMD, to the calculation of the degree of polymerization via the POI of the MMD, and to the usage of a monomer-dependent but otherwise universal factor which correlates the POIs obtained by direct MMD determination and by calibrant-relative calibration. These errors add up to a total of ± 25 %.

Termination Rate Coefficient from SP–PLP–NIR

The accuracy of $\langle k_t \rangle$ deduced from SP–PLP–NIR is highly dependent on signal quality, on deviations of polymerization kinetics from ideality, and on data evaluation. The latter relates, amongst others, to errors in path length, to errors in monochromator slit width, to errors in the degree of monomer conversion, to errors in k_p , to assumptions made concerning monomer concentration, and to the fitting algorithm. Additionally, the accuracy of measured voltage values as well as the temperature dependence of the optical components and thus the constancy of the light intensity have to be considered. It is expected that the total error of $\langle k_t \rangle$ does not exceed $\pm 50\%$ for most of the polymerizations under investigation.

Termination Rate Coefficient from Chemically Initiated Polymerization

The accuracy of $\langle k_t \rangle$ deduced from chemically initiated polymerizations depends on signal quality, deviations of the polymerization kinetics from ideality, consistency of repeated experiments, analysis of the spectra, and data evaluation. The overall error is governed by the accuracy of monomer concentration, of k_p , of k_d as well as of the initiator efficiency, by the determination of the inhibition period, and by the temperature dependence of the optical components. The overall error of $\langle k_t \rangle$ is estimated to be below $\pm 50\%$ for most polymerizations under investigation.

The errors of parameters which are deduced by curve fitting are determined using statistical methods. They are mostly given together with the respective value in the text.

6 Termination Kinetics of 1-Vinylpyrrolidin-2-one Polymerization

1-Vinylpyrrolidin-2-one (VP) is a suitable candidate for detailed studies into the termination kinetics of water-soluble monomers as water represents a good solvent for VP and as poly(VP) is well soluble in both monomer and water. Thus, broad ranges of initial monomer concentration and monomer-to-polymer conversion may be covered. The high propagation rate coefficient of VP is beneficial for the signal-to-noise quality of SP–PLP–NIR experiments. Furthermore, VP polymerization appears to be less or even not prone to inter- and intramolecular chain-transfer reactions^[45] which reduces the complexity of the kinetic scheme^[19,230].

Investigations into the termination kinetics of VP in aqueous solution were performed at 40 °C and initial VP concentrations of 2.63, 4.19, 4.70, 5.21, 7.23, and 8.23 mol·L⁻¹ corresponding to 0.25, 0.40, 0.45, 0.50, 0.70, and 0.80 g·g⁻¹ VP, respectively. The experiments were carried out at 2000 bar to achieve a better signal-to-noise ratio. As the compressibility of the polymerizing system is rather low, there is no reason to assume that high pressure affects the termination mechanism.^[32] To further improve signal-to-noise quality, D₂O was used as the solvent rather than H₂O. As already stated in chapter 5.5.2, D₂O exhibits a largely reduced NIR absorbance in the wavenumber range of interest. Investigations into the radical polymerization of 2-methyl-2-(prop-2-enamido)propane-1-sulfonic acid or acrylic acid in aqueous solution have not provided any indication of experimental $\langle k_t \rangle / k_p$ values being significantly different in H₂O and in D₂O.^[71,231]

Additional experimental data were taken from Hesse^[232] and included in curve fitting. The following section has already been published in the literature.^[113]

6.1 Multidimensional Dependence of the Propagation Rate Coefficient on Reaction Conditions

Propagation rate coefficients need to be known to determine $\langle k_t \rangle$ from the primary experimental quantity $\langle k_t \rangle / k_p$. The dependence of k_p on initial monomer concentration for 40 °C and 2000 bar has been reported by Hesse^[232] to be given by the following expression:

$$k_p / \text{L} \cdot \text{mol}^{-1} \cdot \text{s}^{-1} = 64000 \cdot (0.33 + 0.67 \cdot \exp(-7.7 \cdot w_{\text{VP}}) - 0.27 \cdot w_{\text{VP}}) \quad (\text{eq. 6.1})$$

where w_{VP} is the mass fraction of monomeric VP in water (dideuterium oxide). It was recently shown, that k_p depends on the monomer-to-water ratio, whereas the content of high-molar-mass polymer plays no role.^[43,45] The mass fraction of VP, w_{VP} , during polymerization to high degrees of monomer conversion may be represented by equation 6.2:

$$w_{\text{VP}} = \frac{w_{\text{VP}}^0 \cdot (1 - \alpha)}{1 - w_{\text{VP}}^0 \cdot \alpha} \quad (\text{eq. 6.2})$$

with w_{VP}^0 denoting the initial mass fraction of VP.

As mentioned by Beuermann et al.,^[43] polymer may affect k_p only under conditions of very high polymer content or in case that polymer is of low molar mass and should be better referred to as oligomeric material. Combining equations 6.1 and 6.2 with the volume of activation for propagation of VP, $\Delta^\ddagger V^\circ(k_p) = -11.3 \text{ cm}^3 \cdot \text{mol}^{-1}$,^[232] yields k_p for 40 °C as a function of pressure, initial mass fraction of VP, and degree of monomer conversion:

$$k_p / \text{L} \cdot \text{mol}^{-1} \cdot \text{s}^{-1} = 64000 \cdot \exp(4.34 \cdot 10^{-4} \cdot (p / \text{bar} - 2000)) \cdot \left(0.33 + 0.67 \cdot \exp\left(-7.7 \cdot \left(\frac{w_{VP}^0 \cdot (1-\alpha)}{1-w_{VP}^0 \cdot \alpha}\right)\right) - 0.27 \cdot \left(\frac{w_{VP}^0 \cdot (1-\alpha)}{1-w_{VP}^0 \cdot \alpha}\right) \right) \quad (\text{eq. 6.3})$$

6.2 Dynamic Viscosity of Monomer–Water Mixtures

As termination is diffusion-controlled, the viscosity of the reaction medium matters. Given in figure 6.1 are measured dynamic viscosities for the entire range of monomer–water mixtures at 40 °C and ambient pressure.

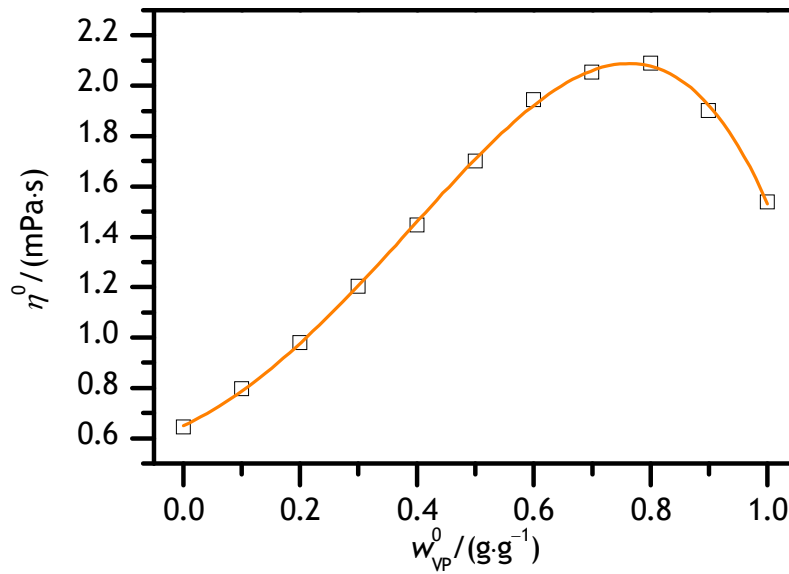


Figure 6.1: Dependence of dynamic viscosity, η^0 , on initial monomer mass fraction at 40 °C and ambient pressure. The line represents the fit of a fourth-order polynomial (equation 6.4).

Viscosity increases towards higher VP content, but passes through a maximum at approximately 0.75 g·g⁻¹ VP in H₂O. The higher viscosity at higher monomer contents is probably due to the larger size of the VP molecule and to stronger intermolecular

interactions resulting from the large dipole moment of VP, which should be similar to the one of 1-methylpyrrolidin-2-one (4.06 D)^[233] and thus significantly above the dipole moment of water (1.85 D)^[234]. As VP cannot act as a hydrogen bond donor, hydrogen-bonded interactions occur only upon the addition of water to pure VP. They result in an enhanced strength of intermolecular interactions and thus of viscosity. The mean molecular size in combination with the increase in the strength of intermolecular interactions due to both the addition of water to VP and of VP to water may qualitatively explain the curvature in figure 6.1. A similar such viscosity maximum has been reported for the 1-vinylimidazole–water system at 70 °C by Bamford and Schofield^[235] as well as for aqueous VP solutions at 50 °C by Senogles and Thomas^[236] and at 60 °C by Karaputadze et al.^[237,238] The detailed understanding of the viscosity–composition curve in figure 6.1 is beyond the scope of this work. The dependence of viscosity on initial monomer mass fraction may be adequately described by the polynomial:

$$\eta_0 / (\text{mPa} \cdot \text{s}) = 0.649 + 1.084 \cdot w_{\text{VP}}^0 + 2.927 \cdot (w_{\text{VP}}^0)^2 - 0.304 \cdot (w_{\text{VP}}^0)^3 - 2.826 \cdot (w_{\text{VP}}^0)^4 \quad (\text{eq. 6.4})$$

6.3 Dependence on Initial Monomer Mass Fraction and Degree of Monomer Conversion

As within the investigations into the termination kinetics of methacrylic acid,^[111] DMPA was used as the photoinitiator. DMPA has the disadvantage of non-ideal photo-decomposition into two radical fragments with clearly different reactivity towards monomer (chapter 5.9.1), but is well soluble in VP–water mixtures. To reduce the effect of non-ideality, DMPA was used at low radical levels,^[217,224] which are achieved by suitably selecting initiator concentration and laser pulse energy.

Relative VP concentration, $c_{\text{M}}(t)/c_{\text{M}}(t=0)$, versus time after applying a laser pulse at $t=0$ is plotted in the upper part of figure 6.2.

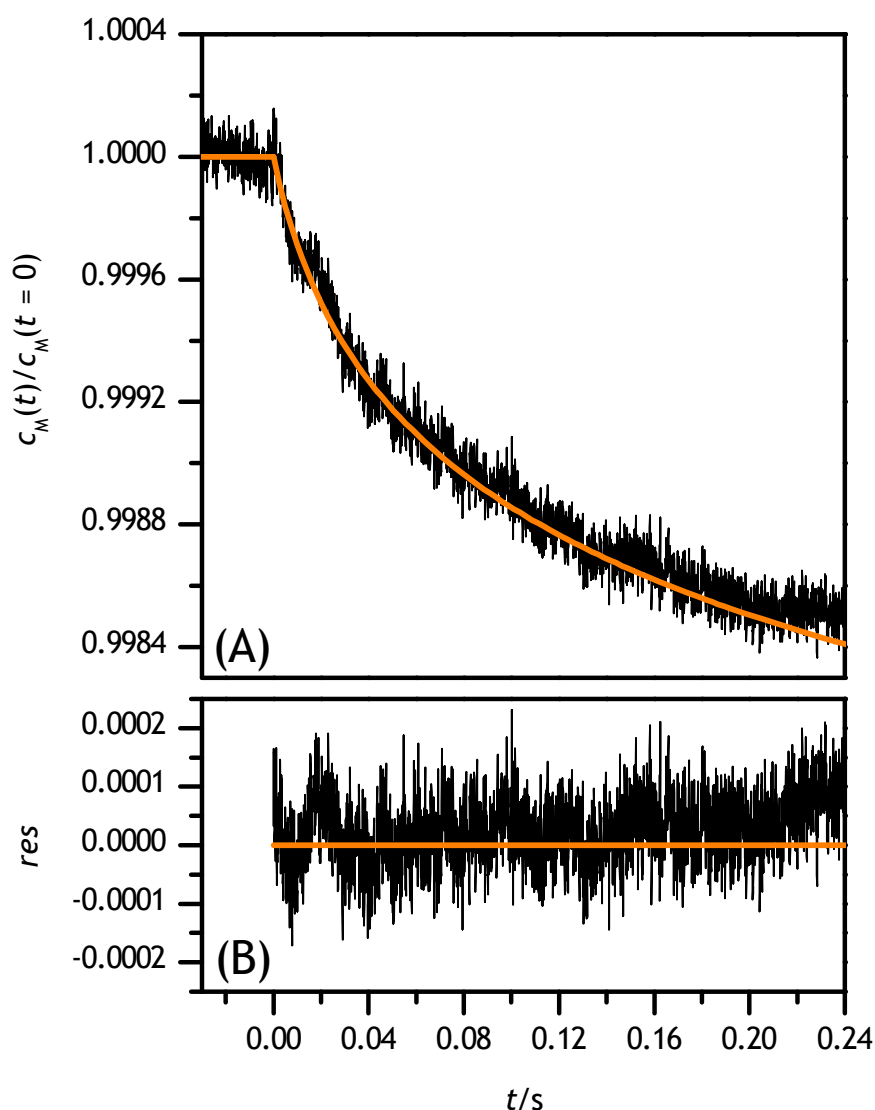


Figure 6.2: (A) Relative monomer concentration plotted versus time after applying an exciplex laser pulse at $t = 0$, during a VP polymerization ($0.45 \text{ g}\cdot\text{g}^{-1}$ in aqueous solution) at 40°C and 2000 bar. The poly(VP) content from preceding polymerization is $0.154 \text{ g}\cdot\text{g}^{-1}$ (corresponding to $\alpha = 0.342$) at $t = 0$. (B) The difference between measured data and fit of equation 3.56 illustrated by the plot of residuals, res .

The signal was obtained during the course of an experiment with an initial VP concentration of $0.45 \text{ g}\cdot\text{g}^{-1}$ and a degree of monomer conversion, from previous laser

pulsing, of 0.342. Monomer concentration prior to laser pulsing, $c_M(t=0)$, is given by the initial monomer concentration and by the degree of overall monomer conversion. To yield better signal-to-noise quality, the signal in figure 6.2 was obtained by averaging 25 subsequently measured SP–PLP–NIR traces which refer to a narrow range of monomer conversion. It has been ensured that polymerization induced by each preceding pulse has ceased, as is demonstrated by the horizontal pretrigger region. The line in figure 6.2 represents a fit of equation 3.56 to the experimental data.

The time interval up to 0.24 s (figure 6.2) refers to chain lengths of up to approximately 13000 monomeric units.^[45] The plot of residuals in the lower part of figure 6.2 indicates that the measured VP concentration versus time trace may be well represented by equation 3.56. That a single chain-length-averaged $\langle k_t \rangle$ value affords for an adequate fit, although k_t is chain-length dependent and decreases with time, is probably due to DMPA acting as the photoinitiator.^[71] The reason behind this discrepancy is seen in the difference in initiation efficiency of the primary radical species. Hesse carried out a few bulk VP polymerization experiments with either DMPA or MMMP.^[113,232] As shown in figure 6.3, the resulting $\langle k_t \rangle$ values for 40 °C and 2000 bar are in close agreement at low degrees of monomer conversion up to $\alpha = 0.15$. Between $\alpha = 0.2$ and $\alpha = 0.3$, the $\langle k_t \rangle$ values obtained with MMMP as the initiator are slightly (20 to 35 %), but systematically higher, which is most likely due to the differences in photoinitiator behavior outlined in the literature.^[217]

In the initial polymerization period (figure 6.3), $\langle k_t \rangle$ is approximately constant. Above $\alpha = 0.12$, $\langle k_t \rangle$ decreases significantly by about one order of magnitude up to $\alpha = 0.4$ (figure 6.4). Such large changes of $\langle k_t \rangle$ are known from investigations into the termination kinetics of several other monomers, such as methacrylic acid,^[111] methyl methacrylate,^[32,110,239] and butyl methacrylate.^[240] Based on the remarks in chapter 3.1.3, the $\langle k_t \rangle$ versus α correlation should primarily depend on control by segmental diffusion and translational diffusion. In the initial period of polymerization, where bulk viscosity is low and thus translational mobility of macroradical coils is high, SD may be rate-determining.

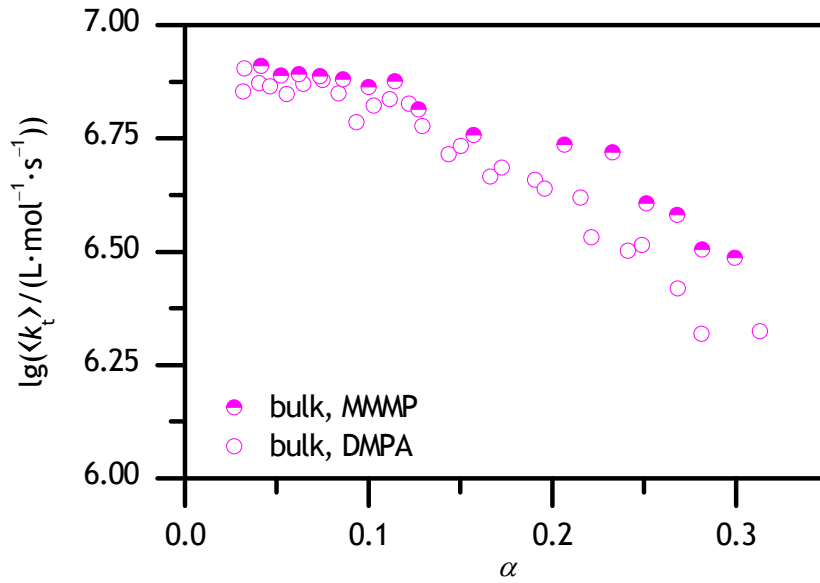


Figure 6.3: Dependence of the chain-length-averaged termination rate coefficient, $\langle k_t \rangle$, on degree of monomer conversion, α , as deduced from laser-induced VP bulk polymerizations at 40 °C and 2000 bar carried out with either DMPA or MMWP being the photoinitiator. $\langle k_t \rangle$ was estimated from measured $\langle k_t \rangle / k_p$ with k_p being taken from equation 6.3. The data were taken from Hesse.^[113,232]

Toward higher monomer-to-polymer conversion, bulk viscosity increases and translational diffusion of radicals may become rate-determining. This is indicated by the decrease in $\langle k_t \rangle$ toward higher conversion, that is, above $\alpha = 0.15$ in bulk polymerization (figure 6.3). Considering reaction diffusion, overall $\langle k_t \rangle$ may be described by equation 6.5 which neglects the diffusion control of k_p at high degrees of monomer conversion. Such diffusion limitation is expected to occur only at very high polymer content, that is, at high initial monomer concentration combined with a high monomer-to-polymer conversion.

$$\langle k_t \rangle = \left(k_{t,SD}^{-1} + \frac{\exp(C_\eta \cdot \alpha)}{k_{t,TD}^0} \right)^{-1} + C_{RD} \cdot (1 - \alpha) \cdot k_p \quad (\text{eq. 6.5})$$

The approximate validity of equation 3.20, which is used in equation 6.5, for aqueous solutions of poly(VP) is supported by viscosity measurements of Sadeghi et al.^[241] Their data for polymer–water solutions show an exponential increase in viscosity toward higher polymer mass fraction.

The $\langle k_t \rangle$ values for polymerization in aqueous solution of 0.20, 0.25, 0.40, 0.45, 0.50, 0.60, 0.70, and 0.80 g·g⁻¹ VP as well as for bulk VP polymerization are presented in figure 6.4 (a combined representation of all data is given by figure A.1 in appendix A.2). The lines represent fits of equation 6.5 to the experimental data with the parameters being estimated via method A, which will be introduced further below. For initial monomer concentrations of up to 0.40 g·g⁻¹ VP, $\langle k_t \rangle$ appears to be constant up to monomer conversions where the system turns inhomogeneous. Therefore, equation 6.5 has not been fitted to these data. The lines in figure 6.4 representing $\langle k_t \rangle$ versus α for monomer contents of 0.40 g·g⁻¹ VP and below were obtained using parameters which were estimated by means of equations 6.6, 6.7, 6.8, and 6.9 (given further below). At initial monomer concentrations above 0.40 g·g⁻¹ VP, $\langle k_t \rangle$ decreases after an initial range of almost constant $\langle k_t \rangle$. The initial range, which is under control by segmental diffusion, becomes less extended toward higher initial monomer content. From the data for $w_{VP}^0 = 0.50$ g·g⁻¹, where the plateau region extends up to about $\alpha = 0.30$, it may be assumed that the plateau-type region ends once a poly(VP) content of about 0.15 g·g⁻¹ is reached. This number indicates that bulk polymerization exhibits constant chain-length-averaged k_t up to $\alpha = 0.15$, which is what is seen in figure 6.4. Along the same argument, polymerization of VP at $w_{VP}^0 = 0.20$ g·g⁻¹ is predicted to show plateau-type behavior up to about $\alpha = 0.75$. This finding is understood as being due to a smaller increase in viscosity at lower VP content which goes with lower poly(VP) concentration at identical monomer conversion.

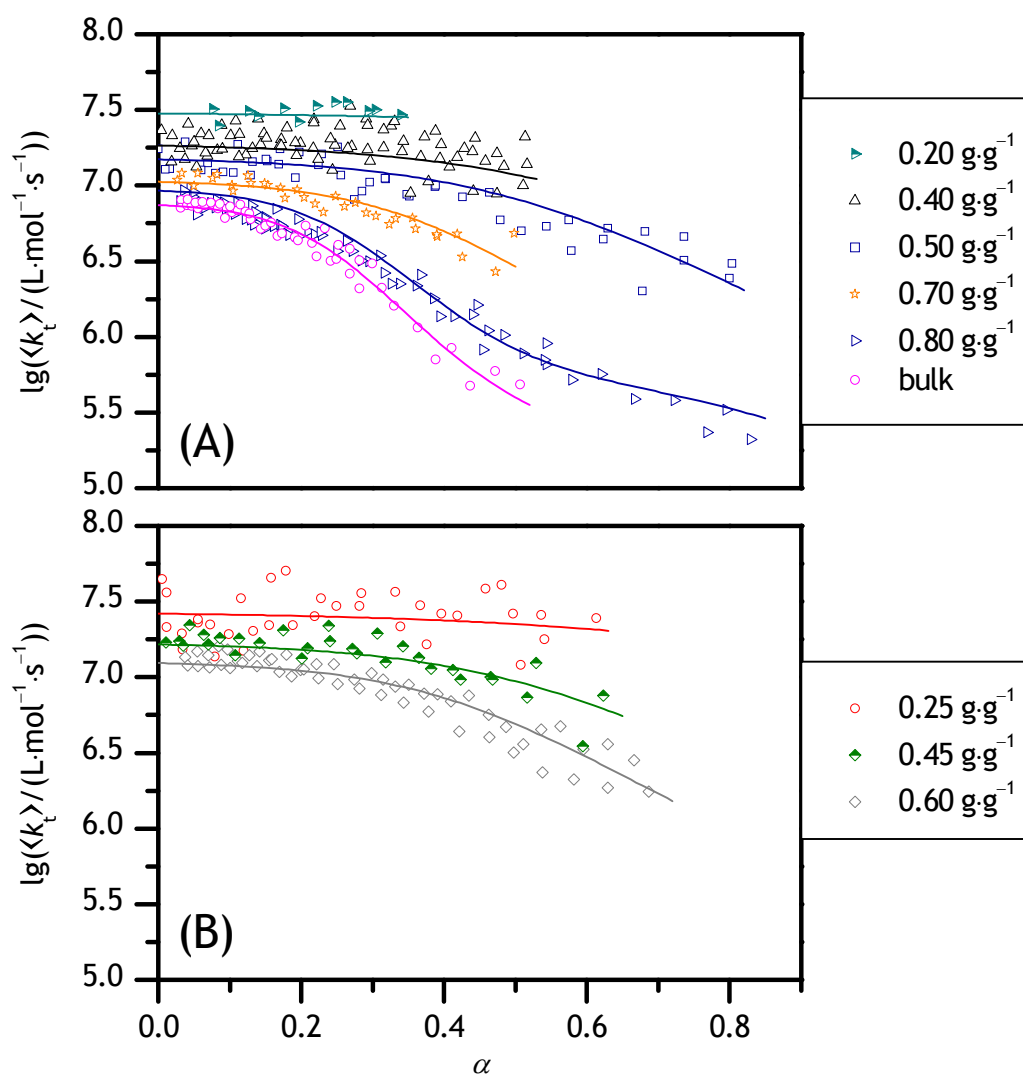


Figure 6.4: Dependence of the chain-length-averaged termination rate coefficient, $\langle k_t \rangle$, on the degree of monomer conversion, α , for VP polymerizations at 40 °C and 2000 bar for various initial monomer contents. The lines are fits of equation 6.5 to the experimental data according to method A. The associated fit parameters are listed in table 6.1 (further below). For initial monomer mass fractions of 0.40 g·g⁻¹ VP and below, the parameters were determined via equations 6.6, 6.7, 6.8, and 6.9 (further below). The data are divided into two figures, (A) and (B). A combined representation of all data is given by figure A.1 in appendix A.2.

The initial plateau value of $\langle k_t \rangle$ increases slightly toward lower initial monomer content. This may, at least partly, be due to the increase in viscosity of the monomer–VP solution upon enhancing VP content. For example, solution viscosity increases by about a factor of two between 0.20 and 0.60 g·g⁻¹ VP (see figure 6.1). In case that $\langle k_t \rangle$ scales with the inverse of solution viscosity, one would expect a lowering of $\langle k_t \rangle$ by 0.3 decimal logarithmic units, which is approximately what the experimental data show for the 0.20 to 0.60 g·g⁻¹ VP range. The plateau value of $\langle k_t \rangle$ is lowest at the highest initial monomer content. This cannot be explained entirely on the basis of the viscosity data in figure 6.1. It should, however, be taken into account that viscosity was measured at ambient pressure, but not at the polymerization pressure of 2000 bar. It needs further to be considered that the dynamic viscosity of the monomer–water mixture probably does not correlate with the rate coefficient which is mainly controlled by segmental diffusion. The mobility of the growing chain end within the polymer coil depends on the interactions of monomer, water, and polymer and, perhaps even more importantly, on the persistence length. The persistence length significantly affects the mobility of the growing chain end just as a leashed dog is much less mobile than an unleashed dog. The importance of the persistence length is, however, not taken into account in the correlation of $\langle k_{t,ini} \rangle$ and dynamic viscosity of the monomer–water mixture.

The decrease of the termination rate coefficient with monomer conversion, after passing the initial plateau region, is more pronounced at higher monomer concentration, where the relative change in viscosity for a given conversion range is larger due to a larger increase in polymer content. At monomer contents of 0.80 g·g⁻¹ VP and above, the decrease of $\langle k_t \rangle$ with monomer conversion becomes less pronounced toward the highest degrees of monomer conversion, which is assigned to $\langle k_t \rangle$ running into control by reaction diffusion.

Two methods, A and B, have been used for fitting equation 6.5 to the experimental $\langle k_t \rangle$ data. The same $k_{t,SD}$ values are used for both methods. They are directly obtained from the mean values of experimental $\langle k_t \rangle$ in the initial polymerization period, $\langle k_{t,ini} \rangle$. The dependence of the so-obtained mean $k_{t,SD}$ values on initial monomer mass fraction may be expressed by the exponential function:

$$k_{t,SD} / (\text{L} \cdot \text{mol}^{-1} \cdot \text{s}^{-1}) = \langle k_{t,ini} \rangle / (\text{L} \cdot \text{mol}^{-1} \cdot \text{s}^{-1}) = 4.87 \cdot 10^7 \cdot \exp\left(-\frac{w_{VP}^0}{0.29}\right) + 5.47 \cdot 10^6 \quad (\text{eq. 6.6})$$

Equation 6.6 is plotted together with the experimental $\langle k_{t,ini} \rangle$ data in figure 6.5.

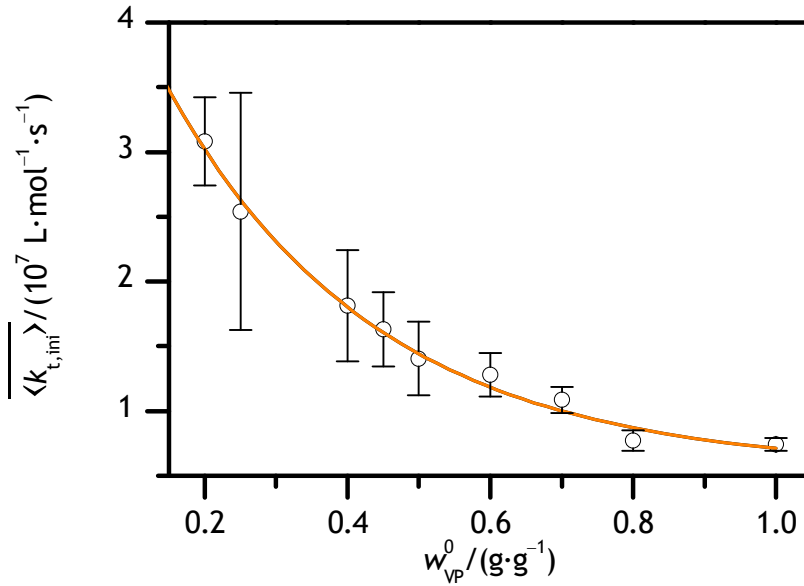


Figure 6.5: Dependence of mean $\langle k_{t,ini} \rangle$ on initial mass fraction of VP, w_{VP}^0 , at 40 °C and 2000 bar; $\langle k_{t,ini} \rangle$ is the mean (plateau) value of experimental $\langle k_t \rangle$ for the initial polymerization period. Error bars indicate the standard deviation. The line refers to equation 6.6.

Even the lowest $\langle k_{t,ini} \rangle$ value in figure 6.5, for bulk VP polymerization, is well above the low-conversion MMA bulk polymerization value of $2.92 \cdot 10^6 \text{ L} \cdot \text{mol}^{-1} \cdot \text{s}^{-1}$, which has been deduced from experimental $\langle k_t \rangle / k_p$ for MMA polymerization at 30 °C and 1000 bar and from $k_p(p, T)$ reported by Beuermann et al.^[32,110] The $k_{t,SD}$ value used for VP at a monomer concentration of $0.60 \text{ g} \cdot \text{g}^{-1}$ in aqueous solution is, by a factor of two, also above $k_{t,SD}$ for $0.60 \text{ g} \cdot \text{g}^{-1}$ MAA in aqueous solution^[111] ($6.5 \cdot 10^6 \text{ L} \cdot \text{mol}^{-1} \cdot \text{s}^{-1}$) at 50 °C and 2000 bar. These differences are not due to viscosity which, at 25 °C and ambient pressure, is $0.584 \text{ mPa} \cdot \text{s}$,^[242] $1.267 \text{ mPa} \cdot \text{s}$,^[243] and $1.539 \text{ mPa} \cdot \text{s}$ (40 °C) for MMA, MAA ($0.60 \text{ g} \cdot \text{g}^{-1}$ in

water), and VP, respectively. Also chain-length-related arguments provide no explanation for the appreciable differences of $k_{t,SD}$ for VP as compared to MMA^[244] and MAA^[111]. The reason behind the differences is most likely the increased hindrance of segmental mobility in MMA and MAA due to the α -methyl group. At modest monomer contents up to $0.25 \text{ g}\cdot\text{g}^{-1}$, equation 6.6 may be used for modeling $\langle k_t \rangle$ up to rather high monomer conversion, as has been shown by Santanakrishnan et al.^[112] This is probably because polymer content and thus viscosity, even at very high conversion, are sufficiently low to allow for fast translational diffusion.

The parameters to be determined by the fitting procedure of equation 6.5 are: $k_{t,TD}^0$, C_η , and C_{RD} . According to theory and as has been shown for ethene polymerization,^[67] C_{RD} for bulk polymerization is independent of conversion, as far as the parameters jump length and polymer molecule diameter are independent of monomer concentration.^[67,103,104] In solution polymerization, C_{RD} depends on initial monomer mass fraction. Fitting to $\langle k_t \rangle$ versus α for VP polymerization at $w_{VP}^0 = 0.80 \text{ g}\cdot\text{g}^{-1}$ yields $C_{RD} = 112$. Under the assumption that C_{RD} linearly scales with VP content, this number allows for estimating C_{RD} at given VP mass fraction by equation 6.7:

$$C_{RD} = 140 \cdot w_{VP}^0 \quad (\text{eq. 6.7})$$

Adopting C_{RD} from equation 6.7 for data taken at lower VP mass fractions circumvents the problem of deducing C_{RD} from data sets which are not sufficiently sensitive toward reaction diffusion. It should thus be stressed that the C_{RD} parameters in table 6.1 and also in table 6.2 (further below) are not individually fitted quantities, but are exclusively based on the estimate of C_{RD} for $w_{VP}^0 = 0.80 \text{ g}\cdot\text{g}^{-1}$. The value for VP bulk polymerization, $C_{RD} = 140$ (see equation 6.7), is well above the associated numbers of 50 for MMA at 60°C ^[244] and 61 for $0.60 \text{ g}\cdot\text{g}^{-1}$ MAA in aqueous solution at 50°C ,^[111] which observation provides another indication for the higher mobility of VP macroradical coils. With C_{RD} being given by equation 6.7, $k_{t,TD}^0$ and C_η are the remaining two correlated fit parameters. Two methods have been applied for estimating $k_{t,TD}^0$.

Method A

From fitting to conversion-dependent $\langle k_t \rangle$ for bulk VP polymerization, $k_{t,TD}^0$ has been found to be $2.2 \cdot 10^8 \text{ L} \cdot \text{mol}^{-1} \cdot \text{s}^{-1}$. As both $k_{t,SD}$ and $k_{t,TD}^0$ refer to diffusional motion which experiences friction by the monomer–water mixture, $k_{t,TD}^0$ is assumed to scale with $k_{t,SD}$. This assumption allows for estimating the variation of $k_{t,TD}^0$ with VP concentration from the measured dependence of $\langle k_{t,ini} \rangle$ on initial VP content according to equation 6.8:

$$\begin{aligned} k_{t,TD}^0 / (\text{L} \cdot \text{mol}^{-1} \cdot \text{s}^{-1}) &= \frac{2.2 \cdot 10^8 \cdot \langle k_{t,ini} \rangle (w_{VP}^0)}{\langle k_{t,ini} \rangle (w_{VP}^0 = 1)} \\ &= \frac{2.2 \cdot 10^8 \cdot \langle k_{t,ini} \rangle (w_{VP}^0)}{7.0 \cdot 10^6 \text{ L} \cdot \text{mol}^{-1} \cdot \text{s}^{-1}} \approx \frac{31 \cdot \langle k_{t,ini} \rangle (w_{VP}^0)}{\text{L} \cdot \text{mol}^{-1} \cdot \text{s}^{-1}} \end{aligned} \quad (\text{eq. 6.8})$$

Fitting of equation 6.5 using equation 6.8, that is applying method A, yields a satisfactory representation of experimental data (figure 6.4). The associated fit parameters, C_η , as well as the values for C_{RD} , $k_{t,SD}$, and $k_{t,TD}^0$ are listed in table 6.1.

Table 6.1: Parameters used for and deduced from fitting equation 6.5 to the experimental data via method A, in which it is assumed that $k_{t,TD}^0$ scales with $\langle k_{t,ini} \rangle$ (see text). The parameter values refer to VP polymerization at 2000 bar and 40 °C.

$w_{VP}^0 / (\text{g} \cdot \text{g}^{-1})$	$k_{t,SD} / (10^6 \text{ L} \cdot \text{mol}^{-1} \cdot \text{s}^{-1})$	C_η	$k_{t,TD}^0 / (10^8 \text{ L} \cdot \text{mol}^{-1} \cdot \text{s}^{-1})$	C_{RD}
0.45	16.1	6.5 ± 0.3	5.0	63
0.50	14.4	6.7 ± 0.2	4.5	70
0.60	11.8	8.0 ± 0.1	3.7	84
0.70	10.0	9.3 ± 0.2	3.1	98
0.80	8.70	13.7 ± 0.2	2.7	112
1.00	7.11	14.9 ± 0.2	2.2	140

The C_η parameters from fitting equation 6.5 to experimental $\langle k_p \rangle$ according to method A are plotted in figure 6.6. A straight line (equation 6.9) passing through the origin may be adequately fitted to the numbers for initial VP mass fractions from 0.45 g·g⁻¹ up to bulk polymerization.

$$C_\eta = 14.75 \cdot w_{VP}^0 \quad (\text{eq. 6.9})$$

This dependence reflects the higher amount of polymer being present at given degree of monomer conversion for polymerizations with higher initial VP content. The extrapolated C_η for $w_{VP}^0 = 0$ is close to zero, which corresponds to conversion-independent $\eta_r(\alpha)$, as is to be expected for the hypothetical case of a polymerization without polymer formation.

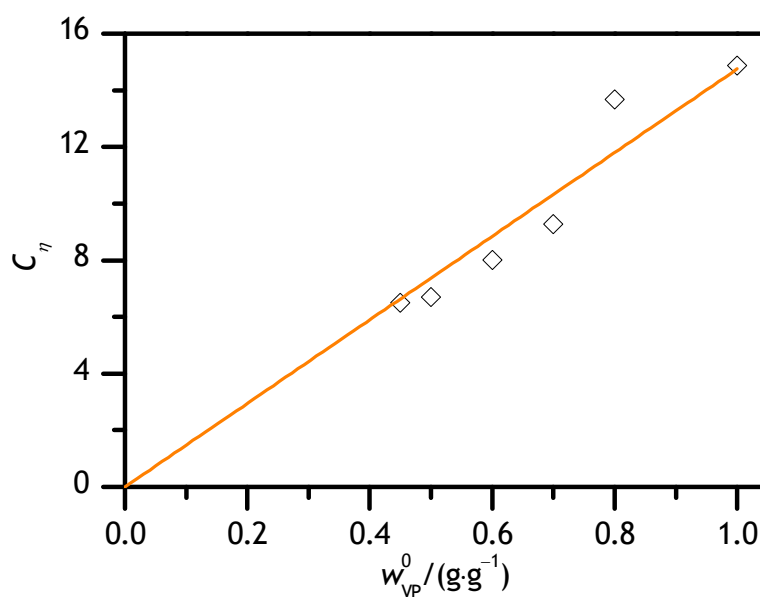


Figure 6.6: Dependence of C_η on the initial mass fraction of VP, w_{VP}^0 , at 40 °C and 2000 bar as obtained by fitting equation 6.5 to the experimental data according to method A; the straight line refers to equation 6.9.

Correlations as in figure 6.6 have also been observed for MAA^[111] and MMA^[110] solution polymerizations with the slope of the straight line, however, being different. Combination of equations 3.20 and 6.9 yields the following dependence of relative viscosity on the mass fraction of polymer, $w_{\text{poly(VP)}}$:

$$\ln(\eta_r(\alpha)) = 14.75 \cdot w_{\text{VP}}^0 \cdot \alpha = 14.75 \cdot w_{\text{poly(VP)}} \quad (\text{eq. 6.10})$$

Equation 6.10 implies that $\eta_r(\alpha)$ in case of polymerization of 0.40 g·g⁻¹ VP to full conversion is close to $\eta_r(\alpha)$ for polymerization of 0.80 g·g⁻¹ VP up to $\alpha = 0.5$, as the polymer mass fraction equals 0.40 g·g⁻¹ in both cases. Further viscosity experiments on the ternary system poly(VP)–VP–water should be helpful for checking the $\eta_r(\alpha)$ versus $w_{\text{poly(VP)}}$ correlation.

The data fits in figure 6.4 indicate that $\langle k_t \rangle$ may be adequately represented via method A with the parameters listed in table 6.1. The variation of $k_{t,\text{SD}}$ and of C_η with monomer mass fraction in aqueous VP solution is similar to the type of behavior observed for MAA,^[111] 0.30 and 0.60 g·g⁻¹ in aqueous solution, and for MMA in solution of toluene.^[110]

Method B

Within this approach, $k_{t,\text{TD}}^0 = 2.2 \cdot 10^8 \text{ L} \cdot \text{mol}^{-1} \cdot \text{s}^{-1}$ has also been adopted for VP bulk polymerization, but the variation of $k_{t,\text{TD}}^0$ with VP content of the aqueous solution has been assumed to scale with inverse viscosity of the aqueous monomer solution. This assumption leads to equation 6.11:

$$k_{t,\text{TD}}^0 / (\text{L} \cdot \text{mol}^{-1} \cdot \text{s}^{-1}) = \frac{2.2 \cdot 10^8 \cdot \eta_0(w_{\text{VP}}^0 = 1)}{\eta_0(w_{\text{VP}}^0)} \quad (\text{eq. 6.11})$$

No viscosity data are available for 2000 bar. Thus, it is assumed that relative viscosity at 2000 bar varies as does relative viscosity at ambient pressure. Moreover, the viscosity data for solution in H₂O (see figure 6.1) have been adopted for D₂O solutions. These two assumptions may affect the fitting of equation 6.5 by method B, which is illustrated in figure 6.7 (a combined representation of all data is given by figure A.2 in appendix A.2). The associated parameter values are given in table 6.2. The lines in figure 6.7 representing $\langle k_t \rangle$ versus α for monomer contents of 0.40 g·g⁻¹ VP and below were obtained using parameters which were estimated by means of equations 6.6, 6.7, 6.11, 6.12 (the latter is given further below).

Adopting the viscosity of H₂O for data analysis results in slightly enhanced $k_{t,TD}^0$ especially at lower monomer concentration, as D₂O viscosity, for example at 40 °C and 1 atm, is by about 20 % above the one of H₂O.^[245,246] The effect on relative viscosity, $\eta_r(\alpha)$, and thus on C_η should be even less.

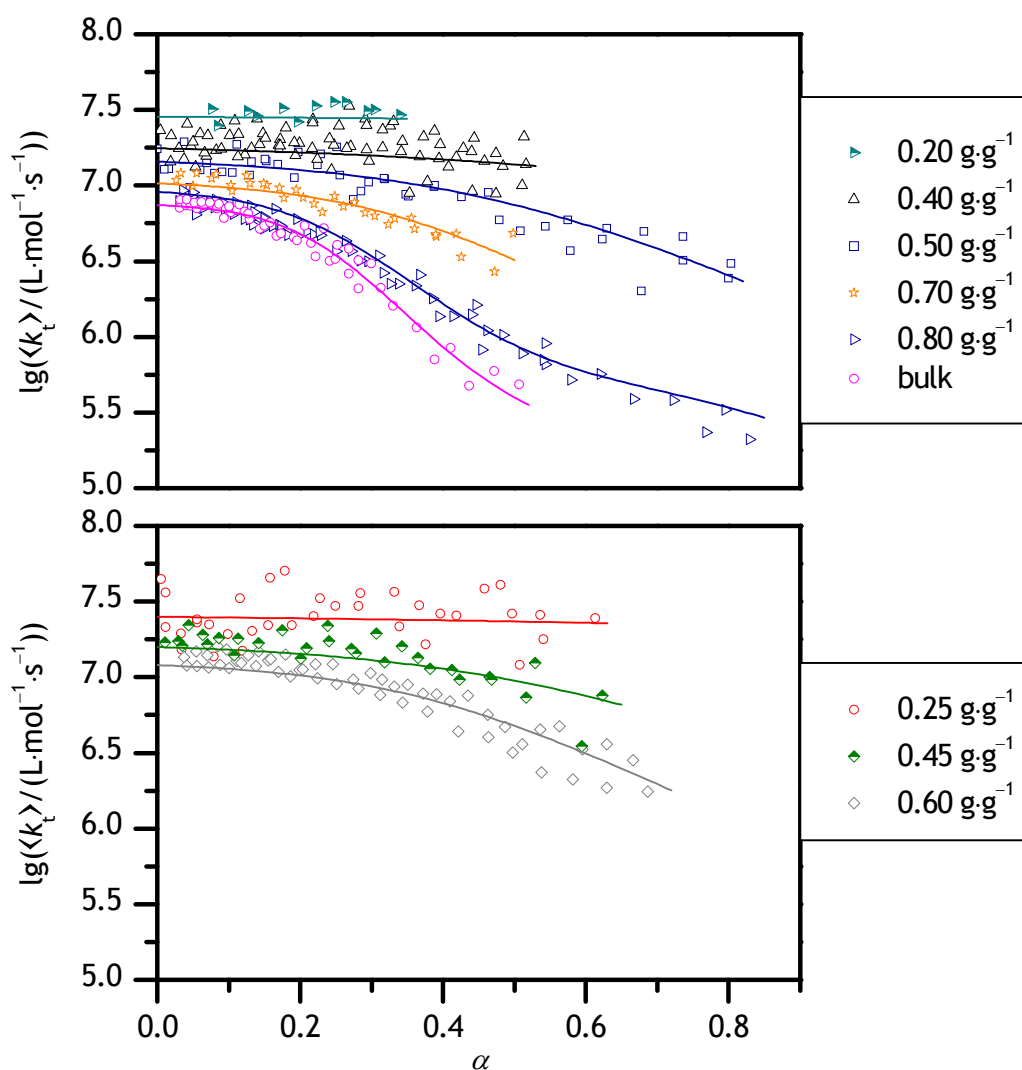


Figure 6.7: Dependence of the chain-length-averaged termination rate coefficient, $\langle k_t \rangle$, on the degree of monomer conversion, α , for VP polymerizations at 40 °C and 2000 bar and various initial monomer concentrations. The lines are fits of equation 6.5 to the experimental data with the parameters listed in table 6.2 corresponding to method B. For initial monomer mass fractions of 0.40 g·g⁻¹ and below, the parameters were determined via equations 6.6, 6.7, 6.11, and 6.12 (the latter is given further below). The data are divided into two figures, (A) and (B). A combined representation of all data is given by figure A.2 in appendix A.2.

With $k_{t,SD}$ and C_{RD} being obtained from equations 6.6 and 6.7, respectively, and with $k_{t,TD}^0$ being estimated via method B (equation 6.11), C_η is the single adjustable parameter. The so-obtained numbers for C_η are listed in table 6.2 and plotted (as diamonds) in figure 6.8. The full line represents a fit of the parameter values from method B, whereas the dashed line represents the C_η values for method A.

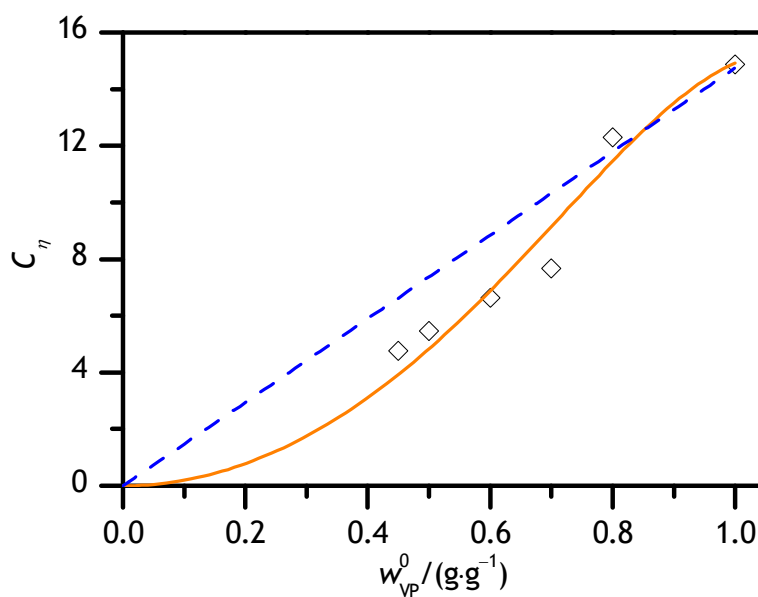


Figure 6.8: Dependence of C_η on initial mass fraction of VP; the full line for method B is constructed from equation 6.12. The dashed line refers to equation 6.9 which is associated with method A.

Table 6.2: Parameters used for and deduced from fitting equation 6.5 to the experimental data via method B, in which it is assumed that $k_{t,TD}^0$ scales with inverse viscosity (see text). The parameter values refer to VP polymerizations at 2000 bar and 40 °C.

$w_{VP}^0 / (g \cdot g^{-1})$	$k_{t,SD} / (10^6 L \cdot mol^{-1} \cdot s^{-1})$	C_η	$k_{t,TD}^0 / (10^8 L \cdot mol^{-1} \cdot s^{-1})$	C_{RD}
0.45	16.1	4.8 ± 0.4	2.1	63
0.50	14.4	5.5 ± 0.1	2.0	70
0.60	11.8	6.6 ± 0.1	1.8	84
0.70	10.0	7.7 ± 0.2	1.6	98
0.80	8.70	12.3 ± 0.2	1.6	112
1.00	7.11	14.9 ± 0.2	2.2	140

The C_η values associated with method B exhibit a sigmoid curvature with respect to initial mass fraction of monomer, which may be represented by:

$$C_\eta = \frac{2.71 \cdot 10^3}{\left(1 + \exp\left(-0.282 \cdot \left(w_{VP}^{0.5} + 31.3\right)\right) - 24.8 \cdot w_{VP}^{0.2} \cdot \exp\left(-0.282 \cdot \left(w_{VP}^{0.5} + 31.3\right)\right)\right)^2} - \frac{2.71 \cdot 10^3}{(1 + \exp(-0.282 \cdot 31.3))^2} \quad (\text{eq. 6.12})$$

Comparison of figures 6.4 and 6.7 shows that both methods A and B are capable of providing an adequate fit to the experimental $\langle k_t \rangle$ data. Thus, both methods may be used for prediction of $\langle k_t \rangle$ in aqueous solution over almost the entire range of VP concentrations and up to very high conversion. A slight weakness of method B is that independent viscosity measurements are required, which should be carried out at the pressures and temperatures of interest. The $\langle k_t \rangle$ analysis via method A, on the other hand, may be performed entirely on the basis of measured $\langle k_t \rangle$ data. The linear correlation of C_η

with mass fraction VP is based entirely on experiments at high VP content and may not apply in dilute solutions. Method A is, however, easily applied.

6.4 Pressure Dependence

In combination with the volume of activation $\Delta^\ddagger V^\circ(\langle k_{t,ini} \rangle) = 14.6 \text{ cm}^3 \cdot \text{mol}^{-1}$,^[113,232] the dependence of $\langle k_{t,ini} \rangle$ on the initial VP mass fraction and on pressure at 40 °C is given by:

$$\langle k_{t,ini} \rangle / (\text{L} \cdot \text{mol}^{-1} \cdot \text{s}^{-1}) = \left(4.87 \cdot 10^7 \cdot \exp\left(-\frac{w_{VP}^0}{0.29}\right) + 5.47 \cdot 10^6 \right) \cdot \exp(5.61 \cdot 10^{-4} \cdot (2 \cdot 10^3 - p / \text{bar})) \quad (\text{eq. 6.13})$$

(valid for $0.20 \leq w_{VP}^0 \leq 1.00$)

Equation 6.13 refers to the initial plateau region of constant chain-length-averaged $\langle k_t \rangle$. At low w_{VP}^0 , this region extends up to high degrees of monomer conversion (figure 6.4). The profit of the equation is the enablement of estimating $\langle k_{t,ini} \rangle$ at ambient pressure. Although high pressure results in an increase of the rate of polymerization, it is usually not used in industrial processes for safety reasons and due to the high costs of pressurization.

7 Propagation Kinetics of the Polymerization of Prop-2-enamides

The polymerization of several prop-2-enamides is of industrial interest. Process optimization requires reliable rate coefficients of the relevant reactions. Moreover, the influence of the amide group versus the influence of the carboxylic acid or carboxylic ester group on kinetics may be investigated by comparison with data determined for (meth)acrylic acid and (meth)acrylates. It can also be investigated whether the α -methyl group at the carbon–carbon double bond has a similar effect on polymerization kinetics of MPAm versus PAm as it has on the polymerization kinetics of MAA versus AA. The polymerization kinetics of several prop-2-enamides^[36,37,40,71,247,248] has already been studied. However, data are scarce or even not available for monomers showing a minor steric demand. By PLP–SEC, Pascal et al. determined the k_p value of MPAm to be $1.1 \cdot 10^3 \text{ L} \cdot \text{mol}^{-1} \cdot \text{s}^{-1}$ at 25 °C, pH = 1, and a monomer concentration of $1 \text{ mol} \cdot \text{L}^{-1}$. Their data reveal an activation energy of $20 \pm 2 \text{ kJ} \cdot \text{mol}^{-1}$.^[248] When these values were measured, the consistency criteria had not yet been developed. Therefore, it is advisable to check these data. Even less data are available for the radical polymerization of M-MPAm and of DM-PAm. Bhattacharya et al. have shown an increase of the initial rate of polymerization of DM-PAm in water towards higher initial monomer concentration.^[249] Investigations into the polymerization kinetics of MPAm and M-MPAm may provide information on the influence of substituents at the nitrogen atom.

Ambient-pressure PLP–SEC experiments to determine k_p were carried out at 25 °C and a monomer mass fraction of $w_{\text{MPAm}} = 0.20 \text{ g} \cdot \text{g}^{-1}$ as well as at 10 °C and monomer mass fractions of $w_{\text{DM-PAm}} = 0.15$ and $0.30 \text{ g} \cdot \text{g}^{-1}$. To determine the Arrhenius pre-exponential factors as well as the Arrhenius activation energies of k_p , additional measurements were performed at 10, 40, 60, and 80 °C and monomer mass fractions of $w_{\text{M-MPAm}} = 0.70$ and $0.80 \text{ g} \cdot \text{g}^{-1}$ as well as of $w_{\text{DM-PAm}} = 0.20, 0.80, \text{ and } 1.00 \text{ g} \cdot \text{g}^{-1}$. To evaluate the volume of activation of k_p , further experiments were carried out at pressures of $p = 1000, 1500, \text{ and } 2000 \text{ bar}$, at 40 °C, and at monomer mass fractions of $w_{\text{PAm}} = 0.20 \text{ g} \cdot \text{g}^{-1}$,

$w_{\text{MPAm}} = 0.20 \text{ g}\cdot\text{g}^{-1}$, and $w_{\text{DM-PAm}} = 0.20$ and $1.00 \text{ g}\cdot\text{g}^{-1}$, respectively. Additional measurements were performed at 500 bar in case of DM-PAm and PAm. Mostly, experiments were carried out at a laser-pulse repetition rate of 20 Hz for M-MPAm, of 150 Hz for PAm, and of 100 Hz for DM-PAm. The number of applied laser pulses was varied such as to keep monomer conversion low. Additional experimental data were taken from the literature^[250] and included in curve fitting. Those values were determined using calibrant-relative calibration and had therefore to be multiplied with the factor which correlates the positions of the POIs obtained by direct MMD determination and by calibrant-relative calibration.

Representative MMDs (black lines) and the associated first-derivative curves (red lines) of a poly(MPAm) sample from PLP in aqueous solution at $w_{\text{MPAm}} = 0.20 \text{ g}\cdot\text{g}^{-1}$, 40 °C, and 2000 bar are depicted in figure 7.1. The full line was obtained by poly(PAm)-relative calibration of the SEC and the dashed line by direct MMD determination. The significant shift of the MMD indicates that the hydrodynamic volume of poly(PAm) in the eluent of the SEC is much larger than the hydrodynamic volume of a poly(MPAm) molecule showing identical molar mass. This is also reflected in the large deviation of the factor which correlates the positions of the POIs obtained by direct MMD determination and by calibrant-relative calibration from unity.

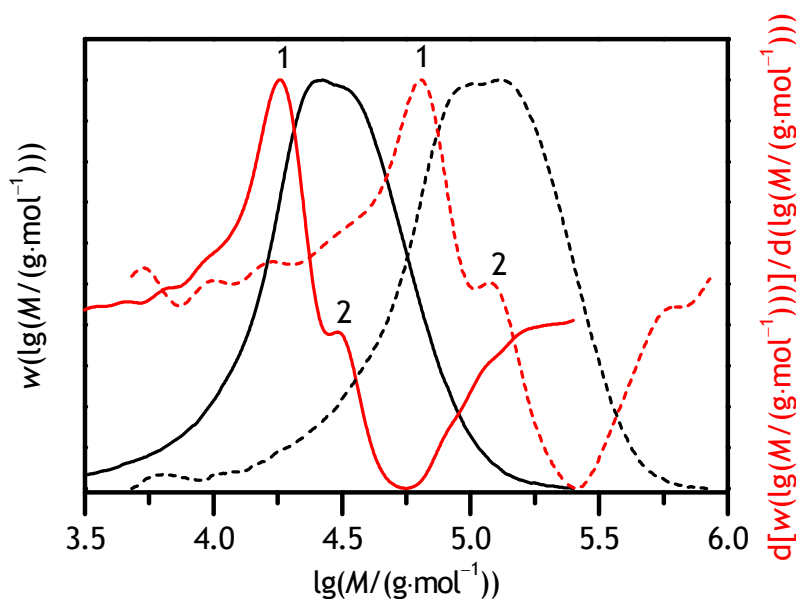


Figure 7.1: MMDs (black lines) and associated first-derivative curves (red lines) obtained from the polymerization of $0.20 \text{ g}\cdot\text{g}^{-1}$ MPAm dissolved in water at 40°C , 2000 bar , and a laser-pulse repetition rate of 20 Hz . The full line was obtained by poly(PAm)-relative calibration of the SEC and the dashed line by direct MMD determination. The numbers indicate the primary and secondary POIs.

Figures 7.2 and 7.3 show representative MMDs (black lines) and the associated first-derivative curves (red lines) of a poly(M-MPAm) sample obtained from PLP at $w_{\text{M-MPAm}} = 0.70 \text{ g}\cdot\text{g}^{-1}$, 40°C , and ambient pressure and of a poly(DM-PAm) sample obtained from PLP at $w_{\text{DM-PAm}} = 0.80 \text{ g}\cdot\text{g}^{-1}$, 10°C , and ambient pressure. These raw MMDs were obtained by polystyrene-relative calibration.

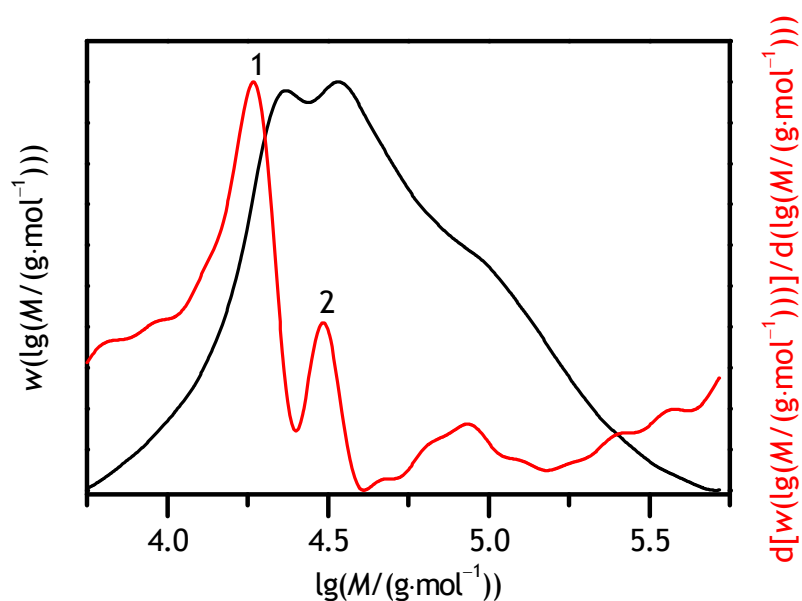


Figure 7.2: MMD (black line) and associated first-derivative curve (red line) obtained from the polymerization of $0.70 \text{ g} \cdot \text{g}^{-1}$ M-MPAm dissolved in water at 40°C , ambient pressure, and at a laser-pulse repetition rate of 20 Hz. The MMD was obtained by polystyrene-relative calibration. The numbers indicate the primary and secondary POIs.

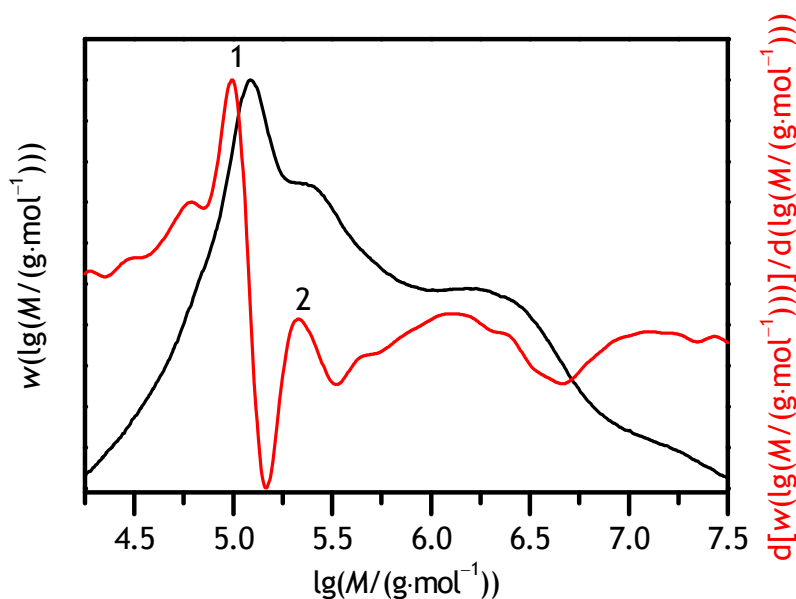


Figure 7.3: MMD (black line) and associated first-derivative curve (red line) obtained from the polymerization of $0.80 \text{ g}\cdot\text{g}^{-1}$ DM-PAm dissolved in water at 10°C , ambient pressure, and at a laser-pulse repetition rate of 100 Hz. The MMD was obtained by polystyrene-relative calibration. The numbers indicate the primary and secondary POIs.

A representative MMD (black line) and the associated first-derivative curve (red line) of a poly(PAm) sample from PLP in aqueous solution at $w_{\text{PAm}} = 0.20 \text{ g}\cdot\text{g}^{-1}$, 40°C , and 1500 bar are depicted in figure 7.4. The MMD was determined by poly(PAm)-relative calibration. Primary and secondary POIs of the MMDs are clearly identified from the maxima of the associated first derivatives. The MMDs of the poly(M-MPAm) and the poly(DM-PAm) samples show high-molar-mass polymer without PLP structure which primarily result from initiation prior to laser irradiation or from post-PLP polymerization. Due to its high molar mass it has negligible impact on the position of the first POI which has been used to determine k_p . The MMD of poly(PAm) shows a weak kink at approximately $10^6 \text{ g}\cdot\text{mol}^{-1}$ which is reflected in a shoulder in the first-derivative curve. This kink is caused by the high-molar-mass limit of the calibration range of the SEC setup. Above this limit, the MMD shown in figure 7.4 does probably not correspond to the true MMD. However, k_p data were only obtained from POI occurring at lower molar mass.

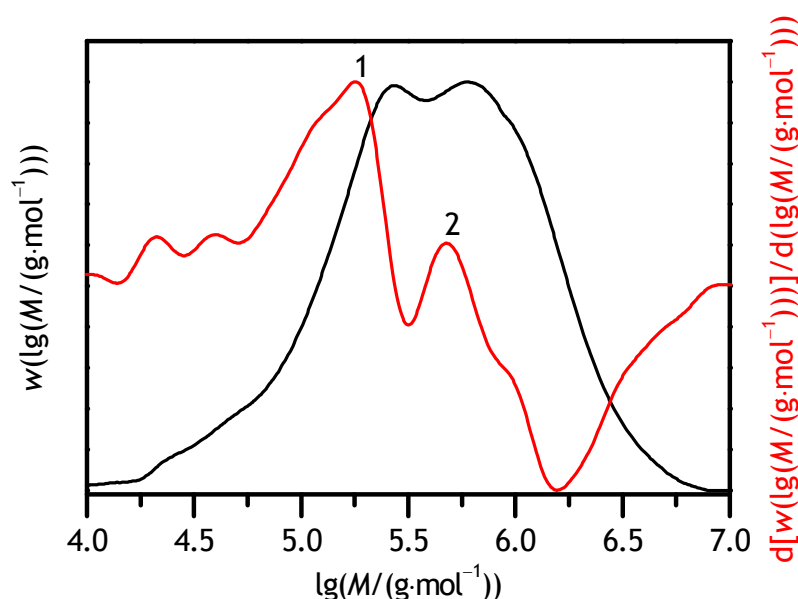


Figure 7.4: MMD (black line) and associated first-derivative curve (red line) obtained from the polymerization of $0.20 \text{ g} \cdot \text{g}^{-1}$ PAm dissolved in water at 40°C , 1500 bar, and at a laser-pulse repetition rate of 150 Hz. The MMD was obtained by poly(PAm)-relative calibration. The numbers indicate the primary and secondary POIs.

The k_p values of all four monomers are listed in appendix A.1. Also given are the monomer mass fraction, the Celsius temperature, the pressure, the photoinitiator concentration, the laser-pulse repetition rate, the number of applied pulses, N_p , the final degree of monomer conversion, the molar mass at the primary POI of the MMD, M_1 , and the ratio of M_1 to the molar mass at the secondary POI of the MMD, M_1/M_2 . The number of laser pulses required to produce a sufficient amount of polymer for analysis strongly depends among others on the preparation of the reaction solution and on laser pulse energy. A few pulses are needed to consume inhibitor and residual oxygen. The amount of oxygen depends on the duration of purging with inert gas prior to PLP, on the flow rate of inert gas, and on the size of the cuvette opening. However, the higher the number of required pulses, the lower is the influence of inhibition. The tables include several data points from experiments where the secondary POI was only reflected as a shoulder (indicated as *Sb*) in the first-derivative curve of the MMD. In many cases the positions of

the primary POI of those experiments are close to the ones observed in polymerizations which were run at the same or very similar reaction conditions, but resulted in both primary and secondary POIs. In the other cases the k_p values follow the trend seen for k_p while varying one variable. Therefore, the propagation rate coefficients deduced from the primary POIs of those experiments are considered reliable. The ratios M_1/M_2 are rather low in case of PAm polymerization. Nevertheless, the data are considered reliable as well because the ratio M_1/M_2 does not vary with pressure. It seems unlikely that any side reaction which influences the MMD results in a pressure-independent M_1/M_2 . Additionally, the volume of activation deduced from determination of k_p as a function of pressure is in a reasonable range. The multimodal MMD may be looked upon as a superposition of several unimodal MMDs, each of which corresponds to polymer that is produced by termination after an integer multiple of t_0 . The low-molar-mass side of the individual MMD, which corresponds to polymer that is produced by termination after $1 \cdot t_0$, is less affected by the overlap with an adjacent unimodal MMD than the other MMDs. M_1 , which was used to determine k_p , is therefore considered to be more reliable than M_2 .

7.1 Dependence on Laser-Pulse Repetition Rate

The propagation rate coefficient of MPAm varies with laser-pulse repetition rate. Shown in figure 7.5 is the dependence of k_p on the degree of polymerization X_1 for $0.20 \text{ g} \cdot \text{g}^{-1}$ MPAm at 25°C and ambient pressure. The red and blue data between degrees of polymerization of 325 and 450 were all determined at a laser-pulse repetition rate of 10 Hz. The difference in X_1 and thus in k_p of red and blue data may be attributed to a renewal of SEC columns although such a strong shift, in spite of a new calibration, is fairly large. k_p data at degrees of polymerization X_1 being lower than 125 were determined by means of the second POI of the MMD because the first POI occurs at molar mass less than the low-molar-mass limit of the calibration range of the SEC setup. The corresponding X_1 values were determined as the half of X_2 . As can be seen, the propagation rate coefficient decreases towards increasing chain length, whereas this

decrease seems to be more significant up to approximately 170 monomeric units. This statement may be made assuming that the red data are systematically shifted for experimental reasons to lower degrees of polymerization and lower k_p . A high consumption of initiator due to a large number of laser pulses may result in low initiator as well as radical concentrations and hence a reduced termination probability. This could explain an increase in molar mass and thus in apparent k_p . Such an effect can, however, be excluded because the number of applied pulses and the initial amount of initiator were the same for the different pulse repetition rates in almost all cases. Furthermore, it should result in a loss of the PLP structure since the control of the termination reaction by the laser is reduced. This was not observed.

What might be taken into account is a dependence of the radical concentration on the laser-pulse repetition rate. At high repetition rates a low amount of radicals terminate between two consecutive laser pulses so that the MMDs correspond to the so-called low termination rate limit.^[85,251] As has already been shown by Beuermann,^[85] this results in higher apparent k_p values at high repetition rates. Additionally, it has been reported in the literature that apparent k_p values determined by PLP–SEC increase towards smaller chains. This effect may be attributed to broadening of the MMD occurring in SEC analysis.^[82,85] A chain-length dependent propagation rate coefficient, which has been described in chapter 3.1.2, may be taken into account as well. The latter two possible explanations base on effects due to too low degrees of polymerization. k_p data at low degrees of polymerization X_1 (figure 7.5) were determined by means of the second POI of the MMD which appears at higher molar mass than the first POI. These values at low degrees of polymerization X_1 may therefore show even higher rate coefficients if the calibration range of the SEC is extended toward lower molar masses and if the k_p values are determined via the first POI. Nevertheless, other k_p data of MPAm shown within this thesis were determined via POIs which usually exhibit a degree of polymerization of some hundreds and thus a chain length in a range where the apparent k_p is almost constant. A laser-pulse repetition rate of 20 Hz, which corresponds to the degrees of polymerization in the range of 200 to 250 in figure 7.5, was usually applied to MPAm polymerization within

this work. Such a dependence of k_p on the degree of polymerization has not been observed, for example, for DM-PAm^[250] or PAm^[199].

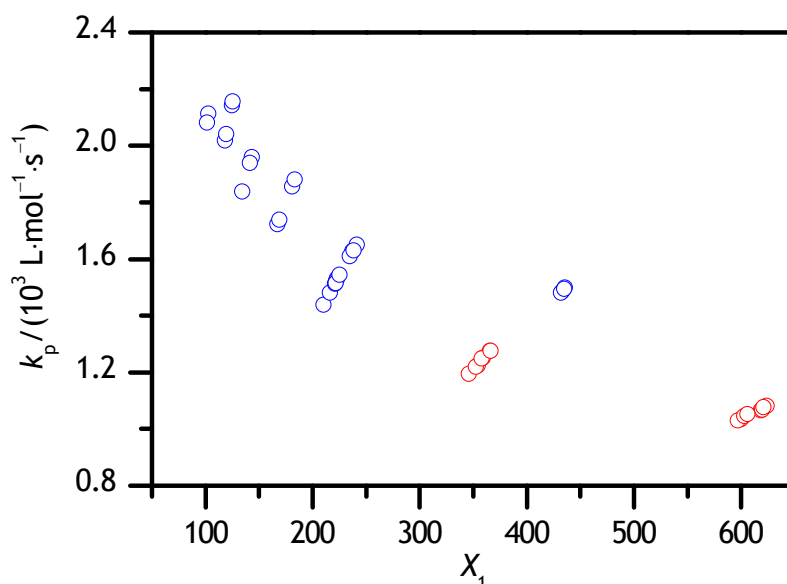


Figure 7.5: Dependence of the propagation rate coefficient on the degree of polymerization X_1 obtained from polymerizations of $0.20 \text{ g} \cdot \text{g}^{-1}$ MPAm in water at 25°C , ambient pressure, and laser-pulse repetition rates between 5 and 60 Hz. Compared to the blue data, the red data have been determined after renewal of the SEC columns.

7.2 Temperature Dependence

Examples of MMDs of poly(M-MPAm) samples prepared at 10 , 40 , and 80°C are shown in figure 7.6A. Figure 7.6B presents the associated first-derivative curves. The MMDs plotted in figure 7.6 were obtained by measuring k_p at a monomer mass fraction of $w_{\text{M-MPAm}} = 0.80 \text{ g} \cdot \text{g}^{-1}$, at an DMPA concentration of $c_{\text{DMPA}} = 1.0 \text{ mmol} \cdot \text{L}^{-1}$, at ambient pressure, and at a pulse repetition rate of 20 Hz . It can clearly be seen that the molar mass of the polymer produced by PLP increases towards higher temperature.

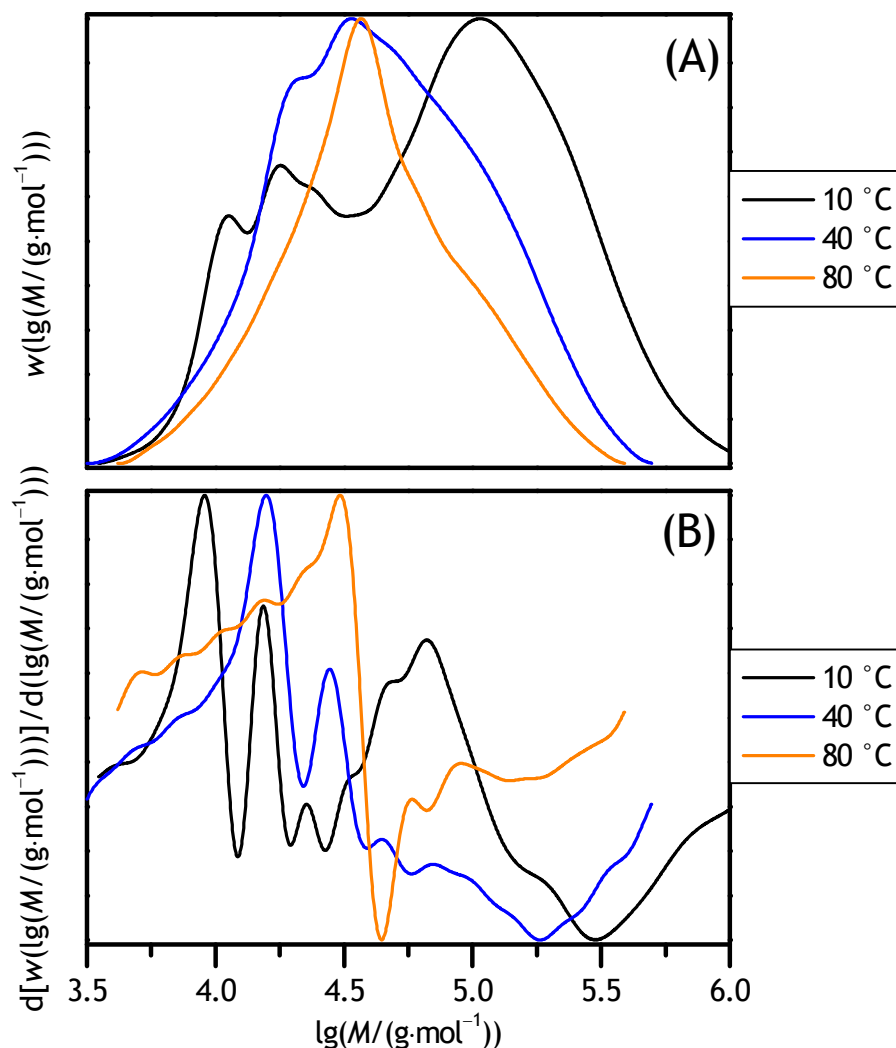


Figure 7.6: MMDs (A) and associated first-derivative curves (B) obtained from polymerizations of $0.80 \text{ g} \cdot \text{g}^{-1}$ M-MPAm dissolved in water at various polymerization temperatures, ambient pressure, and a laser-pulse repetition rate of 20 Hz.

Shown in figures 7.7, 7.8, and 7.9 are the temperature dependences of k_p of MPAm, M-MPAm, and DM-PAm at ambient pressure and four different monomer mass fractions in each case. k_p data of MPAm at 10 °C and, in case of $w_{\text{MPAm}} = 0.04 \text{ g} \cdot \text{g}^{-1}$, at 40 °C were determined by means of the second POI of the MMD because the first POI occurs at a molar mass less than the low-molar-mass limit of the calibration range of the SEC setup.

As expected, the rate coefficient decreases towards lower temperatures. The lines represent linear fits to the experimental data.

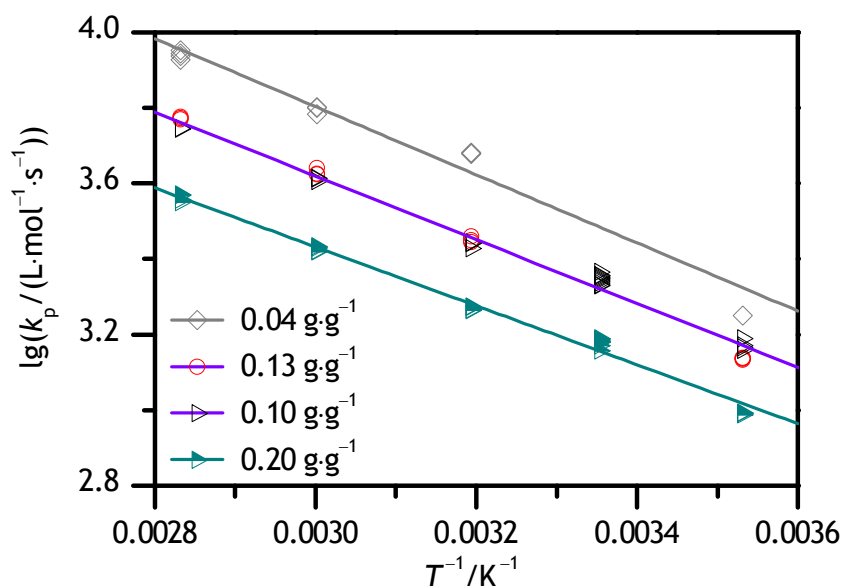


Figure 7.7: Variation of the propagation rate coefficient of MPAm with temperature at ambient pressure, a laser-pulse repetition rate of 20 Hz, and four different monomer mass fractions. The k_p values were taken from the literature.^[250] The lines represent fits of equation 3.49 to the data. Contrary to literature, k_p data at 10 °C and, in case of $w_{\text{MPAm}} = 0.04 \text{ g}\cdot\text{g}^{-1}$, at 40 °C were determined by means of the second POI of the MMD.

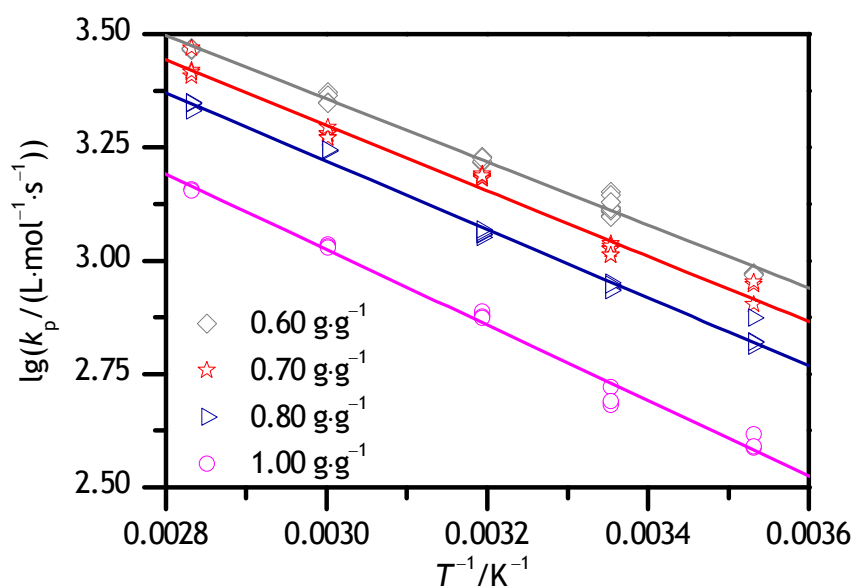


Figure 7.8: Variation of the propagation rate coefficient of M-MPAm with temperature at ambient pressure, a laser-pulse repetition rate of 20 Hz, and four different monomer mass fractions. The lines represent fits of equation 3.49 to the data.

The experimental data show some scatter but may be represented by linear fits in a good manner even in case of MPAm. This indicates that k_p of MPAm is chain-length independent at least for the chain length of polymers produced to determine the Arrhenius parameters. As the k_p values of 0.10 and 0.13 g·g⁻¹ MPAm are quite close, a common line is fitted to the rate coefficients of these two mass fractions. Regarding DM-PAm, the rate coefficients at the highest chosen temperature, 80 °C, have not been taken into account in the fitting procedure because these data seem to be significantly too low compared to the ones at lower temperatures. This indicates that a side reaction occurs which becomes more important at higher temperatures and which consequently exhibits a higher activation energy than propagation. The occurrence of transfer to polymer cannot explain the experimental values because the side reaction has less influence at low monomer concentrations. Decreasing the monomer concentration should result in a lower ratio of the probability of propagation versus the probability of chain transfer to polymer. Especially intermolecular transfer to polymer can be disregarded due to the low polymer

concentration in PLP–SEC experiments. Depropagation or transfer to monomer might explain the experimental data. Concerning depropagation, the difference between real k_p and the experimentally determined value should increase towards lower monomer contents.^[252] However, the low k_p values at 80 °C cannot be ascribed to one of the possible side reactions due to the scatter being too large.

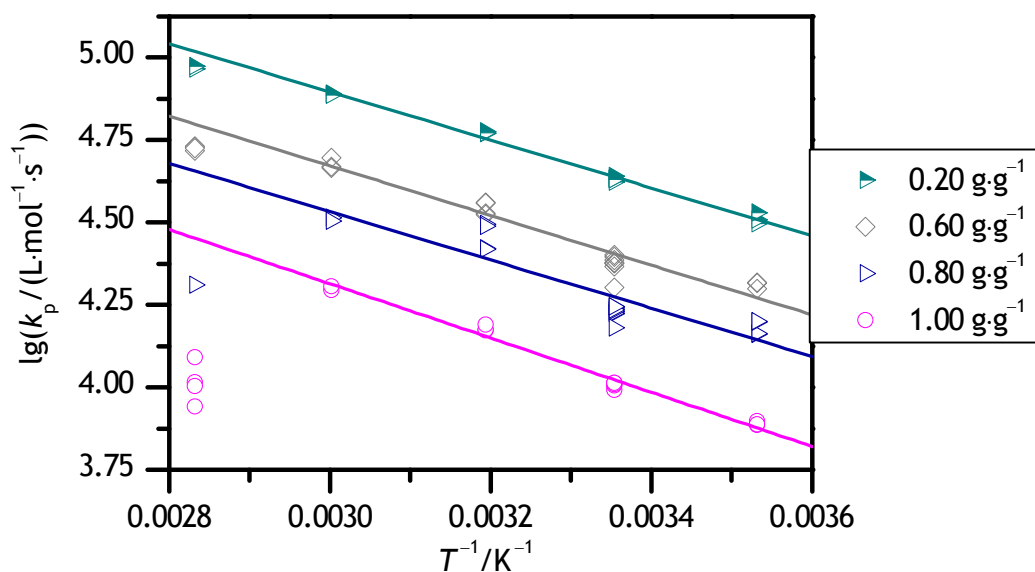


Figure 7.9: Variation of the propagation rate coefficient of DM-PAm with temperature at ambient pressure, a laser-pulse repetition rate of 100 Hz, and four different monomer mass fractions. The lines represent fits of equation 3.49 to the data disregarding the data at the highest temperature.

All Arrhenius pre-exponential factors and activation energies obtained by the linear fits are listed in table 7.1 in combination with associated k_p values at 25 °C and ambient pressure. The propagation rate coefficients are subject to a lower inaccuracy than the pre-exponential factors because the latter quantity was determined by extrapolation to infinite temperature. However, a comparison of k_p values of different monomers is hardly feasible because of the differences in the activation energy.

Table 7.1: Arrhenius activation energies and pre-exponential factors of k_p as well as k_p at 25 °C and ambient pressure of MPAm, M-MPAm, and DM-PAm for various monomer mass fractions.

monomer	$w_M/\text{g}\cdot\text{g}^{-1}$	$A/(10^6 \text{ L}\cdot\text{mol}^{-1}\cdot\text{s}^{-1})$	$E_A/\text{kJ}\cdot\text{mol}^{-1}$	$k_p(25^\circ\text{C})/(\text{L}\cdot\text{mol}^{-1}\cdot\text{s}^{-1})$
MPAm	0.04	$2.14 \leq 3.22 \leq 4.83$	17.3 ± 1.1	3049
	0.10/0.13	$1.28 \leq 1.42 \leq 1.57$	16.2 ± 0.3	2095
	0.20	$0.516 \leq 0.590 \leq 0.673$	14.9 ± 0.3	1432
M-MPAm	0.60	$0.255 \leq 0.279 \leq 0.305$	13.3 ± 0.2	1291
	0.70	$0.249 \leq 0.291 \leq 0.338$	13.8 ± 0.4	1104
	0.80	$0.270 \leq 0.300 \leq 0.334$	14.4 ± 0.3	898
	1.00	$0.283 \leq 0.331 \leq 0.388$	15.9 ± 0.4	537
DM-PAm	0.20	$10.6 \leq 12.1 \leq 13.7$	13.9 ± 0.3	43463
	0.60	$6.03 \leq 8.54 \leq 12.1$	14.4 ± 0.9	25413
	0.80	$2.84 \leq 5.34 \leq 10.0$	14.0 ± 1.6	18780
	1.00	$4.78 \leq 6.07 \leq 7.70$	15.8 ± 0.6	10538

The activation energy of k_p of MPAm decreases with increasing monomer concentration. This is also illustrated in figure 7.10 which shows joint confidence regions for the Arrhenius parameters of k_p for the monomer concentrations under investigation. These are obtained by a nonlinear least-squares fit assuming constant relative errors in k_p and T . The symbols (\times) indicate the best estimates of Arrhenius activation energy and pre-exponential factor. As can be seen in figure 7.10, both activation energy and pre-exponential factor of k_p of MPAm change with monomer concentration.

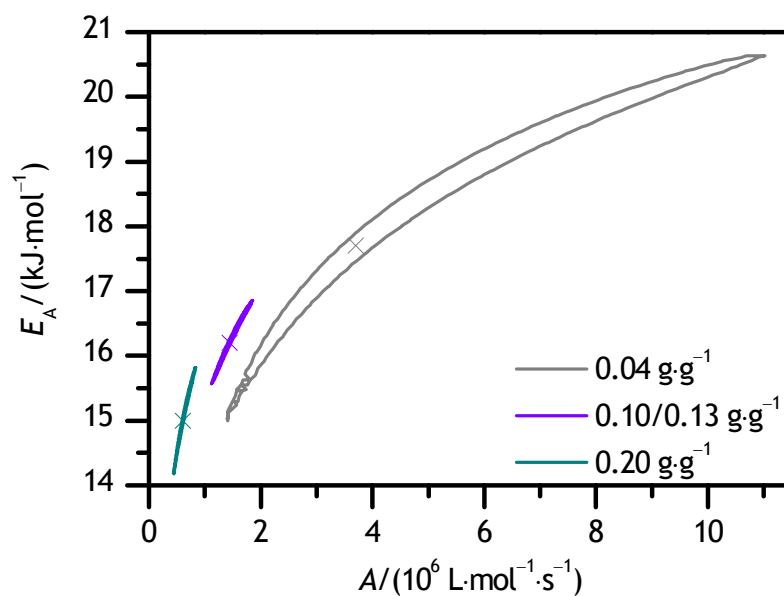


Figure 7.10: 95 % joint confidence region for the Arrhenius parameters of k_p of MPAm for various low monomer mass fractions in aqueous solution. The symbols (×) indicate the best estimates of Arrhenius activation energy and pre-exponential factor.

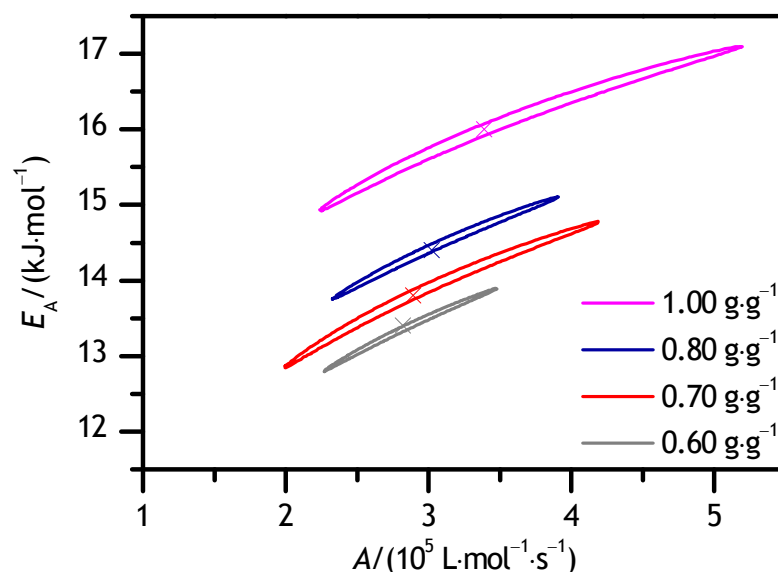


Figure 7.11: 95 % joint confidence region for the Arrhenius parameters of k_p of M-MPAm for various high monomer mass fractions in aqueous solution. The symbols (×) indicate the best estimates of Arrhenius activation energy and pre-exponential factor.

Regarding M-MPAm and DM-PAm, table 7.1 as well as figures 7.11 and 7.12 show that, considering the scatter of the data, the activation energy may be assumed to be independent of the monomer concentration except for bulk polymerization. Both bulk polymerizations show an activation energy that is increased by approximately $2 \text{ kJ}\cdot\text{mol}^{-1}$. Such a behavior has already been reported for VP^[45] and may be explained by the smaller size of the water molecules compared to monomer molecules. Due to the size of the molecules, it may be assumed that at least in case of the coordination of monomer molecules to the macroradical via intermolecular interactions not all coordination sites will be occupied. Hence, the number of molecules which do not coordinate to a macroradical will increase if monomer molecules are preferentially coordinated. Instead, molecules which do not coordinate to a macroradical may form clusters. Taking into account that a single monomer molecule replaces several solvent molecules at the coordination sites, it may further be assumed that the number of clusters is increased by this replacement process. For entropic reasons, the coordination of monomer molecules should be favored

over the coordination of water molecules. According to the fundamental equation of Gibbs energy, this preference increases towards higher temperature. This results in an increased hindrance in the transition state of the propagation step towards higher temperature and therefore a lower k_p value. Such a decrease counteracts the common increase in k_p which may be described by the Arrhenius equation. Since the pre-exponential factor is defined to be temperature independent, it causes the activation energy to be reduced compared to a bulk polymerization which cannot show a variation of the direct environment of the macroradical. Similar to bulk polymerization, the activation energy may be higher in case of monomer concentrations being close to zero compared to polymerizations at intermediate monomer contents. This may be seen in case of the polymerization of MPAm, MAA,^[41] and AA^[38] in aqueous solution. Furthermore, the resonance stabilization may be influenced by a change of the solvent field.^[72] This may especially apply to DM-PAm because the monomer is not capable of forming hydrogen bonds in bulk. The change in resonance stabilization may result in a change in activation energy. Nevertheless, within experimental accuracy, the rate coefficients of MPAm, M-MPAm, and DM-PAm might be represented by a single, concentration-independent activation energy of $16.1 \text{ kJ}\cdot\text{mol}^{-1}$, $14.4 \text{ kJ}\cdot\text{mol}^{-1}$, and $14.5 \text{ kJ}\cdot\text{mol}^{-1}$, respectively. The Arrhenius activation energy of k_p of MPAm is 1 to $2 \text{ kJ}\cdot\text{mol}^{-1}$ higher than the value for the polymerization of MAA at similar monomer mass fractions in aqueous solution.^[41,42] The amino group versus the hydroxy group is the only difference between these two monomers. Compared to the presence of an oxygen atom, the presence of a nitrogen atom, which is less electronegative than an oxygen atom, raises the bonding and antibonding π molecular orbitals of the carbonyl group in energy and thus increases the stability of the radical^[253]. Therefore, a higher activation energy may be expected for k_p of MPAm compared to MAA. This is in agreement with experimental results. Furthermore, the activation energy of k_p of MPAm is lower than the one of k_p of PAm which is approximately $18 \text{ kJ}\cdot\text{mol}^{-1}$.^[199] As has already been found for methacrylates versus acrylates,^[32] an α -methyl group stabilizes the propagating radical^[254] resulting in a higher activation energy of k_p . The lower value in case of MPAm compared to PAm is not well understood so far.

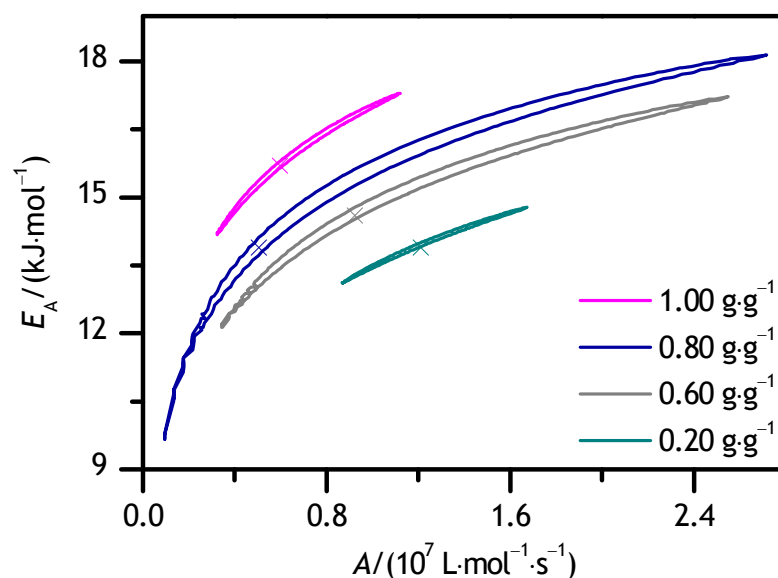


Figure 7.12: 95 % joint confidence region for the Arrhenius parameters of k_p of DM-PAm for various monomer mass fractions in aqueous solution. The symbols (×) indicate the best estimates of Arrhenius activation energy and pre-exponential factor.

The activation energy of k_p of DM-PAm is lower compared to k_p of MPAm due to the absence of the α -methyl group. The activation energy of k_p of DM-PAm is $3.5 \text{ kJ}\cdot\text{mol}^{-1}$ lower than in case of k_p of PAm, too. This fact contradicts what has been found for the comparison of MAA^[41,42] and methyl methacrylate ($22.4 \text{ kJ}\cdot\text{mol}^{-1}$)^[32] as well as for AA (approximately $14 \text{ kJ}\cdot\text{mol}^{-1}$)^[38] versus methyl acrylate ($17.7 \text{ kJ}\cdot\text{mol}^{-1}$)^[25]. Interestingly, the activation energy of M-MPAm is lower than the ones of MPAm and DM-PAm. These findings indicate that a methylation of the amide nitrogen leads to a decrease of the activation energy. To evaluate this, the activation energy of k_p of *N*-methylprop-2-enamide would be of interest. *N,N*,2-trimethylprop-2-enamide does not homopolymerize radically so that a comparison of the three 2-methylprop-2-enamides is not possible. Except for 1-(aziridin-1-yl)-2-methylprop-2-en-1-one, *N,N*-disubstituted 2-methylprop-2-enamides do not undergo radical homopolymerization.^[255–262] This might be due to the steric demand of the bulky *N,N*-disubstituted amide group in combination with the α -methyl group. Anyhow, several *N,N*-disubstituted 2-methylprop-2-enamides have been shown to be

homopolymerizable anionically^[258] or radically by complexing the amide group with a Lewis acid.^[263] Contrary to electronic reasons, steric reasons should thus play a minor role in the inability of polymerizing *N,N*-disubstituted 2-methylprop-2-enamides radically. Remarkable is the conformation of the carbon–carbon double bond versus the carbon–oxygen double bond. Resulting from the repulsion of the dialkylamino group and the α -methyl group only a small fraction of *N,N*,2-trimethylprop-2-enamide^[255,264,265] is in *s-cis* conformation whereas the conformation is predominantly *s-cis* in case of DM-PAm.^[264,265] As surmised by Okamoto and Yuki, this might explain that *N,N*-disubstituted 2-methylprop-2-enamides do not undergo radical homopolymerization.^[255] The argumentation by the conformation is supported by Miyake et al. who determined a poor overlap between the π molecular orbitals of the carbon–carbon and the carbon–oxygen double bonds in case of *N,N*,2-trimethylprop-2-enamide.^[266] A difference in conformations of M-MPAm and MPAm might also explain the difference in activation energies since the energy of the transition state structure should be much less dependent on the conformation of the monomer compared to the energy of the educts. A determination of the activation energy of k_p of other *N*-alkylated 2-methylprop-2-enamides could validate this supposition.

Like in case of MAA^[41] versus AA^[38], the pre-exponential factors of both 2-methylprop-2-enamides, MPAm and M-MPAm, are smaller than the ones of the prop-2-enamides PAm, which is about $7.13 \cdot 10^7 \text{ L} \cdot \text{mol}^{-1} \cdot \text{s}^{-1}$ at a monomer mass fraction of $0.20 \text{ g} \cdot \text{g}^{-1}$,^[199] and DM-PAm as can be seen in table 7.1. The α -methyl group in 2-methylprop-2-enamides induces a hindrance of internal rotational and vibrational motions of the macroradical in the propagation transition state.^[42] The partition function of the transition state is therefore reduced resulting in a lower pre-exponential factor of MPAm and M-MPAm. But it has to be mentioned that this reduction of the pre-exponential factor is much more pronounced for MPAm versus PAm (factor of approximately 120 at a monomer mass fraction of $0.20 \text{ g} \cdot \text{g}^{-1}$) than for MAA versus AA (factor of approximately 10 at a monomer mass fraction of $0.20 \text{ g} \cdot \text{g}^{-1}$)^[33,41]. As can be seen in table 7.2, the Arrhenius pre-exponential factor of bulk DM-PAm polymerization is fairly high. This may be understood because of the lack of an α -methyl group and because

of the size of the amide group which may be assumed to be smaller than the pyrrolidin-2-one group in case of VP. MMA k_p shows a higher pre-exponential factor than MAA and M-MPAm due to the absence of hydrogen bonds and thus a smaller hindrance of internal rotational and vibrational motions of the macroradical in the transition state of propagation. The opposite applies to NVF. This monomer does not contain an α -methyl group but is capable of forming hydrogen bonds. Therefore, k_p of NVF exhibits a pre-exponential factor that is lower compared to VP and DM-PAm.

Table 7.2: Arrhenius pre-exponential factors for bulk polymerizations of several monomers. The values for VP,^[45] MMA,^[22] NVF,^[46] and MAA^[41] were taken from the literature.

monomer	$A/(10^6 \text{ L}\cdot\text{mol}^{-1}\cdot\text{s}^{-1})$
DM-PAm	6.07
VP	3.3
MMA	2.67
NVF	2.0
MAA	0.38
M-MPAm	0.331

7.3 Concentration Dependence

At least in case of MPAm, a decrease of the pre-exponential factor towards higher monomer concentration is noticeable. For further investigations into this behavior k_p has been determined at 25 °C for various monomer mass fractions. The data are shown in figures 7.13, 7.14, and 7.15 together with a fitted line corresponding to equation 7.1. This equation has already been used in case of VP and *N*-vinylformamide (NVF).^[45,46] The monomer content of the solution is represented by the mass fraction. A different quantity may be more useful for a quantitative interpretation of the dependence of k_p on monomer

content. However, an appropriate model is not available so far and monomer mass fractions are common in industry.

$$k_p / (\text{L} \cdot \text{mol}^{-1} \cdot \text{s}^{-1}) = A_p \cdot \left(B_p + (1 - B_p) \cdot \exp \left(-C_p \cdot \frac{w_M}{\text{g} \cdot \text{g}^{-1}} \right) - D_p \cdot \frac{w_M}{\text{g} \cdot \text{g}^{-1}} \right) \quad (\text{eq. 7.1})$$

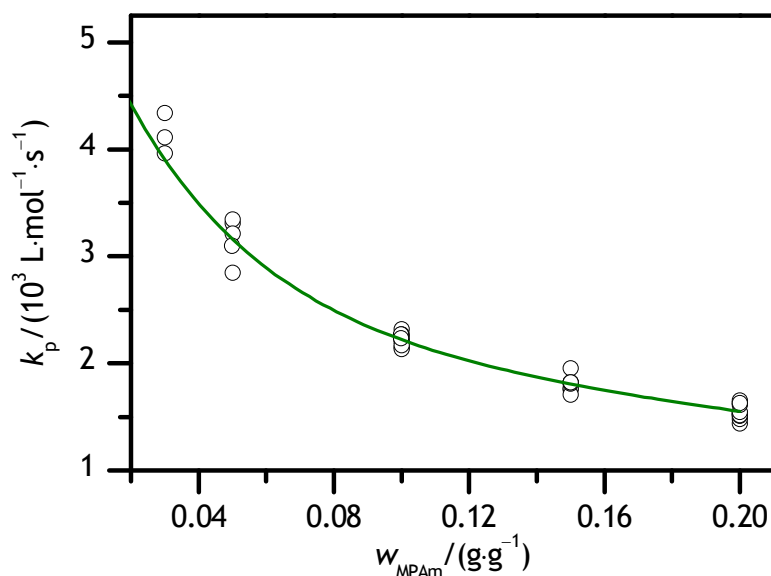


Figure 7.13: Dependence of the propagation rate coefficient on the monomer mass fraction w_{MPAm} for polymerization at 25 °C, ambient pressure and a laser-pulse repetition rate of 20 Hz. The line represents a fit of equation 7.1 to the experimental data. Contrary to literature, k_p data at initial MPAm mass fractions of $0.03 \text{ g} \cdot \text{g}^{-1}$ and $0.05 \text{ g} \cdot \text{g}^{-1}$ were determined by means of the second POI of the MMD.

The measured data are well represented by the lines. The associated fit parameters are listed in table 7.3. The values at $0.03 \text{ g} \cdot \text{g}^{-1}$ MPAm are not considered in the fitting procedure because the chain lengths of these samples are rather small and it cannot be excluded that these high k_p values result from an artifact of the PLP–SEC method or a

chain-length dependence of k_p . In addition, these k_p data and data at an initial MPAm mass fraction of $0.05 \text{ g}\cdot\text{g}^{-1}$ were determined by means of the second POI of the MMD. In case of DM-PAm, the values at 0.03 , 0.05 , 0.10 , 0.15 , and $0.30 \text{ g}\cdot\text{g}^{-1}$ were determined at 10°C and estimated for 25°C by means of the Arrhenius equation and the average activation energy. The estimated k_p values at $0.30 \text{ g}\cdot\text{g}^{-1}$ seem to be reasonable compared the values for 0.20 and $0.40 \text{ g}\cdot\text{g}^{-1}$ determined at 25°C . This indicates that a combined fit of both data sets is possible. The obtained fit parameters in case of M-MPAm are significantly different from the ones of DM-PAm. However, k_p values of M-MPAm are only available in a small concentration range in which the dependence of k_p on monomer mass fraction is almost linear. Therefore, the concentration dependence of k_p of M-MPAm may be adequately represented by different parameters as well.

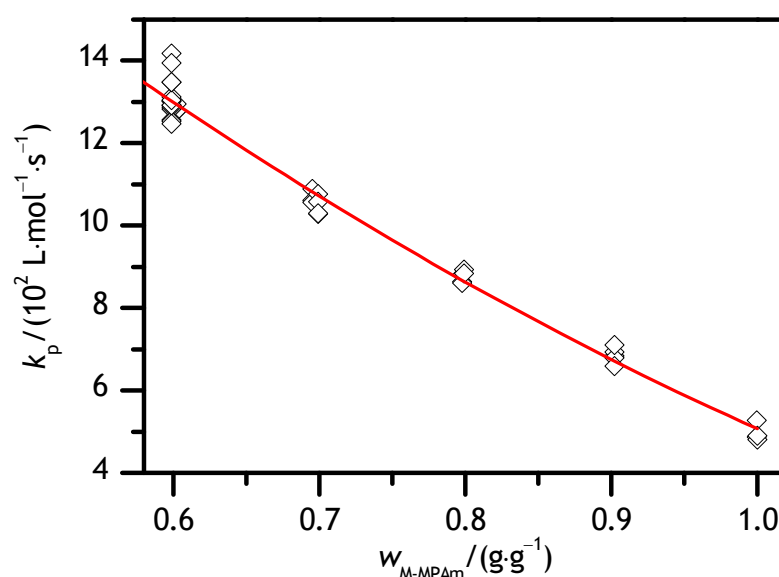


Figure 7.14: Dependence of the propagation rate coefficient on the monomer mass fraction $w_{\text{M-MPAm}}$ for polymerization at 25°C , ambient pressure and a laser-pulse repetition rate of 20 Hz . The line represents a fit of equation 7.1 to the experimental data.

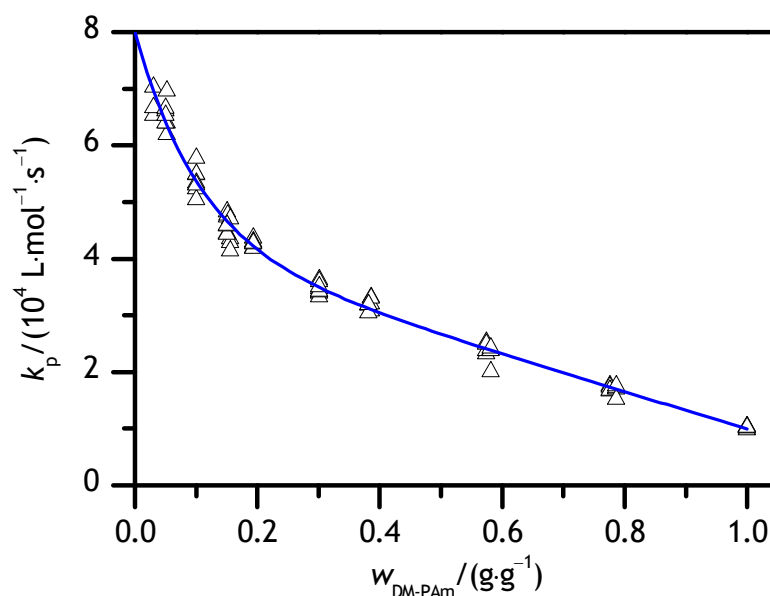


Figure 7.15: Dependence of the propagation rate coefficient on the monomer mass fraction $w_{\text{DM-PAm}}$ for polymerization at 25 °C and ambient pressure. The line represents a fit of equation 7.1 to the experimental data.

Propagation rate coefficients for the polymerization of prop-2-enamide in aqueous solution at 50 °C and ambient pressure were provided by Chovancová et al.^[199] The arithmetic mean values for each monomer mass fraction and the corresponding standard deviations are given in figure 7.16 in combination with a fit of equation 7.1 to the data with the parameter D_p set to zero.

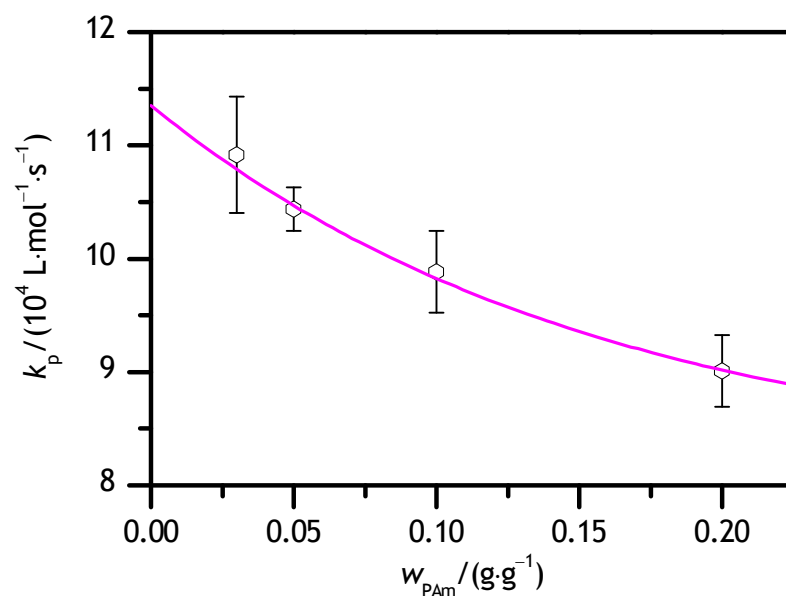


Figure 7.16: Propagation rate coefficients in dependence on the monomer mass fraction w_{PAm} at 50 °C and ambient pressure. The data were provided by Chovancová et al.^[199] The line represents a fit of equation 7.1 to the experimental data with the parameter D_p set to zero.

Table 7.3: Parameters deduced from fitting equation 7.1 to the concentration dependences of k_p of MPAm, M-MPAm, and DM-PAm at 25 °C and ambient pressure. The parameters for PAm are valid for 50 °C.

monomer	$A_p \cdot 10^{-3}$	B_p	C_p	D_p
MPAm	5.88	0.388	24.3	0.646
M-MPAm	3.07	-101	-0.0771	9.01
DM-PAm	80.0	0.535	9.63	0.411
PAm	114	0.714	6.37	0

The k_p value of MPAm at a monomer mass fraction of 0.09 g·g⁻¹ and at 25 °C is about twice as high compared to the rate coefficient determined by Pascal et al.^[248] which is 1 100 L·mol⁻¹·s⁻¹ at a pH of unity but otherwise ostensibly identical reaction conditions. A direct comparison of both values is not possible because within the present work no acid

was added to reduce the pH. However, both values are of the same order of magnitude. What can also be seen in figures 7.13, 7.14, 7.15, and 7.16 is a clear decrease of k_p towards higher monomer concentrations. This behavior has already been found for several other monomers in aqueous solution, for example, *N*-(propan-2-yl)prop-2-enamide,^[37] PAm,^[40] AA,^[38] MAA,^[35,41,47] VP,^[45] and 2-methyl-2-(prop-2-enamido)propane-1-sulfonic acid,^[71] and may be explained by a decrease in the pre-exponential factor of k_p (chapter 3.1.2) under the assumption of the activation energy being independent of monomer concentration.^[41] Replacing monomer molecules in the direct vicinity of the active center by water molecules provides a weaker hindrance in the internal rotational and vibrational motions of the transition state of the propagation step. This is due to stronger intermolecular interactions between monomer and macroradical compared to the intermolecular interactions between water molecules and the macroradical. The dominating intermolecular interactions in case of the polymerization of prop-2-enamides in water are most likely hydrogen bonding and dipole–dipole interactions. The dipole moments of prop-2-enamides, which are, for example, 3.44 D for PAm (*s-cis* conformer),^[267] 3.55 D for propanamide,^[268] the saturated analogue of PAm, and 3.8 D for DM-PAm (*s-cis* conformer),^[269] are rather high compared to the one of water which is 1.85 D.^[234] The dipole–dipole interaction between two monomer molecules should therefore play an important role. In case of DM-PAm, which can act as hydrogen bond acceptor but not as hydrogen bond donor, the addition of a small amount of water to monomer could increase the strength of the intermolecular interactions due to the formation of hydrogen bonds. This would result in a minimum of the pre-exponential factor at high monomer contents which might be seen in table 7.1 and figure 7.12. Such higher pre-exponential factor in combination with a potentially higher activation energy in bulk polymerization may, at 25 °C, still result in a smaller k_p value in bulk polymerization compared to polymerizations in aqueous solution. However, the accuracy of determination of E_A and A does not allow for a verification of this hypothesis.

The required space of water molecules is much smaller compared to monomer molecules. Lowering the monomer concentration may therefore increase the number of molecules in the direct vicinity of the propagating radical. Considering the hindrance described in the

preceding paragraph and neglecting differences in the strength of intermolecular interactions, this gives rise to the expectation of a reduced pre-exponential factor. The effect described in the preceding paragraph is obviously much stronger and dominates. Nevertheless, the combination of both effects might explain the shape of the dependence of k_p on monomer concentration.

The concentration dependence of k_p is shown in figure 7.17 for various monomers in aqueous solution. To allow for a comparison of relative changes in k_p , the propagation rate coefficient has been divided by the parameter \mathcal{A}_p which corresponds to the virtual rate coefficient at a monomer content of zero. These relative rate coefficients are plotted versus the monomer mass fraction because this quantity is common in industry. The relative rate coefficients of various monomers could also be compared with each other on the basis of, for example, the monomer mole fraction. However, such a comparison would show similar results because the molar masses of the monomers are close to each other and significantly higher than the one of water. These molar masses are required to convert mass fractions into mole fractions. In case of concentration-independent activation energies, the lines in figure 7.17 are temperature independent. It can clearly be seen that, compared to NVF, DM-PAm, and VP, the change in k_p of MAA is stronger at intermediate monomer mass fractions but weaker at high monomer contents. The decrease of k_p of MPAm towards higher monomer content up to 0.20 g·g⁻¹ is strongest and exceeds the decrease in case of NVF by almost a factor of two. The rather weak change in k_p of PAm may be an artifact of the low number of data points in a small concentration range.

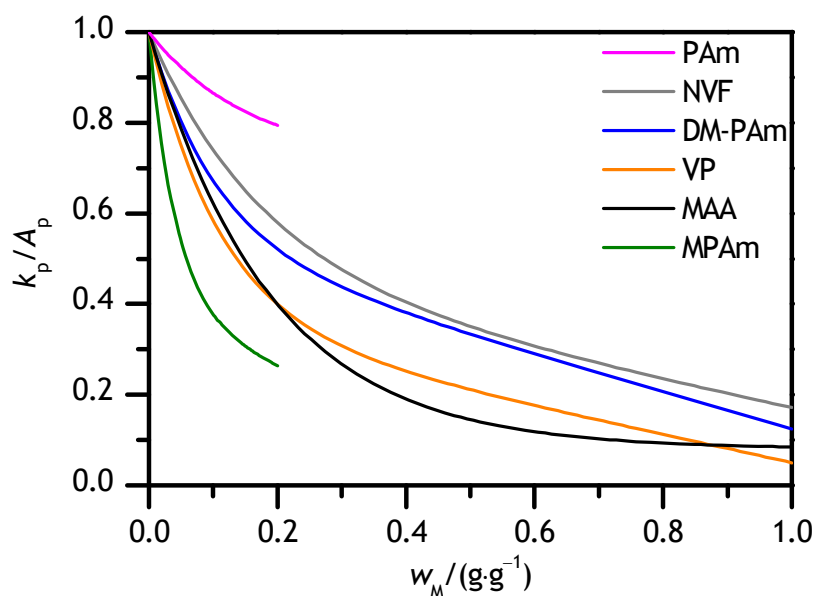


Figure 7.17: Dependence of the relative propagation rate coefficient k_p/A_p on monomer mass fraction in aqueous solution for NVF, DM-PAm, VP, non-ionized MAA, and MPAm at 25 °C and ambient pressure. Functions representing k_p data of NVF,^[46] VP,^[45] and non-ionized MAA^[111] were taken from the literature. The line for PAm is valid for 50 °C.

The fact that the value for parameter C_p is close to zero in case of M-MPAm reflects that the dependence of k_p on monomer mass fraction is almost linear. Such linearity can also be seen in case of DM-PAm at high monomer mass fractions. The linear part in equation 7.1 is introduced to represent experimental data in case of the three prop-2-enamides under investigation as well as VP^[45] and NVF^[46] but may be omitted for MAA^[111]. Classifying the concentration dependence of M-MPAm, k_p requires to divide k_p by the bulk propagation rate coefficient, $k_{p,\text{bulk}}$, because the monomer is not soluble at low monomer concentration. Figure 7.18 shows that the increase of k_p of M-MPAm is slightly stronger compared to DM-PAm. Assuming a concentration-independent activation energy, the change in k_p should be pronounced if the hindrance in the internal rotational and vibrational motions of the transition state of the propagation step of bulk polymerization is much stronger than in solution. The hindrance in bulk polymerization should increase towards higher steric demand of the monomer and stronger

intermolecular interactions. The amide group of DM-PAm is sterically more demanding compared to the amide group of M-MPAm. However, DM-PAm cannot form hydrogen bonds in bulk and it does not contain an α -methyl group and may therefore be accompanied by the same change in k_p with monomer content as M-MPAm.

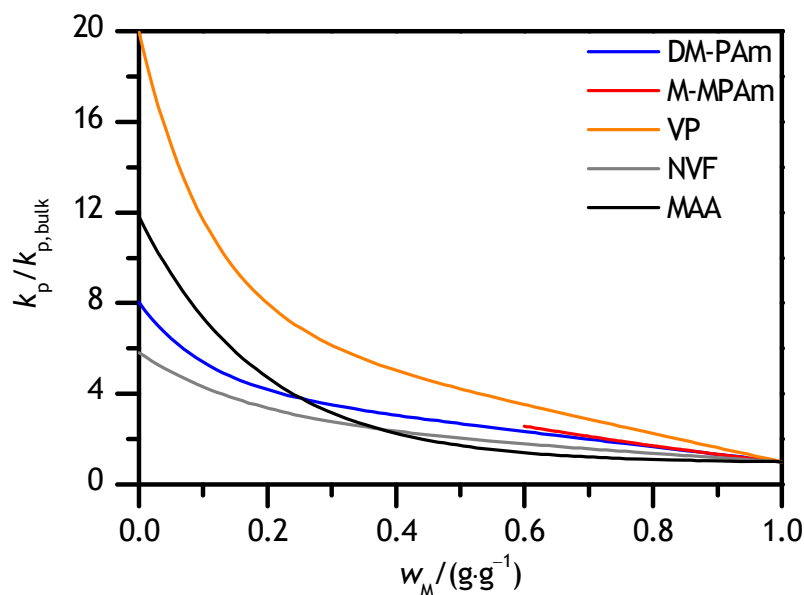


Figure 7.18: Dependence of the relative propagation rate coefficient $k_p/k_{p,bulk}$ on monomer mass fraction in aqueous solution for DM-PAm, M-MPAm, VP, NVF, and non-ionized MAA at 25 °C and ambient pressure. Functions representing k_p data of NVF,^[46] VP,^[45] and non-ionized MAA^[111] were taken from the literature.

The high dipole moment of VP combined with the steric demand of the pyrrolidin-2-one group may result in the strongest change in k_p compared to the monomers mentioned in figures 7.17 and 7.18. NVF, which most probably exhibits a smaller dipole moment than VP^[46] and which is sterically less demanding than VP, obviously shows a rather weak change in k_p . MAA and MPAm contain α -methyl groups and may form strong hydrogen bonds. Therefore, k_p of these two monomers shows strong variation with monomer content. These statements are made under the assumption of a concentration-independent

activation energy. An individual comparison of activation energies and pre-exponential factors would be preferable. However, the scatter of the data as well as the extrapolation to infinite temperature and the associated error make such a comparison hardly feasible.

7.4 Pressure Dependence

Illustrated in figures 7.19, 7.20, 7.21, and 7.22 are propagation rate coefficients as a function of pressure determined at an initiator concentration of approximately $2 \text{ mmol}\cdot\text{L}^{-1}$ and a pulse repetition rate of 150 Hz for PAm, 100 Hz for DM-PAm, and 20 Hz for MPAm as well as M-MPAm. As expected for a chemically controlled bond-forming reaction, the rate coefficient increases towards higher pressure^[144] which corresponds to a negative volume of activation. The volumes of activation of k_p , which were determined via equation 3.48, are given in table 7.4.

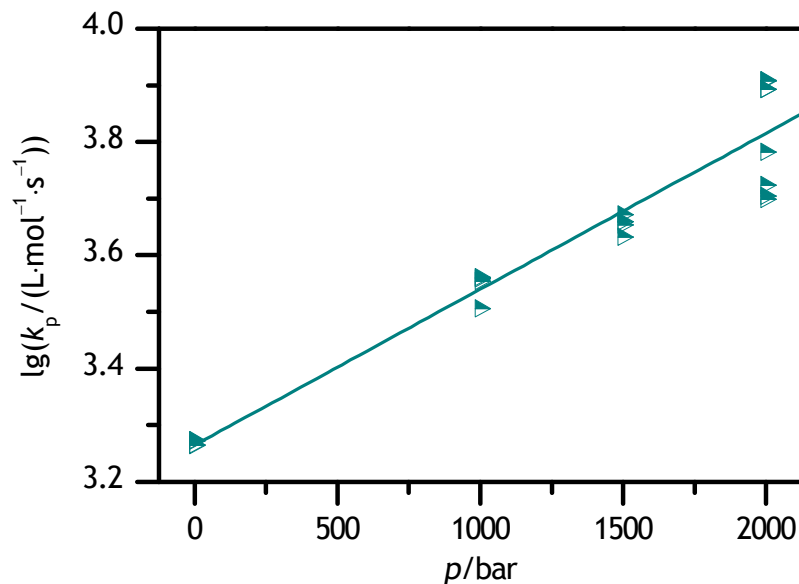


Figure 7.19: Variation of the propagation rate coefficient of MPAm with pressure at 40°C , a laser-pulse repetition rate of 20 Hz, and a monomer mass fraction of $0.20 \text{ g}\cdot\text{g}^{-1}$. The line represents a linear fit to the data.

The absolute value of the volume of activation in case of MPAm is slightly larger than the value for methacrylates which is approximately $-16 \text{ cm}^3 \cdot \text{mol}^{-1}$ [26]. The same applies to DM-PAm versus the acrylate family which exhibits a volume of activation of approximately $-11.5 \text{ cm}^3 \cdot \text{mol}^{-1}$ [25].

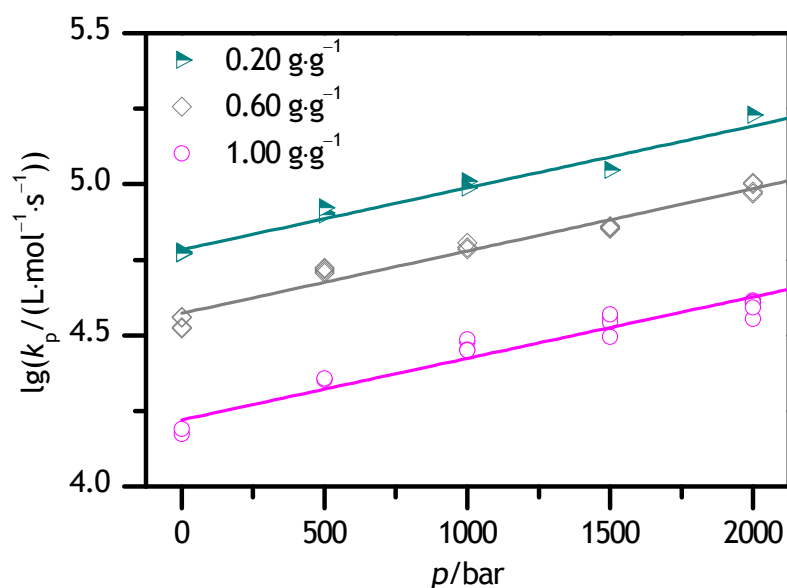


Figure 7.20: Variation of the propagation rate coefficient of DM-PAm with pressure at 40°C , a laser-pulse repetition rate of 100 Hz, and monomer mass fractions of 0.20, 0.60, and $1.00 \text{ g} \cdot \text{g}^{-1}$. The lines represent linear fits to the data.

The slightly more negative volumes of activation in case of the prop-2-enamides might be due to the sterically more demanding amide group compared to the ester group. The length of the carbon–carbon bond formed in the propagation step should show a rather weak dependence on the size of the substituent. Therefore, the partial molar volume of the transition state may be less dependent on substituent size compared to the partial molar volume of the monomer. This would result in larger negative volumes of activation for bulkier substituents of the monomer. The volume of activation of k_p of PAm is, however, close to the one of the acrylate family. As indicated by the family-type behavior of the acrylates and methacrylates,[25,26] only atoms in close vicinity to the double bond of

the monomer seem to influence the volume of activation. In case of prop-2-enamides the number of substituents at the nitrogen atom may have to be taken into account because of the large steric demand of an alkylated amide group. However, neglecting the k_p values at ambient pressure, which were taken from the literature,^[199] results in a volume of activation of $-13.1 \text{ cm}^3 \cdot \text{mol}^{-1}$. The experimental average ambient-pressure rate coefficient would exceed the one estimated by means of the fitted line by approximately 15 %. Therefore, the difference in volumes of activation in case of DM-PAm and PAm could also be ascribed to measuring inaccuracy.

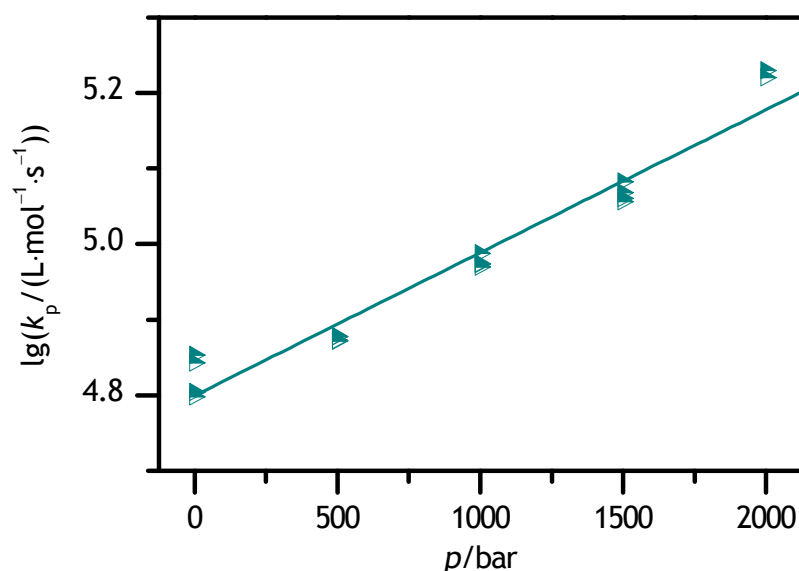


Figure 7.21: Variation of the propagation rate coefficient of PAm with pressure at 40 °C, a laser-pulse repetition rate of 150 Hz, and a monomer mass fraction of $0.20 \text{ g} \cdot \text{g}^{-1}$. Ambient pressure values were provided by Chovancová et al.^[199] The line represents a linear fit to the data.

Surprising is that the volume of activation of k_p of M-MPAm is rather low and almost the same as the one in case of DM-PAm. The volume of activation of k_p of M-MPAm would have been expected to show an even larger absolute value than in case of MPAm because M-MPAm is larger. As this is not the case, maybe other parts than the pure intrinsic

volume of activation have to be taken into account (chapter 3.3). Firstly, it may be assumed that M-MPAm is predominantly in *s-trans* conformation since the *s-cis* conformation is only slightly preferred in case of the less sterically demanding PAm and DM-PAm.^[264] Secondly, the dipole moment of the *s-trans* conformer of methyl acrylate is by approximately 1 D larger than the one of the *s-cis* conformer,^[270] which may be understood qualitatively bearing in mind that the carbonyl oxygen should have a partial negative charge whereas ether oxygen and β -carbon have a partial positive charge. This should be valid for prop-2-enamides as well. Thirdly, the dipole moment of the *s-cis* conformer of PAm is approximately the same as for its saturated analogue.^[267,268] The dipole moment of the M-MPAm monomer might therefore be larger than the apparent dipole moment of the saturated monomeric unit in the polymer. This would result in stronger intermolecular interactions and thus in a shorter distance of monomer and solvent in case of the educts. This solvation contribution to the volume of activation would counteract the intrinsic part resulting in a small overall volume of activation.

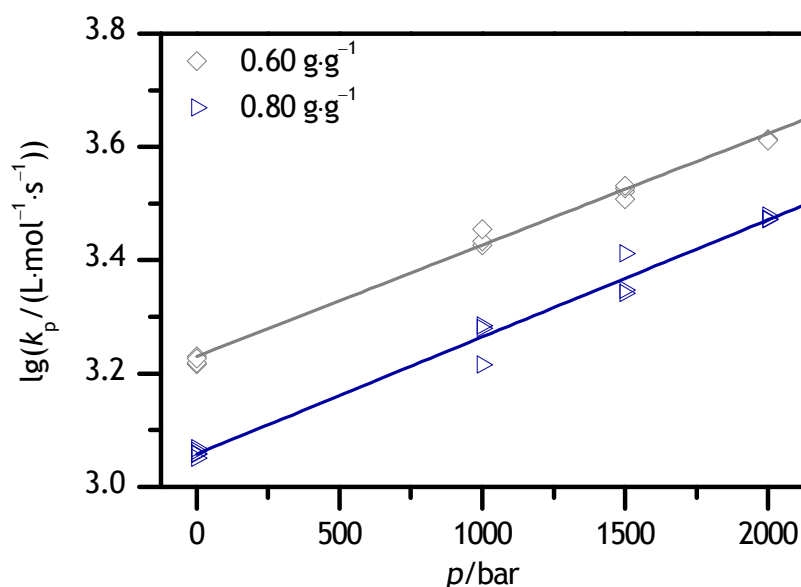


Figure 7.22: Variation of the propagation rate coefficient of M-MPAm with pressure at 40 °C, a laser-pulse repetition rate of 20 Hz, and monomer mass fractions of 0.60 and 0.80 $\text{g} \cdot \text{g}^{-1}$. The lines represent linear fits to the data.

In contrast to M-MPAm, the conformation of MPAm should be predominantly *s-cis* because of the small steric demand of the primary amino group. Such conformation might result in a dipole moment which is similar to the one of its saturated analogue. The difference in conformation might therefore explain that the volume of activation of k_p of MPAm is larger than the one of k_p of M-MPAm. Regarding acrylates and methacrylates, the predominant conformation might be assumed to be *s-cis* in both cases because the even more sterically hindered methyl (*E*)-2-methylbut-2-enoate is predominantly in *s-cis* conformation.^[264]

Furthermore, it stands out that the volumes of activation in case of DM-PAm and M-MPAm in aqueous solution seem to be independent of monomer concentration.

Table 7.4: Volumes of activation of k_p of MPAm, M-MPAm, DM-PAm, and PAm determined at 40 °C.

monomer	$w_M/(\text{g} \cdot \text{g}^{-1})$	$\Delta^\ddagger V^\circ/(\text{cm}^3 \cdot \text{mol}^{-1})$
MPAm	0.20	-16.5 ± 1.1
M-MPAm	0.60	-11.8 ± 0.3
	0.80	-12.4 ± 0.5
DM-PAm	0.20	-12.3 ± 0.7
	0.60	-12.4 ± 0.6
	1.00	-12.2 ± 0.8
PAm	0.20	-11.3 ± 0.6

7.5 Multidimensional Dependence on Reaction Conditions

Assuming concentration-independent activation energy and volume of activation, the dependences of k_p of MPAm on temperature, pressure, and monomer mass fraction may be summarized to equation 7.2.

$$\begin{aligned}
& k_p(w_{\text{MPAm}}, T, p) / (\text{L} \cdot \text{mol}^{-1} \cdot \text{s}^{-1}) = 3.91 \cdot 10^6 \\
& \cdot (0.388 + (1 - 0.388) \cdot \exp(-24.3 \cdot w_{\text{MPAm}}) - 0.646 \cdot w_{\text{MPAm}}) \\
& \cdot \exp\left(-\frac{1.61 \cdot 10^4 - 1.65 \cdot (p/\text{bar})}{8.31441 \cdot (T/\text{K})}\right)
\end{aligned} \tag{eq. 7.2}$$

The data given above were determined by PLP–SEC which is generally performed at low degrees of monomer conversion to avoid significant changes in monomer concentration. Thus, these data refer to the mass fraction in the initial period of polymerization. Assuming that the size of the propagation rate coefficient mainly depends on the amount of monomer in the solution, as already seen for MAA and VP,^[43,45] the mass fraction of MPAm in this equation may be replaced by w_{MPAm}^0 :

$$w_{\text{MPAm}} = \frac{w_{\text{MPAm}}^0 \cdot (1 - \alpha)}{1 - w_{\text{MPAm}}^0 \cdot \alpha} \tag{eq. 7.3}$$

with w_{MPAm}^0 representing the initial mass fraction of 2-methylprop-2-enamide. This equation disregards the amount of polymer produced within the polymerization. The combination of equations 7.2 and 7.3 might be a good representation of all k_p data.

$$\begin{aligned}
& k_p(w_{\text{MPAm}}^0, \alpha, T, p) / (\text{L} \cdot \text{mol}^{-1} \cdot \text{s}^{-1}) = 3.91 \cdot 10^6 \\
& \cdot \left(0.388 + (1 - 0.388) \cdot \exp\left(-24.3 \cdot \frac{w_{\text{MPAm}}^0 \cdot (1 - \alpha)}{1 - w_{\text{MPAm}}^0 \cdot \alpha}\right) - 0.646 \cdot \frac{w_{\text{MPAm}}^0 \cdot (1 - \alpha)}{1 - w_{\text{MPAm}}^0 \cdot \alpha} \right) \\
& \cdot \exp\left(-\frac{1.61 \cdot 10^4 - 1.65 \cdot (p/\text{bar})}{8.31441 \cdot (T/\text{K})}\right)
\end{aligned} \tag{eq. 7.4}$$

Similarly, all k_p data of M-MPAm, DM-PAm, and PAm may be described by equations 7.5, 7.6, and 7.7, respectively.

$$\begin{aligned}
 k_p(w_{M-MPAm}^0, \alpha, T, p) / (\text{L} \cdot \text{mol}^{-1} \cdot \text{s}^{-1}) &= 1.01 \cdot 10^6 \\
 &\cdot \left(-101 + (1 + 101) \cdot \exp \left(0.0771 \cdot \frac{w_{M-MPAm}^0 \cdot (1 - \alpha)}{1 - w_{M-MPAm}^0 \cdot \alpha} \right) - 9.01 \cdot \frac{w_{M-MPAm}^0 \cdot (1 - \alpha)}{1 - w_{M-MPAm}^0 \cdot \alpha} \right) \\
 &\cdot \exp \left(- \frac{1.44 \cdot 10^4 - 1.21 \cdot (p / \text{bar})}{8.31441 \cdot (T / \text{K})} \right)
 \end{aligned} \quad (\text{eq. 7.5})$$

$$\begin{aligned}
 k_p(w_{DM-PAm}^0, \alpha, T, p) / (\text{L} \cdot \text{mol}^{-1} \cdot \text{s}^{-1}) &= 2.81 \cdot 10^7 \\
 &\cdot \left(0.535 + (1 - 0.535) \cdot \exp \left(-9.63 \cdot \frac{w_{DM-PAm}^0 \cdot (1 - \alpha)}{1 - w_{DM-PAm}^0 \cdot \alpha} \right) - 0.411 \cdot \frac{w_{DM-PAm}^0 \cdot (1 - \alpha)}{1 - w_{DM-PAm}^0 \cdot \alpha} \right) \\
 &\cdot \exp \left(- \frac{1.45 \cdot 10^4 - 1.23 \cdot (p / \text{bar})}{8.31441 \cdot (T / \text{K})} \right)
 \end{aligned} \quad (\text{eq. 7.6})$$

$$\begin{aligned}
 k_p(w_{PAm}^0, \alpha, T, p) / (\text{L} \cdot \text{mol}^{-1} \cdot \text{s}^{-1}) &= 9.21 \cdot 10^7 \\
 &\cdot \left(0.714 + (1 - 0.714) \cdot \exp \left(-6.37 \cdot \frac{w_{PAm}^0 \cdot (1 - \alpha)}{1 - w_{PAm}^0 \cdot \alpha} \right) \right) \\
 &\cdot \exp \left(- \frac{1.8 \cdot 10^4 - 1.13 \cdot (p / \text{bar})}{8.31441 \cdot (T / \text{K})} \right)
 \end{aligned} \quad (\text{eq. 7.7})$$

8 Termination Kinetics of the Polymerization of Prop-2-enamides

Water represents a suitable solvent for DM-PAm and its polymer is well soluble in both monomer and water. These attributes allow for covering broad ranges of initial monomer concentration and monomer-to-polymer conversion. Furthermore, polymerization of prop-2-enamide derivatives appears to be associated with less chain-transfer reactions. This is indicated by the PLP-structured MMDs in chapter 7. The high propagation rate coefficient of prop-2-enamide derivatives lacking an α -methyl group may result in high signal-to-noise ratios in SP-PLP-NIR experiments.

Investigations into the termination kinetics of DM-PAm polymerization in aqueous solution were performed at 40 °C and initial monomer concentrations of 2.98, 9.52, and 9.70 mol·L⁻¹ corresponding to 0.30, 0.98, and 1.00 g·g⁻¹ DM-PAm, respectively. The experiments were carried out at 2000 bar to improve the signal-to-noise ratio. Experimental data from the literature^[250] are included in curve fitting. Those values were determined by combining primary experimental $\langle k_t \rangle / k_p$ values with k_p data from PLP-SEC experiments. These k_p values were measured using calibrant-relative calibration for SEC. Therefore, literature data had to be multiplied with the factor which correlates the positions of the POIs obtained by direct MMD determination and by calibrant-relative calibration.

Termination rate coefficients of prop-2-enamide in D₂O were determined by SP-PLP-NIR experiments at 40 °C, 2000 bar, and initial monomer concentrations of 2.85, 4.28, 5.71, and 7.14 mol·L⁻¹ corresponding to 0.20, 0.30, 0.40, and 0.50 g·g⁻¹ PAm, respectively. Further experiments were conducted at 40 °C, an initial monomer concentration of 0.40 g·g⁻¹, and pressures of 500, 1000, and 1500 bar. Chemically initiated polymerizations were performed at 50 °C, ambient pressure, initial monomer contents of 0.10, 0.20 as well as 0.30 g·g⁻¹, and initiator concentrations of 0.25, 0.5, 5, 25, and 50 mmol·L⁻¹.

8.1 Dynamic Viscosity of Monomer–Water Mixtures

The viscosity of the reaction medium is of interest for a detailed analysis of termination kinetics due to its diffusion-controlled nature. Measured dynamic viscosities for the entire range of DM-PAm–water mixtures at 40 °C and ambient pressure are shown in figure 8.1.

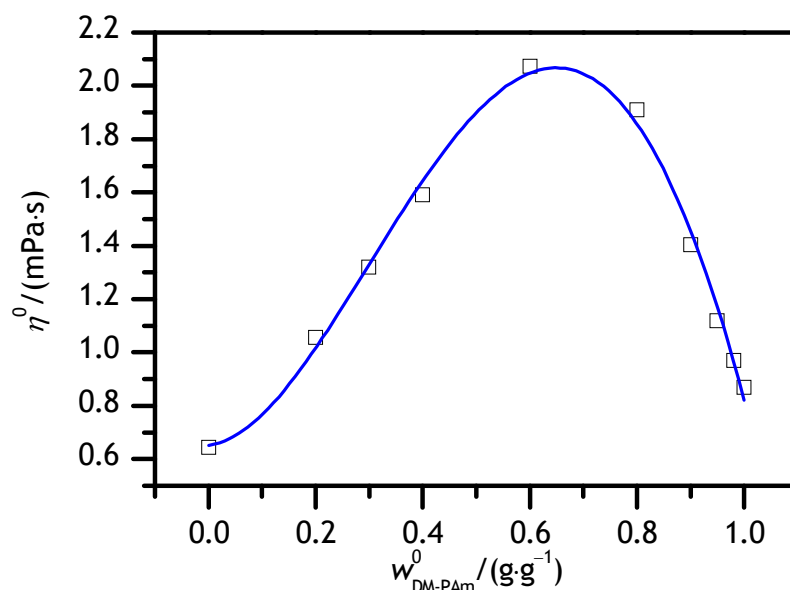


Figure 8.1: Dependence of dynamic viscosity, η^0 , on initial monomer mass fraction of DM-PAm at 40 °C and ambient pressure. The line represents the fit of a fourth-order polynomial.

The dependence of viscosity on monomer content is similar to the one observed for VP (chapter 6.2). The maximum in viscosity is obtained at approximately $0.65 \text{ g} \cdot \text{g}^{-1}$ DM-PAm in water. The occurrence of a maximum may again be explained by the difference of monomer and solvent regarding molecular size, dipole moment, and the ability to form hydrogen bonds. Similar to VP, the dipole moment of DM-PAm (3.8 D, *s-cis* conformer)^[269] is much higher than the dipole moment of water (1.85 D)^[234] and DM-PAm cannot act as hydrogen bond donor. The maximum viscosity of DM-PAm under the chosen conditions is close to the value obtained in case of VP. The bulk

viscosity of DM-PAm is, however, by almost a factor of two lower than for VP. This might be due to the lower dipole moment and to the minor steric demand of DM-PAm. The dependence of dynamic viscosity of DM-PAm on initial monomer mass fraction may be adequately described by the polynomial (given as line in figure 8.1):

$$\eta_0 / (\text{mPa} \cdot \text{s}) = 0.652 + 0.212 \cdot w_{\text{DM-PAm}}^0 + 10.688 \cdot (w_{\text{DM-PAm}}^0)^2 - 13.762 \cdot (w_{\text{DM-PAm}}^0)^3 - 3.032 \cdot (w_{\text{DM-PAm}}^0)^4 \quad (\text{eq. 8.1})$$

8.2 SP–PLP–NIR Investigations into the Dependence of the Termination Rate Coefficient on Initial Monomer Mass Fraction and Degree of Monomer Conversion

DMPA was used as the photoinitiator in case of DM-PAm polymerization. Darocur 1173 was used for PAm polymerization because neither DMPA nor HHMP are sufficiently soluble in dilute aqueous PAm solutions.

Relative monomer concentration, $c_M(t)/c_M(t=0)$, versus time after applying a laser pulse at $t=0$ is plotted in the upper parts of figures 8.2 and 8.3. The signal in figure 8.2 was obtained during the course of an experiment with an initial DM-PAm concentration of $0.40 \text{ g} \cdot \text{g}^{-1}$ and a degree of monomer conversion, from previous laser pulsing, of 0.15. The decrease of relative monomer concentration in a polymerization of $0.40 \text{ g} \cdot \text{g}^{-1}$ PAm at a degree of monomer conversion of 0.11 is depicted in figure 8.3. The signals in case of PAm polymerization have been obtained by averaging two subsequently measured SP–PLP traces. The lines in figures 8.2 and 8.3 represent fits of equation 3.56 to the experimental data. The time intervals up to 0.05 s (figure 8.2) and 0.025 s (figure 8.3) refer to a degree of polymerization of up to approximately $1.16 \cdot 10^4$ and $1.46 \cdot 10^4$ in case of DM-PAm as well as $1.36 \cdot 10^4$ and $1.73 \cdot 10^4$ in case of PAm at 1000 bar and 1500 bar, respectively. The much stronger decrease of relative monomer concentration at 1500 bar compared to the decrease at 1000 bar results in a higher signal-to-noise ratio at higher

pressure. It stands out that the decrease of relative monomer concentration is more pronounced for DM-PAm than for PAm despite the lower k_p value of DM-PAm. This behavior is indicative for a lower $\langle k_t \rangle$ value in case of DM-PAm.

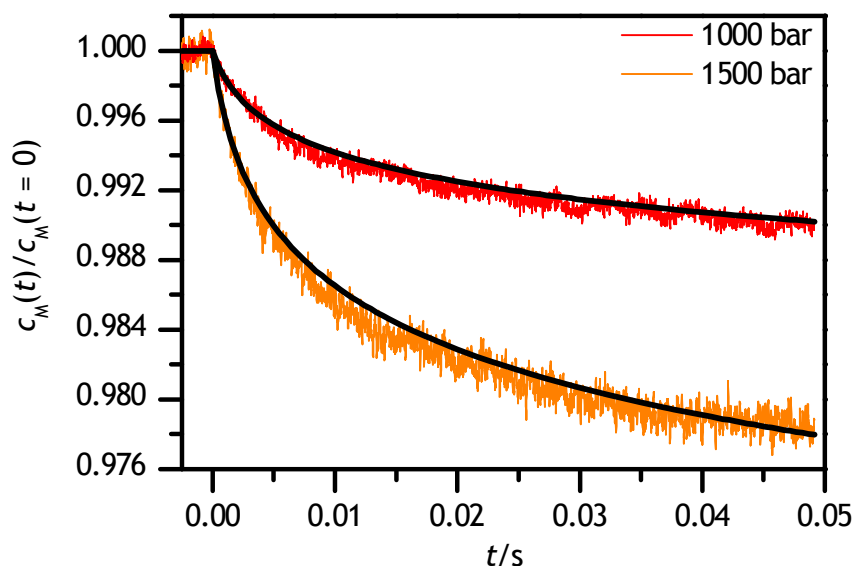


Figure 8.2: Relative monomer concentration plotted versus time after applying a laser pulse at $t = 0$, during DM-PAm polymerizations ($w_{\text{DM-PAm}}^0 = 0.40 \text{ g}\cdot\text{g}^{-1}$ in aqueous solution) at 40°C and 1000 bar (red line) as well as 1500 bar (orange line). The poly(DM-PAm) content from preceding polymerization is $0.060 \text{ g}\cdot\text{g}^{-1}$ (corresponding to a monomer conversion α of 0.15) at $t = 0$. The black lines represent fits of equation 3.56 to the data.

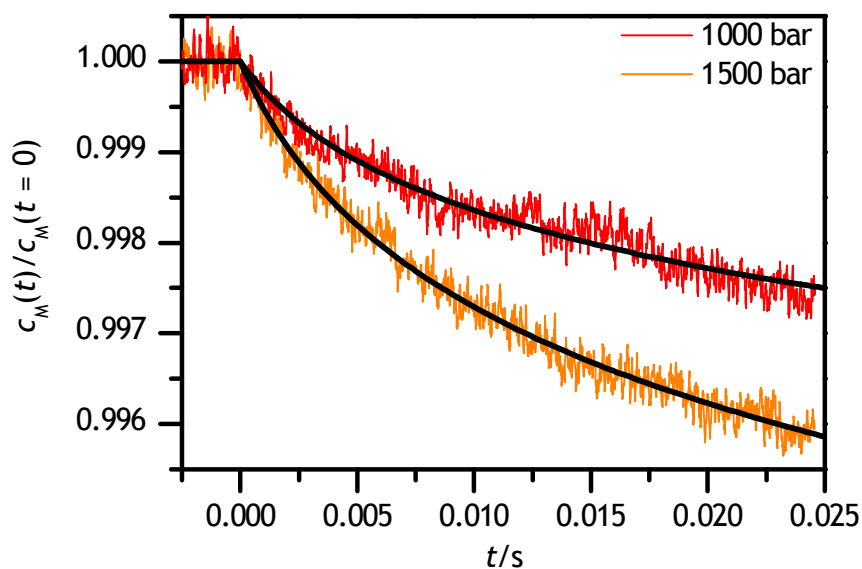


Figure 8.3: Relative monomer concentration plotted versus time after applying a laser pulse at $t = 0$, during PAm polymerizations ($w_{\text{PAm}}^0 = 0.40 \text{ g}\cdot\text{g}^{-1}$ in aqueous solution) at 40°C and 1000 bar (red line) as well as 1500 bar (orange line). The poly(PAm) content from preceding polymerization is $0.044 \text{ g}\cdot\text{g}^{-1}$ (corresponding to $\alpha = 0.11$) at $t = 0$. The black lines represent fits of equation 3.56 to the data.

Chain-length-averaged termination rate coefficients of DM-PAm in dependence on monomer conversion are depicted in figure 8.4 for various initial monomer concentrations. The termination rate coefficient is almost conversion-independent at low degrees of monomer conversion. At initial monomer mass fractions above $0.40 \text{ g}\cdot\text{g}^{-1}$ DM-PAm, a further increase in monomer conversion results in a decrease of $\langle k_t \rangle$. These two conversion ranges may be assigned to segmental and translational diffusion, respectively, being the rate-controlling step. At an initial monomer mass fraction of $0.80 \text{ g}\cdot\text{g}^{-1}$ DM-PAm and a degree of monomer conversion of approximately 0.6 the termination rate coefficient might, aside from scatter, assumed to be controlled by reaction diffusion. In case of initial monomer contents of 0.20, 0.30, and $0.40 \text{ g}\cdot\text{g}^{-1}$ DM-PAm $\langle k_t \rangle$ slightly increases towards high monomer conversion. The $\langle k_t \rangle$ values were determined by means of equation 7.6 which was developed assuming that k_p increases towards higher

monomer conversion. This assumption was made because monomer consumption results in reduced intermolecular interactions of the macroradical with its molecular environment (see chapter 7.3). Nevertheless, assuming a constant k_p value would result in a slight increase of $\langle k_t \rangle$ towards high monomer conversion as well. In case of, for example, $0.20 \text{ g}\cdot\text{g}^{-1}$ DM-PAm in aqueous solution, $\langle k_t \rangle$ increases by a factor of approximately 2.8 in the range of zero conversion to $\alpha = 0.8$ assuming that k_p increases towards higher monomer conversion. In contrast, the increase in $\langle k_t \rangle$ in the same monomer-conversion range will be reduced to a factor of approximately 2.0 if k_p is assumed to be independent of monomer conversion. The increase in mobility of the growing chain end towards higher monomer conversion, due to reduced intermolecular interactions of the macroradical with its molecular environment, may cause an increase of $\langle k_t \rangle$ towards high monomer conversion. Such an increase should be more pronounced for low initial monomer concentrations because the counteracting common decrease of $\langle k_t \rangle$ towards high monomer conversion is less pronounced.

For initial monomer mass fractions below $0.80 \text{ g}\cdot\text{g}^{-1}$ DM-PAm, the monomer conversion at which the plateau-type region ends cannot be easily identified due to the weak or even absent decrease in $\langle k_t \rangle$ at higher monomer conversion. Furthermore, this monomer conversion is almost the same for polymerizations at initial monomer mass fractions of $0.80 \text{ g}\cdot\text{g}^{-1}$ DM-PAm and above. A correlation of the monomer conversion at which the plateau-type region ends with a certain polymer mass fraction, as has been done for VP (chapter 6.3), is therefore hardly feasible. However, this polymer mass fraction may be estimated by means of bulk polymerization to be approximately $0.18 \text{ g}\cdot\text{g}^{-1}$. This value is close to $0.15 \text{ g}\cdot\text{g}^{-1}$ which has been obtained for VP polymerization (chapter 6.3).

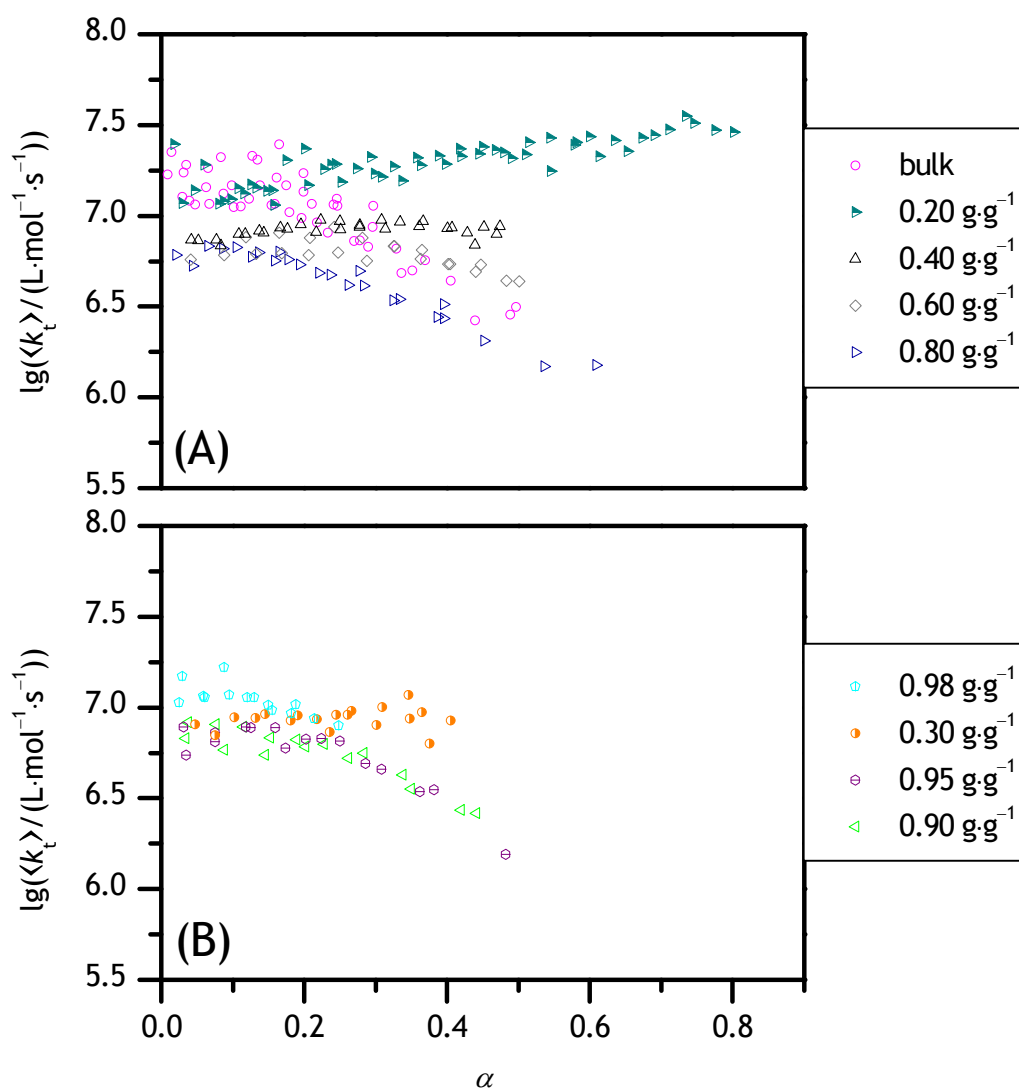


Figure 8.4: Dependence of the chain-length-averaged termination rate coefficient, $\langle k_t \rangle$, on the degree of monomer conversion, α , for DM-PAm polymerizations at 40 °C and 2000 bar for various initial monomer contents. The data are divided into two figures, (A) and (B). A combined representation of all data is given by figure A.3 in appendix A.2.

The $\langle k_t \rangle$ value at low degrees of monomer conversion decreases in passing from 0.20 g·g⁻¹ DM-PAm in water to initial monomer contents of 0.80 g·g⁻¹. Contrary to VP (chapter 6.3), $\langle k_{t,ini} \rangle$ of DM-PAm subsequently increases. This behavior is illustrated in figure 8.5 which shows the mean (plateau) value of experimental $\langle k_t \rangle$ for the initial

polymerization period. The dependence of the plateau value on monomer mass fraction may be represented by equation 8.2.

$$\begin{aligned} \langle k_{t,ini} \rangle / (\text{L} \cdot \text{mol}^{-1} \cdot \text{s}^{-1}) = & 6.64 \cdot 10^7 \cdot (w_{\text{DM-PAm}}^0 - 0.897)^6 \\ & + 1.59 \cdot 10^{-8} \cdot \exp\left(175 \cdot (w_{\text{DM-PAm}}^0 - 0.199)\right)^{0.714} + 6.21 \cdot 10^6 \end{aligned} \quad (\text{eq. 8.2})$$

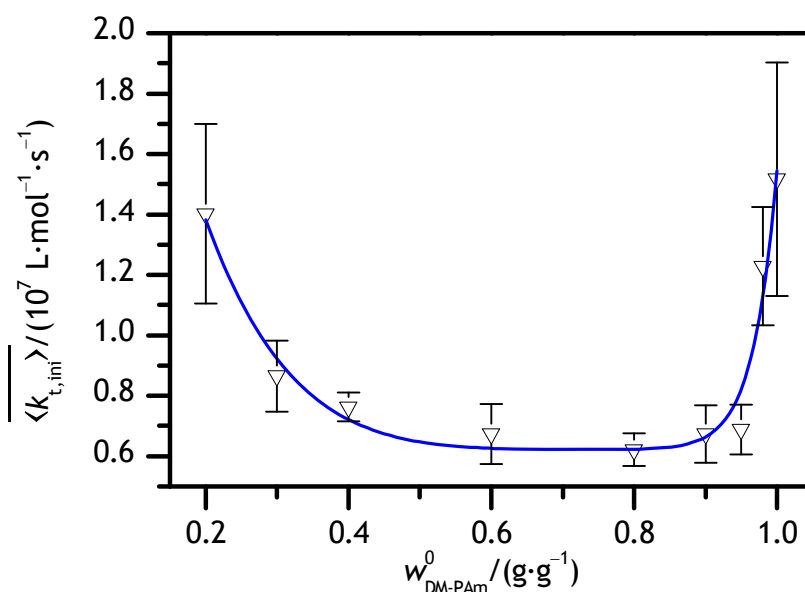


Figure 8.5: Dependence of mean $\langle k_{t,ini} \rangle$ on initial mass fraction of DM-PAm, $w_{\text{DM-PAm}}^0$, at 40 °C and 2000 bar. Error bars indicate the standard deviation. The line refers to equation 8.2.

Diffusion-controlled rate coefficients scale with the inverse of viscosity (equations 3.6 and 3.7). Thus, the product of both quantities would be expected to be constant. The product of $\langle k_{t,ini} \rangle$, which was determined at 40 °C and 2000 bar, and dynamic viscosity of the monomer–water mixture, which was measured at 40 °C and ambient pressure, is shown in figure 8.6. It is not constant (horizontal line in figure 8.6) which implies that $\langle k_{t,ini} \rangle$ does not scale with the inverse of viscosity. However, it has to be considered that the multiplier and the multiplicand have been determined at different pressures. It needs further to be

considered that the dynamic viscosity of the monomer–water mixture probably does not correlate with the rate coefficient which is mainly controlled by segmental diffusion. As already stated for VP (chapter 6.3), the mobility of the growing chain end within the polymer coil depends on the interactions of monomer, water, and polymer and on the persistence length. This is, however, not taken into account in the correlation of $\langle k_{t,ini} \rangle$ and dynamic viscosity of the monomer–water mixture. Nevertheless, the dependence of $\langle k_{t,ini} \rangle$ on initial mass fraction of DM-PAm may partly be explained by means of the dynamic viscosity of the monomer–water mixture. In case of VP (chapter 6.3), the correlation of $\langle k_{t,ini} \rangle$ and dynamic viscosity of the monomer–water mixture is even worse considering that the dependence of viscosity on monomer mass fraction shows a maximum but $\langle k_{t,ini} \rangle$ does not show a minimum. This indicates as well that $\langle k_{t,ini} \rangle$ does not exactly scale with the inverse of viscosity of the monomer–water mixture.

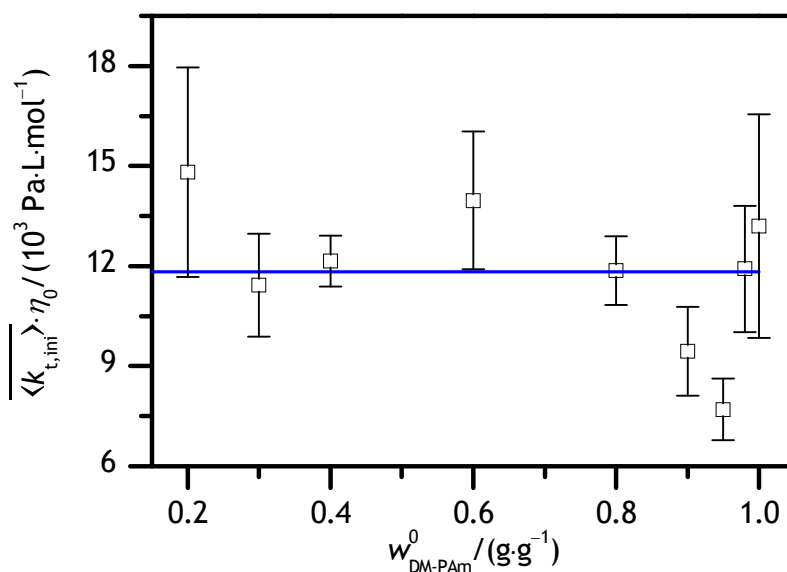


Figure 8.6: Product of mean $\langle k_{t,ini} \rangle$ (40 °C, 2000 bar) and dynamic viscosity of the monomer–water mixture (40 °C, ambient pressure) in dependence on initial DM-PAm mass fraction. Error bars indicate the standard deviation related to $\langle k_{t,ini} \rangle$. The line represents the average value.

The propagation rate coefficient of DM-PAm is six to nine times above the value of VP at 40 °C and 2000 bar (for identical monomer mass fraction). The contribution of termination by reaction diffusion to overall termination might, therefore, be more pronounced in case of DM-PAm compared to VP (see equation 3.19). For the polymerization of, for example, 0.40 g·g⁻¹ DM-PAm in aqueous solution, $k_{t,RD}$ may amount to approximately 28 % of $\langle k_{t,ini} \rangle$ at zero conversion assuming C_{RD} to be 20. This hampers the estimation of $k_{t,SD}$ via the mean value of experimental $\langle k_t \rangle$ for the initial polymerization period. The conversion range, in which $\langle k_t \rangle$ may be assumed to be controlled by reaction diffusion, cannot clearly be seen for any of the chosen initial monomer mass fractions. The presence of such data is necessary to determine C_{RD} . C_{RD} and $k_{t,SD}$ are required for fitting equation 3.56 to experimental data and for determining physically reasonable parameters to describe the conversion dependence of $\langle k_t \rangle$.

Figure 8.7 shows chain-length-averaged termination rate coefficients of PAm as a function of monomer conversion for various initial monomer mass fractions. At initial monomer mass fractions of 0.40 and 0.50 g·g⁻¹ PAm, $\langle k_t \rangle$ seems to be independent of monomer conversion at least up to the degree of monomer conversion at which the system turns inhomogeneous. $\langle k_t \rangle$ may be assumed to be controlled by segmental diffusion. In case of $w_{PAm}^0 = 0.30$ g·g⁻¹ PAm, a control by translational diffusion may set in at a degree of monomer conversion of 0.16. A decrease in $\langle k_t \rangle$ at such low monomer conversion and initial monomer content could not be observed in case of VP or DM-PAm. However, in case of MAA (initial monomer content of 0.30 g·g⁻¹, 50 °C, 2000 bar) the termination rate coefficient decreases above a degree of monomer conversion of approximately 0.2.^[111] The scatter at the lowest monomer concentrations is ascribed to a poor signal-to-noise ratio due to low monomer consumption per laser pulse.

It should be noted that the low-conversion $\langle k_t \rangle$ values for 0.20 g·g⁻¹ and 0.30 g·g⁻¹ as well as for 0.40 g·g⁻¹ and 0.50 g·g⁻¹ PAm are close to each other. The $\langle k_t \rangle$ values determined for initial monomer mass fractions of 0.20 g·g⁻¹ and 0.30 g·g⁻¹ PAm may be represented by a single mean value excluding data above $\alpha = 0.27$ in case of 0.20 g·g⁻¹ PAm and above $\alpha = 0.16$ for 0.30 g·g⁻¹ PAm. The low value for $\langle k_t \rangle$ at $\alpha = 0.29$ for an initial monomer

content of 0.20 g·g⁻¹ PAm may be attributed either to translational diffusion control or to scatter. The $\langle k_t \rangle$ values determined for initial monomer mass fractions of 0.40 g·g⁻¹ and 0.50 g·g⁻¹ PAm may be represented by a single mean value as well. These mean values are depicted in figure 8.7 by horizontal lines. The change in $\langle k_{t,ini} \rangle$ with initial PAm mass fraction, w_{PAm}^0 , may be represented by equation 8.3 under the assumption of a linear dependence of the decadic logarithm of $\langle k_{t,ini} \rangle$ on w_{PAm}^0 .

$$\lg(\langle k_{t,ini} \rangle / (\text{L} \cdot \text{mol}^{-1} \cdot \text{s}^{-1})) = 7.87 - 0.75 \cdot w_{PAm}^0 \quad (\text{eq. 8.3})$$

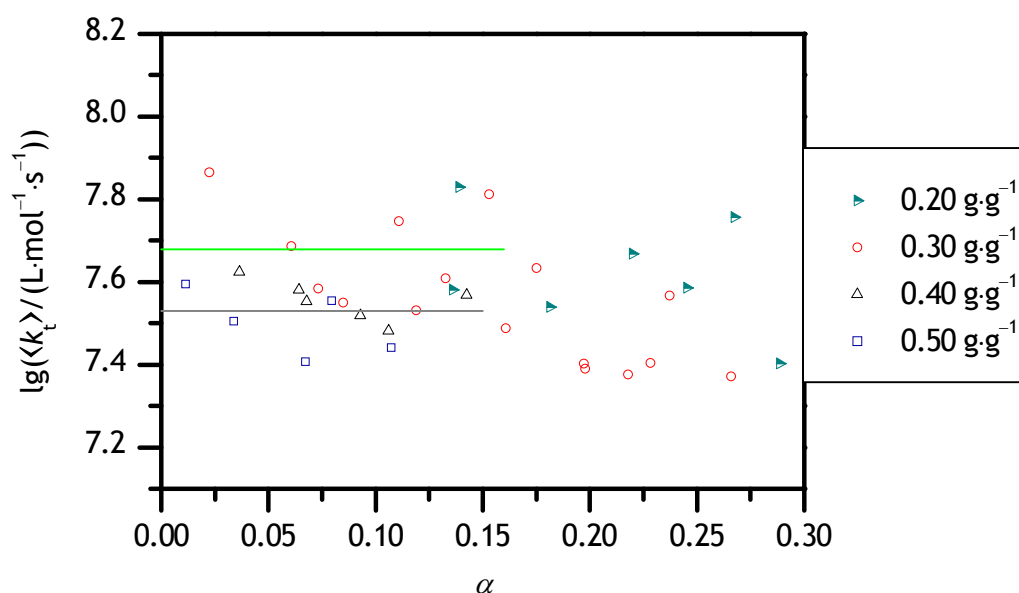


Figure 8.7: Dependence of the chain-length-averaged termination rate coefficient, $\langle k_t \rangle$, on the degree of monomer conversion, α , for PAm polymerizations at 40 °C and 2000 bar for various initial monomer contents. The light green line represents the mean value of $\langle k_{t,ini} \rangle$ for initial monomer mass fractions of 0.20 g·g⁻¹ and 0.30 g·g⁻¹ PAm whereas the gray line represents the mean value for initial monomer mass fractions of 0.40 g·g⁻¹ and 0.50 g·g⁻¹ PAm.

Variation of the initial monomer content by $0.20 \text{ g}\cdot\text{g}^{-1}$ results in a change of $\langle k_{t,\text{ini}} \rangle$ of PAm by a factor of 1.41. The factor which correlates $\langle k_{t,\text{ini}} \rangle$ at initial monomer mass fractions of $0.20 \text{ g}\cdot\text{g}^{-1}$ and $0.40 \text{ g}\cdot\text{g}^{-1}$ amounts to 1.84 in case of DM-PAm and to 1.70 in case of VP, respectively. Therefore, $\langle k_{t,\text{ini}} \rangle$ of PAm shows a weaker dependence on initial monomer mass fraction compared to DM-PAm and VP.

The dependence of k_p of MPAm and of M-MPAm on monomer mass fraction, pressure, and temperature has been reevaluated taking both literature data^[250] and recently measured additional k_p data into account. Therefore, the $\langle k_t \rangle$ values had to be reevaluated as well. Chain-length-averaged termination rate coefficients of MPAm and M-MPAm in dependence on monomer conversion are shown in figures 8.8 and 8.9.

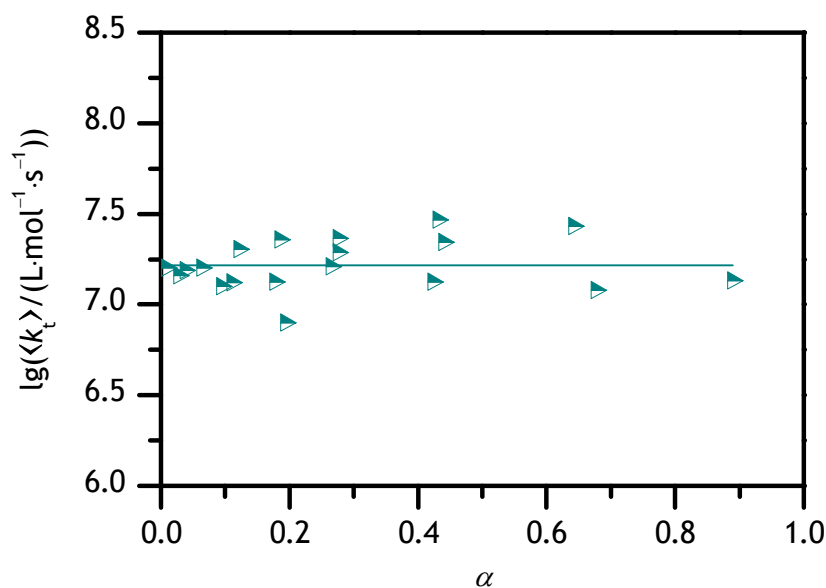


Figure 8.8: Dependence of the chain-length-averaged termination rate coefficient, $\langle k_t \rangle$, on the degree of monomer conversion, α , for MPAm polymerization at 40°C , 2000 bar, and an initial MPAm mass fraction of $0.20 \text{ g}\cdot\text{g}^{-1}$. The line represents the average value.

Measurements could only be performed for an initial monomer mass fraction of $0.20 \text{ g}\cdot\text{g}^{-1}$ in case of MPAm because of the solubility range of the monomer in water (chapter 5.9.3) and because lower monomer contents result in an unsatisfactory signal-to-noise quality. Investigations into the termination kinetics of M-MPAm are limited to the concentration range of 0.60 to $0.80 \text{ g}\cdot\text{g}^{-1}$ M-MPAm in water. The lower mass fraction is given by the solubility limit (chapter 5.9.3). Negligible amounts of poly(M-MPAm) are soluble in its own monomer which hampers detailed studies into the dependence of $\langle k_t \rangle$ on monomer conversion in case of bulk polymerization.

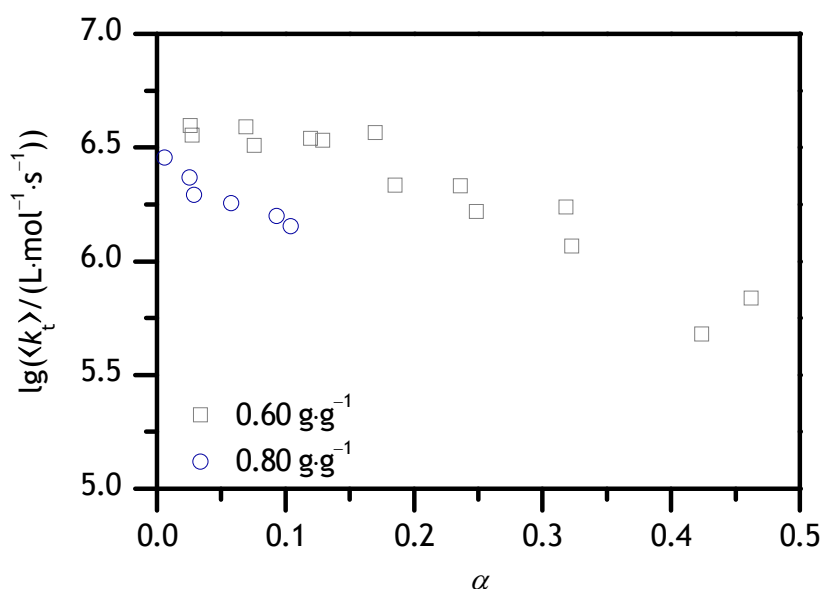


Figure 8.9: Dependence of the chain-length-averaged termination rate coefficient, $\langle k_t \rangle$, on the degree of monomer conversion, α , for M-MPAm polymerizations at 40°C and 2000 bar for two different initial monomer mass fractions.

The termination rate coefficient of MPAm polymerization at $w_{\text{MPAm}}^0 = 0.20 \text{ g}\cdot\text{g}^{-1}$ in aqueous solution is conversion independent up to at least $\alpha = 0.90$. The average value is given by $\lg(\langle k_t \rangle / \text{L}\cdot\text{mol}^{-1}\cdot\text{s}^{-1}) = 7.22$ and is depicted by a horizontal line in figure 8.8. As may be expected for such a low monomer concentration, neither gel effect nor glass effect can be seen.

In M-MPAm polymerization at an initial monomer mass fraction of $0.60 \text{ g}\cdot\text{g}^{-1}$, $\langle k_t \rangle$ is conversion independent up to a degree of monomer conversion of approximately 0.17. At higher monomer conversion the termination rate coefficient decreases. The former monomer conversion range may be ascribed to segmental diffusion control and the latter to translational diffusion control. The decrease in the conversion range in which $\langle k_t \rangle$ is controlled by translational diffusion is much more pronounced compared to the change in $\langle k_t \rangle$ in VP and DM-PAm polymerization. This may indicate a higher C_η value for M-MPAm $\langle k_t \rangle$.

At an initial monomer mass fraction of $0.80 \text{ g}\cdot\text{g}^{-1}$, a rather small conversion range is accessible for M-MPAm polymerization. The two data points at lowest degree of monomer conversion exhibit a higher termination rate coefficient than adjacent data points. A monomer-conversion independent rate coefficient (control by segmental diffusion) would be expected from theory. The higher $\langle k_t \rangle$ may be ascribed to inhibition which may be attributed to residual oxygen or small impurities of the chemicals. Inhibition reduces the monomer consumption per laser pulse. The apparent $\langle k_t \rangle$ value is determined by fitting of equation 3.56 to experimental data. This procedure does not consider the effect of inhibition and consequently initial $\langle k_t \rangle$ values are determined slightly too high. Alternatively, the higher $\langle k_t \rangle$ may be ascribed to translational diffusion being rate-controlling. Translational diffusion control is, however, unlikely to occur at such low monomer conversion considering that at $w_{\text{M-MPAm}}^0 = 0.60 \text{ g}\cdot\text{g}^{-1}$ translational diffusion control does not set in below $\alpha = 0.17$. Similar to VP, $\langle k_{t,\text{ini}} \rangle$ decreases towards higher initial monomer content. Assuming that the two data points at lowest degree of monomer conversion are not influenced by inhibition, the difference in termination rate coefficients of $w_{\text{M-MPAm}}^0 = 0.60 \text{ g}\cdot\text{g}^{-1}$ and $w_{\text{M-MPAm}}^0 = 0.80 \text{ g}\cdot\text{g}^{-1}$ amounts to $\Delta \lg(\langle k_{t,\text{ini}} \rangle / \text{L}\cdot\text{mol}^{-1}\cdot\text{s}^{-1}) \approx 0.1$. Neglecting these two data points, the difference is $\Delta \lg(\langle k_{t,\text{ini}} \rangle / \text{L}\cdot\text{mol}^{-1}\cdot\text{s}^{-1}) \approx 0.3$. At identical reaction conditions the difference amounts to $\Delta \lg(\langle k_{t,\text{ini}} \rangle / \text{L}\cdot\text{mol}^{-1}\cdot\text{s}^{-1}) \approx 0.2$ in case of VP which is in between the two values given above. Therefore, the high $\langle k_t \rangle$ value of the two data points at lowest degree of monomer conversion cannot be easily ascribed to an influence of translational diffusion control or inhibition.

Mean values of $\langle k_{t,ini} \rangle$ for non-ionized AA, DM-PAm, non-ionized MAA, MPAm, PAm, and VP are shown in figure 8.10 for 40 °C, 2000 bar, and an initial monomer mass fraction of 0.20 g·g⁻¹ in aqueous solution. The data were obtained by SP–PLP–NIR experiments. $\lg(\langle k_{t,ini} \rangle)$ of MAA has been estimated by linear extrapolation using data for 0.30 and 0.60 g·g⁻¹ initial monomer mass fraction.^[231] In addition, the value for MAA had to be corrected with respect to temperature because MAA $\langle k_t \rangle$ was determined at 50 °C. A volume of activation of 11 cm³·mol⁻¹, which was determined for 0.30 g·g⁻¹ MAA in aqueous solution,^[231] and an Arrhenius activation energy of 21.1 kJ·mol⁻¹, which was found for 0.10 g·g⁻¹ MAA in aqueous solution,^[11,271] were used. $\langle k_{t,ini} \rangle$ values of AA and VP were taken from the literature.^[113,231,232]

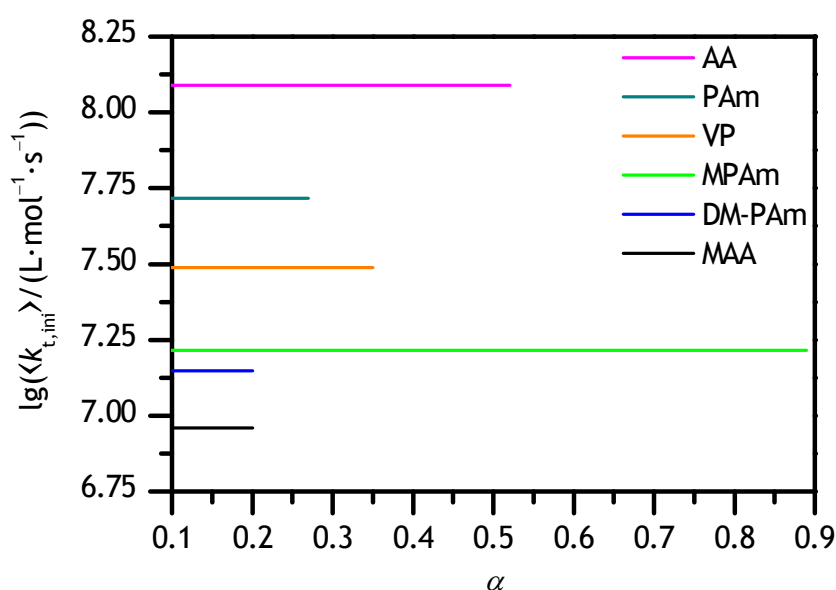


Figure 8.10: $\langle k_{t,ini} \rangle$ values in the monomer conversion range in which $\langle k_t \rangle$ is assumed to be controlled by segmental diffusion for polymerizations of non-ionized AA, DM-PAm, non-ionized MAA, MPAm, PAm, and VP at 40 °C, 2000 bar, and an initial monomer mass fraction of 0.20 g·g⁻¹ in aqueous solution. The sources of $\langle k_{t,ini} \rangle$ values of AA, MAA, and VP are given in the text.

In the following section, $\langle k_{t,ini} \rangle$ is assumed to be mainly determined by $k_{t,SD}$.

For a comparison of termination rate coefficients of several monomers, the chain-length dependence of the termination rate coefficient has to be considered. In SP–PLP–NIR experiments, $\langle k_t \rangle$ is determined by fitting equation 3.56 to experimental $c_M(t)/c_M(t=0)$ versus time traces. The overall termination rate coefficient corresponds to the average over the individual rate coefficients governed by the distribution of radical chain length in the time span under investigation. The degree of polymerization may be determined by $X = k_p \cdot c_M \cdot t$. The $\langle k_{t,ini} \rangle$ values shown in figure 8.10 for various monomers may correspond to different ranges of the degree of polymerization due to differences especially in k_p and in the time span. The maximum degree of polymerization obtained in the time interval is approximately $1 \cdot 10^3$ for MAA,^[111] $4 \cdot 10^3$ for MPAm,^[250] $1 \cdot 10^4$ for VP,^[113] $2 \cdot 10^4$ for DM-PAm as well as PAm, and $5 \cdot 10^4$ for AA^[231]. These maximum degrees of polymerization are significantly above typical values for the crossover chain length u_c ,^[272] which is used as a parameter to describe the chain-length dependence of $k_t(u,u)$ by the composite model (chapter 3.1.3). The exponent β , which is used to describe the high-chain-length regime of $k_t(u,u)$, is usually in the range of 0.15 to 0.30.^[11] Due to the rather small value of β , the sequence of termination rate coefficients shown in figure 8.10 stays most probably unchanged upon correcting for differences in the degree of polymerization (see equation 3.26), except for the sequence of $\langle k_{t,ini} \rangle$ of MPAm and DM-PAm. Nevertheless, $k_{t,SD}$ of DM-PAm may be smaller than in case of MPAm considering that the contribution of $k_{t,RD}$ to $\langle k_{t,ini} \rangle$ of DM-PAm may be rather large.

With the exception of DM-PAm, polymerizations of monomers without an α -methyl group exhibit a termination rate coefficient which is clearly above the one of polymerizations of monomers with an α -methyl group. The reduced steric demand may result in a higher mobility of the growing chain end and in a reduced shielding of the active site. DM-PAm and VP polymerizations show $\langle k_{t,ini} \rangle$ values which are lower than the coefficients for PAm and AA. This may be attributed to the substituents at the carbon–carbon double bond which are more sterically demanding in case of VP and DM-PAm. $\langle k_{t,ini} \rangle$ of MPAm is higher compared to MAA. This finding may be ascribed to carboxylate groups forming stronger hydrogen bonds than amide groups. The mobility of the growing

chain end is expected to decrease towards increasing strength of intermolecular interactions. The rather high $\langle k_{t,ini} \rangle$ value of AA polymerization is unexpected due to the formation of strong hydrogen bonds. Additionally, $\langle k_{t,ini} \rangle$ of AA would have been expected to be close to the value of PAm because of the structural similarity of both monomers. The termination rate coefficient in case of AA was determined neglecting chain-transfer reactions. In addition, high-pressure k_p values^[231] of AA, which were implemented in the primary experimental quantity $\langle k_t \rangle / k_p$, were estimated by means of the average volume of activation of k_p of several acrylates and of k_p values at ambient pressure. An individual volume of activation of k_p of AA has not been determined yet. This results in a large inaccuracy of $\langle k_t \rangle$ of AA polymerization.

The degree of swelling of a macromolecule has to be taken into account when considering termination rate coefficients controlled by segmental diffusion. The mobility of the growing chain end should increase towards higher degree of swelling. A qualitative measure of the degree of swelling may be given by the hydrodynamic volume, which is the basis of separation in SEC. In case that analyte and calibrant macromolecules exhibit identical hydrodynamic volumes, the molar mass of the analyte is assumed to be identical to the one of the calibrant in calibrant-relative (RI detection) calibration. If these two macromolecules consist of monomer units of different molar mass or structure, they feature, however, most likely a difference in total molar mass. This difference is reflected in the factor which correlates the positions of primary points of inflection obtained by direct (MALLS–RI detection) MMD determination and by calibrant-relative (RI detection) calibration. This factor amounts to 3.58 for poly(MPA_m) relative to poly(PAm) in case of the aqueous-solution SEC setup used. The molar mass of MPA_m macromolecules in aqueous solution is thus significantly higher than in case of PAm macromolecules of identical hydrodynamic volume. This is associated with a lower degree of swelling in case of MPA_m. Therefore, the mobility of the growing chain end of a MPA_m macroradical should be reduced compared to a PAm macroradical and $k_{t,SD}$ is lower. This is in line with experimental data. Since *N,N*-dimethylacetamide has been used as eluent in SEC for analysis of poly(VP) and poly(DM-PAm), no such correlation factor is known for aqueous solution.

Hesse^[232] and Barth^[11] have analyzed differences in absolute $k_t(1,1)$ values of various monomers by means of hydrodynamic radii of the monomers, dynamic solution viscosities, and equations 3.6 and 3.7. A detailed analysis in case of $\langle k_{t,ini} \rangle$ values ($k_{t,SD}$ in simplified terms) is hardly feasible. The radius $r_{h,X}$ (see equation 3.7) with respect to $k_{t,SD}$ is related to both monomer size and an “effective” chain length of the moving chain segment. Such radii for the polymers of interest are unknown to the best knowledge of the author. Furthermore, instead of dynamic solution viscosity the microviscosity is required. The microviscosity describes the mobility of the growing chain end and depends on the interactions of monomer, solvent, and polymer as well as on the persistence length. However, microviscosities are difficult to access.

8.3 Pressure Dependence

Termination rate coefficients of DM-PAm, M-MPAm, and PAm polymerization in aqueous solution were determined up to 2000 bar. Termination rate coefficients in dependence on monomer conversion are shown in figure 8.11 for PAm polymerization in aqueous solution at various pressures.

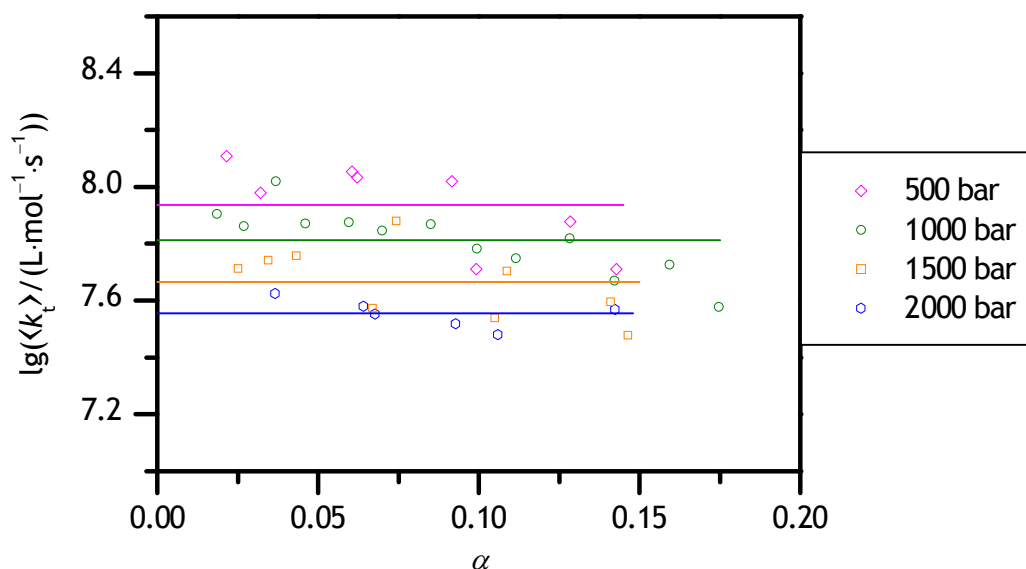


Figure 8.11: Variation of $\langle k_t \rangle$ of PAm with monomer conversion at 40 °C, an initial monomer mass fraction of 0.40 g·g⁻¹, and four different pressures. The horizontal lines represent $\langle k_{t,ini} \rangle$.

A horizontal line has been fitted to the values in the initial plateau region. The corresponding $\langle k_{t,ini} \rangle$ values are depicted in figure 8.12 together with the standard deviations. $\langle k_{t,ini} \rangle$ decreases towards higher pressure which may be attributed to an increase in viscosity. The associated volume of activation of $\langle k_{t,ini} \rangle$ is given in table 8.1. Furthermore, figure 8.11 illustrates that scatter of the data increases towards lower pressure. This may be due to lower monomer consumption per pulse which goes along with a reduced signal-to-noise ratio.

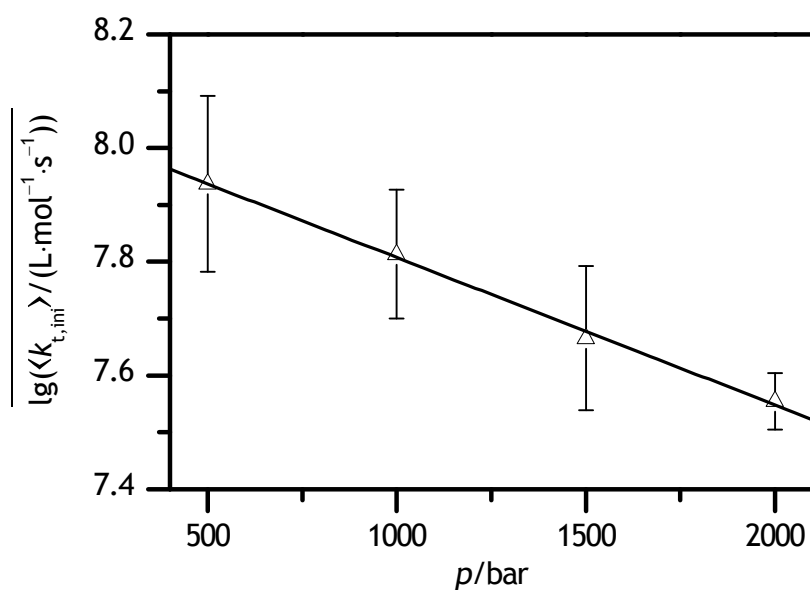


Figure 8.12: Variation of $\langle k_{t,ini} \rangle$ of PAm with pressure at 40 °C and an initial monomer mass fraction of 0.40 g·g⁻¹. The standard deviation is indicated by error bars. The line represents a linear fit to the data.

The dependences of $\langle k_{t,ini} \rangle$ of DM-PAm and M-MPAm polymerization in aqueous solution on pressure are depicted in figures 8.13 and 8.14. The corresponding volumes of activation of $\langle k_{t,ini} \rangle$ are given in table 8.1.

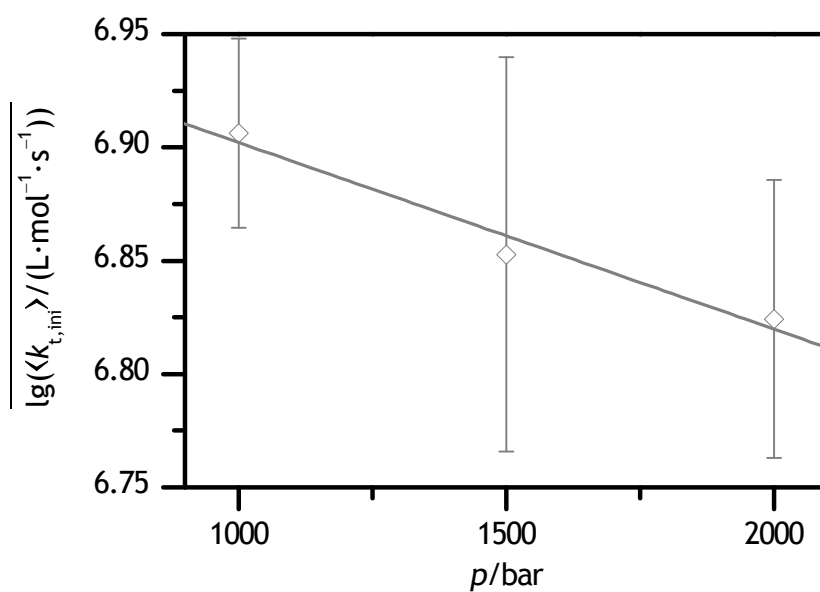


Figure 8.13: Variation of $\langle k_{t,ini} \rangle$ of DM-PAm with pressure at 40 °C and an initial monomer mass fraction of 0.60 g·g⁻¹. The standard deviation is indicated by error bars. The line represents a linear fit to the data.

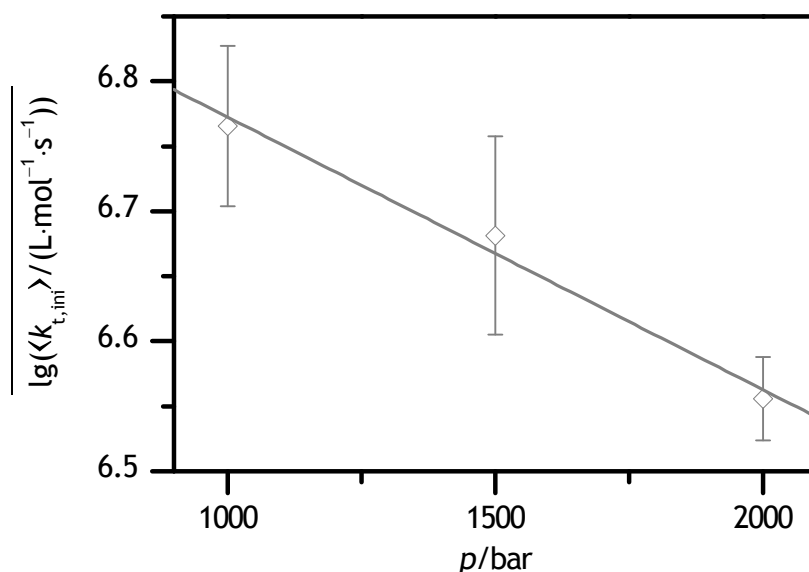


Figure 8.14: Variation of $\langle k_{t,ini} \rangle$ of M-MPAm with pressure at 40 °C and an initial monomer mass fraction of 0.60 g·g⁻¹. The standard deviation is indicated by error bars. The line represents a linear fit to the data.

Table 8.1: Volumes of activation of $\langle k_{t,ini} \rangle$ of M-MPAm, DM-PAm, and PAm determined at 40 °C.

monomer	$w_M / (\text{g} \cdot \text{g}^{-1})$	$\Delta^\ddagger V^\circ / (\text{cm}^3 \cdot \text{mol}^{-1})$
M-MPAm	0.60	12.6 ± 1.4
DM-PAm	0.60	4.9 ± 0.9
PAm	0.40	15.5 ± 0.6

The volume of activation in case of M-MPAm is close to the value obtained for bulk polymerization of dodecyl methacrylate ($\Delta^\ddagger V^\circ(\langle k_{t,ini} \rangle) = 10.8 \text{ cm}^3 \cdot \text{mol}^{-1}$)^[32] whereas the value in case of PAm is close to the values obtained for bulk polymerizations of butyl acrylate ($\Delta^\ddagger V^\circ(\langle k_{t,ini} \rangle) = 16 \text{ cm}^3 \cdot \text{mol}^{-1}$)^[273] VP ($\Delta^\ddagger V^\circ(\langle k_{t,ini} \rangle) = 14.6 \text{ cm}^3 \cdot \text{mol}^{-1}$)^[113,232] styrene ($\Delta^\ddagger V^\circ(\langle k_{t,ini} \rangle) = 14 \text{ cm}^3 \cdot \text{mol}^{-1}$)^[32] and methyl methacrylate ($\Delta^\ddagger V^\circ(\langle k_{t,ini} \rangle) = 15 \text{ cm}^3 \cdot \text{mol}^{-1}$)^[274]. The volume of activation in case of DM-PAm is significantly lower than the values given above. The size of the monomer does not explain

this phenomenon. As mentioned in chapter 8.2, the contribution of termination by reaction diffusion to overall termination might be assumed to be pronounced in the particular case of DM-PAm. This would result in a strong contribution of $k_{t,RD}$ to $\langle k_{t,ini} \rangle$ as can be seen in equation 3.19. The pressure dependence of $k_{t,RD}$ of DM-PAm is unknown. However, in case of butyl acrylate $k_{t,RD}$ has been found to be pressure independent.^[107] If this holds true for DM-PAm, the contribution of a pressure-independent $k_{t,RD}$ to overall termination may explain that the pressure dependence of $\langle k_{t,ini} \rangle$ is weaker compared to other monomers. Additionally, the dependence of the mobility of the growing chain end on pressure might be less pronounced in case of DM-PAm compared to other monomers. This statement cannot be examined because the mobility inside the polymer coil is not accessible experimentally.

Assuming the volumes of activation to be independent of monomer content, the dependences of $\langle k_{t,ini} \rangle$ of DM-PAm and PAm on initial monomer mass fraction and on pressure at 40 °C may be given by equations 8.4 and 8.5, respectively.

$$\begin{aligned} \langle k_{t,ini} \rangle / (\text{L} \cdot \text{mol}^{-1} \cdot \text{s}^{-1}) = & (6.64 \cdot 10^7 \cdot (w_{\text{DM-PAm}}^0 - 0.897)^6 \\ & + 1.59 \cdot 10^{-8} \cdot \exp((175 \cdot (w_{\text{DM-PAm}}^0 - 0.199))^{0.714}) \\ & + 6.21 \cdot 10^6) \cdot \exp(1.88 \cdot 10^{-4} \cdot (2 \cdot 10^3 - p / \text{bar})) \end{aligned} \quad (\text{eq. 8.4})$$

(valid for $0.20 \leq w_{\text{DM-PAm}}^0 \leq 1.00$)

$$\begin{aligned} \langle k_{t,ini} \rangle / (\text{L} \cdot \text{mol}^{-1} \cdot \text{s}^{-1}) = & 10^{7.87 - 0.75 \cdot w_{\text{PAm}}^0} \\ & \cdot \exp(5.97 \cdot 10^{-4} \cdot (2 \cdot 10^3 - p / \text{bar})) \end{aligned} \quad (\text{eq. 8.5})$$

(valid for $0.20 \leq w_{\text{PAm}}^0 \leq 0.50$)

8.4 Chemically Initiated Polymerizations

Chemically initiated polymerizations aiming at the measurement of the dependence of PAm $\langle k_t \rangle$ on initial monomer mass fraction and degree of monomer conversion were

conducted at 50 °C and ambient pressure. The combination of the ratio of k_p to the square root of $\langle k_t \rangle$ with k_p from PLP–SEC yields $\langle k_t \rangle$. Therefore, the dependence of $\langle k_t \rangle$ on monomer conversion may be obtained via two independent methods, the SP–PLP–NIR technique and chemically initiated polymerization. Most chemically initiated polymerizations were carried out twice. The agreement of data determined under identical reaction conditions is mostly satisfactory. Figures 8.15, 8.16, 8.17, and 8.18 show the increase in degree of monomer conversion with time for three different initiator concentrations and initial monomer mass fractions of 0.10 g·g⁻¹, 0.20 g·g⁻¹, and 0.30 g·g⁻¹, respectively.

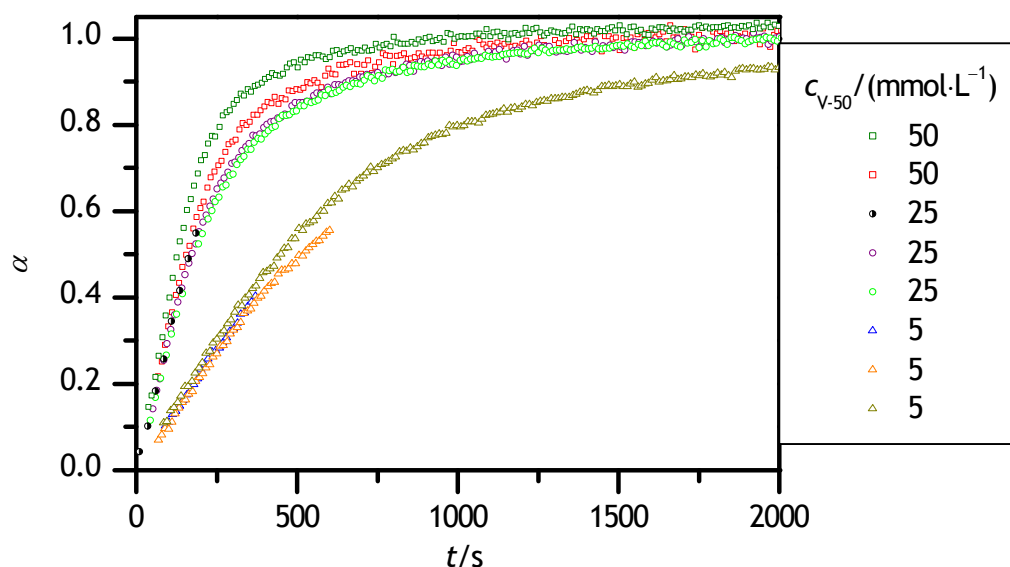


Figure 8.15: Dependence of degree of monomer conversion on time for chemically initiated polymerizations of 0.10 g·g⁻¹ PAm in D₂O at 50 °C, ambient pressure, and three different initial initiator concentrations.

Some of the polymerizations were not conducted to full conversion because small gas bubbles occurred which affect NIR analysis. These are most likely due to purging the solution with argon at ambient temperature prior to polymerization. The solubility of argon decreased while heating up to the desired temperature. The generation of gas

bubbles decreased the concentration of solutes (in the cross section of the NIR light beam) and caused a reduction of absorption bands in the NIR spectrum. Additionally, the baseline changed in absorbance due to scattering.

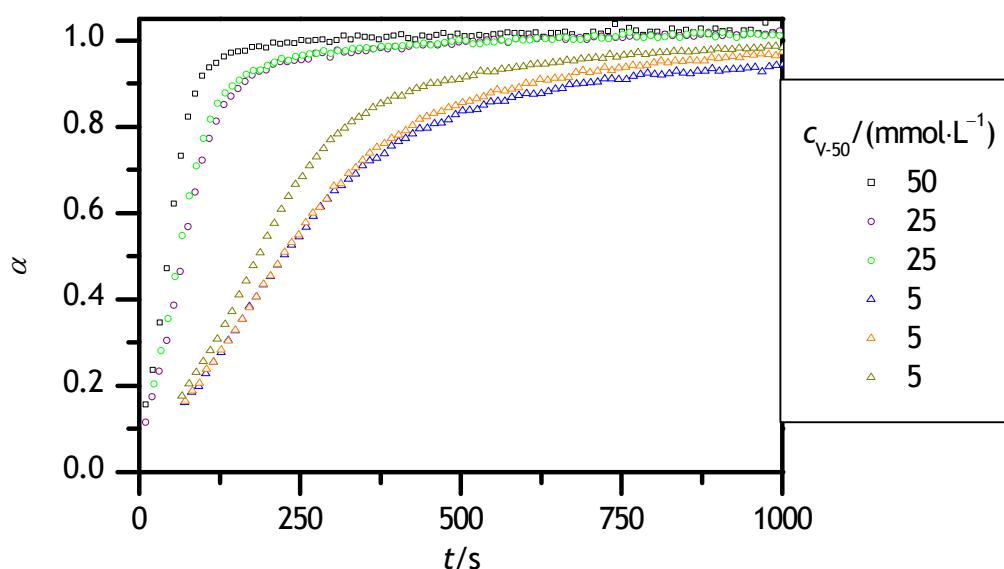


Figure 8.16: Dependence of degree of monomer conversion on time for chemically initiated polymerizations of $0.20 \text{ g}\cdot\text{g}^{-1}$ PAm in D_2O at 50°C , ambient pressure, and three different initial initiator concentrations.

As expected, the rate of polymerization increases towards higher initiator content. The change in degree of monomer conversion with time in case of the polymerization of $0.20 \text{ g}\cdot\text{g}^{-1}$ PAm in D_2O (figure 8.16) at an initial V-50 concentration of $25 \text{ mmol}\cdot\text{L}^{-1}$ would have been expected to be by a factor of $\sqrt{5}$ higher compared to the polymerization at an initial V-50 concentration of $5 \text{ mmol}\cdot\text{L}^{-1}$ (see equation 3.31). The factor is evidently higher indicating an increase in the change in degree of monomer conversion with time towards higher initial initiator concentration. Such an increase cannot be seen in case of the polymerization of $0.10 \text{ g}\cdot\text{g}^{-1}$ PAm in D_2O (figure 8.15).

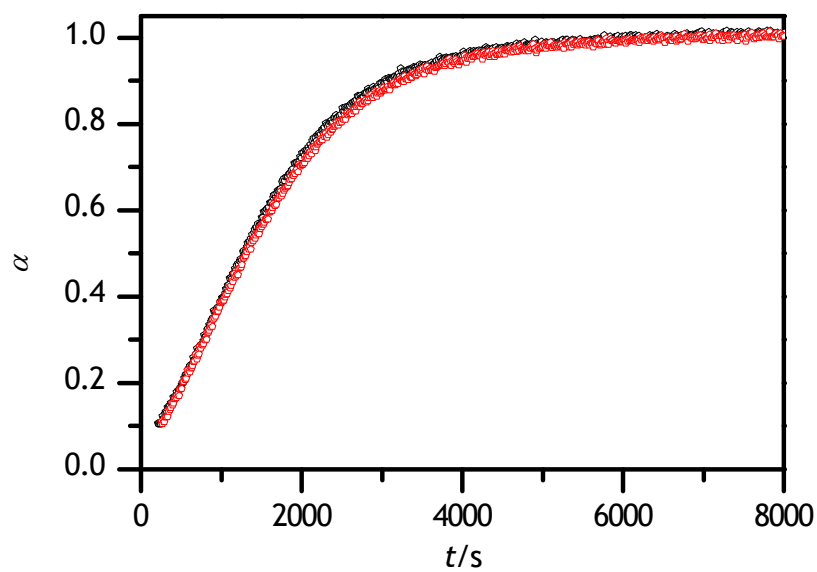


Figure 8.17: Dependence of degree of monomer conversion on time for two chemically initiated polymerizations of $0.20 \text{ g}\cdot\text{g}^{-1}$ PAm in D_2O at 50°C , ambient pressure, and an initial V-50 concentration of $0.25 \text{ mmol}\cdot\text{L}^{-1}$.

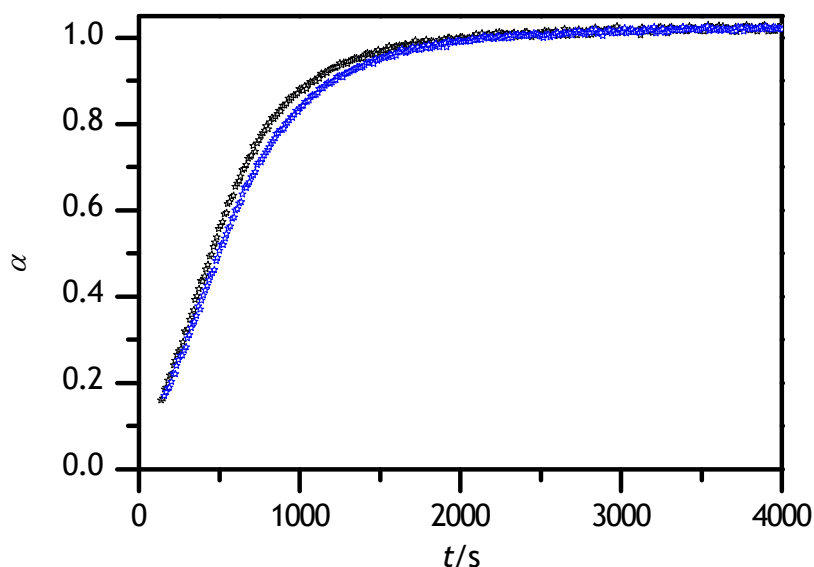


Figure 8.18: Dependence of degree of monomer conversion on time for two chemically initiated polymerizations of $0.30 \text{ g}\cdot\text{g}^{-1}$ PAm in D_2O at 50°C , ambient pressure, and an initial V-50 concentration of $0.5 \text{ mmol}\cdot\text{L}^{-1}$.

By comparison of figures 8.17 and 8.18, it stands out that an increase of initial monomer mass fraction results in a significantly higher rate of polymerization. In terms of initial V-50 content, the change in degree of monomer conversion with time (at a certain degree of monomer conversion) in case of the polymerization depicted in figure 8.18 would have been expected to be by a factor of $\sqrt{2}$ higher compared to the polymerization shown in figure 8.17 (see equation 3.31). The factor is, however, much higher indicating an increase of rate of polymerization towards higher initial monomer mass fraction. This behavior has already been reported by Ishige and Hamielec for initial PAm mass fractions of 0.02, 0.04, 0.08, and $0.16 \text{ g}\cdot\text{g}^{-1}$.^[275] According to equation 3.31, the increase of the degree of monomer conversion with time at a certain degree of monomer conversion would be expected to increase only slightly towards higher initial monomer mass fraction because the change in k_p (figure 7.16) counteracts the changes in k_d (table 5.2) and $\langle k_t \rangle$ (equation 8.3). Checking of temperature inside the cuvette in case of two experiments at $w_{\text{PAm}}^0 = 0.20 \text{ g}\cdot\text{g}^{-1}$ revealed that temperature increases towards higher degree of monomer conversion. Obviously, the heat of polymerization is higher than the heat dissipated with

the setup used. The increase in temperature is expected to be stronger the higher the rate of polymerization. The rate increases towards higher monomer content and higher initiator concentration. In order to allow for a statement regarding the dependence of $\langle k_{t,ini} \rangle$ on initial monomer mass fraction, the termination rate coefficients, which were determined neglecting the increase in temperature, may be extrapolated to zero monomer conversion. The corresponding $\langle k_t \rangle$ values are shown in figure 8.19. Absolute $\langle k_t \rangle$ values were determined by means of equation 7.7 which has been derived using k_p data at monomer mass fractions of up to $0.20 \text{ g}\cdot\text{g}^{-1}$. It is assumed that this equation holds up to an initial PAm mass fraction of $0.30 \text{ g}\cdot\text{g}^{-1}$.

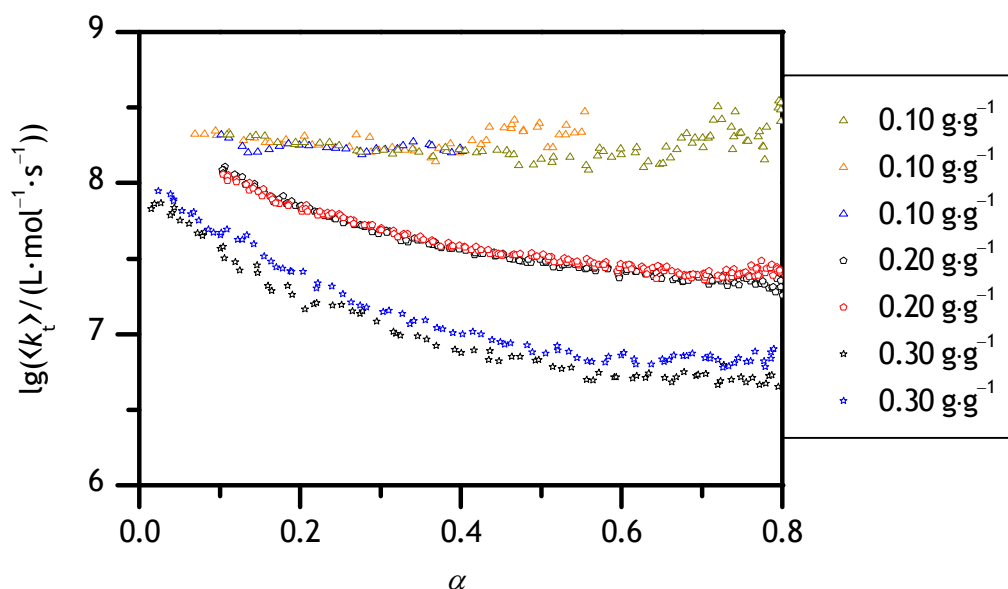


Figure 8.19: Dependence of $\langle k_t \rangle$ on monomer conversion for PAm polymerization at 50°C and ambient pressure. The increase in temperature due to reaction enthalpy has been neglected. Initial V-50 concentrations of $5 \text{ mmol}\cdot\text{L}^{-1}$, $0.25 \text{ mmol}\cdot\text{L}^{-1}$ and $0.5 \text{ mmol}\cdot\text{L}^{-1}$ were used for initial monomer mass fractions of $0.10 \text{ g}\cdot\text{g}^{-1}$, $0.20 \text{ g}\cdot\text{g}^{-1}$, and $0.30 \text{ g}\cdot\text{g}^{-1}$, respectively.

Data are presented up to a degree of monomer conversion of 0.80. At degrees of monomer conversion above 0.80, monomer concentration cannot be accurately

determined due to the low absorbance of the monomer absorption band. Furthermore, diffusion control of k_p might occur which is not easily quantified. The termination rate coefficient in case of an initial PAm mass fraction of $0.10 \text{ g}\cdot\text{g}^{-1}$ seems to be independent of monomer conversion. This indicates that temperature remains constant during polymerization at low monomer and initiator content. Linearly extrapolating $\langle k_t \rangle$ of the polymerization of $w_{\text{PAm}}^0 = 0.20 \text{ g}\cdot\text{g}^{-1}$ to zero monomer conversion results in approximately the same value which is obtained by extrapolation in case of $w_{\text{PAm}}^0 = 0.10 \text{ g}\cdot\text{g}^{-1}$ ($\lg(\langle k_{t,\text{ini}} \rangle / \text{L}\cdot\text{mol}^{-1}\cdot\text{s}^{-1}) \approx 8.3$). Such a small change in $\langle k_{t,\text{ini}} \rangle$ with initial monomer content would contradict the results of SP–PLP–NIR experiments. It can, however, not be ruled out that $\langle k_t \rangle$ is independent of monomer conversion at degrees of monomer conversion below 0.1 in case of $w_{\text{PAm}}^0 = 0.20 \text{ g}\cdot\text{g}^{-1}$ which would result in a value close to $\lg(\langle k_{t,\text{ini}} \rangle / \text{L}\cdot\text{mol}^{-1}\cdot\text{s}^{-1}) = 8.1$. Additionally, extrapolation of $\langle k_t \rangle$ of the polymerization of $w_{\text{PAm}}^0 = 0.30 \text{ g}\cdot\text{g}^{-1}$ to zero monomer conversion results in $\lg(\langle k_{t,\text{ini}} \rangle / \text{L}\cdot\text{mol}^{-1}\cdot\text{s}^{-1}) \approx 8.0$ which is much lower than the one for $w_{\text{PAm}}^0 = 0.10 \text{ g}\cdot\text{g}^{-1}$. $\lg(\langle k_{t,\text{ini}} \rangle / \text{L}\cdot\text{mol}^{-1}\cdot\text{s}^{-1})$ decreases by approximately 0.3 when the initial monomer mass fraction is increased from $0.10 \text{ g}\cdot\text{g}^{-1}$ to $0.30 \text{ g}\cdot\text{g}^{-1}$. According to SP–PLP–NIR experiments and equation 8.3, a decrease by 0.14 would have been expected. The stronger decrease in case of chemically initiated polymerization compared to SP–PLP–NIR experiments may be ascribable to the temperature increase during chemically initiated polymerization.

Two experiments at $w_{\text{PAm}}^0 = 0.20 \text{ g}\cdot\text{g}^{-1}$ were conducted with a thermocouple being inserted in the reaction mixture. The temperature inside the cuvette was monitored which allows for an estimation of $\langle k_t \rangle$ at 50°C . Using an initial V-50 concentration of $5 \text{ mmol}\cdot\text{L}^{-1}$ the temperature increased to 65°C at a degree of monomer conversion of 0.60. At an initial V-50 content of $0.25 \text{ mmol}\cdot\text{L}^{-1}$ the temperature rose only up to 54°C because of the lower rate of polymerization which allows for better heat dissipation. To calculate k_d and k_p and to determine $\langle k_t \rangle$ at 50°C , Arrhenius activation energies of $130 \text{ kJ}\cdot\text{mol}^{-1}$,^[206] $18 \text{ kJ}\cdot\text{mol}^{-1}$,^[199] and $15 \text{ kJ}\cdot\text{mol}^{-1}$ (Arrhenius activation energy of $k_t(1,1)$ of AA in aqueous solution^[11,276]), respectively, were used. The activation energy of $\langle k_t \rangle$ may be closely related (by a factor of approximately one fourth to one third)^[152–155] to the

internal energy of vaporization of the solvent (chapter 3.3), which is approximately $40.7 \text{ kJ}\cdot\text{mol}^{-1}$ for water at 40°C ^[277]. Due to this correlation, the activation energy in case of polymerizations in dilute aqueous solution might be almost independent of the monomer. Thus, the Arrhenius activation energy, which was found to be $15 \text{ kJ}\cdot\text{mol}^{-1}$ for $k_t(1,1)$ of AA in aqueous solution,^[11,276] might be applicable to termination in polymerization of PAm in dilute aqueous solution. Compared to Arrhenius activation energies reported for $\langle k_{t,\text{ini}} \rangle$ of styrene as well as of several acrylates and methacrylates, which are between 6 and $11 \text{ kJ}\cdot\text{mol}^{-1}$,^[32] the value for $k_t(1,1)$ of AA in aqueous solution is much higher. This difference may be ascribed to hydrogen bonding occurring in aqueous solution. The associated termination rate coefficients are shown in figure 8.20.

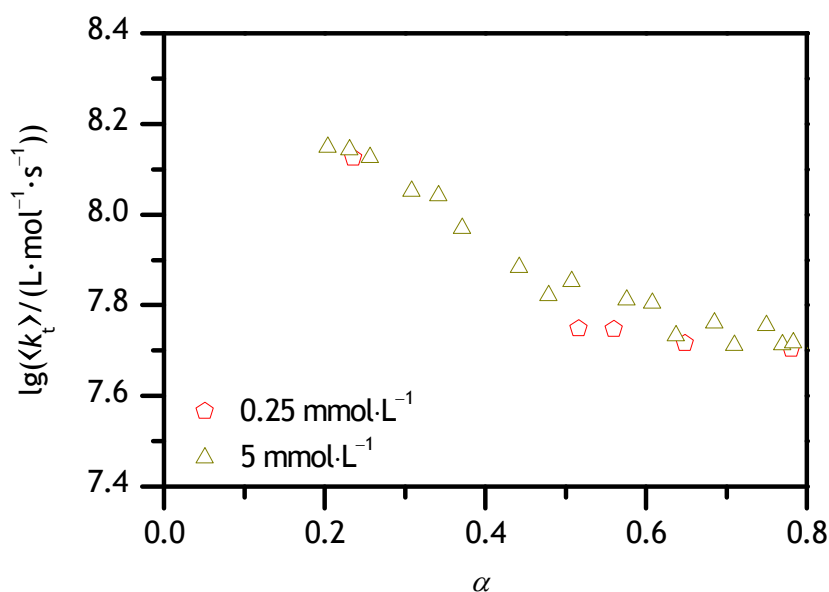


Figure 8.20: Dependence of $\langle k_t \rangle$ on monomer conversion for PAm polymerization at $w_{\text{PAm}}^0 = 0.20 \text{ g}\cdot\text{g}^{-1}$, 50°C and ambient pressure. The values have been corrected for the increase in temperature during polymerization. Two different initial V-50 concentrations were used.

The data determined for both initial V-50 concentrations are in good agreement. This indicates the reliability of the temperature correction. $\langle k_t \rangle$ significantly decreases towards

higher monomer conversion which may be ascribed to translational diffusion control of the termination reaction. At degrees of monomer conversion between 0.6 and 0.8 the decrease in $\langle k_t \rangle$ seems to be weaker than between 0.2 and 0.6. In the high-conversion range $\langle k_t \rangle$ might therefore be subject to reaction diffusion control. In order to determine $\langle k_{t,ini} \rangle$ one would need data at low degrees of monomer conversion. Depending on the rate-controlling step of termination at α below 0.20, $\lg(\langle k_{t,ini} \rangle / \text{L} \cdot \text{mol}^{-1} \cdot \text{s}^{-1})$ may be assumed to be approximately 8.2 in case that segmental diffusion is rate-controlling and 8.4 in case that translational diffusion is rate-controlling. These values may be obtained by linear extrapolation to zero monomer conversion.

The decrease in $\lg(\langle k_t \rangle / \text{L} \cdot \text{mol}^{-1} \cdot \text{s}^{-1})$ for $w_{\text{PAm}}^0 = 0.20 \text{ g} \cdot \text{g}^{-1}$ between degrees of monomer conversion of 0.2 and 0.8 amounts to approximately 0.43 (figure 8.20). In figure 8.19, the decrease in the same conversion range appears to be 0.50. This difference is indicative that the temperature increases during PAm polymerizations under the given conditions.

Direct temperature measurement of the reaction solution is desirable but challenging. A precise thermometer with a low response time is necessary. The thermometer has to be inserted in the reaction mixture in a way that the cuvette is closed to oxygen and that evaporation of the reaction mixture is ruled out. A variation of initiator concentration results in matching $\langle k_t \rangle$ values. This suggests that inhibition plays no major role. Moreover, it has to be ensured that the material of which the thermometer consists does not affect reaction kinetics. Termination rate coefficients for the polymerization of $w_{\text{PAm}}^0 = 0.20 \text{ g} \cdot \text{g}^{-1}$ and an initial V-50 concentration of $0.25 \text{ mmol} \cdot \text{L}^{-1}$ were determined in an experiment with temperature control (figure 8.19, red pentagons) and in a second one without temperature control (figure 8.19, black pentagons). Good agreement of the data indicates that an effect of the thermometer on reaction kinetics is negligible under the chosen reaction conditions. Correct termination rate coefficients could also be determined by a reduction of the initiator concentration which results in a lower rate of polymerization. It needs, however, to be mentioned that this would increase the relative error in initiator concentration through inaccuracies of weighing and through stronger influences of impurities. Attempts to conduct experiments at initiator concentrations below $0.25 \text{ mmol} \cdot \text{L}^{-1}$ failed because the significantly increased inhibition period exceeded

the maximum measurement time which is technically feasible (cooling of the NIR detector over night is required).

SP–PLP–NIR experiments are not prone to changes in temperature because the ratio of surface to volume of the reaction mixture is rather large. Conducting chemically initiated polymerizations at reaction conditions chosen for SP–PLP–NIR experiments could allow for a comparison of data determined by both techniques. The internal cell containing the reaction solution with thermally decomposing initiator would have to be inserted into the preheated high-pressure cell. Closing the high-pressure cell is, however, tedious (duration of approximately 15 min) so that polymerization usually starts before the first NIR spectrum is taken. In case of monomers exhibiting high propagation rate coefficients, like PAm, this hampers taking spectra at low monomer conversion. Furthermore, a laser pulse generates a radical concentration which is usually by a few orders of magnitude above the stationary radical concentration in chemically initiated polymerizations. Thereby, inhibitor is consumed much more readily in SP–PLP–NIR experiments.^[111] The influence of inhibition on kinetics may therefore extend up to higher degrees of monomer conversion in case of chemically initiated polymerizations than in case of SP–PLP–NIR experiments. Moreover, $\langle k_t \rangle$ values obtained by chemically initiated polymerizations at high pressure may show more measurement inaccuracy than in case of SP–PLP–NIR experiments as can be seen for MAA.^[111] In case of MAA this was ascribed to an impact of inhibition. The amount of dissolved oxygen may be assumed to be higher in case of polymerizations inside the internal cell of the high-pressure cell compared to cuvettes, which were used for ambient-pressure experiments, because of differences in sample preparation. Accuracy of data determined by chemically initiated polymerization at ambient pressure is therefore sufficiently high. Direct injection of the reaction solution into the high-pressure cell, which was used within this work, may cause problems regarding heat dissipation because the internal diameter of the high-pressure cell of 22 mm results in an unsatisfactory ratio of surface to volume of the reaction mixture. Moreover, an effect of the material of the internal wall of the cell on kinetics cannot be excluded.

A comparison of data determined by high-pressure SP–PLP–NIR experiments with data derived by chemically initiated polymerization at ambient pressure is hardly feasible

because data in the initial polymerization period are lacking in case of chemically initiated polymerizations and data of SP–PLP–NIR experiments are subject to scatter and accessible in the low-conversion range. However, the termination rate coefficient which may be estimated for $w_{\text{PAm}}^0 = 0.10 \text{ g}\cdot\text{g}^{-1}$, 50 °C, and ambient pressure by equation 8.5 (SP–PLP–NIR) in combination with an activation energy of $15 \text{ kJ}\cdot\text{mol}^{-1}$ (Arrhenius activation energy of $k_t(1,1)$ of AA in aqueous solution^[11,276]) and the volume of activation given in table 8.1 amounts to $\lg(\langle k_{t,\text{ini}} \rangle) = 8.39 \text{ L}\cdot\text{mol}^{-1}\cdot\text{s}^{-1}$. By means of data determined by chemically initiated polymerization, $\lg(\langle k_{t,\text{ini}} \rangle) \approx 8.3 \text{ L}\cdot\text{mol}^{-1}\cdot\text{s}^{-1}$ was estimated. These values are in good agreement.

Additionally, an activation energy of $15 \text{ kJ}\cdot\text{mol}^{-1}$ and the volume of activation given in table 8.1 were used to extrapolate $\langle k_t \rangle$ data for initial PAm mass fractions of $0.20 \text{ g}\cdot\text{g}^{-1}$ and $0.30 \text{ g}\cdot\text{g}^{-1}$ determined by SP–PLP–NIR experiments as well as the average $\langle k_{t,\text{ini}} \rangle$ value for both initial PAm mass fractions (light green line in figure 8.7) to 50 °C and ambient pressure. The so-obtained $\langle k_t \rangle$ values and the average $\langle k_{t,\text{ini}} \rangle$ value (depicted as line) are shown in figure 8.21 together with data from figure 8.20. The line corresponds to $\lg(\langle k_{t,\text{ini}} \rangle) = 8.27 \text{ L}\cdot\text{mol}^{-1}\cdot\text{s}^{-1}$ which is slightly lower than the extrapolated value for $w_{\text{PAm}}^0 = 0.10 \text{ g}\cdot\text{g}^{-1}$ ($\lg(\langle k_{t,\text{ini}} \rangle / \text{L}\cdot\text{mol}^{-1}\cdot\text{s}^{-1}) \approx 8.3$). This indicates that the activation energy and the volume of activation, which were used for extrapolating rate coefficients determined by SP–PLP–NIR experiments to 50 °C and ambient pressure, are reasonable. Taking the inaccuracies of $\langle k_t \rangle$ determination, particularly via SP–PLP–NIR experiments, into account, both methods provide $\langle k_t \rangle$ values which are in good agreement. It might be assumed that termination is controlled by segmental diffusion at degrees of monomer conversion less than 0.15 in case of $w_{\text{PAm}}^0 = 0.20 \text{ g}\cdot\text{g}^{-1}$. A decrease in $\langle k_t \rangle$ towards higher monomer conversion from zero monomer conversion on is unlikely because $\langle k_t \rangle$ at $w_{\text{PAm}}^0 = 0.10 \text{ g}\cdot\text{g}^{-1}$ is almost independent of monomer conversion up to at least $\alpha = 0.8$ (see figure 8.19). The decrease of $\langle k_t \rangle$ values (due to translational diffusion control), which were determined by means of SP–PLP–NIR experiments at an initial monomer mass fraction of $0.30 \text{ g}\cdot\text{g}^{-1}$, above a degree of monomer conversion of 0.16 is stronger than the decrease in $\langle k_t \rangle$ values obtained by chemically initiated polymerization for $w_{\text{PAm}}^0 = 0.20 \text{ g}\cdot\text{g}^{-1}$. This observation is in line with the expectation that a stronger

decrease in $\langle k_t \rangle$ is obtained at higher initial monomer content and thus higher polymer mass fraction at identical degree of monomer conversion.

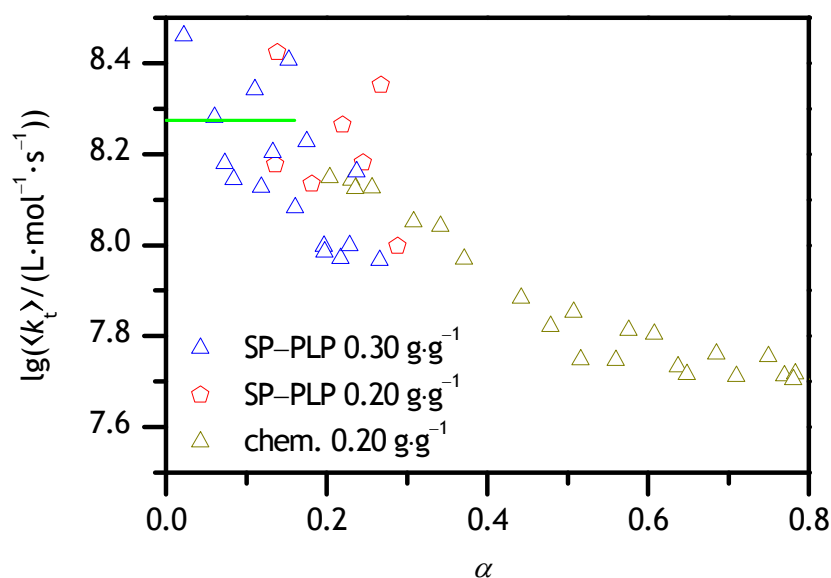


Figure 8.21: Dependence of $\langle k_t \rangle$ on monomer conversion for PAm polymerization at given initial PAm mass fractions, 50 °C and ambient pressure. Data were determined by means of chemically initiated polymerization (chem.) or by SP-PLP-NIR experiments (SP-PLP). The line represents the rate coefficient which is given as light green line in figure 8.7 but extrapolated to 50 °C and ambient pressure (see text).

9 Propagation Kinetics of Sodium Acrylate– 1-Vinylpyrrolidin-2-one Copolymerization

Copolymerization allows for manifold product customization. Copolymers of acrylic acid and 1-vinylpyrrolidin-2-one are sold as, for example, Acrylidone® 1005 or Ultrathix™ P-100 and are used among others in rinse aids, inkjet coatings, membranes, and styling gels.^[278,279] Therefore, investigations into the binary copolymerization kinetics of AA and VP appeared to be rewarding. ¹H NMR analysis of a mixture of both monomers in water, which was prepared at ambient pressure and temperature, revealed that VP undergoes a spontaneous acid-catalyzed reaction in aqueous solution. The ¹H NMR spectrum of the mixture has been recorded in D₂O and is shown in figure 9.1.

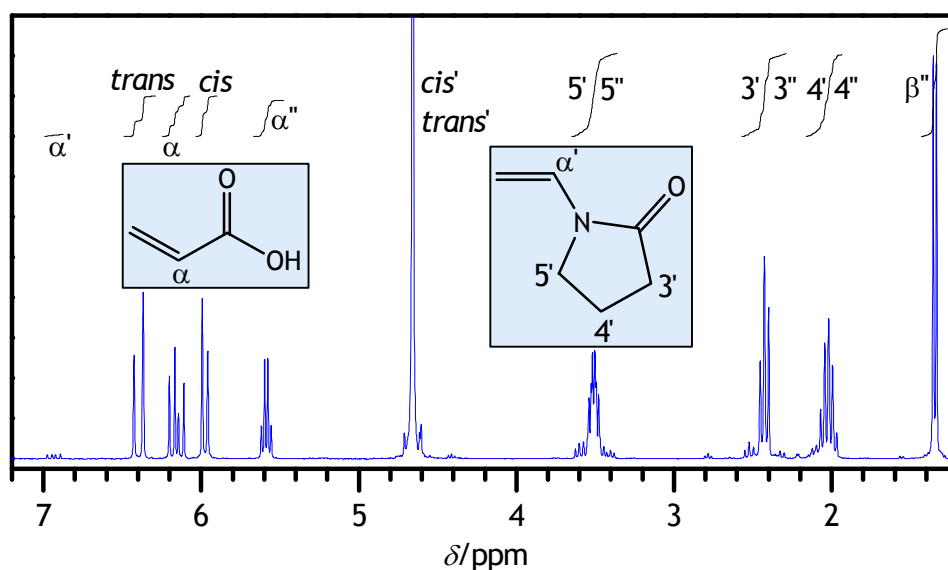
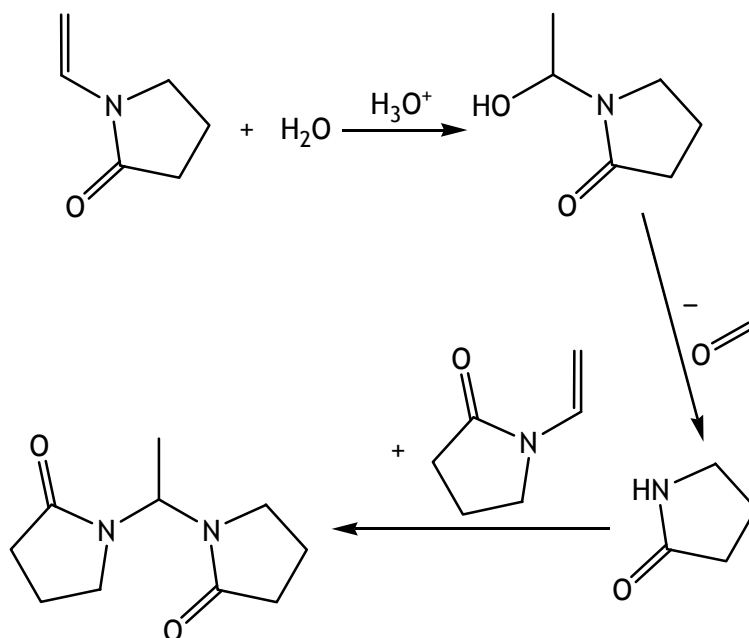


Figure 9.1: ¹H NMR spectrum of a mixture of acrylic acid, 1-vinylpyrrolidin-2-one, and water recorded in D₂O at 35 °C. The mixture was prepared at ambient pressure and temperature. A weak quartet at 9.66 ppm is not shown. Labelings and integral curves are explained in the text. The structures of AA and VP are given with the associated labelings of carbon atoms.

The signals in figure 9.1 are labeled α , β , *cis*, *trans*, 3, 4, and 5 corresponding to the hydrogen atoms joined to the α -carbon, joined to the β -carbon (in case of the reaction product of AA and VP), in *cis* and *trans* position (in case of the monomers) to the first-mentioned hydrogen atom, and joined to the carbon atoms in positions 3, 4, and 5 of the pyrrolidin-2-one ring, respectively. The prime and double prime symbols are used to designate VP and a product of the reaction of AA and VP, respectively. Labelings without prime are used for AA. Relative intensities are given by relative increases of the integral curves. A detailed analysis of the NMR spectrum is given in appendix A.4.

The weakness of those signals, which correspond to the hydrogen atoms joined to the carbon–carbon double bond of VP, indicates that this double bond is consumed by the spontaneous reaction of VP. The structure of the signals in the range of 1.8 ppm to 3.8 ppm indicates that the pyrrolidin-2-one ring is not directly involved in the reaction. Thus, a ring-opening reaction is ruled out. The acid-catalyzed reaction of VP in aqueous solution has already been reported^[280] and is shown in the following reaction scheme.



The very weak doublet at approximately 2.22 ppm in combination with the weak quartet at 9.66 ppm may represent acetaldehyde. The existing ^1H NMR signals of pyrrolidin-2-one,

1-(1-hydroxyethyl)pyrrolidin-2-one, and 1,1-di(pyrrolidin-2-on-1-yl)ethane may show similar chemical shifts because of the structural similarity. The reaction of VP in acidic solution results in monomer consumption and in the production of non-polymerizable molecules. It goes without saying that investigations into the polymerization kinetics of AA and VP in aqueous solution require a detailed kinetic analysis of side reactions. Furthermore, the reaction time prior to the start of the polymerization experiment has to be precisely determined. Influences of all side products on polymerization kinetics have to be studied to allow for an interpretation of determined rate coefficients. However, the side reaction occurs to a negligible extent in more basic solution. Therefore, the copolymerization of VP and sodium acrylate was studied. The ^1H NMR spectrum of a mixture of NaA and VP in water was recorded in D_2O and is shown in figure 9.2.

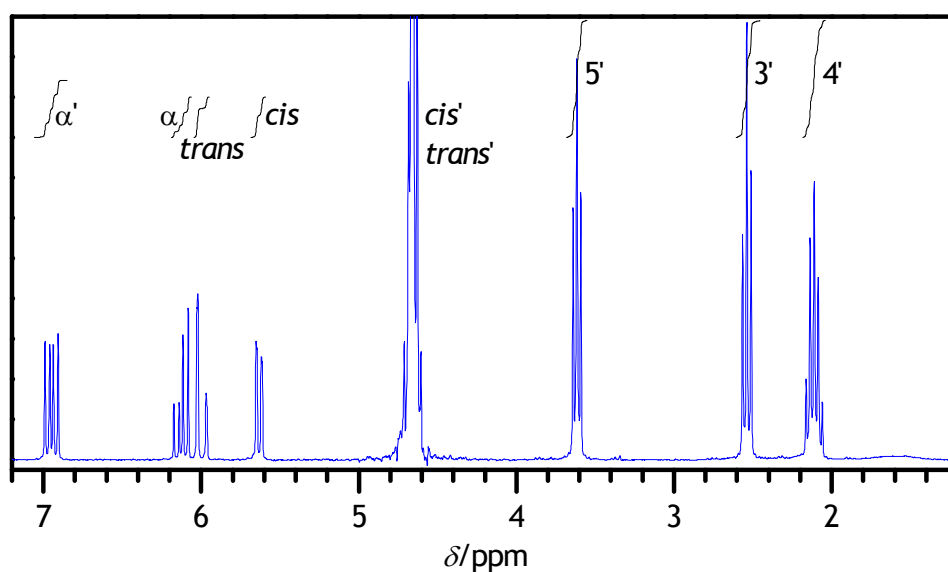


Figure 9.2: ^1H NMR spectrum of a mixture of sodium acrylate, 1-vinylpyrrolidin-2-one, and water recorded in D_2O at 35 °C. The mixture was prepared at ambient pressure and temperature. Labelings and integral curves are explained in the text.

Signal labeling in figure 9.2 is in line with the denotation in figure 9.1 except for the labelings without prime which are used for NaA instead. The spectrum shows only signals which can be unambiguously assigned to either NaA or VP. It stands out that NaA obviously did not transform to AA. A terpolymerization of AA, NaA, and VP may be ruled out.

In binary copolymerization of NaA and VP in aqueous solution monomer composition was varied to determine the monomer reactivity ratios by means of the Mayo–Lewis equation. The change in monomer composition may be associated with a variation in hindrance of the internal rotational and vibrational motions of the activated complex. Such variation in hindrance might affect the individual propagation rate coefficients, k_{11} and k_{12} as well as k_{22} and k_{21} , to a different extent. However, monomer reactivity ratios, which are defined as the ratio of two individual rate coefficients, were determined under the assumption that they are independent of monomer composition. Experiments were conducted at ambient pressure and 25 °C. The total monomer mole fraction was chosen to be 0.05 mol·mol⁻¹ corresponding to mass fractions of 0.215 to 0.245 g·g⁻¹ depending on the monomer composition. The propagation rate coefficient of homopolymerizations in aqueous solution usually changes with monomer content.^[33–38,40–42,45–47,71] Intermolecular interactions of the macroradical with monomer and solvent molecules, respectively, are used to explain this behavior. From this point of view the relative number of monomer and solvent molecules in the direct vicinity of the growing chain end seems to affect the propagation rate coefficient. A quantitative interpretation of the concentration dependence of k_p may presumably be made taking the monomer mole fraction into account rather than the mass fraction. The mass fraction is more common in industry. Compared to the number of electrostatic interactions and the number of formed hydrogen bonds, the mass of a molecule may, at best, negligibly influence the total strength of the intermolecular interactions of the macroradical with monomer and solvent molecules. The mole fraction instead of the mass fraction has been kept constant in copolymerization experiments because both monomers differ in molar mass. The polymer was obtained by PLP at laser-pulse repetition rates of 40 to 400 Hz and an initiator (HHMP) concentration of 2 mmol·L⁻¹. Monomer conversion was kept low to avoid a decrease of the total

monomer content and a monomer composition drift. For most monomer compositions two different laser-pulse repetition rates were applied in separate experiments to check for frequency dependence. Polymer was analyzed by ^1H NMR. It may be assumed that the carboxylic acid groups in the copolymer are fully protonated during NMR analysis because the copolymer was purified by dialysis against demineralized water until constant conductivity was attained. ^1H NMR spectra of produced poly(acrylic acid) (poly(AA)) and poly(VP) samples are depicted in figures 9.3 and 9.4. Signals labeled α and β correspond to the hydrogen atoms at the α -carbon atoms (substituted methylene group) and at the β -carbon atoms (unsubstituted methylene group) of the constitutional units, respectively. 3, 4, and 5 denote signals corresponding to the hydrogen atoms at the carbon atoms in positions 3, 4, and 5 of the pyrrolidin-2-one ring, respectively. Poly(AA) mainly shows signals in the range of approximately 1 ppm to 3 ppm whereas poly(VP) shows signals in the ranges of 1.4 ppm to 2.6 ppm and of 3 ppm to 4 ppm. The copolymer composition may be determined by comparison of signal intensities in the ranges of 1 ppm to 3 ppm and of 3 ppm to 4 ppm. The number of hydrogen atoms of VP units in the copolymer, which show signals in the range at low chemical shift, is twice as high compared to the number of hydrogen atoms of VP units in the copolymer, which show signals in the range at high chemical shift. The same applies to the corresponding signal intensities. This knowledge combined with the signal intensity in the range of 3 ppm to 4 ppm allows for dividing the signal intensity in the range of 1 ppm to 3 ppm into two intensities based on hydrogen atoms of AA units on the one hand and of VP units on the other hand. The ^1H NMR spectrum of a poly(AA-*co*-VP) sample obtained by copolymerization using a mole fraction of VP of $f_{\text{VP}} = 0.30 \text{ mol} \cdot \text{mol}^{-1}$ in the monomer mixture is shown in figure 9.5. The two ranges can easily be distinguished.

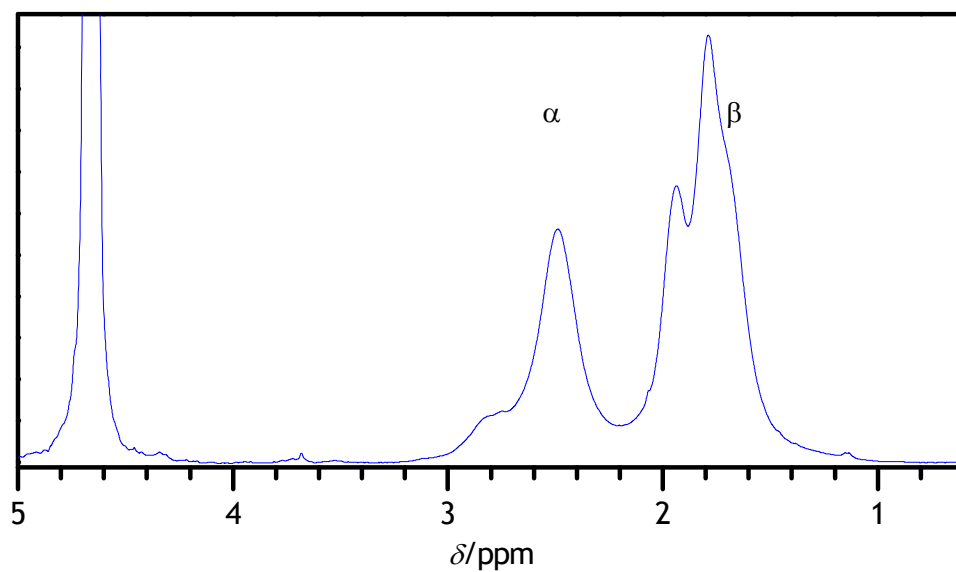


Figure 9.3: ^1H NMR spectrum of poly(acrylic acid) recorded in D_2O at 35°C . Labelings are explained in the text.

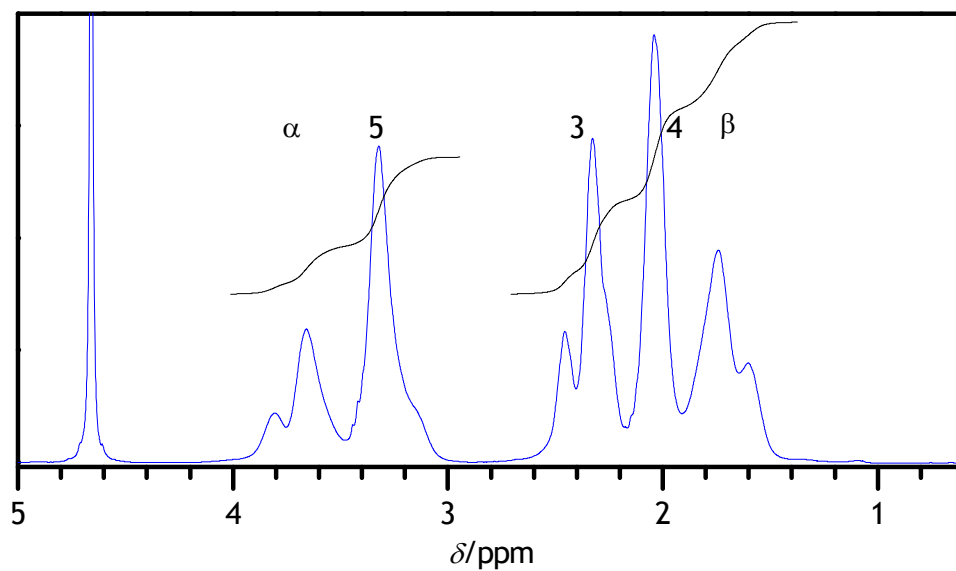


Figure 9.4: ^1H NMR spectrum of poly(1-vinylpyrrolidin-2-one) recorded in D_2O at 35°C . Labelings are explained in the text.

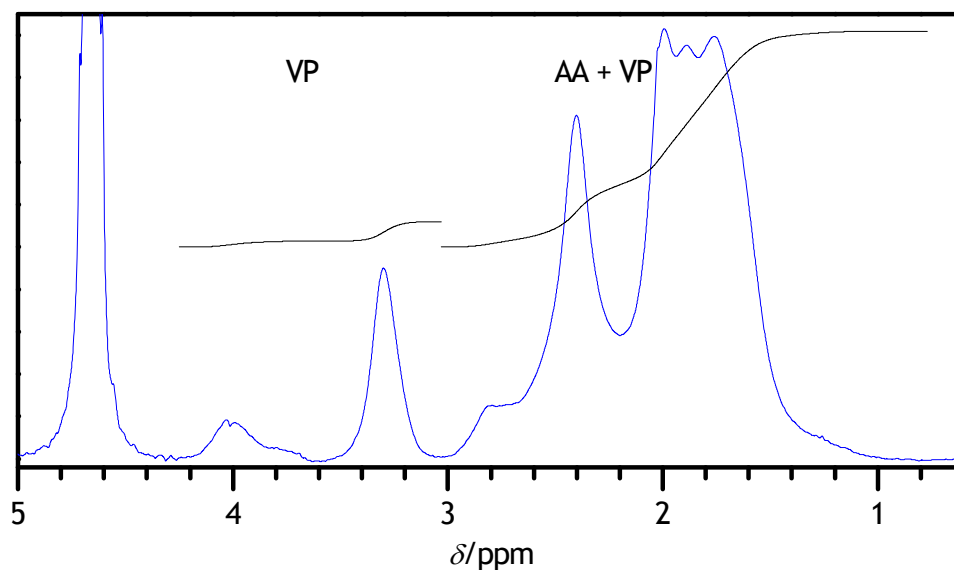


Figure 9.5: ^1H NMR spectrum of a poly[(acrylic acid)-*co*-(1-vinylpyrrolidin-2-one)] sample obtained by copolymerization using a mole fraction of $f_{\text{VP}} = 0.30 \text{ mol} \cdot \text{mol}^{-1}$ in the monomer mixture. The spectrum was recorded in D_2O at 35°C .

Variation of monomer composition and analysis of the produced copolymer results in the data given in figure 9.6. Red symbols denote data determined at higher laser-pulse repetition rate (100–400 Hz) than data depicted as black symbols (40–100 Hz). Error bars were estimated and refer to uncertainties due to NMR analysis. The data indicate that the laser-pulse repetition rate has no influence on the results. The solid line represents a fit of equation 3.36 to all experimental data whereas the dashed line is a representation of equation 3.36 for an ideal azeotropic binary copolymerization with both monomer reactivity ratios being unity.

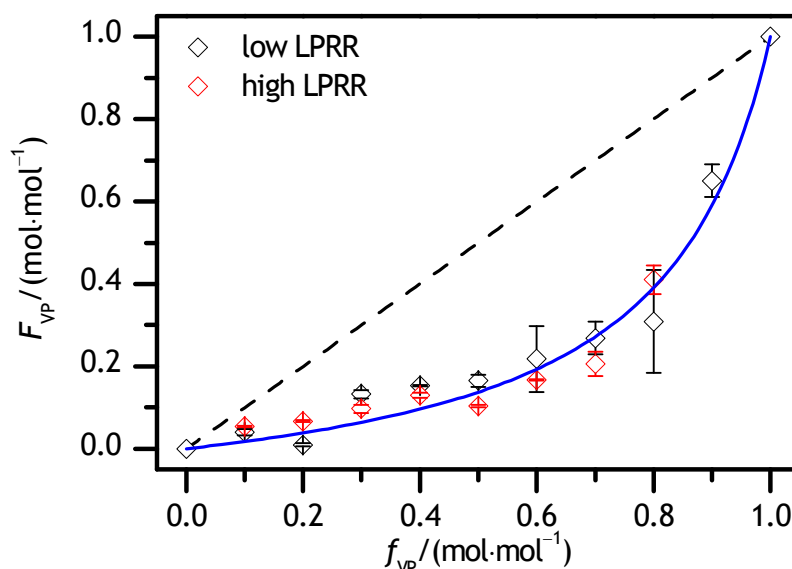


Figure 9.6: Dependence of mole fraction of VP in the copolymer on mole fraction of VP in the monomer mixture. The polymer was obtained at 25 °C, ambient pressure and a total monomer mole fraction including the solvent of 0.05 mol·mol⁻¹. Error bars were estimated and refer to uncertainties due to NMR analysis.

Sodium acrylate is preferably incorporated into the copolymer, as is reflected in the monomer reactivity ratios which are $r_{12} = 0.16 \pm 0.05$ ($M_1 = \text{VP}$, $M_2 = \text{NaA}$) and $r_{21} = 6.28 \pm 1.09$. These values indicate that homopropagation is preferred in case of NaA being the terminal monomer unit whereas cross-propagation is preferred in case of VP being the terminal monomer unit. The copolymer is therefore comprised of blocks of NaA units and statistically incorporated VP units. Additionally, the product of both monomer reactivity ratios is close to unity indicating that it might be an ideal non-azeotropic rather than a statistical non-azeotropic copolymerization. In case of the ideal non-azeotropic copolymerization, the relative rates of incorporation of NaA or VP in the polymer are independent of the terminal monomer unit.

It might have been expected that a macroradical with the terminal monomer unit being sodium acrylate preferentially adds VP because electrostatic repulsion of the carboxylate groups may disfavor NaA addition, which is not the case. Obviously, the sodium

counterions strongly shield the anionic groups resulting in a much weaker electrostatic repulsion of the carboxylate groups.

Monomer reactivity ratios published for the binary copolymerization of AA and VP ($M_1 = \text{VP}$, $M_2 = \text{AA}$) at 30 °C in basic aqueous solution imply that r_{12} is close to zero and $r_{21} \approx 7$.^[48] The pH value was adjusted by addition of sodium hydroxide such that AA may be assumed to be converted to NaA. The monomer reactivity ratios are close to the ones determined in this work. However, a reaction of VP in acidic solution, which may have occurred during sample preparation, was not considered. Chapiro and Trung reported values of $r_{12} = 0.05$ and $r_{21} = 0.48$ for the binary copolymerization of AA and VP at 20 °C in bulk, ethanol (total monomer volume fraction of 0.20 L·L⁻¹), and toluene (total monomer volume fraction of 0.20 L·L⁻¹).^[281] Copolymerization in *N,N*-dimethylformamide (total monomer volume fraction of 0.20 L·L⁻¹, 20 °C) can be represented by $r_{12} = 0.03$ and $r_{21} = 0.67$.^[281] These monomer reactivity ratios are significantly smaller than the values obtained in this work. However, Chapiro and Trung used acrylic acid instead of sodium acrylate. Binary copolymerization of monomers exhibiting an electron-deficient carbon–carbon double bond (like AA) with monomers exhibiting an electron-rich carbon–carbon double bond (like VP) usually show low monomer reactivity ratios because of the strong tendency to form an alternating copolymer. The carbon–carbon double bond of NaA should exhibit a higher electron density than AA because NaA contains a negative charge at the carboxyl group. Assuming that sodium counterions shield the carboxylate groups of NaA, the monomer reactivity ratios of NaA–VP copolymerization are expected to be higher than in case of AA–VP copolymerization which is in accordance to experimental results.

So far, k_p data for homopropagation of sodium acrylate in aqueous solution are scarce. Propagation rate coefficients of AA may be used considering that k_p changes with degree of ionization.^[39,47] As indicated by Wittenberg,^[282] it may be assumed that the ratio of k_p of non-ionized acrylic acid to k_p of NaA is identical to the corresponding ratio in case of non-ionized methacrylic acid and sodium methacrylate. k_p of NaA may therefore be estimated by combining temperature-dependent rate coefficients of AA at different monomer concentrations^[33] with the dependence of k_p of MAA on the degree of

ionization^[47]. The so-obtained rate coefficient amounts to $37\,600\text{ L}\cdot\text{mol}^{-1}\cdot\text{s}^{-1}$ at $25\text{ }^{\circ}\text{C}$ and $0.20\text{ g}\cdot\text{g}^{-1}$ NaA in aqueous solution. This k_p value is close to the rate coefficient at $0.215\text{ g}\cdot\text{g}^{-1}$ NaA which corresponds to an amount fraction of $0.05\text{ mol}\cdot\text{mol}^{-1}$. The k_p value of $0.05\text{ mol}\cdot\text{mol}^{-1}$ VP in water at $25\text{ }^{\circ}\text{C}$ is $7\,400\text{ L}\cdot\text{mol}^{-1}\cdot\text{s}^{-1}$.^[45] Assuming that the individual propagation rate coefficients do not vary with monomer composition, the homopropagation rate coefficients may be taken as k_{11} (VP) and k_{22} (NaA) within the terminal model. Based on these two rate coefficients, it may be concluded that $k_{12} = 46\,300\text{ L}\cdot\text{mol}^{-1}\cdot\text{s}^{-1}$ and $k_{21} = 6\,000\text{ L}\cdot\text{mol}^{-1}\cdot\text{s}^{-1}$. The ratios of the individual rate coefficients reflect the high preference to incorporate NaA in the copolymer. It should be noted that these estimates of cross-propagation rate coefficients rely on the validity of the terminal model which is the exception rather than the rule.

10 Closing Remarks and Outlook

10.1 Experimental Techniques

SP–PLP–NIR Technique

Termination rate coefficients were determined by means of the SP–PLP–NIR technique. Up to date, this method is unrivaled in determination of $\langle k_t \rangle$ up to high degrees of monomer conversion. To obtain monomer conversion versus time profiles of high signal-to-noise quality, high pressure has to be applied which is unfavorable from the industrial point of view. However, $\langle k_t \rangle$ may be extrapolated to ambient pressure via the volume of activation. Moreover, volumes of activation provide insight into reaction mechanisms.

To improve the quality of experimental results, an optimization of the setup is required. The signal of SP–PLP–NIR experiments is subject to electronic noise and so-called ambient vibrations. The latter can be ascribed to, for example, acoustics, air currents, air exhausters, building motion, elevators, pumps, and traffic.^[283] Ambient vibrations cause vibrations of the filament of the tungsten-halogen lamp. This results in oscillations of the signal intensity. To reduce these problems the setup is positioned on a solid granite slab supported by rubber inner tubes. Such passive vibration isolation system is appropriate to reduce vibrations of approximately 10 Hz and above.^[284,285] However, the horizontal natural frequency of passive vibration isolation systems is typically in the range of 2 to 5 Hz.^[284] Ambient horizontal vibrations in upper-floor locations tend to occur in the same frequency range^[283,286] and are therefore amplified by passive vibration isolation systems. An active vibration isolation system, which detects small vibrations electronically and compensates them by means of a counteracting force, could be installed to overcome this problem. Such systems are capable of damping vibrations at low frequency.^[284] At high vibration frequencies, active vibration isolation systems are usually outperformed by passive ones.^[287,288] A system combining both technologies may therefore be rewarding. Such a vibration-isolated table of adequate size has been commercially available for nearly three years at the Technical Manufacturing Corporation. As a result the heavy granite slab would have to be replaced by a lighter one. A specially designed tabletop, which is capable

of damping vibrations passing through the vibration isolation system and vibrations caused by components mounted on the tabletop, should be chosen. Additionally, a renewal of the UV mirrors may increase the signal-to-noise ratio. Within the last decades, significant progress has been made concerning the optimization of the quality of optical windows and of the properties of optical coatings. These improvements result in a higher transmittance of UV mirrors in terms of infrared light and a higher reflectivity in terms of UV light. To allow for a much easier alignment of the halogen lamp, a closed lamp housing is beneficial. This would also reduce stray light. An additional reflector inside the housing would increase the signal intensity. Cooling of low-power lamps may be conducted by convection cooling whereas high-power lamps may be cooled by a fan. Bionically optimized fans, which have been available for a few weeks, are preferred because of the reduced acoustic noise corresponding to weaker pressure waves.

Two paths may be pursued to further improve the quality of experimental results. The first one would be an improvement of the actual components. Replacing the infrared detector by a new one, which exhibits higher detectivity and responsivity in the spectral range of interest, may improve the signal-to-noise ratio. This requires a renewal of the preamplifier (chapter 4.10) in turn. The precise determination of apparent monomer conversion via the USB multifunction data acquisition board relies on a high resolution of the analog input. In case of noise reduction, it appears obvious that the board has to be replaced by a new one with higher resolution. Additionally, the input of the transient recorder could be used in differential mode to reduce electromagnetic noise. SBench 5.3 offers a function to make maximum use of the voltage input range of the transient recorder and thus of the resolution. A compensating voltage can be applied to the input signal via SBench 5.3. Therefore, an input range, which is slightly larger than the difference between lowest and highest input voltage, may be chosen and the input signal may be shifted by the compensating voltage such that the lowest input voltage is close to the lower input limit. Unfortunately, this feature of the present software does not work. In addition, SBench 5.3 occasionally shows problems in averaging several signals and in automatic data storage. These problems can be overcome manually but by a tedious procedure. SBench 5.3 should therefore also be replaced as soon as a new version is available. Fluctuations in infrared

light intensity due to the vibration of the filament of the halogen lamp may be overcome by usage of a tunable infrared laser. A laser with narrow spectral bandwidth supersedes the use of a monochromator as well. Yet, tunable lasers working in the wavenumber range of interest, exhibiting an adequate output power, and showing a preferably noise-free light intensity are, however, scarce if not unavailable.

The second path which may be pursued involves the replacement of the infrared detector by a line scan camera (diode array). With line scan cameras full spectra may be recorded which supersedes the usage of an FTIR spectrometer to determine the overall monomer conversion. The present monochromator can be used as spectrograph, which is required for usage of a line scan camera. However, a spectrograph with higher light-gathering power is desirable. Signal intensity may further be increased by coupling light into the spectrograph by means of a customized circular-to-rectangular fiber bundle. Other optical components would have to be adapted to the opening angle of the fiber bundle. In choosing the material and the length of such a bundle, the transmittance has to be taken into account. Finding an adequate line scan camera is most challenging. The camera has to show high detectivity and responsivity in the wavenumber range of interest. This might be fulfilled by indium gallium arsenide cameras. The number of pixels and the pixel width are related to the wavenumber resolution and the spectral range of the recorded spectrum. In case of the present setup, only the increase in signal intensity after a single laser pulse is detected by the transient recorder. The underlying signal is suppressed by application of a compensating voltage. A high resolution of the monomer concentration is thereby achieved. Determination of the full monomer band means that the underlying signal is not suppressed. Therefore, a significantly higher digital resolution (number of discrete values) of the analog-to-digital converter is necessary to achieve a resolution of monomer concentration which is identical to the one of the present setup. Furthermore, a high line rate is required to ensure a high time resolution. This in turn requires software and hardware which is capable of rapidly recording and processing data. A real-time operating system may be needed for this purpose. The most promising indium gallium arsenide cameras are manufactured by the Goodrich Corporation (Sensors Unlimited). These cameras show maximum line rates of approximately 92 kHz and a maximum digital

resolution of 14 bit. Vastly better line scan cameras are required for SP–PLP–NIR experiments.

Determination of termination rate coefficients at ambient pressure is hardly feasible with the current SP–PLP–NIR setup due to low signal-to-noise quality. For the same reason, termination rate coefficients of monomers, which exhibit high $\langle k_t \rangle$ values and low k_p values even at high pressure, are subject to large scatter. Therefore, the implementation of a new vibration isolation system with an adequate tabletop as well as a renewal of the lamp housing is worthwhile. In addition, the infrared detector should be renewed in the near future accompanied by a renewal of the preamplifier and of the multifunction data acquisition board. SBench 5.3 should be replaced by SBench 6, which is currently in development, as soon as it is available.

Viscometer

Dynamic viscosity was determined at ambient pressure and correlated with termination rate coefficients, which were measured at high pressure. A viscometer capable of measuring data at high pressure is desirable. If such a device determines the kinematic viscosity, a density meter, which is able to measure high-pressure densities, will be needed to calculate dynamic viscosities.

PLP Setup

Exciplex lasers with laser-pulse repetition rates of up to 400 Hz were used for PLP–SEC experiments. A laser-pulse repetition rate of 400 Hz is sufficient for the monomers investigated. Experiments under variation of laser-pulse repetition rate provide information about chain-transfer reactions.^[19,44,232] Investigations at high temperature and high pressure may, however, require repetition rates above 400 Hz. Exciplex lasers, which emit light in the wavelength range of interest at significantly higher laser-pulse repetition rates, are not available up to date. Frequency-tripled solid-state lasers using crystals like Yb:YAG, Nd:YLF, Nd:glass, Nd:YAG, Nd:YCOB or Nd:YVO₄ as laser medium are an

alternative to excimer lasers. Solid-state lasers with significantly higher laser-pulse repetition rates than in case of excimer lasers are available. This advantage usually comes along with low pulse energies. However, PLP experiments are possible using significantly lower pulse energies compared to those used within the present work.^[18,27,29–31] Sometimes low pulse energies are even better for obtaining PLP structures.^[85,251]

Laser-pulse repetition rates should be adapted to the size of the propagation rate coefficient and thus to reaction conditions. It is unlikely that reaction conditions are chosen under which the propagation rate coefficient significantly exceeds $10^6 \text{ L} \cdot \text{mol}^{-1} \cdot \text{s}^{-1}$. Repetition rates above a few kHz may not be needed because the resulting degrees of polymerization would be rather low. Thereby, the relative error in the determined degree of polymerization is increased and a potential chain-length dependence of k_p might have to be taken into account. Additionally, high repetition rates are sometimes even unfavorable for obtaining PLP structures.^[85,251]

Chemically Initiated Polymerizations

In addition to SP–PLP–NIR experiments, chemically initiated polymerizations provide information about termination kinetics. In case of the setup used in this work, the temperature increased during prop-2-enamide polymerization. Temperature constancy is, however, desirable. This may be achieved by low initiator concentrations and by a reduction of the size of the cuvettes while retaining the path length. Otherwise the temperature inside the cuvette has to be measured keeping the requirements mentioned in chapter 8.4 in mind.

10.2 Kinetic Parameters

Termination rate coefficients were determined in dependence of pressure. The volumes of activation determined within the present work were calculated for $\langle k_t \rangle$ at low degrees of monomer conversion. The pressure dependence of the individual parameters $k_{t,SD}$, C_η ,

$k_{t,TD}^0$, and C_{RD} is of interest from industrial and scientific point of view. However, it is challenging to find an adequate system that allows for such detailed analysis. The scatter of the data has to be low, the reaction solution has to stay homogeneous up to high degrees of monomer conversion, and the three conversion ranges, in which $\langle k_t \rangle$ is assumed to be controlled by segmental, translational, and reaction diffusion, have to be observed. Determination of the temperature dependence of the individual parameters $k_{t,SD}$, C_η , $k_{t,TD}^0$, and C_{RD} is even more challenging because the changes in $\langle k_t \rangle$ with temperature are usually rather small.

Investigations into the pressure dependence of chain-transfer reactions may be rewarding as well. They provide relevant information on the reaction mechanism as well as on the influence of chain transfer on SP–PLP–NIR results. As already done at ambient pressure,^[19,44,232] variation of the laser-pulse repetition rate in high-pressure PLP–SEC experiments may provide insight into the pressure dependence of chain-transfer reactions. Additionally, high-pressure SP–PLP–EPR experiments may be conducted. Among others, the Grampp group (Graz, Austria) and the Lorró group (Lausanne, Switzerland)^[289] developed a setup which allows for EPR measurements at high pressure. However, irradiation of the sample by a laser is difficult so far.

10.3 Monomers

Within the present work, propagation and termination rate coefficients of several prop-2-enamides were determined. They allow for modeling polymerization and for optimization of production processes. A detailed understanding of the magnitude of the rate coefficients as well as of the corresponding Arrhenius activation energies and volumes of activation is of particular interest. For this purpose, propagation and termination kinetics of *N*-methylprop-2-enamide may be studied. Additionally, kinetics could be investigated under variation of the length of the alkyl chains, which are joined to the α -carbon atom or the amide nitrogen atom. One of the industrially most important prop-2-enamides is *N*-(propan-2-yl)prop-2-enamide (*N*-isopropylacrylamide). Propagation

rate coefficients have already been determined but show significant scatter.^[37] Furthermore, activation energies of $\langle k_t \rangle$ of the polymerization of several monomers in aqueous solution may be determined.

Concerning sodium acrylate–1-vinylpyrrolidin-2-one copolymerization, the dependence of monomer reactivity ratios on pressure, temperature, overall monomer concentration, and monomer composition may be investigated. Determination of monomer reactivity ratios is usually made by assuming that they are independent of monomer composition although their definitions allow for a variation with composition. k_{11} and k_{22} may be determined by replacing one monomer at a time by its saturated (non-polymerizable) analogue. This is associated with the assumption that monomer and its saturated analogue influence the rate coefficient to the same extent. Such behavior has already been reported for MAA^[43] and VP^[45]. Moreover, copolymer-averaged effective propagation and termination rate coefficients may be determined. Of course, investigations into the polymerization kinetics of other comonomers in aqueous solution are of scientific and industrial interest as well. Acrylic acid^[290] and 1-vinylpyrrolidin-2-one^[291], for example, are widely used as comonomers with other monomers.

Acknowledgements

I would like to thank Prof. Dr. Michael Buback for giving me the opportunity to work on such an interesting topic and for his continuous support.

Thanks go to Prof. Dr. Philipp Vana for all the suggestions made and for being co-supervisor for my thesis.

I am indebted to Igor Lacík, DSc, and Marek Stach, PhD, (both Polymer Institute, Slovak Academy of Sciences, Bratislava, Slovak Republic) for fruitful cooperation, many discussions, providing insight into challenging SEC analyses, and determination of numerous SEC traces. Contributions of further coworkers at the Polymer Institute of the Slovak Academy of Sciences in Bratislava are also gratefully acknowledged.

Thanks owe to Prof. Robin A. Hutchinson (Department of Chemical Engineering, Queen's University, Kingston, Canada) for helpful discussions and introduction to the software package PREDICI®.

I am grateful to Lucia Učňová, PhD, (Institute of Chemical Sciences and Engineering, École Polytechnique Fédérale de Lausanne, Lausanne, Swiss Confederation) Anna Chovancová (Polymer Institute, Slovak Academy of Sciences, Bratislava, Slovak Republic), Sandhya Santana Krishnan, PhD, and Calista Preusser (both Department of Chemical Engineering, Queen's University, Kingston, Canada) for sharing results.

Thanks are given to Prof. Dr. Alex M. van Herk (Department of Chemical Engineering and Chemistry, Eindhoven, Netherlands) for providing the program Contour.

Gratitude is expressed to former and current members of the Buback and Vana workgroups for the nice working atmosphere as well as for suggestions and support. Special thanks go to Arne Wolpers, Hendrik Kattner, Hendrik Schröder, Dr. Johannes

Barth (BASF SE, Ludwigshafen, Federal Republic of Germany), Nicolai Sörensen, Nils Wittenberg, Sebastian Smolne, and Wibke Meiser for fruitful discussions, support, and pleasant conversations. I wish to thank Hendrik Schröder and Nils Wittenberg for proofreading the present thesis.

I would particularly like to thank Dr. Hans-Peter Vögele for his awareness of problems, constant willingness to discuss and solve problems, suggestions for improvement as well as maintenance and expeditious repair of the spectrometers. The assistance regarding the repair of the SP–PLP–NIR setup and the programming with Agilent VEE is also gratefully acknowledged.

Many thanks owe to Dr. Pascal Hesse (BASF SE, Ludwigshafen, Federal Republic of Germany) for discussions and introduction in experimental and theoretical basics.

I wish to thank Dr. Tatiana Sergeeva (Max Planck Institute for Biophysical Chemistry, Göttingen, Federal Republic of Germany) for discussions and support regarding improvement of experimental results of SP–PLP–NIR experiments.

I would like to thank Andreas Knorr, Annika von Roden, Hans-Joachim Schlette, Volker Meyer, and all other staff members of the electronic, glassblowing, and mechanical workshops for their mostly quick and scrupulous processing of production and repair orders. In this context, thanks go to Prof. Dr. Dirk Schwarzer, Prof. Dr. Hans-Jürgen Troe, and especially Reinhard Bürsing for repairing the lasers. I am particularly obliged to Andreas Knorr for his willingness to explain the basics of the electronic circuits of the SP–PLP–NIR setup and for his permanent readiness for troubleshooting.

Thanks are given to institute staff members Clemens Heymann, Marion Diegmann, Dr. Markus Hold, Michael Schlote, and Norbert Neisen for making work easier as well as Heike Rohmann, Ingrid Jünke, Sandra Lotze, Stefanie Kindler, Ute Friesen-Lippke, and Werner Noack for support and enjoyable hours.

I wish to thank Reinhard Machinek and other staff members of the NMR facility for NMR analysis and for discussions regarding required conditions.

Financial Support by the BASF SE and the Deutsche Forschungsgemeinschaft (German Research Foundation) within the framework of the European Graduate School 585 “Microstructural Control in Free-Radical Polymerization” is gratefully acknowledged. I am obliged to BASF members and former members of the European Graduate School for advices and suggestions.

I am indebted to my family for continuous support in moral and financial terms during my studies.

Finally, I would like to thank my friends for the distraction from work and the enjoyable time. Special thanks go to the “Master semester” for the pleasant admission to the circle of friends and the joint activities.

Appendix A: Experimental Data

A.1 Propagation Rate Coefficients

Propagation Rate Coefficients of 2-Methylprop-2-enamide

Table A.1: PLP conditions and propagation rate coefficients for the polymerization of 0.20 g·g⁻¹ MPAm in aqueous solution at 25 °C and ambient pressure. Data printed in red were, in contrast to the values printed in blue, determined after renewal of the SEC columns. Values printed in bold were obtained by means of the second POI of the MMD.

$C_{\text{Darocur}} /$ (mmol·L ⁻¹)	$\nu_{\text{LPRR}} /$ Hz	N_{p}	$\alpha \cdot 100$	$M_1 /$ (10 ³ g·mol ⁻¹)	M_1 / M_2	$k_{\text{p}} /$ (10 ³ L·mol ⁻¹ ·s ⁻¹)
3	60	300	0.62	0.99	0.57	2.11
3	60	300	0.62	0.99	0.57	2.08
3	50	300	0.71	1.05	0.52	2.02
3	50	300	0.71	1.04	0.51	2.04
3	50	600	1.46	1.06	0.52	2.14
3	50	600	1.46	1.07	0.52	2.16
3	40	300	0.73	1.00	0.41	1.96
3	40	300	0.73	1.01	0.42	1.94
3	40	600	0.92	1.14	0.46	1.84
3	30	300	0.35	1.54	0.50	1.86
3	30	300	0.35	1.56	0.50	1.88
3	30	600	1.30	1.42	0.44	1.72
3	30	600	1.30	1.44	0.44	1.74
3	20	300	1.06	2.02	0.46	1.63
3	20	300	1.06	2.00	0.45	1.61
3	20	600	0.53	2.05	0.47	1.65

Table A.1 (Continued)

$c_{\text{Darocur}} /$ (mmol·L ⁻¹)	$\nu_{\text{LPRR}} /$ Hz	N_{p}	$\alpha \cdot 100$	$M_1 /$ (10 ³ g·mol ⁻¹)	M_1 / M_2	$k_{\text{p}} /$ (10 ³ L·mol ⁻¹ ·s ⁻¹)
3	20	600	0.53	2.03	0.46	1.63
2	20	100	0.45	1.79	0.46	1.44
2	20	100	0.45	1.84	0.47	1.48
2	20	300	1.11	1.90	0.48	1.53
2	20	300	1.11	1.89	0.48	1.53
0.6	20	100	0.29	1.88	0.48	1.51
0.6	20	100	0.29	1.88	0.49	1.52
0.6	20	300	0.98	1.92	0.48	1.55
0.6	20	300	0.98	1.92	0.49	1.55
3	10	300	1.00	3.69	0.44	1.49
3	10	300	1.00	3.68	0.44	1.48
3	10	600	1.58	3.71	0.45	1.50
3	10	600	1.58	3.70	0.45	1.50
3	10	500	2.37	3.02	0.52	1.22
3	10	500	2.37	3.01	0.50	1.22
3	10	500	2.37	2.94	0.50	1.20
3	10	500	2.37	3.00	0.49	1.22
3	10	1000	4.16	3.05	0.52	1.25
3	10	1000	4.16	3.11	0.50	1.28
3	10	1000	4.16	3.05	0.52	1.25
3	10	1000	4.16	3.11	0.50	1.28
3	5	300	1.95	5.11	0.51	1.04
3	5	300	1.95	5.26	0.48	1.07
3	5	300	1.95	5.08	0.51	1.03

Table A.1 (Continued)

$c_{\text{Darocur}} /$ (mmol·L ⁻¹)	$\nu_{\text{LPRR}} /$ Hz	N_{p}	$\alpha \cdot 100$	$M_1 /$ (10 ³ g·mol ⁻¹)	M_1 / M_2	$k_{\text{p}} /$ (10 ³ L·mol ⁻¹ ·s ⁻¹)
3	5	300	1.95	5.27	0.48	1.07
3	5	1000	3.33	5.13	0.52	1.05
3	5	1000	3.33	5.31	0.49	1.08
3	5	1000	3.33	5.15	0.52	1.05
3	5	1000	3.33	5.28	0.49	1.08

Table A.2: PLP conditions and propagation rate coefficients for the polymerization of 0.20 g·g⁻¹ MPAm in aqueous solution at 40 °C, a laser-pulse repetition rate of 20 Hz, and $c_{\text{Darocur}} = 2 \text{ mmol}\cdot\text{L}^{-1}$. Values printed in bold were obtained by direct MMD determination. The corresponding data determined by poly(PAm)-relative calibration are marked by an asterisk.

p/bar	N_p	$\alpha\cdot 100$	$M_1/$ ($10^4 \text{ g}\cdot\text{mol}^{-1}$)	M_1/M_2	$k_p/$ ($10^3 \text{ L}\cdot\text{mol}^{-1}\cdot\text{s}^{-1}$)
1 000	800	4.04	4.52	<i>Sh</i>	3.58*
1 000	800	4.04	4.57	<i>Sh</i>	3.62
1 000	1 000	7.46	4.52	0.61	3.64*
1 000	1 000	7.46	3.97	0.50	3.20
1 500	600	5.70	5.81	0.59	4.56*
1 500	600	5.70	5.97	0.49	4.69
1 500	800	8.41	5.65	0.60	4.50*
1 500	800	8.41	5.38	0.52	4.29
2 000	400	6.99	6.50	0.60	5.06*
2 000	400	6.99	6.41	0.54	4.99
2 000	600	9.65	6.70	0.60	5.30*
2 000	600	9.65	7.66	0.57	6.05
2 000	300	5.24	10.13	0.48	7.81
2 000	300	5.24	10.12	0.48	7.81
2 000	600	6.78	10.41	0.49	8.10
2 000	600	6.78	10.39	0.49	8.07
2 000	600	6.78	10.04	0.49	7.81

Propagation Rate Coefficients of *N*,2-Dimethylprop-2-enamide

Table A.3: PLP conditions and propagation rate coefficients for the polymerization of M-MPAm in aqueous solution at ambient pressure, $\nu_{\text{LPRR}} = 20$ Hz and $\phi_{\text{DMPA}} = 1 \text{ mmol}\cdot\text{L}^{-1}$.

$w_{\text{M-MPAm}}/$ ($\text{g}\cdot\text{g}^{-1}$)	$\theta/$ $^{\circ}\text{C}$	N_{P}	$\alpha\cdot 100$	$M_1/$ ($10^4 \text{ g}\cdot\text{mol}^{-1}$)	M_1/M_2	$k_{\text{p}}/$ ($10^3 \text{ L}\cdot\text{mol}^{-1}\cdot\text{s}^{-1}$)
0.70	10	20	3.01	2.70	0.61	0.80
0.70	10	40	3.21	2.70	0.60	0.80
0.70	10	20	2.98	2.98	0.57	0.88
0.70	10	40	3.11	3.03	0.60	0.90
0.80	10	20	3.04	2.54	0.61	0.66
0.80	10	30	3.17	2.55	0.60	0.66
0.80	10	10	2.90	2.49	0.60	0.65
0.80	10	40	3.50	2.53	0.59	0.66
0.80	10	20	2.98	2.88	0.52	0.75
0.70	40	15	2.95	5.12	0.60	1.52
0.70	40	15	2.95	5.10	0.59	1.51
0.70	40	15	2.95	5.24	0.60	1.55
0.70	40	30	3.05	5.15	0.60	1.53
0.70	40	30	3.05	5.16	0.61	1.53
0.70	40	30	3.05	5.18	0.61	1.54
0.80	40	15	2.83	4.33	0.56	1.13
0.80	40	15	2.83	4.39	0.58	1.14
0.80	40	30	2.99	4.40	0.57	1.15
0.80	40	30	2.99	4.44	0.57	1.16
0.80	40	30	2.99	4.49	0.57	1.17

Table A.3 (Continued)

$w_{\text{M-MPAm}} /$ ($\text{g} \cdot \text{g}^{-1}$)	$\theta /$ $^{\circ} \text{C}$	N_{p}	$\alpha \cdot 100$	$M_1 /$ ($10^4 \text{ g} \cdot \text{mol}^{-1}$)	M_1 / M_2	$k_{\text{p}} /$ ($10^3 \text{ L} \cdot \text{mol}^{-1} \cdot \text{s}^{-1}$)
0.70	60	15	2.78	6.40	0.52	1.90
0.70	60	15	2.78	6.43	0.49	1.91
0.70	60	15	2.78	6.62	0.55	1.97
0.70	60	30	3.10	6.27	0.53	1.86
0.70	60	30	3.10	6.29	0.53	1.87
0.80	60	15	2.81	6.73	0.58	1.75
0.80	60	15	2.81	6.71	0.57	1.75
0.80	60	30	3.32	6.69	0.58	1.75
0.80	60	30	3.32	6.73	0.59	1.76
0.70	80	15	2.99	9.90	0.67	2.94
0.70	80	15	2.99	8.58	0.60	2.55
0.70	80	30	3.17	8.82	0.54	2.62
0.70	80	30	3.17	8.75	0.54	2.60
0.80	80	15	2.85	8.40	0.52	2.19
0.80	80	15	2.85	8.30	0.50	2.16
0.80	80	15	2.85	8.22	0.49	2.14
0.80	80	30	3.00	8.53	0.52	2.22
0.80	80	30	3.00	8.58	0.53	2.23
0.80	80	30	3.00	8.55	0.53	2.23

Propagation Rate Coefficients of *N,N*-Dimethylprop-2-enamide**Table A.4:** PLP conditions and propagation rate coefficients for the polymerization of DM-PAm in aqueous solution at ambient pressure and $\nu_{\text{LPRR}} = 100$ Hz.

$w_{\text{DM-PAm}} /$ (g·g ⁻¹)	$\theta /$ °C	$c_{\text{DMPA}} /$ (mmol·L ⁻¹)	N_{p}	$\alpha \cdot 100$	$M_1 /$ (10 ⁴ g·mol ⁻¹)	M_1 / M_2	$k_{\text{p}} /$ (10 ⁴ L·mol ⁻¹ ·s ⁻¹)
0.15	10	0.02	30	4.22	4.83	0.50	3.19
0.15	10	0.02	30	4.22	4.76	0.51	3.14
0.15	10	0.02	50	5.55	5.19	0.51	3.45
0.15	10	0.02	50	5.55	4.57	0.46	3.04
0.15	10	0.06	30	4.03	4.79	0.50	3.26
0.15	10	0.06	30	4.03	4.78	0.49	3.25
0.15	10	0.06	50	3.15	4.96	0.50	3.36
0.15	10	0.06	50	3.15	4.98	0.51	3.37
0.20	10	1	10	3.40	6.12	0.53	3.53
0.20	10	1	20	3.33	6.30	0.52	3.23
0.20	10	1	20	3.33	6.62	0.52	3.39
0.30	10	0.02	30	4.01	7.76	0.49	2.66
0.30	10	0.02	30	4.01	7.25	0.45	2.49
0.30	10	0.02	50	5.24	7.37	0.45	2.55
0.30	10	0.02	50	5.24	7.64	0.45	2.64
0.30	10	0.06	30	4.65	7.09	0.48	2.44
0.30	10	0.06	30	4.65	7.29	0.49	2.51
0.30	10	0.06	50	5.91	7.25	0.47	2.51
0.30	10	0.06	50	5.91	7.42	0.50	2.57

Table A.4 (Continued)

$w_{\text{DM-PAm}} /$ (g·g ⁻¹)	$\theta /$ °C	$c_{\text{DMPA}} /$ (mmol·L ⁻¹)	N_{p}	$\alpha \cdot 100$	$M_1 /$ (10 ⁴ g·mol ⁻¹)	M_1 / M_2	$k_{\text{p}} /$ (10 ⁴ L·mol ⁻¹ ·s ⁻¹)
0.80	10	1	10	2.46	11.10	0.46	1.45
0.80	10	1	10	2.46	11.15	0.46	1.46
0.80	10	1	30	4.73	11.94	0.44	1.58
0.80	10	1	30	4.73	12.03	0.45	1.59
1.00	10	1	10	0.45	7.58	0.47	0.79
1.00	10	1	10	0.45	7.36	0.47	0.77
1.00	10	1	30	0.83	7.38	0.46	0.77
1.00	10	1	30	0.83	7.39	0.46	0.77
0.20	40	1	10	1.87	11.56	0.42	5.88
0.20	40	1	10	1.87	11.75	0.42	5.97
0.20	40	1	15	4.05	11.53	0.44	5.93
0.20	40	1	15	4.05	11.53	0.44	5.93
0.80	40	1	10	0.75	20.40	0.34	2.64
0.80	40	1	10	0.75	20.29	0.34	2.63
0.80	40	1	30	4.87	23.67	0.36	3.13
0.80	40	1	30	4.87	23.32	0.35	3.08
1.00	40	1	10	0.74	14.27	0.35	1.49
1.00	40	1	10	0.74	14.31	<i>Sh</i>	1.49
1.00	40	1	30	1.45	14.82	<i>Sh</i>	1.55
1.00	40	1	30	1.45	14.80	0.36	1.55

Table A.4 (Continued)

$w_{\text{DM-PAm}}/$ ($\text{g}\cdot\text{g}^{-1}$)	$\theta/$ $^{\circ}\text{C}$	$c_{\text{DMPA}}/$ ($\text{mmol}\cdot\text{L}^{-1}$)	N_{p}	$\alpha\cdot 100$	$M_1/$ ($10^4 \text{ g}\cdot\text{mol}^{-1}$)	M_1/M_2	$k_{\text{p}}/$ ($10^4 \text{ L}\cdot\text{mol}^{-1}\cdot\text{s}^{-1}$)
0.20	60	1	5	2.70	15.10	<i>Sh</i>	7.75
0.20	60	1	5	2.70	15.07	<i>Sh</i>	7.74
0.20	60	1	10	4.12	14.92	0.38	7.72
0.20	60	1	10	4.12	14.87	0.36	7.69
0.80	60	1	10	2.02	25.06	0.30	3.27
0.80	60	1	10	2.02	24.51	0.29	3.20
1.00	60	1	10	0.81	18.91	<i>Sh</i>	1.97
1.00	60	1	10	0.81	19.39	<i>Sh</i>	2.02
0.20	80	1	10	4.46	17.85	<i>Sh</i>	9.25
0.20	80	1	10	4.46	18.16	<i>Sh</i>	9.41
0.80	80	1	30	5.40	15.37	<i>Sh</i>	2.04
1.00	80	1	10	1.41	11.80	<i>Sh</i>	1.24
1.00	80	1	10	1.41	9.89	<i>Sh</i>	1.04
1.00	80	1	30	2.99	8.30	<i>Sh</i>	0.88
1.00	80	1	30	2.99	9.55	<i>Sh</i>	1.01

Table A.5: PLP conditions and propagation rate coefficients for the polymerization of DM-PAm in aqueous solution at 40 $^{\circ}\text{C}$, $c_{\text{DMPA}} = 2 \text{ mmol}\cdot\text{L}^{-1}$, and $\nu_{\text{LPRR}} = 100 \text{ Hz}$.

$w_{\text{DM-PAm}}/$ ($\text{g}\cdot\text{g}^{-1}$)	$p/$ bar	N_{p}	$\alpha\cdot 100$	$M_1/$ ($10^5 \text{ g}\cdot\text{mol}^{-1}$)	M_1/M_2	$k_{\text{p}}/$ ($10^4 \text{ L}\cdot\text{mol}^{-1}\cdot\text{s}^{-1}$)
0.20	500	25	5.65	1.70	0.44	8.38
0.20	500	40	12.45	1.57	0.40	8.05
0.20	500	60	15.72	1.52	0.39	7.93

Table A.5 (Continued)

$w_{\text{DM-PAm}}/$ ($\text{g}\cdot\text{g}^{-1}$)	$p/$ bar	N_{p}	$\alpha\cdot 100$	$M_1/$ ($10^5 \text{ g}\cdot\text{mol}^{-1}$)	M_1/M_2	$k_{\text{p}}/$ ($10^4 \text{ L}\cdot\text{mol}^{-1}\cdot\text{s}^{-1}$)
0.60	500	15	4.38	3.08	0.41	5.24
0.60	500	25	9.20	2.96	0.39	5.16
0.60	500	40	13.70	2.96	0.36	5.29
0.60	500	60	17.37	2.79	0.35	5.08
1.00	500	40	3.31	2.13	<i>Sh</i>	2.25
1.00	500	60	4.48	2.15	<i>Sh</i>	2.28
0.20	1000	25	9.59	1.98	0.42	10.22
0.20	1000	25	9.59	1.88	0.40	9.72
1.00	1000	15	0.90	2.88	<i>Sh</i>	3.00
1.00	1000	15	0.90	2.94	0.25	3.07
1.00	1000	25	1.85	2.71	<i>Sh</i>	2.84
1.00	1000	25	1.85	2.69	0.26	2.82
0.20	1500	25	10.91	2.18	0.39	11.17
0.20	1500	25	10.91	2.17	0.38	11.15
1.00	1500	15	3.01	2.96	0.23	3.13
1.00	1500	15	0.94	3.49	0.26	3.65
1.00	1500	25	2.47	3.32	<i>Sh</i>	3.49
1.00	1500	25	2.47	3.53	<i>Sh</i>	3.72
0.20	2000	20	2.97	3.49	0.47	16.94
1.00	2000	5	0.65	3.96	<i>Sh</i>	4.13
1.00	2000	7	1.34	3.90	0.44	4.08
1.00	2000	7	1.34	3.88	0.42	4.06
1.00	2000	20	0.11	3.44	0.15	3.58
1.00	2000	20	0.11	3.76	0.19	3.91

Propagation Rate Coefficients of Prop-2-enamide

Table A.6: PLP conditions and propagation rate coefficients for the polymerization of 0.20 g·g⁻¹ PAm in aqueous solution at 40 °C, $\nu_{\text{LPRR}} = 150$ Hz, and $\phi_{\text{DMPA}} = 2$ mmol·L⁻¹.

p/bar	N_p	$\alpha \cdot 100$	$M_1/$ (10 ⁵ g·mol ⁻¹)	M_1/M_2	$k_p/$ (10 ⁴ L·mol ⁻¹ ·s ⁻¹)
500	60	9.80	1.07	<i>Sh</i>	7.55
500	60	9.80	1.06	<i>Sh</i>	7.46
500	60	8.20	1.08	<i>Sh</i>	7.55
500	60	8.20	1.06	0.39	7.44
1000	30	4.47	1.42	0.37	9.41
1000	30	4.47	1.42	0.36	9.41
1000	55	9.30	1.37	0.36	9.32
1000	55	9.30	1.43	0.37	9.72
1500	30	7.99	1.73	0.37	11.70
1500	30	7.99	1.79	0.38	12.09
1500	25	6.36	1.70	0.35	11.39
1500	25	6.36	1.72	0.34	11.49
2000	40	6.98	2.52	<i>Sh</i>	16.61
2000	40	6.98	2.57	<i>Sh</i>	16.97

A.2 Termination Rate Coefficients

Termination Rate Coefficients of 1-Vinylpyrrolidin-2-one

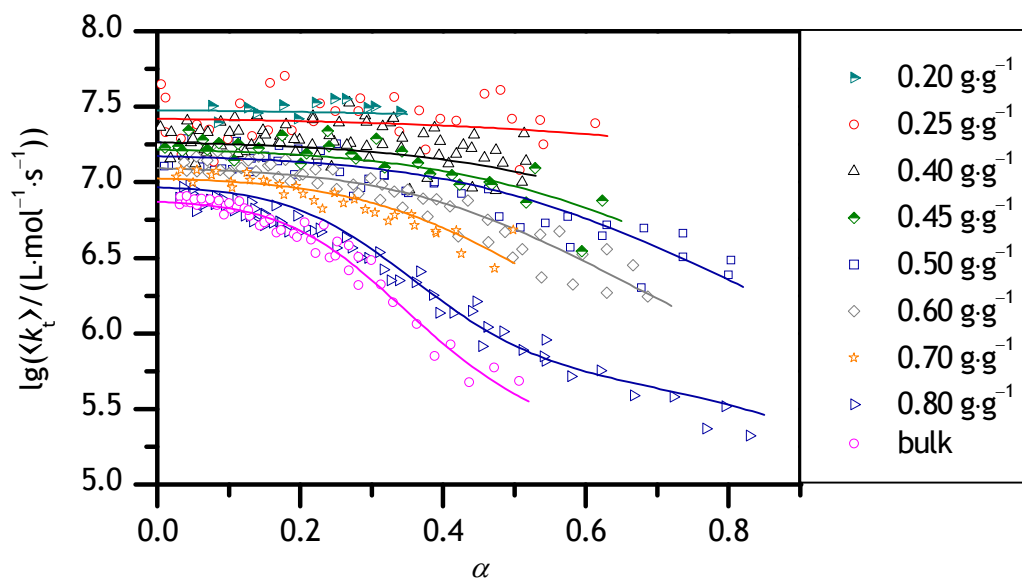


Figure A.1: Dependence of the chain-length-averaged termination rate coefficient, $\langle k_t \rangle$, on the degree of monomer conversion, α , for VP polymerizations at 40 °C and 2000 bar for various initial monomer contents of VP. The lines are fits of equation 6.5 to the experimental data according to method A. The associated fit parameters are listed in table 6.1. For initial monomer mass fractions of 0.40 g·g⁻¹ and below, the parameters were determined via equations 6.6, 6.7, 6.8, and 6.9.

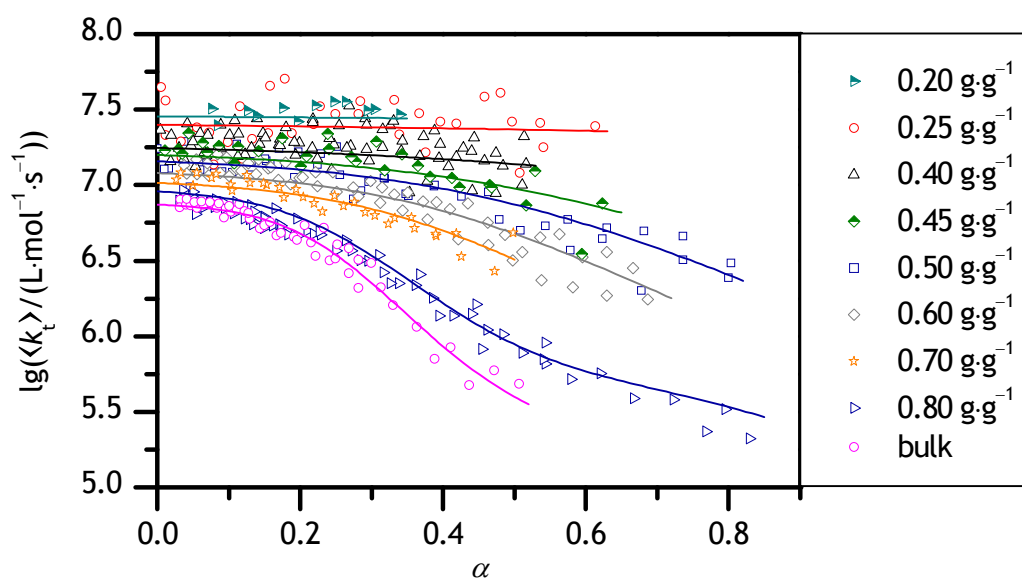


Figure A.2: Dependence of the chain-length-averaged termination rate coefficient, $\langle k_t \rangle$, on the degree of monomer conversion, α , for VP polymerizations at 40 °C and 2000 bar for various initial monomer concentrations. The lines are fits of equation 6.5 to the experimental data with the parameters listed in table 6.2 corresponding to method B. For initial monomer mass fractions of 0.40 g·g⁻¹ and below, the parameters were determined via equations 6.6, 6.7, 6.11, and 6.12.

Table A.7: Termination rate coefficients for VP polymerization at 40 °C and 2000 bar for an initial monomer mass fraction of 0.25 g·g⁻¹.

α	$\lg(\langle k_t \rangle / \text{L} \cdot \text{mol}^{-1} \cdot \text{s}^{-1})$
0.005	7.65
0.012	7.33
0.012	7.56
0.033	7.29
0.034	7.18
0.056	7.38
0.056	7.36
0.073	7.35
0.079	7.14
0.099	7.28
0.116	7.52
0.120	7.18
0.132	7.30
0.156	7.35
0.158	7.66
0.178	7.70
0.189	7.35
0.219	7.40
0.228	7.52
0.250	7.47
0.281	7.47
0.284	7.56
0.331	7.56

Table A.7 (Continued)

α	$\lg(\langle k_t \rangle / \text{L} \cdot \text{mol}^{-1} \cdot \text{s}^{-1})$
0.339	7.33
0.366	7.47
0.376	7.22
0.396	7.42
0.419	7.41
0.458	7.58
0.481	7.61
0.496	7.42
0.507	7.08
0.536	7.41
0.541	7.25
0.613	7.39

Table A.8: Termination rate coefficients for VP polymerization at 40 °C and 2000 bar for an initial monomer mass fraction of 0.40 g·g⁻¹.

α	$\lg(\langle k_t \rangle / \text{L} \cdot \text{mol}^{-1} \cdot \text{s}^{-1})$
0.004	7.37
0.019	7.16
0.019	7.33
0.038	7.17
0.054	7.12
0.069	7.20
0.082	7.23
0.101	7.33
0.113	7.19
0.123	7.20
0.143	7.27
0.148	7.34
0.170	7.27
0.172	7.31
0.194	7.20
0.199	7.28
0.217	7.44
0.224	7.17
0.244	7.10
0.248	7.27
0.269	7.53
0.271	7.26
0.293	7.24

Table A.8 (Continued)

α	$\lg(\langle k_t \rangle / \text{L} \cdot \text{mol}^{-1} \cdot \text{s}^{-1})$
0.297	7.16
0.316	7.25
0.326	7.40
0.342	7.23
0.353	6.95
0.368	7.19
0.378	7.03
0.395	7.18
0.408	7.12
0.428	7.24
0.441	6.96
0.458	7.16
0.475	6.95
0.484	7.13
0.511	7.00
0.514	7.32

Table A.9: Termination rate coefficients for VP polymerization at 40 °C and 2000 bar for an initial monomer mass fraction of 0.45 g·g⁻¹.

α	$\lg(\langle k_t \rangle / \text{L} \cdot \text{mol}^{-1} \cdot \text{s}^{-1})$
0.011	7.23
0.030	7.24
0.035	7.21
0.044	7.35
0.063	7.28
0.070	7.22
0.086	7.26
0.108	7.15
0.113	7.25
0.142	7.22
0.175	7.31
0.201	7.12
0.209	7.19
0.238	7.34
0.240	7.24
0.271	7.19
0.278	7.16
0.307	7.29
0.319	7.10
0.342	7.20
0.365	7.13
0.382	7.06
0.412	7.05

Table A.9 (Continued)

α	$\lg(\langle k_t \rangle / \text{L} \cdot \text{mol}^{-1} \cdot \text{s}^{-1})$
0.423	6.98
0.465	7.00
0.468	6.98
0.516	6.87
0.529	7.09
0.594	6.55
0.623	6.88

Table A.10: Termination rate coefficients for VP polymerization at 40 °C and 2000 bar for an initial monomer mass fraction of 0.50 g·g⁻¹.

α	$\lg(\langle k_t \rangle / \text{L} \cdot \text{mol}^{-1} \cdot \text{s}^{-1})$
0.000	7.24
0.010	7.11
0.016	7.11
0.038	7.29
0.046	6.99
0.060	7.10
0.069	7.15
0.080	7.08
0.091	7.09
0.105	7.09
0.111	7.27
0.129	7.07
0.132	7.16
0.151	7.17
0.152	7.16
0.169	7.14
0.170	7.24
0.192	7.05
0.198	7.22
0.224	7.13
0.228	7.21
0.251	7.26
0.256	7.07

Table A.10 (Continued)

α	$\lg(\langle k_t \rangle / \text{L} \cdot \text{mol}^{-1} \cdot \text{s}^{-1})$
0.275	6.91
0.285	6.96
0.296	7.02
0.317	7.05
0.318	7.04
0.348	6.94
0.352	6.93
0.387	6.99
0.388	7.00
0.425	6.93
0.463	6.96
0.479	6.77
0.508	6.70
0.544	6.73
0.574	6.77
0.578	6.57
0.623	6.65
0.630	6.72
0.678	6.30
0.681	6.70
0.736	6.51
0.736	6.66
0.800	6.39
0.803	6.49

Table A.11: Termination rate coefficients for VP polymerization at 40 °C and 2000 bar for an initial monomer mass fraction of 0.70 g·g⁻¹.

α	$\lg(\langle k_t \rangle / \text{L} \cdot \text{mol}^{-1} \cdot \text{s}^{-1})$
0.027	7.03
0.050	7.00
0.076	7.05
0.103	7.00
0.130	7.01
0.153	7.00
0.178	6.92
0.205	6.92
0.232	6.83
0.261	6.86
0.292	6.82
0.323	6.74
0.356	6.78
0.391	6.66
0.426	6.53
0.033	7.08
0.056	7.08
0.082	7.07
0.105	6.96
0.126	7.07
0.149	7.01
0.171	6.98
0.195	6.97

Table A.11 (Continued)

α	$\lg(\langle k_t \rangle / \text{L} \cdot \text{mol}^{-1} \cdot \text{s}^{-1})$
0.220	6.88
0.248	6.93
0.276	6.89
0.305	6.80
0.333	6.78
0.360	6.71
0.390	6.68
0.419	6.68
0.473	6.43
0.499	6.68

Table A.12: Termination rate coefficients for VP polymerization at 40 °C and 2000 bar for an initial monomer mass fraction of 0.80 g·g⁻¹.

α	$\lg(\langle k_t \rangle / \text{L} \cdot \text{mol}^{-1} \cdot \text{s}^{-1})$
0.050	6.96
0.063	6.88
0.081	6.90
0.110	6.89
0.129	6.77
0.133	6.74
0.135	6.82
0.150	6.78
0.165	6.84
0.173	6.73
0.195	6.78
0.219	6.68
0.227	6.69
0.264	6.63
0.284	6.50
0.310	6.54
0.326	6.35
0.368	6.41
0.395	6.13
0.446	6.21
0.455	5.91
0.541	5.85
0.544	5.96

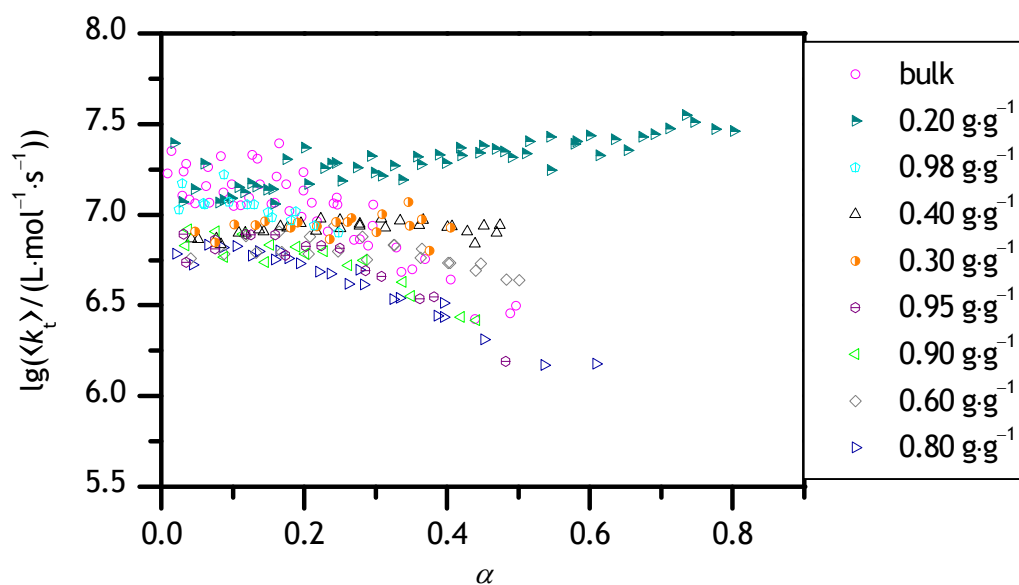
Termination Rate Coefficients of *N,N*-Dimethylprop-2-enamide

Figure A.3: Conversion dependence of the chain-length-averaged termination rate coefficient, $\langle k_t \rangle$, for DM-PAm polymerizations at 40 °C and 2000 bar for various initial monomer contents.

Table A.13: Termination rate coefficients for DM-PAm polymerization at 40 °C and 2000 bar for an initial monomer mass fraction of 0.30 g·g⁻¹.

α	$\lg(\langle k_t \rangle / \text{L} \cdot \text{mol}^{-1} \cdot \text{s}^{-1})$
0.048	6.91
0.075	6.85
0.102	6.95
0.132	6.94
0.145	6.96
0.181	6.93
0.191	6.96
0.218	6.93
0.236	6.87
0.245	6.96
0.261	6.96
0.267	6.98
0.301	6.90
0.309	7.00
0.346	7.07
0.348	6.94
0.365	6.98
0.376	6.80
0.405	6.93

Table A.14: Termination rate coefficients for DM-PAm polymerization at 40 °C and 2000 bar for an initial monomer mass fraction of 0.98 g·g⁻¹.

α	$\lg(\langle k_t \rangle / \text{L} \cdot \text{mol}^{-1} \cdot \text{s}^{-1})$
0.025	7.03
0.030	7.17
0.060	7.06
0.061	7.06
0.088	7.22
0.095	7.07
0.120	7.05
0.130	7.06
0.150	7.01
0.155	6.98
0.182	6.97
0.188	7.02
0.214	6.94
0.249	6.90

Table A.15: Termination rate coefficients for DM-PAm bulk polymerization at 40 °C and 2000 bar.

α	$\lg(\langle k_t \rangle / \text{L} \cdot \text{mol}^{-1} \cdot \text{s}^{-1})$
0.039	7.08
0.067	7.06
0.111	7.05
0.154	7.06
0.180	7.02
0.218	6.96
0.269	6.86
0.329	6.82
0.405	6.64
0.497	6.50

Termination Rate Coefficients of Prop-2-enamide

Table A.16: Termination rate coefficients for PAm polymerization at 40 °C and 2000 bar for an initial monomer mass fraction of 0.20 g·g⁻¹.

α	$\lg(\langle k_t \rangle / \text{L} \cdot \text{mol}^{-1} \cdot \text{s}^{-1})$
0.136	7.58
0.139	7.83
0.182	7.54
0.220	7.67
0.245	7.59
0.267	7.76
0.289	7.40

Table A.17: Termination rate coefficients for PAm polymerization at 40 °C and 2000 bar for an initial monomer mass fraction of 0.40 g·g⁻¹.

α	$\lg(\langle k_t \rangle / \text{L} \cdot \text{mol}^{-1} \cdot \text{s}^{-1})$
0.037	7.62
0.064	7.58
0.068	7.55
0.093	7.52
0.106	7.48
0.142	7.57

Table A.18: Termination rate coefficients for PAm polymerization at 40 °C and 2000 bar for an initial monomer mass fraction of 0.30 g·g⁻¹.

α	$\lg(\langle k_t \rangle / \text{L} \cdot \text{mol}^{-1} \cdot \text{s}^{-1})$
0.023	7.86
0.061	7.69
0.073	7.58
0.085	7.55
0.111	7.75
0.119	7.53
0.133	7.61
0.153	7.81
0.161	7.49
0.175	7.63
0.197	7.40
0.198	7.39
0.218	7.38
0.228	7.40
0.237	7.57
0.266	7.37

Table A.19: Termination rate coefficients for PAm polymerization at 40 °C and 2000 bar for an initial monomer mass fraction of 0.50 g·g⁻¹.

α	$\lg(\langle k_t \rangle / \text{L} \cdot \text{mol}^{-1} \cdot \text{s}^{-1})$
0.012	7.60
0.034	7.50
0.067	7.41
0.080	7.55
0.107	7.44

Table A.20: Termination rate coefficients for PAm polymerization at 40 °C and 1500 bar for an initial monomer mass fraction of 0.40 g·g⁻¹.

α	$\lg(\langle k_t \rangle / \text{L} \cdot \text{mol}^{-1} \cdot \text{s}^{-1})$
0.025	7.71
0.035	7.74
0.043	7.76
0.067	7.57
0.074	7.88
0.105	7.54
0.109	7.70
0.141	7.60
0.147	7.48

Table A.21: Termination rate coefficients for PAm polymerization at 40 °C and 1000 bar for an initial monomer mass fraction of 0.40 g·g⁻¹.

α	$\lg(\langle k_t \rangle / \text{L} \cdot \text{mol}^{-1} \cdot \text{s}^{-1})$
0.019	7.91
0.027	7.86
0.037	8.02
0.046	7.87
0.060	7.88
0.070	7.85
0.085	7.87
0.099	7.78
0.112	7.75
0.128	7.82
0.142	7.67
0.159	7.73
0.175	7.58

Table A.22: Termination rate coefficients for PAm polymerization at 40 °C and 500 bar for an initial monomer mass fraction of 0.40 g·g⁻¹.

α	$\lg(\langle k_t \rangle / \text{L} \cdot \text{mol}^{-1} \cdot \text{s}^{-1})$
0.022	8.11
0.032	7.98
0.061	8.05
0.062	8.03
0.092	8.02
0.099	7.71
0.129	7.88
0.143	7.71

A.3 Densities and Viscosities

Table A.23: Densities, kinematic viscosities, and dynamic viscosities of VP–H₂O mixtures at various monomer mass fractions, 40 °C, and ambient pressure.

$w_{\text{VP}}^0 / (\text{g} \cdot \text{g}^{-1})$	$\rho^0 / (\text{g} \cdot \text{cm}^{-3})$	$\nu^0 / (\text{mm}^2 \cdot \text{s}^{-1})$	$\eta^0 / (\text{mPa} \cdot \text{s})$
0.00	0.9922	0.649	0.644
0.10	0.9992	0.798	0.797
0.20	1.0051	0.975	0.979
0.30	1.0106	1.191	1.204
0.40	1.0160	1.424	1.447
0.50	1.0203	1.668	1.702
0.60	1.0248	1.897	1.944
0.70	1.0268	1.999	2.053
0.80	1.0283	2.032	2.089
0.90	1.0277	1.850	1.901
1.00	1.0244	1.502	1.539

Table A.24: Densities, kinematic viscosities, and dynamic viscosities of DM-PAm–H₂O mixtures at various monomer mass fractions, 40 °C, and ambient pressure.

$w_{\text{DM-PAm}}^0 / (\text{g} \cdot \text{g}^{-1})$	$\rho^0 / (\text{g} \cdot \text{cm}^{-3})$	$\nu^0 / (\text{mm}^2 \cdot \text{s}^{-1})$	$\eta^0 / (\text{mPa} \cdot \text{s})$
0.00	0.9922	0.649	0.644
0.20	0.9928	1.065	1.057
0.30	0.9931	1.329	1.320
0.40	0.9930	1.603	1.592
0.60	0.9898	2.094	2.072
0.80	0.9765	1.957	1.911
0.90	0.9632	1.458	1.404
0.95	0.9576	1.169	1.119
0.98	0.9517	1.019	0.970
1.00	0.9476	0.918	0.870

A.4 Analysis of ¹H NMR Spectra

¹H NMR Spectrum Shown in Figure 9.1

¹H NMR (300 MHz, D₂O, 35 °C): δ/ppm = 9.65 (q, J = 2.6 Hz, acetaldehyde-CH), 6.94 (dd, J = 15.9 Hz, J = 9.1 Hz, α'), 6.40 (d, J = 17.2 Hz, *trans*), 6.16 (dd, J = 17.3 Hz, J = 10.7 Hz, α), 5.98 (d, J = 10.5 Hz, *cis*), 5.59 (q, J = 6.1 Hz, α''), 4.73–4.60 (m, *cis'*, *trans'*), 3.65–3.36 (m, 5', 5''), 2.57–2.29 (m, 3', 3''), 2.22 (d, J = 3.1 Hz, acetaldehyde-CH₃), 2.15–1.94 (m, 4', 4''), 1.35 (d, J = 6.4 Hz, β'').

¹H NMR Spectrum Shown in Figure 9.2

¹H NMR (300 MHz, D₂O, 35 °C): δ/ppm = 6.95 (dd, J = 15.9 Hz, J = 9.1 Hz, α'), 6.13 (dd, J = 17.4 Hz, J = 10.0 Hz, α), 6.00 (d, J = 17.0 Hz, *trans*), 5.63 (d, J = 9.9 Hz, *cis*), 4.73–4.60 (m, *cis'*, *trans'*), 3.62 (t, J = 7.3 Hz, 5'), 2.54 (t, J = 8.1 Hz, 3'), 2.18–2.04 (m, 4').

A.5 Copolymer Composition

Table A.25: Copolymer composition, associated uncertainty ascribable to NMR analysis, and laser-pulse repetition rate used for PLP of VP and NaA at various monomer compositions, 25 °C, and a total monomer mole fraction of 0.05 mol·mol⁻¹.

$f_{VP}/(\text{mol}\cdot\text{mol}^{-1})$	$F_{VP}/(\text{mol}\cdot\text{mol}^{-1})$	$\Delta F_{VP}/(\text{mol}\cdot\text{mol}^{-1})$	ν_{LPRR}/Hz
0.10	0.040	0.008	100
0.10	0.054	0.002	400
0.20	0.010	0.005	100
0.20	0.067	0.003	400
0.30	0.133	0.010	100
0.30	0.097	0.010	400
0.40	0.154	0.002	80
0.40	0.131	0.006	400
0.50	0.165	0.015	70
0.50	0.103	0.003	200
0.60	0.218	0.080	60
0.60	0.167	0.002	200
0.70	0.269	0.040	50
0.70	0.206	0.030	200
0.80	0.309	0.125	40
0.80	0.410	0.035	100
0.90	0.650	0.040	50

Appendix B: C++ Source Codes

The following C++ source codes were written based on the source codes developed by Feldermann.^[208]

B.1 Script for the Calibration of the Laser and the UV Diode

Calibration.cpp

```
1  /* Script for the calibration of the charging voltage of the
2  Lextra 50 UV laser and a UV diode mounted in front of the
3  measuring cell with a joulemeter (Gentec, ED-200). The laser pulse
4  energy can be plotted as a function of the charging voltage or of
5  the voltage at the UV diode. A straight line may be fitted to
6  these data. Thereby the chosen charging voltage allows for a rough
7  estimate of the applied pulse energy whereas the exact pulse
8  energy can be calculated by means of the voltage at the UV diode.
9  Effective January 2012. */
10
11 // The following standard files are included
12 #include <iostream>
13 #include <fstream>
14 #include <conio.h>
15 #include "../..../cbw.h"
16
17 using namespace std;
18
19 // Declaration of global variables
20 float voltage;
21 char path[100];
```

```
22 int Channel;
23 int BoardNum = 0;
24 int ULStat = 0;
25
26 // Function for the provision of a file for the data
27 void input() {
28
29     // Declaration of local variables
30     char name[100];
31     char date[100];
32     char dir[100];
33
34     // Reading in the path and the name of the file
35     cout << "Enter user name" << endl;
36     cin >> name;
37     strcpy_s (dir, "\\benutzer\\");
38     strcat_s (dir, name);
39     strcat_s (dir, "\\Eichung\\");
40     cout << "Enter date" << endl;
41     cin >> date;
42
43     // Provision of the folder for the file to be saved in
44     _makepath_s(path, "d", dir, date , ".txt");
45
46 }
47
48 /* Function for reading in the voltage at channels 0
49 (Gentec detector) or 1 (UV diode)*/
50 void import() {
51
52     /* Declaration of local variables
```



```
53     "Range" characterizes the voltage input range (BIP10VOLTS
54     stands for the bipolar voltage range of -10 - +10 V)
55     "DataValue" is the digital value collected from "Channel" */
56     int Range = BIP10VOLTS;
57     unsigned short int DataValue = 0;
58
59     ULStat = cbAIn (BoardNum, Channel, Range, &DataValue);
60     ULStat = cbToEngUnits (BoardNum, Range, DataValue, &voltage);
61
62 }
63
64 // Main function
65 void main() {
66
67     input();
68
69     // Declaration of local variables
70     int n;
71     int j;
72     float UVd;
73     float UVl;
74     float Gentec;
75
76     cout << "Enter number of laser pulses" << endl;
77     cin >> n;
78
79     // Declaration of local variables
80     float RevLevel = (float)CURRENTREVNUM;
81
82     // Declaration of the revision level of the Universal Library
83     ULStat = cbDeclareRevision(&RevLevel);
```

```
84
85     /* Initiate error handling with the parameters
86     "PRINTALL" (all warnings and errors encountered will be
87     printed) and "STOPALL" (if any error is encountered,
88     the program will stop) */
89     cbErrHandling (PRINTALL, STOPALL);
90
91     // Configuration of port B as digital output
92     int PortNum, Direction;
93     PortNum = FIRSTPORTB;
94     Direction = DIGITALOUT;
95     ULStat = cbDConfigPort (BoardNum, PortNum, Direction);
96
97     // Writing header in path
98     ofstream Outfile (path);
99     Outfile << "PulseIndex  Voltage/V          Energy/mJ" << endl;
100
101     /* Beginning of the loop consisting of measurement
102     and data storage */
103     for (j = 1; j<n+1; j++) {
104
105         // Open UV iris diaphragm, and activate UV diode
106         ULStat = cbDOut(BoardNum, PortNum, 10);
107         Sleep (500);
108
109         /* Read voltage of the UV diode at channel 1
110         before triggering the laser */
111         Channel = 1;
112         import();
113         UVd = voltage;
114
```

```
115         // Reset of the UV diode
116         ULStat = cbDOut(BoardNum, PortNum, 8);
117         Sleep (200);
118
119         /* Activate UV diode, arm laser, i.e. set bit 0 to 1;
120         laser triggers at transition 1 to 0 */
121         ULStat = cbDOut(BoardNum, PortNum, 11);
122         Sleep (200);
123
124         // Triggering the laser
125         ULStat = cbDOut(BoardNum, PortNum, 10);
126         Sleep (10);
127
128         /* Reading channel 0 (Gentec) and channel 1 (UV diode)
129         while triggering the laser */
130         Channel = 0;
131         import();
132         Gentec = voltage;
133         Channel = 1;
134         import();
135         UV1 = voltage;
136
137         // Reset of UV diode
138         ULStat = cbDOut(BoardNum, PortNum, 8);
139         Sleep (200);
140
141         float difference = UV1 - UVd;
142
143         // Write data in file
144         Outfile << j;
145         Outfile << "          " << difference;
```

```
146         Outfile << "      " << Gentec << endl;
147
148         /* Print number of the laser pulse as well as the
149         signal intensities (voltage) of the Gentec and the
150         UV diode on the screen */
151         cout << "\nIndex of the pulse: ";
152         cout << j;
153         cout << "\nEnergy at the Gentec detector: ";
154         cout << Gentec << " mJ";
155         cout << "\nVoltage at the UV diode in V: ";
156         cout << difference << " V\n";
157
158     }
159
160     Outfile.close();
161
162     // Close UV iris diaphragm
163     ULStat = cbDOut(BoardNum, PortNum, 0);
164
165     cout << "\nThe recording of data is completed.";
166     cout << "\n\nPlease press any key to exit the program.";
167     _getch();
168
169 }
```

B.2 Script for the Electronic Control of the SP–PLP–NIR Setup

Measurement.cpp

```
1 /* Script for the electronic control of the SP-PLP-NIR setup
2 by the miniLAB 1008 (Measurement Computing Corp.) 12-bit data
```

```
3 acquisition board while recording time-resolved data with the
4 M2i.4650-exp (Spectrum Systementwicklung Microelectronic GmbH)
5 16-bit transient recorder and the software SBench.
6 Effective January 2012. */
7
8 // The following standard files are included
9 #include <iostream>
10 #include <fstream>
11 #include <conio.h>
12 #include "../..../cbw.h"
13
14 using namespace std;
15
16 // Declaration of global variables
17 char name[50];
18 char dir[70];
19 unsigned short int DataValue;
20 int ULStat = 0;
21 int BoardNum = 0;
22 int Channel;
23 int Range;
24 float voltage;
25 float EngUnits;
26 char signalname[10];
27 char file[20];
28 char no[5];
29 char path[100];
30
31 // Function for the reference to a folder for the created file
32 void input() {
33
```

```
34     // Reading in the path
35     cout << "Enter user name" << endl;
36     cin >> name;
37     strcpy_s (dir, "\\benutzer\\");
38     strcat_s (dir, name);
39     strcat_s (dir, "\\Signale\\");
40
41 }
42
43 /* Function for reading in the voltage at channels 1 (UV diode),
44 2 (uncompensable IR signal) or 3 (compensable IR signal) */
45 void import() {
46     DataValue = 0;
47     ULStat = cbAIn (BoardNum, Channel, Range, &DataValue);
48     ULStat = cbToEngUnits (BoardNum, Range, DataValue, &voltage);
49
50 }
51
52 /* Function for output of the compensating voltage via analog
53 output channel 1 */
54 void compensation() {
55     Range = UNI5VOLTS;
56     Channel = 1;
57     DataValue = 0;
58     ULStat =
59     cbFromEngUnits (BoardNum, Range, EngUnits, &DataValue);
60     ULStat = cbAOut (BoardNum, Channel, Range, DataValue);
61
62 }
63
64 // Main function
```

```
65 void main() {
66
67     input();
68
69     // Declaration of local variables
70     float RevLevel = (float)CURRENTREVNUM;
71     int PortNum;
72     int Direction = DIGITALOUT;
73     int a;
74     float Ia;
75     float Ib;
76     float I002c;
77     float I002o;
78     float I002;
79     int answer;
80     int number = 0;
81     float I003o;
82     float I003c;
83     float I003;
84     float I02c;
85     float I02o;
86     float I02;
87     int check;
88     float I03o;
89     float I03c;
90     float I03;
91     int samprate;
92     int n;
93     float UVvoltage;
94     int j;
95     float UVd;
```

```
96     float UV1;
97     float I3o;
98     float I2o;
99     float I2c;
100    float I2;
101    int reply;
102    int reply2;
103
104    // Declaration of the revision level of the Universal Library
105    ULStat = cbDeclareRevision(&RevLevel);
106
107    /* Initiate error handling with the parameters
108    "PRINTALL" (all warnings and errors encountered will be
109    printed) and "STOPALL" (if any error is encountered,
110    the program will stop) */
111    cbErrHandling (PRINTALL, STOPALL);
112
113    // Configuration of port B as digital output
114    PortNum = FIRSTPORTB;
115    ULStat = cbDConfigPort (BoardNum, PortNum, Direction);
116
117    // -----Beginning of the measurement-----
118
119    // -----measureI002-----
120    measureI002:
121
122    // Close IR iris diaphragm
123    ULStat = cbDOut(BoardNum, PortNum, 0);
124
125    Sleep (2000);
126
```



```
127     // Determination of "I002c" as average of 1000 measurements
128     a = 0;
129     Ib = 0;
130     for (a = 0; a<1000; a++) {
131         Channel = 2;
132         Range = BIP1VOLTS;
133         import();
134         Ia = voltage;
135         Ib = Ib + Ia;
136         Sleep (1);
137     }
138     I002c = Ib/1000;
139
140     // Open IR iris diaphragm
141     ULStat = cbDOut(BoardNum, PortNum, 4);
142
143     Sleep (1000);
144
145     // Determination of "I002o" as average of 1000 measurements
146     a = 0;
147     Ib = 0;
148     for (a = 0; a<1000; a++) {
149         Channel = 2;
150         Range = BIP1VOLTS;
151         import();
152         Ia = voltage;
153         Ib = Ib + Ia;
154         Sleep (1);
155     }
156     I002o = Ib/1000;
157
```

```
158      // Determination of "I002"
159      I002 = I002o - I002c;
160
161      cout << "I002 is: ";
162      cout << I002 << " V" << endl;
163 // -----End of I002 determination-----
164
165 // -----question1-----
166      question1:
167      cout << "I002 okay? Enter 1 if yes or 2 if no. "
168      "Don't enter letters!!! ";
169      cin >> answer;
170      if (answer==1)
171          goto proceed;
172      else if (answer==2)
173          goto measureI002;
174      else
175          goto question1;
176 // -----End of question1-----
177
178 // -----proceed-----
179      proceed:
180      cout << "Enter signal name" << endl;
181      cin >> signalname;
182
183 // -----again-----
184      again:
185      /* The following commands increment the number affix
186      of the file */
187      number = number + 1;
188      strcpy_s (file, signalname);
```

```
189     strcat_s (file, "_");
190     _itoa_s (number, no, 10);
191     strcat_s (file, no);
192
193     // Provision of the folder and file for data to be saved in
194     _makepath_s(path, "d", dir, file , ".txt");
195     ofstream Outfile (path);
196     Outfile << I002 << endl;
197
198 // -----reexamine-----
199     reexamine:
200     // Close IR iris diaphragm
201     ULStat = cbDOut(BoardNum, PortNum, 0);
202
203     Sleep(2000);
204
205     // Determination of "I02c" as an average of 1000 measurements
206     a = 0;
207     Ib = 0;
208     for (a = 0; a<1000; a++) {
209         Channel = 2;
210         Range = BIP1VOLTS;
211         import();
212         Ia = voltage;
213         Ib = Ib + Ia;
214         Sleep (1);
215     }
216     I02c = Ib/1000;
217
218     // Open IR iris diaphragm
219     ULStat = cbDOut(BoardNum, PortNum, 4);
```

```
220
221     Sleep (1000);
222
223     // Determination of "I02o" as an average of 1000 measurements
224     a = 0;
225     Ib = 0;
226     for (a = 0; a<1000; a++) {
227         Channel = 2;
228         Range = BIP1VOLTS;
229         import();
230         Ia = voltage;
231         Ib = Ib + Ia;
232         Sleep (1);
233     }
234     I02o = Ib/1000;
235
236     // Determination of "I02"
237     I02 = I02o - I02c;
238
239     cout << "I02 is: " << I02 << " V" << endl;
240
241 // -----question2-----
242     /* Question whether I02 should be checked
243     or whether pulsing should be started */
244     question2:
245     cout << "Should I02 be checked? If yes, press 1, if no "
246     "press 2. Don't enter letters!!! ";
247     cin >> check;
248
249     if (check==1)
250         goto reexamine;
```

```
251     else if (check==2)
252         goto write_I02;
253     else
254         goto question2;
255 // -----End of question2-----
256
257 // -----write_I02-----
258     write_I02:
259     Outfile << I02 << endl;
260
261     // Setting the compensating voltage to 0 V
262     EngUnits = 0;
263     compensation();
264
265     Sleep (1000);
266
267     // Determination of "I003o" as average of 1000 measurements
268     a = 0;
269     Ib = 0;
270     for (a = 0; a<1000; a++) {
271         Channel = 3;
272         Range = BIP10VOLTS;
273         import();
274         Ia = voltage;
275         Ib = Ib + Ia;
276         Sleep (1);
277     }
278     I003o = Ib/1000;
279
280     // Close IR iris diaphragm
281     ULStat = cbDOut(BoardNum, PortNum, 0);
```

```
282
283     Sleep(2000);
284
285     // Determination of "I003c" as average of 1000 measurements
286     a = 0;
287     Ib = 0;
288     for (a = 0; a<1000; a++) {
289         Channel = 3;
290         Range = BIP10VOLTS;
291         import();
292         Ia = voltage;
293         Ib = Ib + Ia;
294         Sleep (1);
295     }
296     I003c = Ib/1000;
297
298     // Determination of "I003"
299     I003 = I003o - I003c;
300
301     // Setting the compensating voltage
302     EngUnits = I003o;
303     compensation();
304
305     Sleep(1000);
306
307     // Determination of "I03c" as an average of 1000 measurements
308     a = 0;
309     Ib = 0;
310     for (a = 0; a<1000; a++) {
311         Channel = 3;
312         Range = BIP10VOLTS;
```

```
313         import();
314         Ia = voltage;
315         Ib = Ib + Ia;
316         Sleep (1);
317     }
318     I03c = Ib/1000;
319
320     // Open IR iris diaphragm
321     ULStat = cbDOut(BoardNum, PortNum, 4);
322
323     Sleep(1000);
324
325     // Determination of "I03o" as an average of 1000 measurements
326     a = 0;
327     Ib = 0;
328     for (a = 0; a<1000; a++) {
329         Channel = 3;
330         Range = BIP10VOLTS;
331         import();
332         Ia = voltage;
333         Ib = Ib + Ia;
334         Sleep (1);
335     }
336     I03o = Ib/1000;
337
338     // Determination of "I03"
339     I03 = I03o - I03c;
340
341     cout << "I03 is: " << I03 << " V" << endl;
342     Outfile << I03 << endl;
343
```

```
344     cout << "Which sampling rate (in kHz) has been chosen "
345     "in SBench?" << endl;
346     cin >> samprate;
347     cout << "Enter the number of pulses to apply "
348     "for averaging purposes" << endl;
349     cin >> n;
350     UVvoltage = 0;
351
352     // Start pulse sequence
353     for (j = 1; j<n+1; j++) {
354         cout << "Pulse index: ";
355         cout << j << endl;
356
357         // Activate UV diode
358         ULStat = cbDOut(BoardNum, PortNum, 6);
359
360         Sleep (1000);
361         Channel = 1;
362         Range = BIP10VOLTS;
363         import();
364         UVd = voltage;
365
366         // Reset UV diode, open UV iris diaphragm
367         ULStat = cbDOut(BoardNum, PortNum, 12);
368
369         Sleep (200);
370
371     /* Activate UV diode, arm laser, i.e. set bit 0 to 1; laser
372     triggers at transition 1 to 0 */
373         ULStat = cbDOut(BoardNum, PortNum, 15);
374
```



```
375         Sleep (200);
376
377         // Trigger the laser
378         ULStat = cbDOut(BoardNum, PortNum, 14);
379
380         Sleep (1500);
381
382         /* Reading in channel 1 (UV diode)
383         while triggering the laser */
384         Channel = 1;
385         Range = BIP10VOLTS;
386         import();
387         UVl = voltage;
388         UVvoltage = UVvoltage + UVl - UVd;
389
390         // Close UV iris diaphragm, reset UV diode
391         ULStat = cbDOut(BoardNum, PortNum, 4);
392
393         EngUnits = 0;
394         compensation();
395         Sleep (1000);
396
397         /* Determination of "I3o" as an average of
398         1000 measurements */
399         a = 0;
400         Ib = 0;
401         for (a = 0; a<1000; a++) {
402             Channel = 3;
403             Range = BIP10VOLTS;
404             import();
405             Ia = voltage;
```

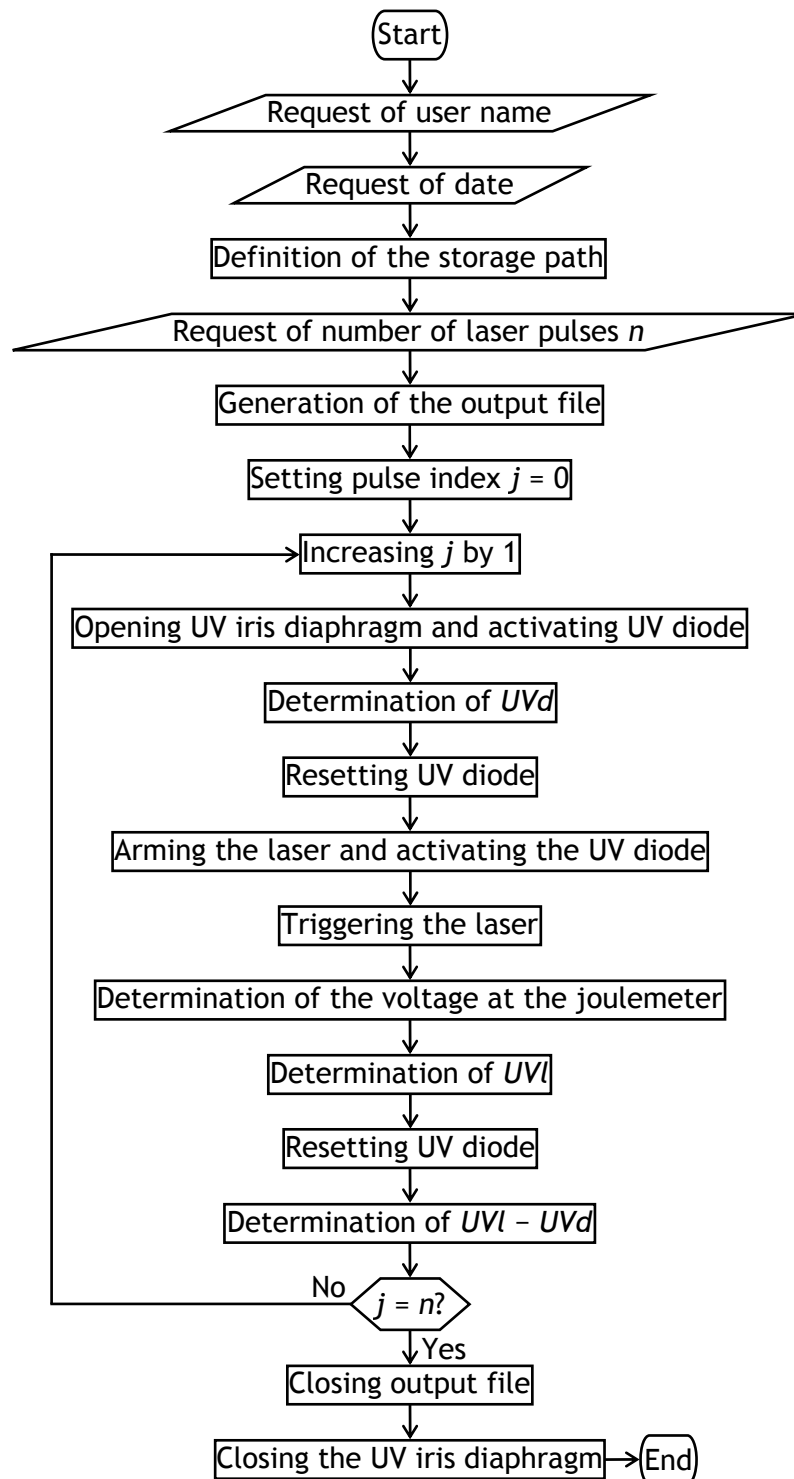
```
406             Ib = Ib + Ia;
407             Sleep (1);
408         }
409         I3o = Ib/1000;
410
411         cout << "I3o is: " << I3o << " V" << endl;
412         EngUnits = I3o;
413         compensation();
414         Sleep (1000);
415
416     }
417
418     // Determination of "I2o" as an average of 1000 measurements
419     a = 0;
420     Ib = 0;
421     for (a = 0; a<1000; a++) {
422         Channel = 2;
423         Range = BIP1VOLTS;
424         import();
425         Ia = voltage;
426         Ib = Ib + Ia;
427         Sleep (1);
428     }
429     I2o = Ib/1000;
430
431     // Close IR iris diaphragm
432     ULStat = cbDOut(BoardNum, PortNum, 0);
433
434     Sleep (2000);
435
436     // Determination of "I2c" as an average of 1000 measurements
```

```
437     a = 0;
438     Ib = 0;
439     for (a = 0; a<1000; a++) {
440         Channel = 2;
441         Range = BIP1VOLTS;
442         import();
443         Ia = voltage;
444         Ib = Ib + Ia;
445         Sleep (1);
446     }
447     I2c = Ib/1000;
448
449     // Determination of "I2"
450     I2 = I2o - I2c;
451
452     cout << "I2 is: " << I2 << " V" << endl;
453
454     // Write data into the file
455     Outfile << UVvoltage/n << endl;
456     Outfile << I2 << endl;
457     Outfile << I003 << endl;
458     Outfile << I02o << endl;
459     Outfile << I2o << endl;
460     Outfile << I002o << endl;
461     Outfile << n << endl;
462     Outfile << samprate << endl;
463     Outfile << I03o << endl;
464     Outfile << I003o << endl;
465
466     Outfile.close();
467
```

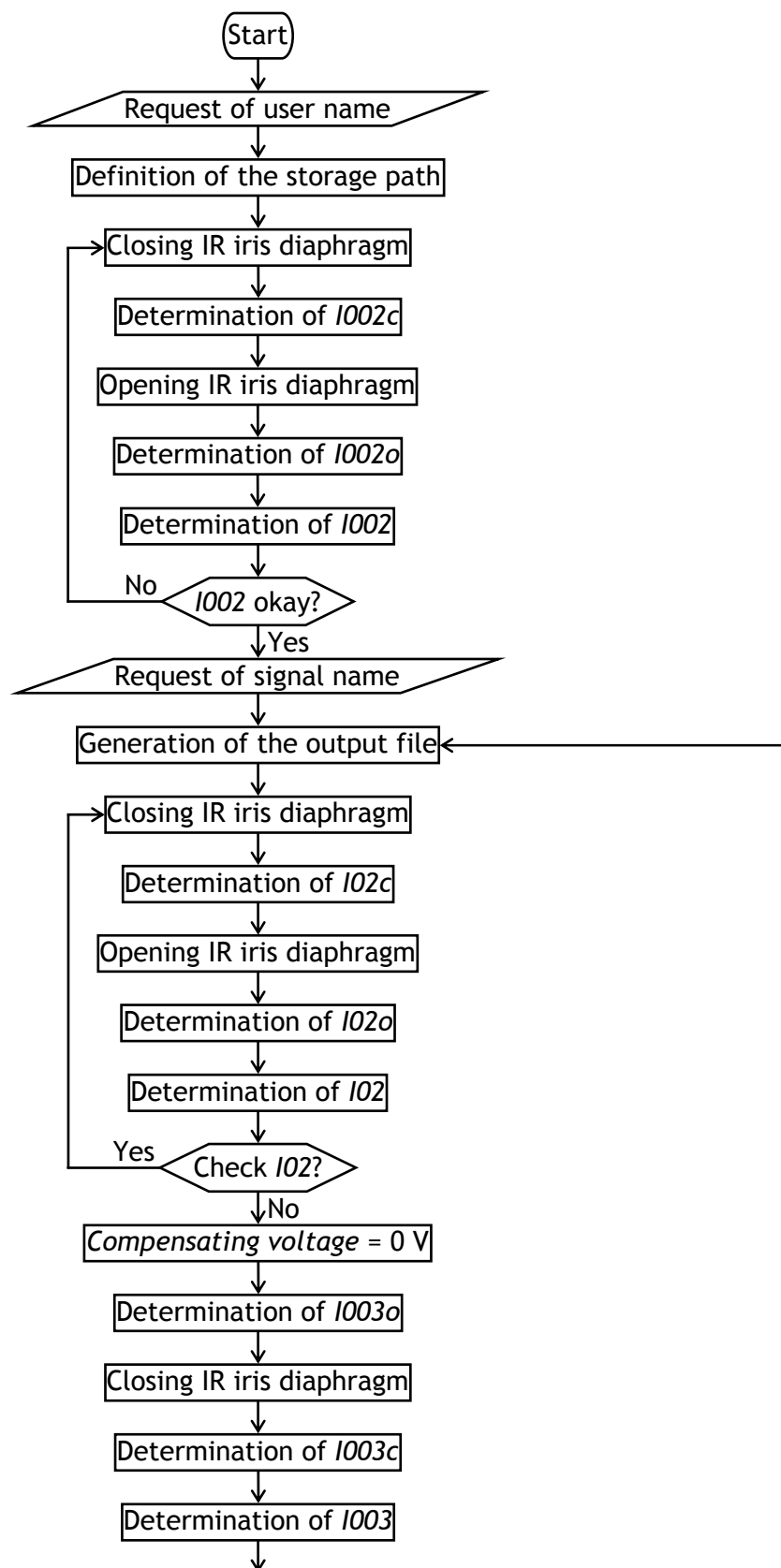
```
468 // -----question3-----
469     question3:
470     cout << "Apply another pulse sequence?  If yes, press 1, "
471     "if no press 2. Don't enter letters!!!  ";
472     cin >> reply;
473     if (reply==1)
474         goto again;
475     else if (reply==2)
476     {
477         cout << "Quit the program?  If yes, press 1, if "
478         "no press 2. Don't enter letters!!!  ";
479         cin >> reply2;
480     }
481     else
482         goto question3;
483 // -----End of question3-----
484
485     if (reply2==2)
486         goto question3;
487     else if ((reply2!=1) && (reply2!=2))
488         goto question3;
489
490     EngUnits = 0;
491     compensation();
492
493     cout << "\nThe recording of data is completed.";
494     cout << "\n\nPlease press any key to exit the program.";
495     _getch();
496
497 }
```

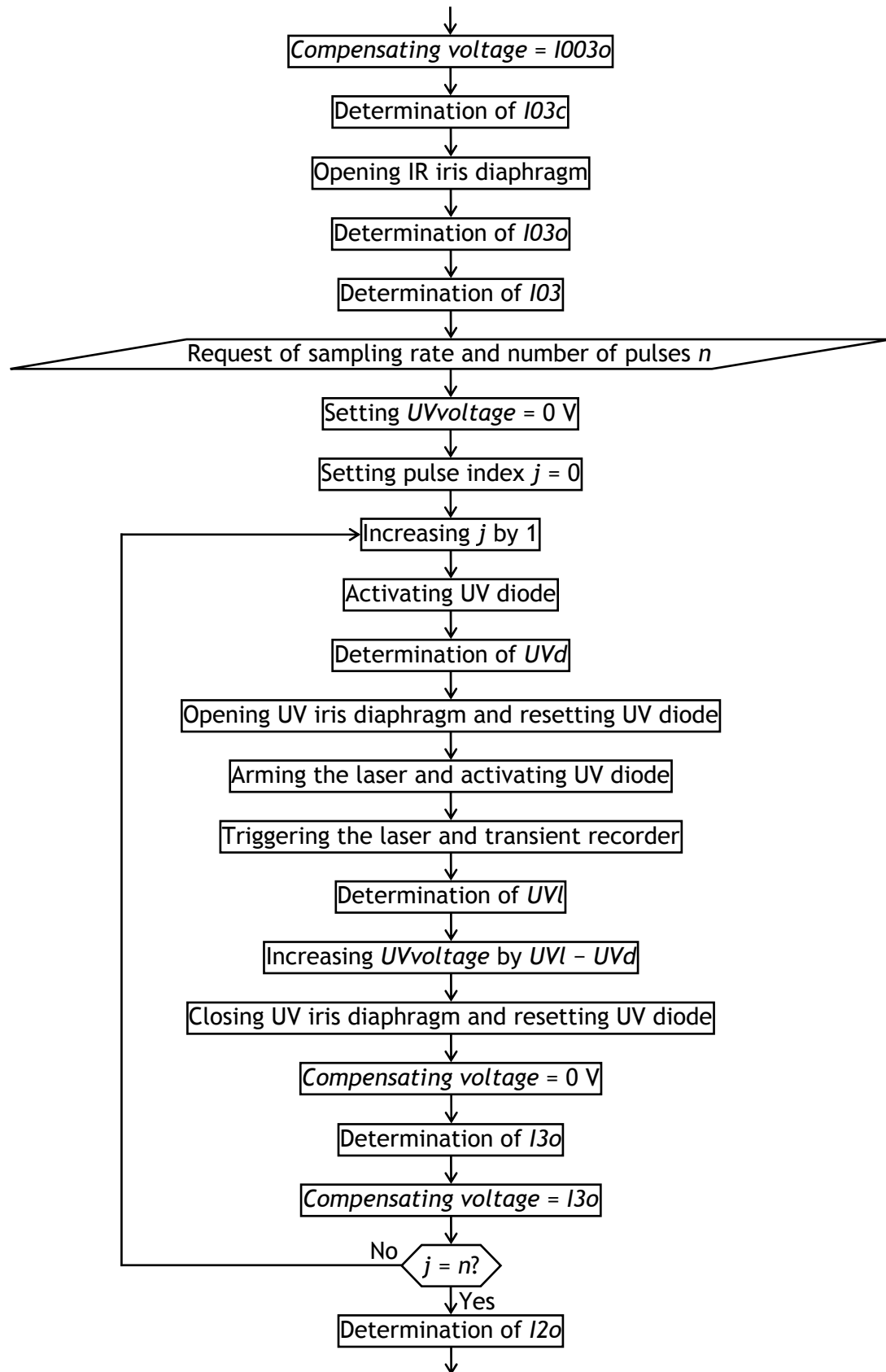
Appendix C: Flowcharts

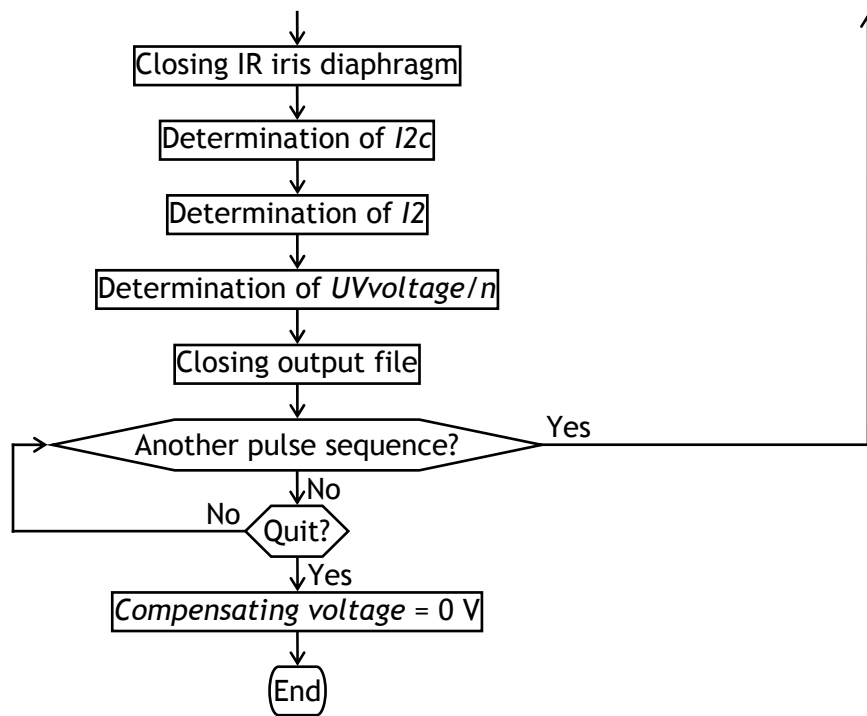
C.1 Flowchart of the Main Steps of Laser Calibration



C.2 Flowchart of the Main Steps of SP–PLP–NIR Experiments







Appendix D: MATLAB[®] Functions

The following MATLAB[®] functions were written based on the ones developed by Junkers.^[209] The new functions are written for MATLAB[®] R2011a (MathWorks, version 7.12).

D.1 Function for the Adjustment of *I002* Values

I002.m

```
1 function I002
2
3 % Program for loading all .txt-files generated by the
4 % data acquisition board (by Measurement.cpp) and
5 % adjusting the I002 values.
6 % Effective September 2011. v. 1.0 Thomas Junkers (31.01.2003)
7 % v. 2.0 Jens Schrooten (19.09.2011)
8
9 matrix = [];
10
11 %%%%%%%%%% Input of general information %%%%%%%%%%
12 disp('The following text files were found in the current path:')
13 dir *.txt
14 name = input(...)
15     'Enter the signal name (without number affix)!    ','s');
16 quant = input('How many text files were recorded?    ');
17 disp(' ')
18
19 %%%%%%%%%% Read files %%%%%%%%%%
20 for i = 1:quant;
```

```
21
22     % Read signal name
23     for a = 1:length(name)
24         filename(a) = name(a);
25     end
26
27     % Read number affix
28     c = num2str(i);
29     y = 0;
30     for b = length(name) + 1:length(name) + length(c)
31         y = y + 1;
32         filename(b) = c(1,y);
33     end
34
35     % Define file extension (.txt)
36     txt = '.txt';
37     for d = length(name) + length(c) + 1:...
38         length(name) + length(c) + 4
39         filename(d) = txt(d - length(name) - length(c));
40     end
41
42     s1 = exist(filename,'file');
43     if s1==2
44         dummy = load(filename);
45         matrix = [matrix dummy];
46     else
47         disp(' ');
48         disp('NUMBER OF SIGNALS WAS WRONG! PLEASE RESTART!');
49     end
50
51     disp(filename);
```

```
52
53 end
54
55 if isempty(matrix)
56     return;
57 end
58 disp(' ')
59 disp('          ...have been loaded')
60
61 %%%%%%%%% Input of physical quantities %%%%%%%%%
62 disp('Please input the following experimental parameters:');
63 disp(' ');
64 epseff = input('Epsilon_eff (cm^2/mol):    ');
65 if isempty(epseff)
66     return;
67 end
68 disp(' ');
69 d = input('Optical path length of the inner cell (mm):    ');
70 if isempty(d)
71     return;
72 end
73 d = d/10;
74 disp(' ');
75 M = input('Molar mass (g/mol):    ');
76 if isempty(M)
77     return;
78 end
79 disp(' ');
80 rho=input('Density (g/cm^3):    ');
81 if isempty(rho)
82     return;
```

```
83 end
84 disp(' ');
85 n = input('Mean value for every 2^n data points: n = ');
86 if isempty(n)
87     disp(' ');
88     disp('The following default value for n has been chosen: 4');
89     n = 4;
90 end
91 disp(' ');
92 kp = input('Propagation rate coefficient (L/mol*s): ');
93 if isempty(kp)
94     disp(' ');
95     disp('The following default value has been chosen: 1');
96     kp = 1;
97 end
98 disp(' ');
99 yi = input(['y-intercept of the function fitted to the data '...
100     'determined by LaserCalibration.cpp (mJ): ']);
101 if isempty(yi)
102     disp(' ');
103     disp('The following default value has been chosen: 1');
104     yi = 1;
105 end
106 disp(' ');
107 sl = input(['Slope of the function fitted to the data '...
108     'determined by LaserCalibration.cpp (mJ/V): ']);
109 if isempty(sl)
110     disp(' ');
111     disp('The following default value has been chosen: 1');
112     sl = 1;
113 end
```

```
114
115 disp(' ');
116 disp(' ');
117
118 disp(matrix)
119
120 ft = input('How many FT-NIR spectra are there? ');
121 if isempty(ft)
122     return;
123 end
124 disp('_____');
125
126 %%%%%%%%% Adjustment of I002 values %%%%%%%%%
127 conversion1 = 0;
128 start = 0;
129 disp(['The first FT-NIR spectrum should be the one '...
130       'at 0 % monomer conversion.']);
131
132 for i = 1:ft - 1
133
134     inter = input(['How many signals have been recorded '...
135                   'until the next FT-NIR spectrum? ']);
136     if isempty(inter)
137         return;
138     end
139     conversion2 = input(['Monomer conversion from '...
140                          'next spectrum (%): ']);
141     if isempty(conversion2)
142         return;
143     end
144     disp(' ');
```

```
145     first = start + 1;
146     last = start + inter;
147
148     m = 0;
149     for a = first:last
150         y = matrix(10,a);
151         m = m + y;
152     end
153     UPulse = (conversion2 - conversion1)/m;
154     nP = 0;
155     for a = first:last
156         i02 = matrix(2,a);
157         i2 = matrix(5,a);
158         conversion1neu = conversion1 + (UPulse*nP);
159         nP = nP + matrix(10,a);
160         conversion2neu = conversion1 + (UPulse*nP);
161         [newi002] = correction(M,rho,epseff,...
162             d,i02,i2,conversion1neu,conversion2neu);
163         matrix(1,a) = newi002;
164     end
165     conversion1 = conversion2;
166
167     start = last;
168
169 end
170
171 disp(matrix)
172
173
174 %%%%%%%%%%% Saving of the data %%%%%%%%%%%
175 disp('_____');
```

```
176 yesno = input('Overwrite existing files (1 for YES)? ');
177 if yesno ~= 1
178     disp('DATA NOT SAVED');
179     return;
180 elseif isempty(yesno)
181     disp('DATA NOT SAVED');
182     return;
183 end
184
185 for i = 1:quant
186     clear filename;
187
188     % Read signal name
189     for a = 1:length(name)
190         filename(a) = name(a);
191     end
192
193     % Read number affix
194     c = num2str(i);
195     y = 0;
196     for b = length(name) + 1:length(name) + length(c)
197         y = y + 1;
198         filename(b) = c(1,y);
199     end
200
201     % Define file extension (.txt)
202     txt = '.txt';
203     for de = length(name) + length(c) + 1:...
204         length(name) + length(c) + 4
205         filename(de) = txt(de - length(name) - length(c));
206     end
```

```
207
208     vektor = matrix(:,i);
209     save(filename,'vektor','-ascii')
210 end
211
212 %%%%%%%%%%% Saving physical quantities %%%%%%%%%%%
213 intake = [epseff;d;M;rho;n;kp;yi;sl;];
214 save ('exParamet','intake','-ascii')
215
216 %%%%%%%%%% Set starting parameters for the fitting procedure %%%%%%%%%%
217 disp(['The following values will be saved as '...
218     'starting parameters for the Levenberg-Marquardt '...
219     'curve fit (can be changed by editor):'])
220 disp ('q = 100      w = 0.001');
221 q = 100;
222 w = 0.001;
223 start = [q;w];
224 save('startParamet','start','-ascii');
225
226 %%%%%%%%%%% Subfunction %%%%%%%%%%%
227 function [newi002] = correction(M,rho,epseff,...
228     d,i02,i2,conversion1neu,conversion2neu)
229 medrho1 = conversion1neu * rho/100;
230 medrho2 = conversion2neu * rho/100;
231 newi0021 = i02 * (10^(- d * medrho1 * epseff/M));
232 newi0022 = i2 * (10^(- d * medrho2 * epseff/M));
233 newi002 = (newi0021 + newi0022)/2;
```


D.2 Function for the Calculation of the Relative Monomer Concentration Versus Time Profile and for the Curve Fitting to Experimental Data

analyze.m

```
1 function analyze
2
3 % Program for analysis of time-resolved SP-PLP-NIR signals
4 % by means of voltages determined by the data acquisition board
5 % (by Measurement.cpp). Effective September 2011.
6 % v. 2.10 Thomas Junkers (17.06.2004)
7 % v. 3.0 Jens Schrooten (19.09.2011)
8
9 format long;
10
11 % Importing file with time-resolved data from transient recorder
12 [file1_txt, path1] = uigetfile('*.txt', ['Choose file (*.txt) '...
13     'with time-resolved data from transient recorder']);
14 trans = importdata([path1 file1_txt], ' ');
15 dummy1 = trans(1:length(trans),2);
16
17 % Importing file with data from the data acquisition board
18 [file2_txt, path2] = uigetfile('*.txt',...
19     'Choose file (*.txt) with data from data acquisition board');
20 dummy2 = importdata([path2 file2_txt]);
21
22 % Loading of the parameters input with I002.m
23 % (physical quantities and starting parameters for the
24 % fitting procedure). The file exParamet has to be
25 % in the "Current Folder"
26 supi = exist('exParamet','file');
```

```
27 if supi~=0
28     load exParamet;
29     epseff = exParamet(1,1);
30     d = exParamet(2,1);
31     M = exParamet(3,1);
32     rho = exParamet(4,1);
33     n = exParamet(5,1);
34     kp = exParamet(6,1);
35     yi = exParamet(7,1);
36     sl = exParamet(8,1);
37 else
38     disp(['File exParamet with values '...
39         'epseff, d, M, rho, n , kp, yi, and sl not found!']);
40     return
41 end
42 supi2 = exist('startParamet','file');
43 if supi2~=0
44     load startParamet;
45     q = startParamet(1,1);
46     w = startParamet(2,1);
47 elseif supi2 == 0
48     disp('File startParamet with values q and w not found!');
49     return
50 end
51
52 % Assigning default names to save output files
53 % default name = file name of the imported measured data
54 % affix _fitdat for fitting results
55 % affix _concdat for pure concentration vs time profiles
56 % File name for fitting results
57 % Removal of file extension (.txt)
```

```
58 for i = 1:length(file1_txt) - 4
59     file1(i) = file1_txt(i);
60 end
61 extension1 = '_fitdat';
62 k = 0;
63 for i = 1:length(file1) + 7
64     if i<=length(file1)
65         default1(i) = file1(i);
66     else
67         k = k + 1;
68         default1(i) = extension1(k);
69     end
70 end
71 % File name for concentration vs time profiles
72 % Removal of file extension (.txt)
73 for i = 1:length(file2_txt) - 4
74     file2(i) = file2_txt(i);
75 end
76 extension2 = '_concdat';
77 k = 0;
78 for i = 1:length(file2) + 8
79     if i<=length(file2)
80         default2(i) = file2(i);
81     else
82         k = k + 1;
83         default2(i) = extension2(k);
84     end
85 end
86
87 % Determining the number of values determined by
88 % the transient recorder
```

```
89 m = length(dummy1);
90
91 % Cache data of the files
92 Iabs = dummy2(:);
93
94 % Reading physical parameters
95 gainfac = 100;
96 I002 = Iabs(1,1);
97 I02 = Iabs(2,1);
98 calib = Iabs(4,1);
99 I2 = Iabs(5,1);
100 Lp = Iabs(10,1);
101 samprate = Iabs(11,1);
102
103 % Determination of acquisition time after the laser pulse
104 acqtime = (3/4*m-1)/(1000*samprate);
105
106 % Determination of the laser pulse energy in mJ
107 disp(' ');
108 disp('Laser energy (in mJ):');
109 medener = yi + calib*sl;
110 disp(medener);
111
112 % Determination of the averaged conversion for a pulse sequence
113 % Change of density until start of the pulse sequence
114 rhoi0 = M*log10(abs(I002/I02))/d/epseff;
115 % Change of density until end of the pulse sequence
116 rhoi1 = M*log10(abs(I002/I2))/d/epseff;
117 % Averaged change of density
118 medrho = abs((rhoi0 + rhoi1)/2);
119 % Averaged monomer density during a pulse sequence
```

```
120 edrho = rho - medrho;
121 % Averaged monomer concentration during a pulse sequence
122 edconc = abs(edrho/M);
123 % Averaged monomer conversion (in %) during a pulse sequence
124 mconversion = (1 - edconc/(rho/M))*100;
125 disp('Mean monomer conversion (in %):');
126 disp(mconversion);
127
128 % Determination of the time needed for a single propagation step
129 tp = 1/(edconc*1000*kp);
130 disp('Time needed for a single propagation step (in s):');
131 disp(tp);
132 disp('_____');
133
134 % Averaging of sequences of 2^n data points
135 % determined by the transient recorder
136 for i = 1:m/(2^n);
137     tei = dummy1(2^n*(i - 1) + 1:2^n*i);
138     mit(i) = mean(tei);
139 end
140
141 % Plotting the data
142 % Setting of the part of the pretrigger region to be fitted
143 % and determination of the mean value
144 prt = 30;
145 pr = dummy1(fix((1 - prt/100)*m/4) + 1:m/4);
146 mi = mean(pr);
147 % Calculation of the concentration vs time profile
148 x = 100;
149 aaa = 1/(epseff*d*(rho/M + rhoi0/M));
150 [t,y] = conctimeprof (m,x,n,samprate,mit,mi,gainfac,Lp,aaa,I02);
```

```
151 % Plotting and saving the data
152 % Determination of the duration of the conc-time-prof
153 maxt = max(t);
154 plotsignal(t,y);
155 s1 = t(:);
156 s2 = y(:);
157 clear t;
158 clear y;
159
160 % Question about setting the pretrigger
161 pret_quest = input...
162     ('Pretrigger (30 %) okay? (press "5" for NO) ');
163
164 % Plotting the data after resetting of the pretrigger
165 if pret_quest==5
166     disp(' ');
167     prt = input(['How many data values (in %) of the '...
168         'pretrigger region should be used '...
169         'for calculation? ']);
170     pr = dummy1(fix((1 - prt/100)*m/4) + 1:m/4);
171     mi = mean(pr);
172     x = 100;
173     % Calculation of the concentration vs time profile
174     [t,y] = ...
175         conctimeprof (m,x,n,samprate,mit,mi,...
176             gainfac,Lp,aaa,I02);
177     % Plotting and saving the data
178     plotsignal(t,y);
179     s1 = t(:);
180     s2 = y(:);
181     clear t;
```

```
182     clear y;
183     clear x;
184 end
185 disp(' ');
186
187 % Saving the concentration vs time profile in ASCII
188 flop = input(['Save concentration vs time profile in ASCII '...
189     '(will be saved as plotted)? (press "1" for YES)    ']);
190 if isempty(flop)
191     disp('No ASCII file has been saved')
192 elseif flop==1
193     file = [s1 s2];
194     disp(' ');
195     flop2 = input(['Use default name? '...
196         '(In case it already exists, it will '...
197         'be overwritten.) (press "1" for NO)    ']);
198     filename = default2;
199     if isempty(flop2)
200         disp(' ');
201         filename = input('Please input another filename:', 's');
202     elseif flop2~=1
203         disp(' ');
204         filename = input('Please input another filename:', 's');
205     end
206     disp('The following file name is used:');
207     disp(filename);
208     save (filename, 'file', '-ascii', '-double', '-tabs');
209 end
210 disp(' ');
211
212 % Determination of kt for a certain chain-length interval
```

```
213 kt_chain_quest = input(['Average kt for a certain '...
214     'chain-length interval? (press "1" for YES)    ']);
215 if isempty(kt_chain_quest)
216     kt_chain_quest = 0;
217 end
218 disp(' ');
219 if kt_chain_quest==1
220     check = 0;
221     while check==0
222         % Choice of the maximum degree of polymerization
223         chainlength = input(['What is the maximum '...
224             'chain length for averaging?    ']);
225         timeind = chainlength*tp;
226         disp(['Acquisition time needed '...
227             'for data evaluation (in s):    ']);
228         disp(timeind);
229         % Definition of the maximum percentage of the data
230         % up to which kt is averaged
231         startpot = timeind/maxt*100;
232         check = 1;
233         % If degree of polymerization is out of range
234         if startpot > 100
235             chainlength = fix(maxt/tp);
236             disp(' ');
237             disp('          W A R N I N G ');
238             disp(' Chain length exhibits time! ');
239             disp(' Maximum chain length is:');
240             disp(chainlength);
241             check = 0;
242             disp(' ');
243         end
```



```
244     end
245     interval = 100 - startpot;
246     fitnum = 1;
247
248 % Determination of kt for a various percentage intervals
249 else
250     disp(['Each fit is applied to a certain percentage '...
251         'of the data of the post-trigger region.']);
252     interval = input(['Choose the increment '...
253         'of this percentage (in %):    ']);
254     if isempty(interval)
255         interval = 100;
256     end
257     disp(' ');
258     startpot = input(['Percentage of data '...
259         'to start with (in %):    ']);
260     if isempty(startpot)
261         startpot = interval;
262     elseif startpot==0
263         startpot = interval;
264     end
265     disp(' ');
266     fitnum = input(['How many fits shall be applied '...
267         '(press "0" for escape)?    ']);
268     if isempty(fitnum)
269         fitnum = 1;
270     end
271
272 end
273
274 % If number of fits equals zero
```

```
275 if fitnum==0
276     error('No fitting done. ');
277 end
278
279 % Preparing the saving of data using a default name
280 supi = exist(default1,'file');
281 if supi~=0
282     disp('File name already exists in the current directory!');
283     default1 = input(['Please input alternative file name '...
284         '(without file extension):    '], 's');
285 end
286 fn = default1;
287 fid = fopen(fn, 'a');
288 fprintf(fid, ['Key    Percentage of data    '...
289     'Fitting time range/s '...
290     'lg(kt/kp) ln(kt/kp) (2*kt*cR0)/Hz    kp/(2*kt) '...
291     'SSE Adj. R squared  RMS error  Iterations Exitflag\r']);
292 fclose(fid);
293
294 % Determination of percentage ranges
295 % and applying fits with applyfit.m
296 intermed = interval*fitnum;
297 % Correction of number of fits in case the percentage
298 % of the last fit exceeds 100 %
299 if intermed > 100
300     fitnum = fix((100-startpot)/interval);
301 end
302 % Correction of interval in case the percentage
303 % of the second fit exceeds 100 %
304 if startpot + interval > 100
305     if startpot~=100
```

```
306         interval = 100 - startpot;
307     end
308 end
309
310 % Initializing of parameters for fitting procedure
311 pot = startpot - interval;
312 val1 = 0;
313 x = 0;
314 runind = 0;
315
316 % Setting plot style
317 ax_ = subplot(1,1,1);
318 set(ax_,'Box','on');
319 legh_ = [];
320 legt_ = {};
321
322 % Fitting procedure
323 for har = 1:fitnum + 1
324     if x~=100
325         pot = pot + interval;
326         runind = runind + 1;
327         x = pot;
328         if val1==1
329             x = 100;
330         end
331         % Calculation of the concentration vs time profile
332         [t,y] = conctimeprof ...
333             (m,x,n,samprate,mit,mi,gainfac,Lp,aaa,I02);
334         % Fitting the data
335         [x,lgktp,ktp,P1,P2,sse,adjrsquare,rmse,iterations,...
336             exitflag,ax_,legh_, legt_] = applyfit(t,y,q,w,...
```

```
337         runind,x,fitnum,ax_,legh_, legt_);
338     % Handing fit results over
339     result = [x lgktp ktkp P1 P2 sse adjrsquare rmse ...
340             iterations exitflag];
341
342     clear t;
343     clear y;
344
345     % Saving fit results
346     if runind==1
347         overres = result;
348     else
349         intoverres = overres;
350         overres = [intoverres;result];
351     end
352
353     % Determination of time after trigger used for fitting
354     x2 = x*maxt/100;
355
356     % Saving all variables of the fitting procedure in file
357     fid = fopen(fn, 'a');
358     fprintf(fid, ' %.5f', x);
359     fprintf(fid, ' %.5f', x2);
360     fprintf(fid, ' %.5f', lgktp);
361     fprintf(fid, ' %.5f', ktkp);
362     fprintf(fid, ' %.8f', P1);
363     fprintf(fid, ' %.8e', P2);
364     fprintf(fid, ' %.4e', sse);
365     fprintf(fid, ' %.4f', adjrsquare);
366     fprintf(fid, ' %.8f', rmse);
367     fprintf(fid, ' %.0f', iterations);
```

```
368         fprintf(fid, ' %.0f\r', exitflag);
369         fclose(fid);
370
371         % If last fit has been applied and less than 100 %
372         % of the data have been used
373         if fitnum==runind
374             if x < 100
375                 val1 = 1;
376             end
377         end
378
379     end
380 end
381
382 % Setting plot style
383 legend(ax_,legh_, leg_);
384 hold off;
385 legend(ax_,legh_, leg_);
386
387 % Saving kt for a certain chain-length interval
388 if kt_chain_quest==1
389     fid = fopen(fn, 'a');
390     fprintf(fid, 'Key   max. chain length\r');
391     fprintf(fid, ' %.2f\r', chainlength);
392     fclose(fid);
393 end
394
395 % Saving all quantities determined by means of the
396 % data acquisition board in the file
397 fid = fopen(fn, 'a');
398 fprintf(fid, ['Key   Conversion/%%   Laser energy/mJ '...]
```

```
399     'Epsilon_eff/(cm^2/mol)    Path length/cm  '...
400     'Total acq. time after laser pulse/s  '...
401     'Virtual molar mass/(g/mol) n    Density/(g/ml)\r']]);
402 fprintf(fid, ' %.2f', mconversion);
403 fprintf(fid, ' %.4f', medener);
404 fprintf(fid, ' %.3f', epseff);
405 fprintf(fid, ' %.4f', d);
406 fprintf(fid, ' %.6f', acqtime);
407 fprintf(fid, ' %.2f', M);
408 fprintf(fid, ' %.2f', n);
409 fprintf(fid, ' %.4f\r', rho);
410 fclose(fid);
411
412 % Display results
413 disp('_____');
414 disp(overres);
```

conctimeprof.m

```
1 function [t,y] =...
2     conctimeprof (m,x,n,samprate,mit,mi,gainfac,Lp,aaa,I02)
3
4 % Function for the determination of cM/cM0 and
5 % the corresponding point of time as well as
6 % averaging of 2^n data points.
7 % Effective September 2011.
8 % v. 1.0 Thomas Junkers, v. 2.0 Jens Schrooten (19.09.2011)
9
10 t = zeros (1, (fix(3/4*m/(2^n)*x/100) + m/(4*2^n)));
11 y = zeros (1, (fix(3/4*m/(2^n)*x/100) + m/(4*2^n)));
12
```

```
13 % Choice of data to be fitted
14 % (pretrigger and percentage x of the post-trigger)
15 for i = 1:(fix(3/4*m/(2^n)*x/100) + m/(4*2^n));
16     % Point in time of the measurement of the data value
17     % (trigger at 0 s)
18     t(i) = 1/(1000*samprate)*((i - 1)*2^n + 2^(n - 1) - 0.5 - m/4);
19
20     y(i) = 1 - aaa/Lp*log10(abs((I02*gainfac + Lp*(mit(i)...
21         - mi))/(I02*gainfac)));
22 end
```

plotsignal.m

```
1 function plotsignal(xaxis,yaxis,ax_)
2
3 % Function for plotting the signals with providing
4 % the possibility to add further data. Effective September 2011.
5 % v. 1.0 Thomas Junkers, v. 2.0 Jens Schrooten (19.09.2011)
6
7 % Setting plot style
8 f_ = clf;
9 figure(f_);
10 ax_ = subplot(1,1,1);
11 set(ax_,'Box','on');
12 hold on;
13 title('Concentration vs time profile')
14 xlabel('\itt\rm/s')
15 ylabel('\itc\rm_M/\itc\rm_M^0')
16
17 % Reading data
18 xaxis = xaxis(:);
```

```
19 yaxis = yaxis(:);
20
21 % Plotting the data
22 line(xaxis,yaxis,'Parent',ax_,'Color',[0.666667 0 0.333333],...
23      'LineStyle','none', 'LineWidth',1,...
24      'Marker','.', 'MarkerSize',5);
```

applyfit.m

```
1 function [x,lgktpk,ktkp,P1,P2,sse,adjrsquare,rmse,...
2      iterations,exitflag,ax_,legh_,legt_] = applyfit...
3      (xaxis,yaxis,q,w,a1,x,fitnum,ax_,legh_, legt_)
4
5 % Function for fitting a mathematical function to the data.
6 % Effective September 2011.
7 % v. 1.0 Thomas Junkers, v. 2.0 Jens Schrooten (19.09.2011)
8
9 disp('_____');
10 disp(' ');
11 disp('Fit no.:')
12 disp(a1);
13 disp('Percentage of data included for fitting:');
14 disp(x);
15 tic;
16
17 % Reading data
18 xaxis = xaxis(:);
19 yaxis = yaxis(:);
20
21 % Setting options for the fitting procedure
22 ex_ = 0 > xaxis;
```

```

23 fo_ = fitoptions('Method','NonlinearLeastSquares','Robust',...
24     'on','Algorithm','Levenberg-Marquardt','MaxFunEvals',...
25     10000,'MaxIter',1000,'TolFun',1e-50,'TolX',1e-10);
26 st_ = [q w];
27 set(fo_,'StartPoint',st_);
28 set(fo_,'Exclude',ex_);
29 ft_ = fittype('(P1*x + 1)^(-P2)','dependent',...
30     'y','independent','x',...
31     'coefficients',{'P1', 'P2'});
32
33 % Fitting of the data
34 [cf_,gof,output] = fit(xaxis,yaxis,ft_ ,fo_);
35
36 % Reading goodness-of-fit statistics and
37 % information associated with the fitting algorithm
38 sse = getfield(gof,{1,1},'sse');
39 adjrsquare = getfield(gof,{1,1},'adjrsquare');
40 rmse = getfield(gof,{1,1},'rmse');
41 exitflag = getfield(output,{1,1},'exitflag');
42 iterations = getfield(output,{1,1},'iterations');
43
44 dumdum = coeffvalues(cf_);
45 P1 = dumdum(1,1);
46 P2 = dumdum(1,2);
47 ktkp = -log(2*P2);
48 lgktkp = -log10(2*P2);
49
50 % Displaying information associated with the fitting and results
51 disp(cf_);
52 disp('Sum of squares due to error:');
53 disp(sse);

```

```
54 disp('Root mean squared error (standard error):');
55 disp(rmse);
56 disp('Number of iterations:');
57 disp(iterations);
58 disp('Exitflag:');
59 disp(exitflag);
60 disp('ln(kt/kp):');
61 disp(ktkp);
62 disp('lg(kt/kp):');
63 disp(lgktkp);
64
65 toc;
66
67 % Plotting data and fits
68 [ax_,legh_, legt_] = plotfit(cf_,x,fitnum,a1,ax_,legh_, legt_);
```

plotfit.m

```
1 function [ax_,legh_,legt_] =...
2     plotfit(cf_,percent,fitnum,runind,ax_,legh_, legt_)
3
4 % Function for plotting a fit in an open figure.
5 % Effective September 2011
6 % v. 1.0 Thomas Junkers
7 % v. 2.0 Jens Schrooten (19.09.2011)
8
9 % Setting number of fit and plot style
10 fitnum = fitnum + 1;
11 colormap(hsv(fitnum));
12 cmap = colormap;
13 h = plot(cf_,'fit',0.95);
```

```
14 set(h(1),'Color',...
15      [cmap(runind,1) cmap(runind,2) cmap(runind,3)],...
16      'LineStyle','- ', 'LineWidth',2,'Marker','none',...
17      'MarkerSize',6);
18 xlabel('\itt\rm/s')
19 ylabel('\itc\rm_M/\itc\rm_M^0')
20
21 % Setting of the legend
22 percent = int2str(percent);
23 legh_(end+1) = h(1);
24 legt_{end+1} = percent;
```


Abbreviations and Symbols

This index lists abbreviations of words and phrases as well as symbols of physical quantities. The Latin alphabet is indexed ahead of the Greek alphabet, lower case letters ahead of upper case, upright symbols ahead of italic, and single-letter symbols ahead of multiple-letter ones. The first letter is used for distinction. The abbreviations and symbols are listed in alphabetical order. Numbers were considered where necessary for a clear differentiation.

Symbols of units as well as mathematical symbols, operators, and functions are given in the IUPAC Green Book.^[292,293]

a	Kuhn–Mark–Houwink–Sakurada parameter
amp	amplification factor
a_p	Kuhn–Mark–Houwink–Sakurada parameter of the polymer under investigation
a_{st}	Kuhn–Mark–Houwink–Sakurada parameter of the polymer used as calibration standard
A	species A
AA	acrylic acid
ADC	analog-to-digital converter
ANSI	American National Standards Institute
A	Arrhenius pre-exponential factor
A'	pre-exponential factor
A_{10}	decadic absorbance
$A_{10,bi}$	decadic absorbance before applying pulse sequence i
$A_{10,eff}$	effective decadic absorbance
A_{int}	integrated decadic absorbance
$A_{int}(t)$	integrated decadic absorbance at time t
$A_{int}(t = 0)$	integrated decadic absorbance at time zero

A_p	parameter to describe the dependence of the propagation rate coefficient on monomer mass fraction
b	number of the corresponding maximum in the first derivative of the MMD
B	species B
BD	beam dump
Bo	bolt
B	monochromator slit width
B_p	parameter to describe the dependence of the propagation rate coefficient on monomer mass fraction
c	solute concentration
c_{Darocur}	concentration of 2-hydroxy-2-methyl-1-phenylpropan-1-one
c_{DMPA}	concentration of 2,2-dimethoxy-1,2-diphenylethan-1-one
c_I	initiator concentration
c_I^0	initial initiator concentration
c_M	overall monomer concentration
c_M^0	initial monomer concentration
c_{M1}	instantaneous monomer concentration of the comonomer M_1
c_{M2}	instantaneous monomer concentration of the comonomer M_2
$c_{M,p,bi}$	monomer concentration before applying pulse sequence i
$c_{M,p,i}$	average monomer concentration occurring during pulse sequence i
$c_M(t)$	monomer concentration at time t after application of the laser pulse
$c_M(t=0)$	monomer concentration when applying the laser pulse at time zero
c_R	radical concentration
$c_R(t)$	radical concentration at time t after application of the laser pulse
$c_R(t=0)$	radical concentration when applying the laser pulse at time zero
c_{V-50}	concentration of initiator V-50
c_X	concentration of molecule X
C	high-pressure capillary
CaF_2	calcium difluoride

CASRN	Chemistry Abstracts Service registry number
CB	cell body
C_{RD}	reaction-diffusion constant
C_p	parameter to describe the dependence of the propagation rate coefficient on monomer mass fraction
$C_{tr,X}$	chain-transfer constant with X being the molecule to which the radical function is transferred
C_η	proportionality factor between logarithmic, relative dynamic viscosity of the reaction solution and monomer conversion
d	doublet
dd	doublet of doublet
dm	diffusion mean
$d\lambda/dx$	reciprocal linear dispersion
d	diameter
D	detector
DMAc	<i>N,N</i> -dimethylacetamide
DMPA	2,2-dimethoxy-1,2-diphenylethan-1-one
DM-PAm	<i>N,N</i> -dimethylprop-2-enamide
DO	digital output
D ₂ O	dideuterium oxide
Dr.	Doktor (German: Doctor), academic title
DSc	Doctor of Science
D_p	parameter to describe the dependence of the propagation rate coefficient on monomer mass fraction
D_s	individual diffusion coefficient
D_S^A	diffusion coefficient of species A
D_S^B	diffusion coefficient of species B
eq.	equation
et al.	et alii (Latin: and others)
e	total order of a reaction

EM	ellipsoidal mirror
EPR	electron paramagnetic resonance
E_0	difference of zero-point energies of the reactants and of the transition state
E_A	Arrhenius activation energy
E_p	energy of a laser pulse
E_λ	energy of a photon of the laser wavelength λ
f	initiator efficiency
f_1	mole fraction of component 1 in the monomer mixture
f_2	mole fraction of component 2 in the monomer mixture
f_i	mole fraction of component i in the monomer mixture
f_j	mole fraction of component j in the monomer mixture
f_L	focal length
f_n	natural frequency
f_{VP}	mole fraction of 1-vinylpyrrolidin-2-one in the monomer mixture
F	filter
FID	free induction decay
Fl	flange
FT	Fourier-transformation
FTIR	Fourier-transform infrared
FT-NIR	Fourier-transform near-infrared
F_1	mole fraction of component 1 in the copolymer
F_{VP}	mole fraction of 1-vinylpyrrolidin-2-one in the copolymer
gm	geometric mean
g	acceleration of free fall
GBP	gain–bandwidth product
hm	harmonic mean
h	index being 1 or 2
h_{cap}	distance of the two marks in a capillary viscometer
h_P	Planck constant

$h\nu$	photochemical excitation
H	heating jacket
HHMP	2-hydroxy-1-[4-(2-hydroxyethoxy)phenyl]-2-methylpropan-1-one
H ₂ O	dihydrogen oxide
HPC	high-pressure cell
i	index number
I	initiator
InAs	indium arsenide
Inc.	Incorporated
InSb	indium antimonide
IR	infrared
ISA	Industry Standard Architecture
IUPAC	International Union of Pure and Applied Chemistry
$I002$	signal at channel 2 prior to polymerization
$I003$	signal at channel 3 before applying a laser pulse sequence without application of a compensating voltage
$I02$	signal at channel 2 before applying a laser pulse sequence
$I03$	signal at channel 3 before applying a laser pulse sequence while applying a compensating voltage
$I2$	signal at channel 2 after applying a laser pulse sequence
$I002_{ai}$	$I002$ value after applying pulse sequence i
$I002_{bi}$	$I002$ value before applying pulse sequence i
$I002c$	signal at channel 2 prior to polymerization with electromagnetic shutter Sh2 being closed
$I003c$	signal at channel 3 before applying a laser pulse sequence without application of a compensating voltage, with electromagnetic shutter Sh2 being closed
$I02c$	signal at channel 2 before applying a laser pulse sequence with electromagnetic shutter Sh2 being closed

$I03c$	signal at channel 3 before applying a laser pulse sequence while applying a compensating voltage, with electromagnetic shutter Sh2 being closed
$I2c$	signal at channel 2 after applying a laser pulse sequence with electromagnetic shutter Sh2 being closed
$I002_i$	$I002$ value of pulse sequence i
$I002o$	signal at channel 2 prior to polymerization with electromagnetic shutter Sh2 being open
$I003o$	signal at channel 3 before applying a laser pulse sequence without application of a compensating voltage, with electromagnetic shutter Sh2 being open
$I02o$	signal at channel 2 before applying a laser pulse sequence with electromagnetic shutter Sh2 being open
$I03o$	signal at channel 3 before applying a laser pulse sequence while applying a compensating voltage, with electromagnetic shutter Sh2 being open
$I2o$	signal at channel 2 after applying a laser pulse sequence with electromagnetic shutter Sh2 being open
$I3o$	signal at channel 3 after applying a single laser pulse without application of a compensating voltage with electromagnetic shutter Sh2 being open
$I(\tilde{\nu})$	light intensity behind the sample cell at a certain wavenumber
$I_0(\tilde{\nu})$	light intensity in front of the sample cell at a certain wavenumber
j	index number
J	spin–spin coupling constant
k	index number
k_{11}	rate coefficient of homopropagation of the monomer M_1
k_{22}	rate coefficient of homopropagation of the monomer M_2
k_B	Boltzmann constant
k_d	rate coefficient of the initiator decomposition
k_D	diffusion-controlled rate coefficient

k_{HC}	empirical constant of the Hagenbach–Couette correction
k_{hij}	propagation rate coefficient in a binary copolymerization in accordance with the PUE model
k_i	rate coefficient of initiation
k_{ii}	rate coefficient of homopropagation of the monomer M_i
k_{iii}	propagation rate coefficient corresponding to a propagation step with the penultimate monomer unit, the terminal monomer unit, and the monomer molecule being of type M_i
k_{ijj}	propagation rate coefficient corresponding to a propagation step with the types of the penultimate monomer unit, the terminal monomer unit, and the monomer molecule being M_i , M_i , and M_j , respectively
k_{ji}	rate coefficient of cross-propagation with the types of the terminal monomer unit and the monomer molecule being M_i and M_j , respectively
k_{jii}	propagation rate coefficient corresponding to a propagation step with the types of the penultimate monomer unit, the terminal monomer unit, and the monomer molecule being M_j , M_i , and M_i , respectively
k_{jij}	propagation rate coefficient corresponding to a propagation step with the types of the penultimate monomer unit, the terminal monomer unit, and the monomer molecule being M_j , M_i , and M_j , respectively
k_{Osc}	instrument constant
k_p	rate coefficient of propagation
$\langle k_p \rangle$	chain-length averaged rate coefficient of propagation
$k_{p,\text{bulk}}$	propagation rate coefficient of bulk polymerization
$k_{p,C}$	rate coefficient of the chemical reaction of the propagation
$k_{p,\text{copo}}$	overall propagation rate coefficient in a copolymerization
$k_{p,D}$	rate coefficient of the diffusive stage of propagation
$k_{p,D}^0$	rate coefficient of the diffusive stage of propagation at a monomer-to-polymer conversion being equal to zero
$k_{p,X}$	rate coefficient of the first propagation step of radical X^\bullet

k_t	rate coefficient of termination
$\langle k_t \rangle$	chain-length averaged rate coefficient of termination
k_t^0	rate coefficient of termination of two hypothetically coiled radicals of chain length unity
$k_t(1,1)$	rate coefficient of termination of two radicals with chain length unity
$k_{t,C}$	rate coefficient of the chemical reaction of the termination
$k_{t,comb}$	rate coefficient of combination
$k_{t,disp}$	rate coefficient of disproportionation
$k_{t,DM}$	termination rate coefficient of the termination mechanism which is based on diffusion occurring by motion of the macroradical or segments of it
$\langle k_{t,ini} \rangle$	mean (plateau) value of experimental $\langle k_t \rangle$ for the initial polymerization period
$k_t(u,v)$	rate coefficient of termination corresponding to a reaction of radicals of chain length u and v , respectively
$k_{t,RD}$	termination rate coefficient based on reaction diffusion
$k_{tr,X}$	rate coefficient of chain transfer to molecule X
$k_{t,SD}$	termination rate coefficient based on segmental diffusion
$k_{t,TD}$	termination rate coefficient based on translational diffusion
$k_{t,TD}^0$	termination rate coefficient based on translational diffusion at a monomer-to-polymer conversion of zero
k_x	general rate coefficient
K	Kuhn–Mark–Houwink–Sakurada parameter
K_P	Kuhn–Mark–Houwink–Sakurada parameter of the polymer under investigation
K_{St}	Kuhn–Mark–Houwink–Sakurada parameter of the polymer used as calibration standard
l	index number
l_{cap}	length of the capillary
$l_{p^0,rt}$	path length at ambient pressure and temperature

l_{rc}	path length at reaction conditions
L	lens
La	lamp
LIF	Lighting Industry Federation
LPRR	laser-pulse repetition rate
m	multiplet
$\dots - m_{hi}^\bullet$	macroradical with a terminal monomer unit of type M_i and an adjacent, penultimate monomer unit M_h
$\dots - m_i^\bullet$	macroradical with a terminal monomer unit of type M_i
$\dots - m_{ij}^\bullet$	macroradical with a terminal monomer unit of type M_j and an adjacent, penultimate monomer unit M_i
$\dots - m_j^\bullet$	macroradical with a terminal monomer unit of type M_j
m_M	monomer mass
m_{Sol}	solvent mass
M	monomer
M_1	monomer 1
M_2	monomer 2
MAA	methacrylic acid
MALLS	multi-angle laser light scattering
M_b	monomer b
M_i	monomer i
M_j	monomer j
MMA	methyl methacrylate
MMD	molar-mass distribution
MMMP	2-methyl-1-[4-(methylsulfanyl)phenyl]-2-(morpholin-4-yl)propan-1-one
M-MPAm	<i>N</i> ,2-dimethylprop-2-enamide
MPAm	2-methylprop-2-enamide
M	molar mass
M_1	molar mass at the primary point of inflection of the MMD
M_2	molar mass at the secondary point of inflection of the MMD

$M_{\text{D}_2\text{O}}$	molar mass of D_2O
$M_{\text{H}_2\text{O}}$	molar mass of H_2O
M_{M}	monomer molar mass
M_{POI}	molar mass at the point of inflection
M_{r}	relative molecular mass
$M_{\text{r,P}}$	relative molecular mass of the polymer under investigation
$M_{\text{r,St}}$	relative molecular mass of the polymer used as calibration standard
M_{virt}	virtual molar mass
$MWCO$	molecular-weight cut-off
n	refractive index
n_{abs}	amount of absorbed photons
n_i	number of pulses applied during pulse sequence i
n_l	sum of the number of laser pulses applied during sequences l
n_{M}	amount of monomer at monomer conversion α
n_{M}^0	initial amount of monomer
n_{tot}	amount of photons entering the sample cell
NaA	sodium acrylate
NAED	National Association of Electrical Distributors
Na_2HPO_4	disodium hydrogenphosphate
NaNO_3	sodium nitrate
Nd:YCOB	neodymium-doped yttrium calcium oxyborate
Nd:glass	neodymium-doped glass
Nd:YAG	neodymium-doped yttrium aluminum garnet
Nd:YLF	neodymium-doped yttrium lithium fluoride
Nd:YVO ₄	neodymium-doped yttrium orthovanadate
NiMH	nickel–metal hydride
NIR	near infrared
NMR	nuclear magnetic resonance
NTC	negative temperature coefficient
N_{A}	Avogadro constant

N_p	number of applied laser pulses
OPA	operational amplifier
p.a.	pro analysi (Latin: for analysis), purity grade
$p a_{D^+}$	negative decadic logarithm of the activity of deuterium ions
pH	negative decadic logarithm of the activity of hydrogen ions
poly(AA)	poly(acrylic acid)
poly(AA- <i>co</i> -VP)	poly[(acrylic acid)- <i>co</i> -(1-vinylpyrrolidin-2-one)]
poly(DM-PAm)	poly(<i>N,N</i> -dimethylprop-2-enamide)
poly(M-MPAm)	poly(<i>N</i> ,2-dimethylprop-2-enamide)
poly(MPAm)	poly(2-methylprop-2-enamide)
poly(PAm)	poly(prop-2-enamide)
poly(VP)	poly(1-vinylpyrrolidin-2-one)
puriss.	purissimum (Latin: the purest), purity grade
p	pressure
p°	ambient pressure
P	polymer under investigation
PAm	prop-2-enamide
PC	personal computer
PCIe	Peripheral Component Interconnect Express
PFA	perfluoroalkoxy
PG	pressure gauge
PhD	philosophiae doctor (Latin: doctor of philosophy)
PID	Proportional–Integral–Derivative
PLP	pulsed-laser polymerization
POI	point of inflection
PR	positioning ring
Prof.	Professor (German: professor), official title for full professors at German universities
PT	PTFE tube
PTFE	polytetrafluoroethylene

PUE	penultimate-unit effect
P_X	macromolecule with a degree of polymerization of X
P_{X+Y}	macromolecule with a degree of polymerization of $X + Y$
$P_Y^=$	macromolecule with a degree of polymerization of Y carrying an unsaturated chain end
q	quartet
\tilde{q}^\ddagger	partition function per volume of the activated complex
\tilde{q}_M	partition function per volume of the monomer
\tilde{q}_R	partition function per volume of the radical
Q	quartz window
rpm	revolutions per minute
r_{12}	monomer reactivity ratio of the comonomers M_1 and M_2 in accordance with the terminal model
r_{21}	monomer reactivity ratio of the comonomers M_1 and M_2 in accordance with the terminal model
r_c	capture radius
r_{cap}	inside radius of the capillary
res	residual
$r_{h,X}$	hydrodynamic radius of the monomer or the macroradical with a degree of polymerization X
r_{ij}	monomer reactivity ratio of the comonomers M_i and M_j in accordance with the penultimate model
r_{ij}	monomer reactivity ratio of the comonomers M_i and M_j in accordance with the terminal model
r_{jj}	monomer reactivity ratio of the comonomers M_i and M_j in accordance with the penultimate model
®	registered trademark
R	organic substituent group
R_0^\bullet	primary radical
R_1^\bullet	radical with one monomeric unit

RD	reaction diffusion
RG	Rotglas (German: red glass)
RI	refractive index
RS-232	Recommended Standard 232
R_X^\bullet	radical with a degree of polymerization of X
R_{X+1}^\bullet	radical with a degree of polymerization of $X + 1$
R_Y^\bullet	radical with a degree of polymerization of Y
R	gas constant
s	jump distance
s_i	chain-end reactivity ratio with the terminal monomer unit and the monomer being of type i
S	sample
ScP	screw press
SD	segmental diffusion
SEC	size-exclusion chromatography
Sh	electromagnetic shutter
SP	single laser pulse
SP–PLP–EPR	single pulse–pulsed-laser polymerization in conjunction with electron paramagnetic resonance spectroscopy
SP–PLP–NIR	single pulse–pulsed-laser polymerization in conjunction with near-infrared spectroscopy
SPu	sealing punch
St	polymer used as calibration standard
SV	storage vessel
SW	sapphire window
Sync	synchronization
Sh	shoulder
t	triplet
t	time
t_0	time interval between two consecutive laser pulses

T	sheathed thermocouple
TD	translational diffusion
TTL	transistor–transistor logic
T	thermodynamic temperature
n	chain length of a growing radical
n_c	crossover chain length
USB	Universal Serial Bus
UV	ultraviolet
UVM	UV mirror
$U_{\text{post}}(t)$	voltage determined by the transient recorder after applying a laser pulse
$\overline{U_{\text{pre}}}$	average value of a chosen number of voltage values determined before applying the laser pulse
UVd	signal of the UV diode without laser pulsing
UVl	signal of the UV diode while applying a laser pulse
vs	versus
ν	chain length of a growing radical
V	stop valve
VEE	Visual Engineering Environment
VP	1-vinylpyrrolidin-2-one
VSMOW	Vienna Standard Mean Ocean Water
V	irradiated sample volume
V_h	hydrodynamic volume
V_{sol}	volume of the solution
$w_{\text{DM-PAm}}$	mass fraction of <i>N,N</i> -dimethylprop-2-enamide
$w_{\text{DM-PAm}}^0$	initial mass fraction of <i>N,N</i> -dimethylprop-2-enamide
w_{M}	monomer mass fraction
$w_{\text{M-MPAm}}$	mass fraction of <i>N</i> ,2-dimethylprop-2-enamide
$w_{\text{M-MPAm}}^0$	initial mass fraction of <i>N</i> ,2-dimethylprop-2-enamide
w_{MPAm}	mass fraction of 2-methylprop-2-enamide
w_{MPAm}^0	initial mass fraction of 2-methylprop-2-enamide

w_{PAm}	mass fraction of prop-2-enamide
w_{PAm}^0	initial mass fraction of prop-2-enamide
$w_{\text{poly(VP)}}$	mass fraction of poly(1-vinylpyrrolidin-2-one)
w_{VP}	mass fraction of 1-vinylpyrrolidin-2-one
w_{VP}^0	initial mass fraction of 1-vinylpyrrolidin-2-one
X	molecule to which the radical function is transferred by chain transfer
X^\bullet	radical formed by chain transfer
XeF	xenon fluoride
X	degree of polymerization
X_1	degree of polymerization at the primary point of inflection of the molar-mass distribution
X_2	degree of polymerization at the secondary point of inflection of the molar-mass distribution
X_b	degree of polymerization at the b^{th} point of inflection of the molar-mass distribution
Yb:YAG	ytterbium-doped yttrium aluminum garnet
Y	degree of polymerization
ZnSe	zinc selenide
α	monomer-to-polymer conversion
$\bar{\alpha}$	average degree of monomer conversion
α_{ai}	degree of monomer conversion after applying pulse sequence i
α_{ak}	degree of monomer conversion after applying pulse sequence k
α_{bi}	degree of monomer conversion before applying pulse sequence i
α_{bj}	degree of monomer conversion before applying pulse sequence j
α_i	arithmetic mean of the degrees of monomer conversion before and after applying pulse sequence i
β	power-law exponent
β	composite-model exponent for the high-chain-length regime
β_s	composite-model exponent for the small-chain-length regime

δ	chemical shift
ΔF_{VP}	uncertainty of the copolymer composition ascribable to NMR analysis
$\Delta^\ddagger G^\circ$	standard Gibbs energy of activation
$\Delta \tilde{\nu}$	spectral range exiting the monochromator
$\Delta \rho_{art,ai}$	artificial density loss after applying pulse sequence i
$\Delta \rho_{art,bi}$	artificial density loss before applying pulse sequence i
$\overline{\Delta \rho_{art,i}}$	absolute value of the arithmetic mean of the artificial densities
$\Delta^\ddagger V^\circ$	volume of activation
ε_{eff}	effective decadic molar absorption coefficient
ε_{int}	integrated molar decadic absorption coefficient
$\varepsilon(\tilde{\nu})$	molar decadic absorption coefficient at a certain wavenumber
η	dynamic viscosity
$[\eta]$	intrinsic viscosity
η^0	dynamic viscosity of the reaction solution at a monomer-to-polymer conversion of zero
$\eta(\alpha)$	dynamic viscosity of the reaction solution at a certain monomer-to-polymer conversion α
$\eta_r(\alpha)$	relative dynamic viscosity of the reaction solution at a certain monomer-to-polymer conversion α
θ	Celsius temperature
κ	transmission coefficient
κ_c	conductivity
κ_T	isothermal compressibility
K_{cell}	conductivity cell constant
λ	wavelength
ν	kinematic viscosity
$\tilde{\nu}$	wavenumber
ν^0	kinematic viscosity of the reaction solution at a monomer-to-polymer conversion of zero
ν_{LPRR}	laser-pulse repetition rate

ν_n	resonance frequency of the nucleus under investigation
$\tilde{\nu}_{\text{peak}}$	wavenumber at the maximum of the absorption band
ν_{ref}	resonance frequency of a standard
ρ	density
ρ^0	solution density at reaction conditions and zero monomer conversion
ρ_{aqPAm}	density of an aqueous solution of prop-2-enamide
$\rho_{\text{art},i}$	artificial density occurring while applying pulse sequence i
$\rho_{\text{DM-PAm}}$	density of <i>N,N</i> -dimethylprop-2-enamide
ρ_{M}	monomer density
$\rho_{\text{M-MPAm}}$	density of <i>N</i> ,2-dimethylprop-2-enamide
ρ_{Osc}	density of the oscillator
$\rho_{p^\circ, \text{rt}}^0$	solution density at ambient pressure, ambient temperature, and zero monomer conversion
ρ_{sol}	density of the solution
ρ_{Sol}	solvent density
ρ_{VP}	density of 1-vinylpyrrolidin-2-one
ρ_{VSMOW}	density of Vienna Standard Mean Ocean Water
Φ	quantum yield

References

- [1] L. H. Baekeland, *Chemiker-Zeitung* **1909**, *33*, 317–318.
- [2] H. Staudinger, *Ber. dtsh. Chem. Ges. A/B* **1920**, *53*, 1073–1085.
- [3] *Plastics – the Facts 2012 – An analysis of European plastics production, demand and waste data for 2011*, Plastics Europe, EuPC, EuPR, EPRO, 2012, pp. 1–36.
- [4] M. Akbari, M. H. Fazelipour, A. S. Goharizi, *Biotechnol. Bioproc. Eng.* **2011**, *16*, 407–412.
- [5] L. Yunkai, X. Tingwu, O. Zhiyun, L. Xiongcai, L. Honglu, H. Zhongyong, Y. Peiling, *J. Appl. Polym. Sci.* **2009**, *113*, 3510–3519.
- [6] L. Aktay, A. F. Johnson, M. Holzapfel, *Comp. Mater. Sci.* **2005**, *32*, 252–260.
- [7] W. A. Livesey, A. Robinson, *The Repair of Vehicle Bodies*, 5th edition, Butterworth-Heinemann, Oxford, London 2005, p. 559.
- [8] H.-G. Elias, *Makromoleküle – Industrielle Polymere und Synthesen*, 6th edition, Vol. 3, WILEY-VCH, Weinheim 2001, p. 211.
- [9] G. Wypych, *Handbook of Polymers*, ChemTec Publishing, Toronto 2012, pp. 247–249.
- [10] M. Buback, M. Egorov, T. Junkers, E. Panchenko, *Macromol. Rapid Commun.* **2004**, *25*, 1004–1009.
- [11] J. Barth, *Radical Polymerization Kinetics in Systems with Transfer Reactions Studied by Pulsed-Laser-Polymerization and Online EPR-Detection*, PhD thesis, <http://hdl.handle.net/11858/00-1735-0000-0006-B075-2>, Göttingen, 2011.
- [12] M. Buback, H. Hippler, J. Schweer, H.-P. Vögele, *Makromol. Chem., Rapid Commun.* **1986**, *7*, 261–265.
- [13] C. Barner-Kowollik, M. Buback, M. Egorov, T. Fukuda, A. Goto, O. F. Olaj, G. T. Russell, P. Vana, B. Yamada, P. B. Zetterlund, *Prog. Polym. Sci.* **2005**, *30*, 605–643.
- [14] O. F. Olaj, I. Bitai, F. Hinkelmann, *Makromol. Chem.-Macromol. Chem. Phys.* **1987**, *188*, 1689–1702.
- [15] S. Beuermann, *Pure Appl. Chem.* **2003**, *75*, 1091–1096.

- [16] S. Beuermann, M. Buback, *Pure Appl. Chem.* **1998**, *70*, 1415–1418.
- [17] S. Beuermann, M. Buback, T. P. Davis, R. G. Gilbert, R. A. Hutchinson, A. Kajiwar, B. Klumperman, G. T. Russell, *Macromol. Chem. Phys.* **2000**, *201*, 1355–1364.
- [18] C. Barner-Kowollik, F. Günzler, T. Junkers, *Macromolecules* **2008**, *41*, 8971–8973.
- [19] A. N. Nikitin, R. A. Hutchinson, M. Buback, P. Hesse, *Macromolecules* **2007**, *40*, 8631–8641.
- [20] S. Beuermann, M. Buback, G. T. Russell, *Macromol. Rapid Commun.* **1994**, *15*, 351–355.
- [21] R. G. Gilbert, *Pure Appl. Chem.* **1996**, *68*, 1491–1494.
- [22] S. Beuermann, M. Buback, T. P. Davis, R. G. Gilbert, R. A. Hutchinson, O. F. Olaj, G. T. Russell, J. Schweer, A. M. van Herk, *Macromol. Chem. Phys.* **1997**, *198*, 1545–1560.
- [23] R. A. Hutchinson, S. Beuermann, D. A. Paquet, J. H. McMin, *Macromolecules* **1997**, *30*, 3490–3493.
- [24] M. Buback, U. Geers, C. H. Kurz, *Macromol. Chem. Phys.* **1997**, *198*, 3451–3464.
- [25] M. Buback, C. H. Kurz, C. Schmaltz, *Macromol. Chem. Phys.* **1998**, *199*, 1721–1727.
- [26] M. Buback, C. H. Kurz, *Macromol. Chem. Phys.* **1998**, *199*, 2301–2310.
- [27] B. Dervaux, T. Junkers, M. Schneider-Baumann, F. E. Du Prez, C. Barner-Kowollik, *J. Polym. Sci., Part A: Polym. Chem.* **2009**, *47*, 6641–6654.
- [28] T. Junkers, D. Voll, C. Barner-Kowollik, *e-Polymers* **2009**, *076*, 1–8.
- [29] R. Siegm, S. Beuermann, *Macromolecules* **2010**, *43*, 3699–3704.
- [30] C. Barner-Kowollik, F. Bennet, M. Schneider-Baumann, D. Voll, T. Rölle, T. Fäcke, M. S. Weiser, F. K. Bruder, T. Junkers, *Polym. Chem.* **2010**, *1*, 470–479.
- [31] T. Junkers, M. Schneider-Baumann, S. P. S. Koo, P. Castignolles, C. Barner-Kowollik, *Macromolecules* **2010**, *43*, 10427–10434.
- [32] S. Beuermann, M. Buback, *Prog. Polym. Sci.* **2002**, *27*, 191–254.
- [33] I. Lacík, S. Beuermann, M. Buback, *Macromolecules* **2001**, *34*, 6224–6228.
- [34] S. Beuermann, M. Buback, P. Hesse, F.-D. Kuchta, I. Lacík, A. M. van Herk, *Pure Appl. Chem.* **2007**, *79*, 1463–1469.

- [35] F.-D. Kuchta, A. M. van Herk, A. L. German, *Macromolecules* **2000**, *33*, 3641–3649.
- [36] F. Ganachaud, M. J. Monteiro, R. G. Gilbert, *Macromol. Symp.* **2000**, *150*, 275–281.
- [37] F. Ganachaud, R. Balic, M. J. Monteiro, R. G. Gilbert, *Macromolecules* **2000**, *33*, 8589–8596.
- [38] I. Lacík, S. Beuermann, M. Buback, *Macromolecules* **2003**, *36*, 9355–9363.
- [39] I. Lacík, S. Beuermann, M. Buback, *Macromol. Chem. Phys.* **2004**, *205*, 1080–1087.
- [40] S. A. Seabrook, M. P. Tonge, R. G. Gilbert, *J. Polym. Sci., Part A: Polym. Chem.* **2005**, *43*, 1357–1368.
- [41] S. Beuermann, M. Buback, P. Hesse, I. Lacík, *Macromolecules* **2006**, *39*, 184–193.
- [42] S. Beuermann, M. Buback, P. Hesse, S. Kukučková, I. Lacík, *Macromol. Symp.* **2007**, *248*, 23–32.
- [43] S. Beuermann, M. Buback, P. Hesse, S. Kukučková, I. Lacík, *Macromol. Symp.* **2007**, *248*, 41–49.
- [44] M. Buback, P. Hesse, I. Lacík, *Macromol. Rapid Commun.* **2007**, *28*, 2049–2054.
- [45] M. Stach, I. Lacík, D. Chorvát, M. Buback, P. Hesse, R. A. Hutchinson, L. Tang, *Macromolecules* **2008**, *41*, 5174–5185.
- [46] M. Stach, I. Lacík, P. Kasák, D. Chorvát, A. J. Saunders, S. Santanakrishnan, R. A. Hutchinson, *Macromol. Chem. Phys.* **2010**, *211*, 580–593.
- [47] I. Lacík, L. Učňová, S. Kukučková, M. Buback, P. Hesse, S. Beuermann, *Macromolecules* **2009**, *42*, 7753–7761.
- [48] S. Ponratnam, S. L. Kapur, *J. Polym. Sci., Polym. Chem. Ed.* **1976**, *14*, 1987–1992.
- [49] S. Santanakrishnan, M. Stach, I. Lacík, R. A. Hutchinson, *Macromol. Chem. Phys.* **2012**, *213*, 1330–1338.
- [50] E. E. L. Kathmann, C. L. McCormick, *Macromolecules* **1993**, *26*, 5249–5252.
- [51] M. Haque, *A Kinetic Study of Acrylamide/ Acrylic Acid Copolymerization*, Master thesis, <http://hdl.handle.net/10012/5193>, Waterloo, 2010.
- [52] M. Buback, R. G. Gilbert, G. T. Russell, D. J. T. Hill, G. Moad, K. F. O'Driscoll, J. Shen, M. A. Winnik, *J. Polym. Sci., Part A: Polym. Chem.* **1992**, *30*, 851–863.
- [53] A. N. Nikitin, R. A. Hutchinson, *Macromolecules* **2005**, *38*, 1581–1590.
- [54] S. Penczek, G. Moad, *Pure Appl. Chem.* **2008**, *80*, 2163–2193.

- [55] H.-G. Elias, *Macromolecules – Chemical Structures and Synthesis*, 6th edition, Vol. 1, WILEY-VCH, Weinheim 2005, pp. 326–327.
- [56] H.-G. Elias, *Macromolecules – Chemical Structures and Synthesis*, 6th edition, Vol. 1, WILEY-VCH, Weinheim 2005, pp. 312–321.
- [57] D. S. Achilias, *Macromol. Theory Simul.* **2007**, *16*, 319–347.
- [58] M. J. Ballard, D. H. Napper, R. G. Gilbert, *J. Polym. Sci., Part A: Polym. Chem.* **1984**, *22*, 3225–3253.
- [59] T. G. Carswell, D. J. T. Hill, D. I. Londero, J. H. O'Donnell, P. J. Pomery, C. L. Winzor, *Polymer* **1992**, *33*, 137–140.
- [60] P. B. Zetterlund, H. Yamazoe, B. Yamada, D. J. T. Hill, P. J. Pomery, *Macromolecules* **2001**, *34*, 7686–7691.
- [61] P. B. Zetterlund, S. Yamauchi, B. Yamada, *Macromol. Chem. Phys.* **2004**, *205*, 778–785.
- [62] A. Beer, *Ann. Phys. Chem.* **1852**, *86*, 78–88.
- [63] J. H. Lambert, *Photometria sive de Mensura et Gradibus Luminis, Colorum et Umbrae*, Eberhard Klett, Augsburg 1760, p. 391.
- [64] P. Bouguer, *Essai d'Optique, sur la gradation de la lumiere*, Claude Jombert, Paris 1729, pp. 63–67.
- [65] M. von Smoluchowsky, *Z. Phys. Chem.* **1917**, *92*, 129–168.
- [66] A. Einstein, *Ann. Phys.* **1905**, *17*, 549–560.
- [67] M. Buback, *Makromol. Chem.-Macromol. Chem. Phys.* **1990**, *191*, 1575–1587.
- [68] H. Yamazoe, P. B. Zetterlund, B. Yamada, D. J. T. Hill, P. J. Pomery, *Macromol. Chem. Phys.* **2001**, *202*, 824–829.
- [69] M. J. Ballard, R. G. Gilbert, D. H. Napper, P. J. Pomery, P. W. O'Sullivan, J. H. O'Donnell, *Macromolecules* **1986**, *19*, 1303–1308.
- [70] S. Zhu, Y. Tian, A. E. Hamielec, D. R. Eaton, *Polymer* **1990**, *31*, 154–159.
- [71] S. Beuermann, M. Buback, P. Hesse, T. Junkers, I. Lacík, *Macromolecules* **2006**, *39*, 509–516.
- [72] S. C. Thickett, R. G. Gilbert, *Polymer* **2004**, *45*, 6993–6999.
- [73] K. J. Laidler, M. C. King, *J. Phys. Chem.* **1983**, *87*, 2657–2664.

- [74] H. Eyring, *J. Chem. Phys.* **1935**, *3*, 107–115.
- [75] E. R. Cohen, T. Cvitaš, J. G. Frey, B. Holmström, K. Kuchitsu, R. Marquardt, I. Mills, F. Pavese, M. Quack, J. Stohner, H. L. Strauss, M. Takami, A. J. Thor, *IUPAC Green Book – Quantities, Units and Symbols in Physical Chemistry*, 3rd edition, IUPAC & RSC Publishing, Cambridge 2008, p. 67.
- [76] J. P. A. Heuts, R. G. Gilbert, L. Radom, *Macromolecules* **1995**, *28*, 8771–8781.
- [77] G. Moad, E. Rizzardo, D. H. Solomon, A. L. J. Beckwith, *Polym. Bull.* **1992**, *29*, 647–652.
- [78] P. B. Zetterlund, W. K. Busfield, I. D. Jenkins, *Macromolecules* **2002**, *35*, 7232–7237.
- [79] A. A. Gridnev, S. D. Ittel, *Macromolecules* **1996**, *29*, 5864–5874.
- [80] J. P. A. Heuts, G. T. Russell, G. B. Smith, A. M. van Herk, *Macromol. Symp.* **2007**, *248*, 12–22.
- [81] G. B. Smith, J. P. A. Heuts, G. T. Russell, *Macromol. Symp.* **2005**, *226*, 133–146.
- [82] R. X. E. Willemse, B. B. P. Staal, A. M. van Herk, S. C. J. Pierik, B. Klumperman, *Macromolecules* **2003**, *36*, 9797–9803.
- [83] O. F. Olaj, P. Vana, M. Zoder, A. Kornherr, G. Zifferer, *Macromol. Rapid Commun.* **2000**, *21*, 913–920.
- [84] O. F. Olaj, M. Zoder, P. Vana, A. Kornherr, I. Schnöll-Bitai, G. Zifferer, *Macromolecules* **2005**, *38*, 1944–1948.
- [85] S. Beuermann, *Macromolecules* **2002**, *35*, 9300–9305.
- [86] G. B. Smith, G. T. Russell, M. Yin, J. P. A. Heuts, *Eur. Polym. J.* **2005**, *41*, 225–230.
- [87] J. P. A. Heuts, G. T. Russell, *Eur. Polym. J.* **2006**, *42*, 3–20.
- [88] J. P. A. Heuts, G. T. Russell, G. B. Smith, *Aust. J. Chem.* **2007**, *60*, 754–764.
- [89] H.-G. Elias, *Macromolecules – Chemical Structures and Synthesis*, 6th edition, Vol. 1, WILEY-VCH, Weinheim 2005, p. 324.
- [90] R. Szymanski, *Macromol. Theory Simul.* **2011**, *20*, 8–12.
- [91] M. Buback, M. Egorov, R. G. Gilbert, V. Kaminsky, O. F. Olaj, G. T. Russell, P. Vana, G. Zifferer, *Macromol. Chem. Phys.* **2002**, *203*, 2570–2582.
- [92] M. Buback, L. H. Garcia-Rubio, R. G. Gilbert, D. H. Napper, J. Guillot, A. E. Hamielec, D. Hill, K. F. O'Driscoll, O. F. Olaj, J. C. Shen, D. Solomon, G. Moad,

- M. Stickler, M. Tirrell, M. A. Winnik, *J. Polym. Sci., Part C: Polym. Lett.* **1988**, *26*, 293–297.
- [93] S. W. Benson, A. M. North, *J. Am. Chem. Soc.* **1959**, *81*, 1339–1345.
- [94] S. W. Benson, A. M. North, *J. Am. Chem. Soc.* **1962**, *84*, 935–940.
- [95] S. K. Soh, D. C. Sundberg, *J. Polym. Sci., Part A: Polym. Chem.* **1982**, *20*, 1315–1329.
- [96] G. V. Schulz, *Z. Phys. Chem.* **1956**, *8*, 290–317.
- [97] M. Buback, B. Huckestein, G. T. Russell, *Macromol. Chem. Phys.* **1994**, *195*, 539–554.
- [98] H.-H. Schuh, H. Fischer, *Helv. Chim. Acta* **1978**, *61*, 2130–2164.
- [99] H. Fischer, *Chem. Phys. Lett.* **1983**, *100*, 255–258.
- [100] H. Schuh, H. Fischer, *Int. J. Chem. Kinet.* **1976**, *8*, 341–356.
- [101] H. Fischer, H. Paul, *Acc. Chem. Res.* **1987**, *20*, 200–206.
- [102] G. T. Russell, R. G. Gilbert, D. H. Napper, *Macromolecules* **1993**, *26*, 3538–3552.
- [103] M. Buback, J. Schweer, *Z. Phys. Chem. Neue Folge* **1989**, *161*, 153–165.
- [104] J. Schweer, *Bestimmung individueller Geschwindigkeitskoeffizienten radikalischer Polymerisationen aus Laserpulsexperimenten mit Infrarotspektroskopischer Umsatzdetektion im Mikrosekunden-Bereich*, PhD thesis, Göttingen, 1988.
- [105] P. E. M. Allen, C. R. Patrick, *Makromol. Chem.* **1964**, *72*, 106–118.
- [106] G. T. Russell, D. H. Napper, R. G. Gilbert, *Macromolecules* **1988**, *21*, 2133–2140.
- [107] M. Buback, B. Degener, *Makromol. Chem.-Macromol. Chem. Phys.* **1993**, *194*, 2875–2883.
- [108] R. G. W. Norrish, R. R. Smith, *Nature* **1942**, *150*, 336–337.
- [109] E. Trommsdorff, H. Köhle, P. Lagally, *Makromol. Chem.-Macromol. Chem. Phys.* **1948**, *1*, 169–198.
- [110] S. Beuermann, M. Buback, G. T. Russell, *Macromol. Chem. Phys.* **1995**, *196*, 2493–2516.
- [111] S. Beuermann, M. Buback, P. Hesse, R. A. Hutchinson, S. Kukučková, I. Lacík, *Macromolecules* **2008**, *41*, 3513–3520.
- [112] S. Santanakrishnan, L. Tang, R. A. Hutchinson, M. Stach, I. Lacík, J. Schrooten, P. Hesse, M. Buback, *Macromol. React. Eng.* **2010**, *4*, 499–509.

- [113] J. Schrooten, M. Buback, P. Hesse, R. A. Hutchinson, I. Lacík, *Macromol. Chem. Phys.* **2011**, *212*, 1400–1409.
- [114] O. F. Olaj, G. Zifferer, *Macromolecules* **1987**, *20*, 850–861.
- [115] O. F. Olaj, A. Kornherr, G. Zifferer, *Macromol. Theory Simul.* **1998**, *7*, 501–508.
- [116] G. Moad, D. H. Solomon, *The Chemistry of Radical Polymerization*, 2nd edition, Elsevier Ltd, Amsterdam 2006, p. 245.
- [117] G. B. Smith, G. T. Russell, J. P. A. Heuts, *Macromol. Theory Simul.* **2003**, *12*, 299–314.
- [118] M. J. Roedel, *J. Am. Chem. Soc.* **1953**, *75*, 6110–6112.
- [119] K. Horie, M. Barón, R. B. Fox, J. He, M. Hess, J. Kahovec, T. Kitayama, P. Kubisa, E. Maréchal, W. Mormann, R. F. T. Stepto, D. Tabak, J. Vohlídal, E. S. Wilks, W. J. Work, *Pure Appl. Chem.* **2004**, *76*, 889–906.
- [120] K. J. Laidler, *Pure Appl. Chem.* **1996**, *68*, 149–192.
- [121] J. J. Kurland, *J. Polym. Sci., Polym. Chem. Ed.* **1980**, *18*, 1139–1145.
- [122] L. B. Levy, *Plant/Oper. Prog.* **1987**, *6*, 188–189.
- [123] H. Becker, H. Vogel, *Chem. Eng. Technol.* **2006**, *29*, 1227–1231.
- [124] S. Schulze, H. Vogel, *Chem. Eng. Technol.* **1998**, *21*, 829–837.
- [125] R. Shenoy, C. N. Bowman, *Macromolecules* **2010**, *43*, 7964–7970.
- [126] C. E. Barnes, *J. Am. Chem. Soc.* **1945**, *67*, 217–220.
- [127] T. Alfrey, Jr., G. Goldfinger, *J. Chem. Phys.* **1944**, *12*, 205–209.
- [128] F. R. Mayo, F. M. Lewis, *J. Am. Chem. Soc.* **1944**, *66*, 1594–1601.
- [129] I. Sakurada, "Kongo Jugo (Mixed Polymerization)", in: *Konjugo Hanno (High Polymerization Reaction)*, Kobunshi Kagaku Kyokai (Polymer Chemistry Association), Ed., Tokyo 1946, pp. 35–41.
- [130] I. Sakurada, *Polym. J.* **2012**, *44*, 11–13.
- [131] T. Fukuda, Y. D. Ma, H. Inagaki, *Macromolecules* **1985**, *18*, 17–26.
- [132] T. Fukuda, Y. D. Ma, K. Kubo, H. Inagaki, *Macromolecules* **1991**, *24*, 370–375.
- [133] S. A. Jones, G. S. Prementine, D. A. Tirrell, *J. Am. Chem. Soc.* **1985**, *107*, 5275–5276.
- [134] D. J. T. Hill, J. H. O'Donnell, P. W. O'Sullivan, *Macromolecules* **1982**, *15*, 960–966.

- [135] E. Merz, T. Alfrey, G. Goldfinger, *J. Polym. Sci.* **1946**, *1*, 75–82.
- [136] P. B. Zetterlund, S. Tagashira, K. Izumi, Y. Nagano, M. Azukizawa, H. Yamazoe, M. Kumagai, B. Yamada, *Macromolecules* **2002**, *35*, 8209–8215.
- [137] J. P. A. Heuts, R. G. Gilbert, I. A. Maxwell, *Macromolecules* **1997**, *30*, 726–736.
- [138] T. Fukuda, Y. D. Ma, H. Inagaki, *Makromol. Chem., Rapid Commun.* **1987**, *8*, 495–499.
- [139] H. Eyring, *Chem. Rev.* **1935**, *17*, 65–77.
- [140] E. R. Cohen, T. Cvitaš, J. G. Frey, B. Holmström, K. Kuchitsu, R. Marquardt, I. Mills, F. Pavese, M. Quack, J. Stohner, H. L. Strauss, M. Takami, A. J. Thor, *IUPAC Green Book – Quantities, Units and Symbols in Physical Chemistry*, 3rd edition, IUPAC & RSC Publishing, Cambridge 2008, pp. 65–66.
- [141] R. A. Alberty, *Pure Appl. Chem.* **2001**, *73*, 1349–1380.
- [142] S. D. Hamann, W. J. le Noble, *J. Chem. Educ.* **1984**, *61*, 658–660.
- [143] Y. Sueishi, N. Nishimura, K. Hirata, K. Kuwata, *Bull. Chem. Soc. Jpn.* **1988**, *61*, 4253–4257.
- [144] R. van Eldik, T. Asano, W. J. le Noble, *Chem. Rev.* **1989**, *89*, 549–688.
- [145] N. Nishimura, T. Tanaka, T. Motoyama, *Can. J. Chem.* **1987**, *65*, 2248–2253.
- [146] Y. Yoshimura, M. Nakahara, *J. Chem. Phys.* **1984**, *81*, 4080–4086.
- [147] J. Schroeder, J. Troe, *Chem. Phys. Lett.* **1985**, *116*, 453–459.
- [148] S. R. Logan, *J. Chem. Educ.* **1982**, *59*, 279–281.
- [149] K. J. Laidler, *J. Chem. Educ.* **1984**, *61*, 494–498.
- [150] J. H. van't Hoff, *Études de dynamique chimique*, Frederik Muller & Co., Amsterdam 1884, pp. 114–118.
- [151] S. Arrhenius, *Z. Phys. Chem.* **1889**, *4*, 226–248.
- [152] H. Eyring, J. Hirschfelder, *J. Phys. Chem.* **1937**, *41*, 249–257.
- [153] R. H. Ewell, H. Eyring, *J. Chem. Phys.* **1937**, *5*, 726–736.
- [154] R. H. Ewell, *J. Appl. Phys.* **1938**, *9*, 252–269.
- [155] S. Glasstone, K. J. Laidler, H. Eyring, *International Chemical Series – The Theory of Rate Processes – The Kinetics of Chemical Reactions, Viscosity, Diffusion and Electrochemical*

- Phenomena*, 1st edition, Louis P. Hammett, Ed., McGraw-Hill Book Company, New York, London 1941, pp. 477–495.
- [156] S. Glasstone, K. J. Laidler, H. Eyring, *International Chemical Series – The Theory of Rate Processes – The Kinetics of Chemical Reactions, Viscosity, Diffusion and Electrochemical Phenomena*, 1st edition, Louis P. Hammett, Ed., McGraw-Hill Book Company, New York, London 1941, p. 523.
- [157] S. Glasstone, K. J. Laidler, H. Eyring, *International Chemical Series – The Theory of Rate Processes – The Kinetics of Chemical Reactions, Viscosity, Diffusion and Electrochemical Phenomena*, 1st edition, Louis P. Hammett, Ed., McGraw-Hill Book Company, New York, London 1941, pp. 506–507.
- [158] P. Kratochvil, U. W. Suter, *Pure Appl. Chem.* **1989**, *61*, 211–241.
- [159] H.-G. Elias, *Macromolecules – Chemical Structures and Synthesis*, 6th edition, Vol. 1, WILEY-VCH, Weinheim 2005, pp. 77–78.
- [160] Z. Grubisic, P. Rempp, H. Benoit, *J. Polym. Sci., Part B: Polym. Lett.* **1967**, *5*, 753–759.
- [161] P. J. Flory, *J. Chem. Phys.* **1945**, *13*, 453–465.
- [162] W. Kuhn, *Kolloid-Zeitschrift* **1934**, *68*, 2–15.
- [163] H. Mark, "Über die Entstehung und Eigenschaften hochpolymerer Festkörper", in: *Der feste Körper – Vorträge an der Tagung der Physikalischen Gesellschaft Zürich anlässlich der Feier ihres 50jährigen Bestehens*, Raymund Sänger, Ed., S. Hirzel, Leipzig 1938, pp. 65–104.
- [164] R. Houwink, *J. Prakt. Chem.* **1940**, *157*, 15–18.
- [165] I. Sakurada, *Polym. J.* **2012**, *44*, 5–10.
- [166] I. Sakurada, "Yoekichu ni okeru itojo-bunshi no katachi narabini yoekinendo to bunshiryo no kankei (Shape of threadlike molecules in solution, and relationship between solution viscosity and molecular weight)", in: *Nihon Kagaku Sen'i Kenkyusho Koenshu (Collected lectures of the Japanese Institute for Chemical Fibers Research)*, Tokyo 1940, pp. 33–44.
- [167] W. F. Reed, *Macromol. Chem. Phys.* **1995**, *196*, 1539–1575.
- [168] P. J. Wyatt, *Anal. Chim. Acta* **1993**, *272*, 1–40.

- [169] T. P. Davis, K. F. O'Driscoll, M. C. Piton, M. A. Winnik, *Macromolecules* **1989**, *22*, 2785–2788.
- [170] M. Buback, M. Busch, R. A. Lämmel, *Macromol. Theory Simul.* **1996**, *5*, 845–861.
- [171] O. F. Olaj, I. Bitai, *Angew. Makromol. Chem.* **1987**, *155*, 177–190.
- [172] B. O'Shaughnessy, D. Vavylonis, *Macromol. Theory Simul.* **2003**, *12*, 401–412.
- [173] G. Zifferer, A. Kornherr, I. Schnöll-Bitai, O. F. Olaj, *Macromol. Symp.* **2004**, *217*, 289–294.
- [174] M. Buback, R. G. Gilbert, R. A. Hutchinson, B. Klumperman, F. D. Kuchta, B. G. Manders, K. F. O'Driscoll, G. T. Russell, J. Schweer, *Macromol. Chem. Phys.* **1995**, *196*, 3267–3280.
- [175] R. A. Hutchinson, M. T. Aronson, J. R. Richards, *Macromolecules* **1993**, *26*, 6410–6415.
- [176] J. W. Verhoeven, *Pure Appl. Chem.* **1996**, *68*, 2223–2286.
- [177] S. Wartewig, *IR and Raman Spectroscopy – Fundamental Processing*, WILEY-VCH, Weinheim 2003, pp. 35–49.
- [178] F. J. Harris, *Proc. IEEE* **1978**, *66*, 51–83.
- [179] K. H. Michaelian, *Infrared Phys.* **1989**, *29*, 87–100.
- [180] H.-G. Elias, *Macromolecules – Chemical Structures and Synthesis*, 6th edition, Vol. 1, WILEY-VCH, Weinheim 2005, pp. 93–94.
- [181] J. L. L. M. Poiseuille, *Comp. Ren. S. Acad. Sci.* **1840**, *11*, 961–967.
- [182] G. H. L. Hagen, "Über die Bewegung des Wassers in cylindrischen, nahe horizontalen Leitungen", in: *Abhandlungen der Königlichen Akademie der Wissenschaften zu Berlin – Aus dem Jahre 1869*, G. Vogt, Ed., Buchdruckerei der Königlichen Akademie der Wissenschaften, Berlin 1870, Vol. II, pp. 1–14.
- [183] J. L. L. M. Poiseuille, *Comp. Ren. S. Acad. Sci.* **1840**, *11*, 1041–1044.
- [184] J. L. L. M. Poiseuille, *Comp. Ren. S. Acad. Sci.* **1840**, *11*, 1044–1048.
- [185] J. L. L. M. Poiseuille, *Comp. Ren. S. Acad. Sci.* **1840**, *11*, 112–115.
- [186] Information brochure, *DMA Externe Meßzellen*, Anton PAAR, Graz, pp. 4–5.
- [187] R. K. Harris, E. D. Becker, S. M. Cabral de Menezes, P. Granger, R. E. Hoffman, K. W. Zilm, *Pure Appl. Chem.* **2008**, *80*, 59–84.

-
- [188] Sigma-Aldrich Chemie, *Technical Information*, **2012**.
- [189] M. Buback, *Angew. Chem. Int. Ed. Engl.* **1991**, *30*, 641–653.
- [190] T. C. Poulter, *Phys. Rev.* **1932**, *40*, 860–871.
- [191] M. B. Huglin, *J. Appl. Polym. Sci.* **1965**, *9*, 4003–4024.
- [192] C. Kowollik, *Propagation and Termination Kinetics in Free-Radical Bulk Copolymerizations of Acrylate/Acrylate and Acrylate/Methacrylate Systems Studied by Pulsed Laser Techniques*, PhD thesis, Göttingen, 1999.
- [193] B. Degener, *Laserinduzierte radikalische Polymerisation von Butylacrylat in einem weiten Umsatzbereich*, PhD thesis, Göttingen, 1992.
- [194] N. Tanaka, G. Girard, R. Davis, A. Peuto, N. Bignell, *Metrologia* **2001**, *38*, 301–309.
- [195] F. Kohlrausch, *Praktische Physik*, 22nd edition, Vol. 3, B. G. Teubner, Stuttgart 1968, p. 40.
- [196] *Guideline on the Use of Fundamental Physical Constants and Basic Constants of Water*, The International Association for the Properties of Water and Steam, Gaithersburg, Maryland, 2001, pp. 1–7.
- [197] D. R. Lide, *Handbook of Chemistry and Physics*, 84th edition, CRC Press, Boca Raton 2004, p. 3/228.
- [198] Material Safety Data Sheet, *EG-Sicherheitsdatenblatt – N-Methyl methacrylamide*, ABCR, Karlsruhe, 2007, pp. 1–3.
- [199] A. Chovancová, L. Učňová, I. Lacík, Report, *PLP-SEC STUDIES ON ACRYLAMIDE AQUEOUS-PHASE POLYMERIZATION*, Bratislava, 2012, pp. 1–27.
- [200] W. Wagner, A. Pruss, *J. Phys. Chem. Ref. Data* **2002**, *31*, 387–535.
- [201] R. J. Sension, B. S. Hudson, *J. Chem. Phys.* **1989**, *90*, 1377–1389.
- [202] A. B. Sieval, A. L. Demirel, J. W. M. Nissink, M. R. Linford, J. H. van der Maas, W. H. de Jeu, H. Zuilhof, E. J. R. Sudholter, *Langmuir* **1998**, *14*, 1759–1768.
- [203] J. T. Lyon, H. G. Cho, L. Andrews, *Organometallics* **2007**, *26*, 6373–6387.
- [204] R. A. Nyquist, *Variables in Data Interpretation of Infrared and Raman Spectra – Interpreting Infrared, Raman, and Nuclear Magnetic Resonance Spectra*, Vol. 1, Academic Press, San Diego, London 2001, p. 60.
-

- [205] J. J. Max, C. Chapados, *J. Chem. Phys.* **2009**, *131*, 184505-1–184505-13.
- [206] Information brochure, *V-50 – 2,2'-Azobis (2-amidinopropane) dihydrochloride*, Wako, Osaka, p. 3.
- [207] P. K. Glasoe, F. A. Long, *J. Phys. Chem.* **1960**, *64*, 188–190.
- [208] A. Feldermann, *Terminierungskinetik radikalischer Homo- und Copolymerisationen bis zu hohen Monomerumsätzen*, PhD thesis, <http://hdl.handle.net/11858/00-1735-0000-0006-B0B5-0>, Göttingen, 2003.
- [209] T. Junkers, *Novel Single Pulse–Pulsed Laser Polymerization Methods for the Determination of Chain-Length Dependent Termination Kinetics in Conventional and Controlled Free-Radical Polymerization*, PhD thesis, Göttingen, 2006.
- [210] A. M. van Herk, *J. Chem. Educ.* **1995**, *72*, 138–140.
- [211] A. M. van Herk, T. Dröge, *Macromol. Theory Simul.* **1997**, *6*, 1263–1276.
- [212] P. S. Engel, C. Steel, *Acc. Chem. Res.* **1973**, *6*, 275–281.
- [213] M. Buback, H. Frauendorf, O. Janssen, P. Vana, *J. Polym. Sci., Part A: Polym. Chem.* **2008**, *46*, 6071–6081.
- [214] M. Buback, H. Frauendorf, F. Günzler, P. Vana, *J. Polym. Sci., Part A: Polym. Chem.* **2007**, *45*, 2453–2467.
- [215] M. Buback, H. Frauendorf, F. Günzler, P. Vana, *Polymer* **2007**, *48*, 5590–5598.
- [216] R. G. W. Norrish, F. W. Kirkbride, *J. Chem. Soc.* **1932**, 1518–1530.
- [217] M. Buback, A. Kuelpmann, *Macromol. Chem. Phys.* **2003**, *204*, 632–637.
- [218] P. Vana, T. P. Davis, C. Barner-Kowollik, *Aust. J. Chem.* **2002**, *55*, 315–318.
- [219] H. Fischer, R. Baer, R. Hany, I. Verhoolen, M. Walbiner, *J. Chem. Soc., Perkin Trans. 2* **1990**, 787–798.
- [220] C. J. Groenenboom, H. J. Hageman, T. Overeem, A. J. M. Weber, *Makromol. Chem.-Macromol. Chem. Phys.* **1982**, *183*, 281–292.
- [221] C. Barner-Kowollik, P. Vana, T. P. Davis, *J. Polym. Sci., Part A: Polym. Chem.* **2002**, *40*, 675–681.
- [222] Z. Szablan, T. Junkers, S. P. S. Koo, T. M. Lovestead, T. P. Davis, M. H. Stenzel, C. Barner-Kowollik, *Macromolecules* **2007**, *40*, 6820–6833.
- [223] M. Buback, M. Busch, C. Kowollik, *Macromol. Theory Simul.* **2000**, *9*, 442–452.

- [224] M. Buback, C. Kowollik, C. Kurz, A. Wahl, *Macromol. Chem. Phys.* **2000**, *201*, 464–469.
- [225] Catalog, *BOLA Katalog – Profi-Laborbedarf aus Hochleistungskunststoffen – PTFE | PFA | FEP*, Bohlender, Grünsfeld, 2010, pp. 219–225.
- [226] Flowserve Corporation, Specification Sheet, *PFA vs. PTFE: Debunking The Myth*, Cookeville, 1999, pp. 1–2.
- [227] Y. V. Sytyi, B. I. Molchanov, M. M. Gudimov, Y. V. Zherdev, A. I. Soshko, E. S. Golovastov, A. N. Tynnyi, N. G. Kalinin, *Mat. Sci.* **1974**, *7*, 457–458.
- [228] Catalog, *BOLA Katalog – Profi-Laborbedarf aus Hochleistungskunststoffen – PTFE | PFA | FEP*, Bohlender, Grünsfeld, 2010, p. 231.
- [229] H. E. Gottlieb, V. Kotlyar, A. Nudelman, *J. Org. Chem.* **1997**, *62*, 7512–7515.
- [230] A. N. Nikitin, R. A. Hutchinson, *Macromol. Theory Simul.* **2006**, *15*, 128–136.
- [231] S. Kukučková, *Laser Initiated Polymerization Of Water Soluble Monomers*, PhD thesis, Bratislava, 2006.
- [232] P. Hesse, *Radical Polymerization Kinetics in Aqueous Solution and in Systems with Secondary and Tertiary Radicals Studied by Novel Pulsed- Laser Techniques*, PhD thesis, Göttingen, 2008.
- [233] C. M. Lee, W. D. Kumler, *J. Am. Chem. Soc.* **1961**, *83*, 4593–4596.
- [234] D. R. Lide, *Handbook of Chemistry and Physics*, 84th edition, CRC Press, Boca Raton 2004, p. 9/46.
- [235] C. H. Bamford, E. Schofield, *Polymer* **1981**, *22*, 1227–1235.
- [236] E. Senogles, R. Thomas, *J. Polym. Sci., Part C: Polym. Symp.* **1975**, *49*, 203–210.
- [237] T. M. Karaputadze, V. I. Shumskii, Y. E. Kirsh, *Vysokomol. Soedin. A* **1978**, *20*, 1853–1859.
- [238] T. M. Karaputadze, V. I. Shumskii, Y. E. Kirsh, *Polym. Sci. U.S.S.R.* **1978**, *20*, 2084–2091.
- [239] R. Sack-Kouloumbri, G. Meyerhoff, *Makromol. Chem.-Macromol. Chem. Phys.* **1989**, *190*, 1133–1152.
- [240] M. Buback, T. Junkers, *Macromol. Chem. Phys.* **2006**, *207*, 1640–1650.
- [241] R. Sadeghi, M. T. Zafarani-Moattar, *J. Chem. Thermodyn.* **2004**, *36*, 665–670.

- [242] N. V. Sastry, J. George, *Int. J. Thermophys.* **2003**, *24*, 1089–1104.
- [243] J. T. Chen, W. C. Chang, *J. Chem. Eng. Data* **2005**, *50*, 1753–1756.
- [244] S. Beuermann, *Laserinduzierte radikalische Polymerisation von Methylmethacrylat in Substanz und in Lösung in einem weiten Zustandsbereich*, PhD thesis, Göttingen, 1994.
- [245] *Revised Release on Viscosity and Thermal Conductivity of Heavy Water Substance*, The International Association for the Properties of Water and Steam, Lucerne, Switzerland, 2007, pp. 1–17.
- [246] *Release on the IAPWS Formulation 2008 for the Viscosity of Ordinary Water Substance*, The International Association for the Properties of Water and Steam, Berlin, Germany, 2008, pp. 1–9.
- [247] P. Pascal, M. A. Winnik, D. H. Napper, R. G. Gilbert, *Macromolecules* **1993**, *26*, 4572–4576.
- [248] P. Pascal, D. H. Napper, R. G. Gilbert, M. C. Piton, M. A. Winnik, *Macromolecules* **1990**, *23*, 5161–5163.
- [249] A. Bhattacharya, A. Das, P. C. Mondal, *J. Radioanal. Nucl. Chem.* **2000**, *246*, 237–238.
- [250] J. Schrooten, *Untersuchung der Kinetik der Puls-Laser-induzierten radikalischen Polymerisation von (Meth)acrylamiden in wässriger Phase*, Diploma thesis, Göttingen, 2007.
- [251] J. Sarnecki, J. Schweer, *Macromolecules* **1995**, *28*, 4080–4088.
- [252] W. Wang, R. A. Hutchinson, *Macromolecules* **2008**, *41*, 9011–9018.
- [253] H. Zipse, "Radical Stability – A Theoretical Perspective", in: *Radicals in Synthesis I – Methods and Mechanisms*, Andreas Gansäuer, Ed., Springer-Verlag, Berlin, Heidelberg 2006, *Topics in Current Chemistry* Vol. 263, p. 167.
- [254] H. Zipse, "Radical Stability – A Theoretical Perspective", in: *Radicals in Synthesis I – Methods and Mechanisms*, Andreas Gansäuer, Ed., Springer-Verlag, Berlin, Heidelberg 2006, *Topics in Current Chemistry* Vol. 263, pp. 167–172.
- [255] Y. Okamoto, H. Yuki, *J. Polym. Sci., Part A: Polym. Chem.* **1981**, *19*, 2647–2650.
- [256] T. Otsu, B. Yamada, T. Mori, M. Inoue, *J. Polym. Sci., Part C: Polym. Lett.* **1976**, *14*, 283–285.

-
- [257] J. Zabransky, M. Houska, J. Kalal, *Makromol. Chem.-Macromol. Chem. Phys.* **1985**, *186*, 247–253.
- [258] T. Suzuki, J. Kusakabe, K. Kitazawa, T. Nakagawa, S. Kawauchi, T. Ishizone, *Macromolecules* **2010**, *43*, 107–116.
- [259] T. Kodaira, F. Aoyama, *J. Polym. Sci., Part A: Polym. Chem.* **1974**, *12*, 897–910.
- [260] B. Yamada, T. Saya, T. Ohya, T. Otsu, *Makromol. Chem.-Macromol. Chem. Phys.* **1982**, *183*, 963–969.
- [261] B. Yamada, T. Saya, T. Otsu, *Makromol. Chem.-Macromol. Chem. Phys.* **1982**, *183*, 627–643.
- [262] B. Yamada, M. Azukizawa, T. Hirayama, *Polym. Bull.* **2000**, *43*, 457–464.
- [263] J. Moens, G. Smets, *J. Polym. Sci.* **1957**, *23*, 931–948.
- [264] G. Montaudo, V. Librando, S. Caccamese, P. Maravigna, *J. Am. Chem. Soc.* **1973**, *95*, 6365–6370.
- [265] G. Montaudo, P. Maravigna, S. Caccamese, V. Librando, *J. Org. Chem.* **1974**, *39*, 2806–2809.
- [266] G. Miyake, L. Caporaso, L. Cavallo, E. Y.-X. Chen, *Macromolecules* **2009**, *42*, 1462–1471.
- [267] K. M. Marstokk, H. Mollendal, S. Samdal, *J. Mol. Struct.* **2000**, *524*, 69–85.
- [268] K. M. Marstokk, H. Mollendal, S. Samdal, *J. Mol. Struct.* **1996**, *376*, 11–24.
- [269] M. Asada, T. Mitsugi, K. Fujii, R. Kanzaki, Y. Umebayashi, S. Ishiguro, *J. Mol. Liq.* **2007**, *136*, 138–146.
- [270] M. F. Ruiz-López, X. Assfeld, J. I. García, J. A. Mayoral, L. Salvatella, *J. Am. Chem. Soc.* **1993**, *115*, 8780–8787.
- [271] J. Barth, M. Buback, *Macromolecules* **2011**, *44*, 1292–1297.
- [272] C. Barner-Kowollik, G. T. Russell, *Prog. Polym. Sci.* **2009**, *34*, 1211–1259.
- [273] S. Beuermann, M. Buback, C. Schmaltz, *Ind. Eng. Chem. Res.* **1999**, *38*, 3338–3344.
- [274] M. Buback, C. Kowollik, *Macromolecules* **1998**, *31*, 3211–3215.
- [275] T. Ishige, A. E. Hamielec, *J. Appl. Polym. Sci.* **1973**, *17*, 1479–1506.
- [276] J. Barth, W. Meiser, M. Buback, *Macromolecules* **2012**, *45*, 1339–1345.

- [277] D. R. Lide, *Handbook of Chemistry and Physics*, 84th edition, CRC Press, Boca Raton 2004, p. 6/4.
- [278] Information brochure, *Performance & Industrial Chemicals – Reference Guide*, International Speciality Products, USA, 2005, p. 28.
- [279] Information brochure, *UltraThix P-100 – A Multi-Benefit Rheology Modifier*, International Speciality Products, USA, 2011, p. 1.
- [280] E. Senogles, R. A. Thomas, *J. Chem. Soc., Perkin Trans. 2* **1980**, 825–828.
- [281] A. Chapiro, L. D. Trung, *Eur. Polym. J.* **1974**, 10, 1103–1106.
- [282] N. F. G. Wittenberg, *Personal Communication*, **2012**.
- [283] CVI Melles Griot, *All Things Photonic – The CVI Melles Griot Technical Guide*, Vol. 2, Iss. 1, Albuquerque 2009, p. 9.3.
- [284] Information brochure, *Compendium – Principles of Halcyonics Active Vibration Isolation Technology*, Accurion, Göttingen, p. 1.
- [285] CVI Melles Griot, *All Things Photonic – The CVI Melles Griot Technical Guide*, Vol. 2, Iss. 1, Albuquerque 2009, p. 9.23.
- [286] CVI Melles Griot, *All Things Photonic – The CVI Melles Griot Technical Guide*, Vol. 2, Iss. 1, Albuquerque 2009, p. 9.22.
- [287] D. Bogner, Accurion, *Personal Communication*, **2010**.
- [288] N. Henze, Linos Photonics, *Personal Communication*, **2010**.
- [289] B. Náfrádi, R. Gaál, A. Sienkiewicz, T. Fehér, L. Forró, *J. Magn. Reson.* **2008**, 195, 206–210.
- [290] M. Alger, *Polymer Science Dictionary*, 2nd edition, Chapman & Hall, London 1997, p. 6.
- [291] M. Alger, *Polymer Science Dictionary*, 2nd edition, Chapman & Hall, London 1997, p. 606.
- [292] E. R. Cohen, T. Cvitaš, J. G. Frey, B. Holmström, K. Kuchitsu, R. Marquardt, I. Mills, F. Pavese, M. Quack, J. Stohner, H. L. Strauss, M. Takami, A. J. Thor, *IUPAC Green Book – Quantities, Units and Symbols in Physical Chemistry*, 3rd edition, IUPAC & RSC Publishing, Cambridge 2008, pp. 105–106.
- [293] E. R. Cohen, T. Cvitaš, J. G. Frey, B. Holmström, K. Kuchitsu, R. Marquardt, I. Mills, F. Pavese, M. Quack, J. Stohner, H. L. Strauss, M. Takami, A. J. Thor,

IUPAC Green Book – Quantities, Units and Symbols in Physical Chemistry, 3rd edition, IUPAC & RSC Publishing, Cambridge 2008, pp. 183–193.

Curriculum Vitae



Personal Details

Name	Jens Schrooten
Date and Place of Birth	15/05/1984, Göttingen
Citizenship	German

Education

05/2008–present	doctoral studies in chemistry at the University of Göttingen
05/2008–present	doctoral dissertation research, „Investigations into the Propagation and Termination Kinetics of the Radical Polymerization of Polar Monomers in Aqueous Solution“
23/04/2008	graduate chemist (Diplom)
10/2003–04/2008	diploma studies in chemistry at the University of Göttingen
10/2005–04/2008	main studies
06/2007–12/2007	diploma thesis, „Untersuchung der Kinetik der Puls-Laser-induzierten radikalischen Polymerisation von (Meth)acrylamiden in wässriger Phase“ (Investigations into the Kinetics of the Pulsed-Laser-Induced Radical Polymerization of (Meth)acrylamides in Aqueous Phase)
26/10/2005	intermediate diploma examination
10/2003–09/2005	basic studies
18/06/2003	German Abitur at the Otto-Hahn-Gymnasium Göttingen

Scholarships

01/2009–03/2010	scholarship holder of the Institute of Physical Chemistry at the University of Göttingen
05/2008–12/2008	scholarship holder of the DFG-funded European Graduate School 585: „Microstructural Control in Free-Radical Polymerization“

Göttingen, 25/09/2012